Photochemical and Spectroscopic Studies of Ketoaziridines

Gulácsy, Christina

Award date:
2016

Awarding institution:
University of Bath

Photochemical and Spectroscopic Studies of Ketoaziridines

Christina Elizabeth Gulácsy

A thesis submitted for the degree of Doctor of Philosophy

University of Bath

Department of Chemistry

April 2016

Abstract

While alcohols have successfully undergone kinetic resolutions, amines pose a challenge due to their nucleophilic nature. Aziridines were identified as potential substrates as a result of their synthetic utility and reduced nucleophilicity. Using a helical aminopyridine catalyst, the kinetic resolutions of ketoaziridines were explored. Initial attempts revealed anomalous kinetic behaviour [slow conversion and non-first order]. Non-buffered noncatalytic control reactions demonstrated unexpected reaction dynamics, as gauged by HPLC and ^{1}H NMR. Stopped-flow spectroscopy revealed photochemical sensitivity of the aziridine. As a result of this new information, the project evolved into a study of the photochemical behaviour of ketoaziridines and their spectroscopic properties.

UV-vis absorbance and fluorescence spectroscopy were used to probe the photochemical reactivity of ketoaziridines. These studies suggested a two-step mechanism where an azomethine ylide formed a reactive intermediate, ultimately to form 2,5-diphenyloxazole. Kinetic analysis revealed the mechanism was autocatalytic with respect to oxazole formation. TD-DFT calculations suggested the mechanism proceeded *via* a diradical species upon irradiation. This mechanistic route was studied by investigating the presence of a magnetic field effect on the kinetics of absorption and emission changes, in collaboration with the Manchester Institute of Biotechnology. Further studies demonstrated a radical species, derived from the irradiation of aziridine, may be used as a photoinitiator in the polymerization of methyl methacrylate. This work also involved development of a synthetic platform to diphenyloxazoles, where functionality may be installed in the initial steps. Use of this strategy allowed for the synthesis of a natural product, texaline.

Table of Contents

Acknowledgements

I would first like to thank Dr. Dave Carbery for giving me the chance to join his group and work on this project. I greatly appreciate all of the advice, support, and enthusiasm given to me throughout my Ph.D. Thank you for the opportunity to follow this odd and exciting chemistry!

I must next thank Dr. Chris Pudney who was instrumental in helping me become a spectroscopist. Thank you for all of your help since my first stopped-flow experiment, you helped me discover another area of science that I enjoy. Your encouragement and enthusiasm could not be more appreciated!

To my buddy throughout my 3 years, Giles Prentice, thank you. The "buffer zone," wine nights, and discovery that you are actually capable of cleaning (on move out day) will be missed. You have been a great help throughout my Ph.D., whether it be data discussions or providing me with unhelpful cycling knowledge I somehow still retain. Thank you for keeping me entertained!

Ciara Byrne, my first and last undergraduate. I am so lucky to have had your company for 2 years. You were an important part of this project and I could not have asked for a better student or friend!

I would like to thank the Carbery group: Dr. Fabienne Pradaux-Caggiano, Dr. Alex Murray, Chris Molloy, and Matt Camilleri. Thank you for your chemistry discussions and disco ball Fridays. It has been a fun and interesting 3 years!

The Pudney group, Dragana Catici and Hannah Jones, it has been a pleasure getting to know you. Dragana, thank you for being a good friend and for teaching me about ribosomes!

Thank you also to Dr. Dan Pantoş and the Pantoş group: Dr. Liam Emmett, Simone Limberti, Afi Dehkordi, Tibi Gianga, and Dora Rasadean. You have all been incredibly helpful and have made my lab and writing-up period enjoyable!

To the Frost group: Dr. Barrie Marsh, Dr. Sean Goggins, Dr. Will Mahy, Sinead Cabezas-Hayes, Jamie Leitch, Andy Paterson, and Callum Heron, thank you for the abuse and for allowing me to invade your office for chats!

Thank you also to Dr. John Lowe for all of your help and for not running away whenever I came to find you with a new experiment idea or question!

Dan Heathcote, you have been a key part of my Ph.D. these last two years. My sanity would be long gone by now had it not been for you. You survived my thesis and I know we are both glad it is over! You made this time more enjoyable and kept me smiling. Thank you for being there and supporting me!

Most importantly I must thank my family. I cannot thank you enough for all of your love and support! I am incredibly lucky to have such wonderful parents who helped me pursue my dream. I would not be here without all of you!

Abbreviations

°C	Degrees Centigrade
C	Conversion
Ac	Acetyl
Ar	Aryl
Boc	*tert*-Butoxycarbonyl
Bu	Butyl
Bz	Benzyl
Cbz	Carboxybenzyl
Cl-PIQ	2-Phenyl-7-chloro-1,2-dihydroimidazo[1,2-*a*]quinoline
DABCO	1,4-Diazabicyclo[2.2.2]octane
DCC	*N*,*N'*-Dicyclohexylcarbodiimide
DCE	1,2-Dichloroethane
DCM	Dichloromethane
DHIP	2,3-Dihydroimidazo-[1,2-*a*]pyridine
DMAD	Dimethylacetylenedicarboxylate
DMAP	4-Dimethylaminopyridine
DME	Dimethoxyethane
DMF	Dimethylformamide
DMSO	Dimethyl sulfoxide
EAF	Ethyl Azidoformate
ee	Enantiomeric Excess
EPA	Ether-*Iso*pentane-Ethanol
Eq.	Equivalents
ESI	Electrospray Ionisation
Et	Ethyl
Fmoc	Fluorenylmethyloxycarbonyl
GC	Gas Chromatography
GPC	Gel Permeation Chromatography
h	Hours
HeAP	Helical Aminopyridine
HPLC	High Performance Liquid Chromatography

hν	Light
^{i}Pr	Isopropyl
IR	Infrared Spectroscopy
IUPAC	International Union of Pure and Applied Chemistry
K	Kelvin
KR	Kinetic Resolution
LDA	Lithium Diisopropylamide
m-CPBA	Meta-Chloroperoxybenzoic acid
Me	Methyl
MeCN	Acetonitrile
min	Minutes
MMA	Methyl Methacrylate
MS	Mass Spectrometry
MSH	*O*-Mesitylenesulfonylhydroxylamine
MTHF	2-Methyltetrahydrofuran
mW	Milliwatt
NBS	*N*-Bromosuccinimide
NCS	*N*-Chlorosuccinimide
NMM	*N*-Methylmorpholine
NMR	Nuclear Magnetic Resonance
Nu	Nucleophile
PDI	Poly-Dispersity Index
Ph	Phenyl
Phth	Phthalimide
PMMA	Poly-Methyl Methacrylate
PQ^{2+}	4,4´-Dimethylbipyridiniumdication
p-Tol	Para-Toluyl
RF	Response Factor
RT	Room Temperature
s	Selectivity Factor
T	Tesla
TD-DFT	Time-Dependent Density Functional Theory
TFA	Trifluoroacetic Acid

THF	Tetrahydrofuran
TLC	Thin-Layer Chromatography
UV	Ultraviolet
V	Volt
Δ	Heat
$\Delta G^{\ddagger}$	Activation Energy
Δε	Molar Absorptivity

Chapter I: Introduction

Table of Contents

1.1. Properties of Aziridines

1.1.1. General Properties

Aziridines are important organic molecules in synthetic chemistry with various properties enabling their synthetic utility. The pK_a of the aziridinium ion was measured to be 7.98, making aziridines less basic than alkylamines, but more basic than arylamines.[1] Due to their trigonal ring, they are geometrically constrained and are less prone to nitrogen inversion as they have a higher barrier attributable to bond strain. This strain also means the ring is capable of opening using mild conditions, however, not as readily as epoxides due to nitrogen being less electronegative than oxygen.

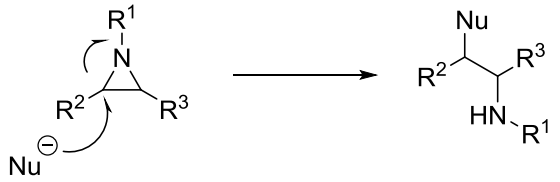

Scheme 1. Nucleophilic ring-opening of aziridine.

Ring-cleavage of aziridines takes place through nucleophilic attack at carbon, similar to epoxides. Asymmetric aziridines are usually attacked at the less substituted side when ring-opening, but this may be changed depending on the electronics of the molecule. In order to ring-open on the more substituted side, a weakly activating group on the nitrogen, such as an electron-withdrawing functionality, may be used.[1] This exception was observed, as shown in Scheme 2, where the *N*-substituent was weakly activating and the nucleophile was sterically hindered or a weak Lewis base. In this case, the quaternary carbon atom was attacked instead of the less substituted atom due to the substitution on the nitrogen.

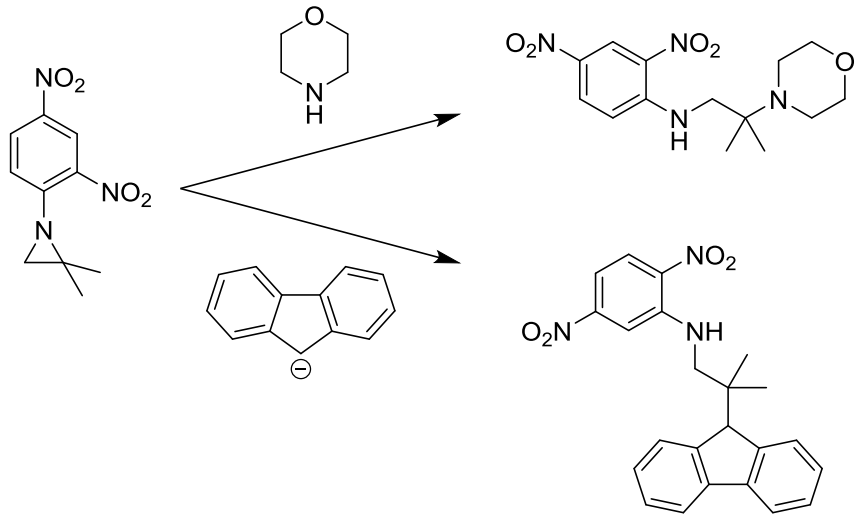

Scheme 2. Demonstration of attack at the quaternary carbon over the least substituted.

Aziridines have limited interaction with Lewis acids as compared with epoxides. This interaction may only take place when the substitution on the nitrogen does not contain oxygen. However, activation towards ring-opening of the aziridine may still be achieved for oxygen containing *N*-substituents, where coordination to the Lewis acid takes place through the oxygen lone pairs.[1]

1.1.2. Importance of N-Substituent

Functionalization of the nitrogen allows activation for ring-opening, as well as, protection of the nitrogen.[2] In order to assist with ring-opening activation, the substituent should help stabilise an amide anion that forms during the ring-opening. Aziridines were categorised by Ham in 1964 as "activated" or "non-activated."[3] "Activated" refers to substituents able to stabilise a negative charge during ring-opening when the aziridine nitrogen reacts with the nucleophile. When the nitrogen is capable of stabilising this charge, the activation energy required is reduced and acid catalysts are not needed. In the case of "non-activated" aziridines, an acid catalyst is essential for the reaction to take place with a nucleophile. Effective activating groups are ones containing double bonded oxygen. The resonance between the X=O and nitrogen allows for stabilisation of charge.

When studying carbonyl type substituents, electrophilicity is critical as ring-opening does not typically occur when the acyl group is more electrophilic. Acyl transfer is more likely to occur under this condition (Scheme 3). However, when using a less

electrophilic substituent on the nitrogen, ring-opening will occur, in addition to a side reaction taking place where the nitrogen is deacylated, affecting the yield.

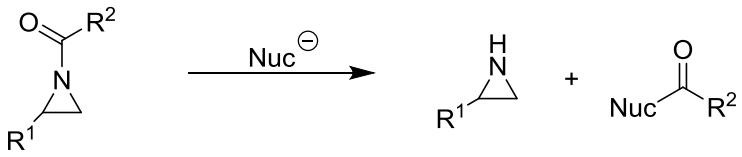

Scheme 3. Acyl transfer from the aziridine due to the presence of a carbonyl substituent.

1.1.3. Bond Angle Strain and Distortion

In saturated 3-membered heterocycles the bond angles are distorted, as they are approximately 60°, as opposed to the normal 109.5° for sp^3 hybridised atoms. Because of this, the molecule's hybridisation is altered to relieve the bond-angle distortion where the orbitals are overlapped resulting in the atoms being of a p nature. The distortion between the orbitals aids in relieving bond angle strain, which alters the bond angle to 60°. The nitrogen lone pair also contains more s character, resulting in its reduced basicity in comparison with aliphatic secondary amines.[4]

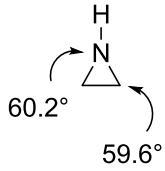

Figure 1. Aziridine internal bond angles where C-C-N is 59.6° and C-N-C is 60.2°.

Due to the ring strain present in aziridines, they are less prone to pyramidal inversion at the nitrogen. In the planar transition state, the planar nitrogen angle differs from the usual tetrahedral angle of 109.5°, resulting in increased angle strain which raises the energy barrier to inversion ($\Delta G^{\ddagger} \approx 71$ kJ mol^{-1}), as opposed to secondary amines ($\Delta G^{\ddagger} \approx$ 25 kJ mol^{-1}). The energy barrier may be further influenced by the substitution on the nitrogen. Electron-withdrawing groups are capable of stabilising this transition state, lowering the energy barrier to inversion. Sterics also play a role as they may destabilise the pyramidal transition state. To raise the energy barrier to inversion, electron-withdrawing groups with a lone pair may be used as the interaction between the lone pairs on the nitrogen and substituents are not favoured.[4] Padwa and Battisti synthesised *N*-chlorobenzoylphenylaziridine, and due to its slow inversion, it was possible to isolate the two invertomers using thick layer chromatography (Figure 2).[5]

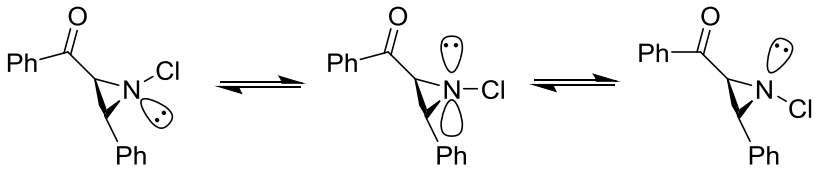

Figure 2. Isolated invertomers of *N*-chlorobenzoylphenylaziridine.

Also of note is the electrocyclic method of ring-opening aziridines. When heated or irradiated with UV light, an aziridine may open and form an azomethine ylide, creating a 1,3-dipole which may then be trapped to make compounds such as pyrrolidines. As this ring-opening is stereospecific, *S*- and *W*-dipoles are derived from *cis*- and *trans*-aziridines, respectively (Figure 3); *S*-dipoles are more reactive as they retain geometry and react with a wide range of dipolarophiles, while *W*-dipoles are less reactive and require more reactive dipolarophiles.[1]

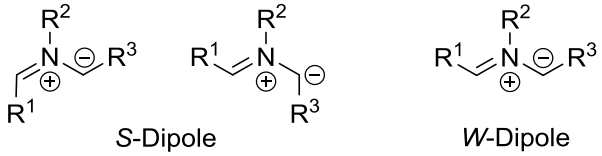

Figure 3. *S*- and *W*-dipoles derived from *cis*- and *trans*-aziridine.

Unless azomethine ylides have stabilising groups, they cannot be isolated. They are useful intermediates for 1,3-dipolar cycloaddition reactions and may be generated from aziridines, either thermally or photochemically, in the presence of electron-withdrawing groups on the adjacent carbons of the aziridine (Scheme 4). Using heat to open the ring generates an azomethine ylide stereopecifically where the ring opens in a conrotatory manner. Alternatively, when photochemical methods are used, the ring also opens stereospecifically but in a disrotatory fashion (Figure 4).[4]

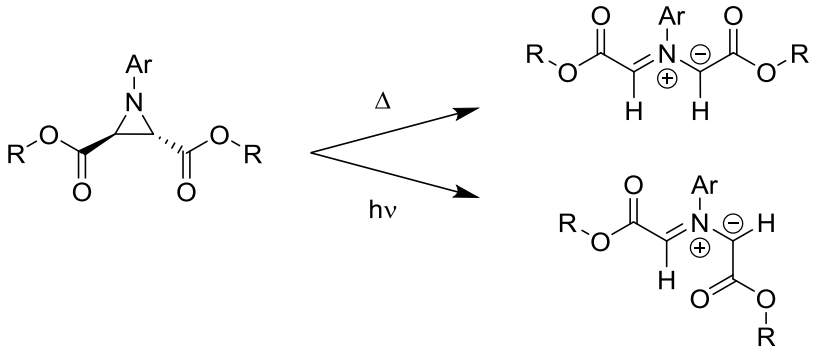

Scheme 4. Generation of azomethine ylides *via* thermal or photochemical means.[4]

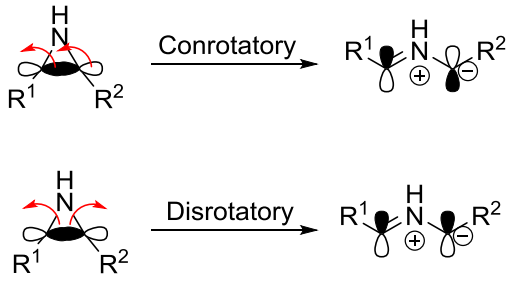

Figure 4. Conrotatory and disrotatory ring-opening of aziridines to azomethine ylides.

Commonly selected activating substituents are sulfonyl groups. These are used due to their ability to effectively stabilise the negative charge, allowing for simpler ring-opening. In addition, *N*-sulfonyl aziridines are readily synthesised, often forming solids, which aids in scale-up. The main drawback of these groups is their inability to be removed by mild conditions. While they are effective for ring-opening reactions, the issue then arises with their removal which may either not be possible, or may cause a subsequent reduction in yield and/or stereoselectivity.

1.2. Synthesis of Aziridines

1.2.1. Synthesis via *Nitrenes*

The idea to generate an *in situ* nitrene was proposed by Atkinson and Rees in 1969, where lead tetraacetate was used to dehydrogenate the free amine on 3-aminobenzoxazolin-2-one to form the active nitrene species (**1**, Figure 5).[6] The nitrene added to olefins to form aziridines, and also to 1,2-conjugated dienes to form vinyl aziridines. The main drawbacks of this methodology were the use of hazardous chemicals and the required substitution on the amine.

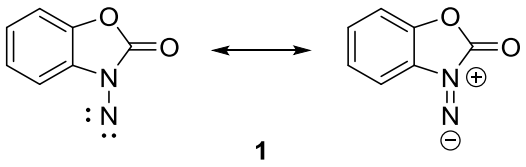

1

Figure 5. Active nitrene species used by Atkinson and Rees.

The use of chloramine-T was proposed by Komatsu *et al*. in 1998 in combination with CuCl, where the copper centre was directly involved in the aziridination step.[7] Sharpless further developed the use of chloramine-T by using it with an organic oxidant, phenyltrimethylammonium tribromide. Alkenes which were electron-rich or neutral efficiently underwent aziridination at room temperature.[8]

Most methods synthesise aziridines with sulfonyl substituents, which are difficult to remove. The use of trichloroethylsulfamate was proposed by Guthikonda and Du Bois, a group easily removed by metallic zinc under mild conditions.[9] This Rh(I)-catalysed process was applicable to a wide variety of alkenes, including cyclic alkenes and those with electron-withdrawing and alkyl substituents (Scheme 5). Yields between 57 and 95% were achieved.

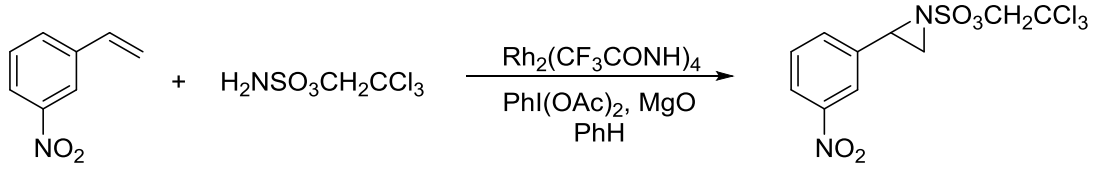

Scheme 5. Guthikonda and Du Bois aziridine synthesis.

McLaughlin *et al*. introduced a green synthesis for aziridination of *α,β*-unsaturated carbonyl compounds utilising a solvent free microwave reaction with high yields (79-97%) and low reaction times (1-4 hours).[10] Ethyl azidoformate (EAF) served as a nitrene source, with thermal or photochemical decomposition forming a reactive carbethoxynitrene species (Scheme 6). The reactive nitrene species was thermally generated by microwave irradiation. EAF as the nitrene source was previously used by Lwowski in 1965 for the photochemical aziridination of cyclohexene.[11]

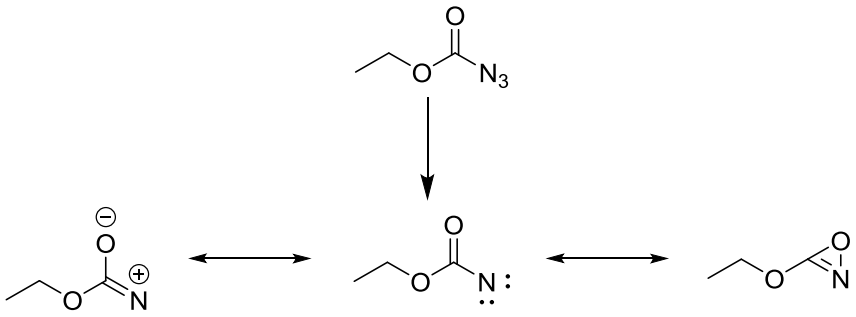

Scheme 6. Decomposition of ethyl azidoformate to generate active nitrenes species and its resonance forms.

Yudin utilised the versatility of aziridines to generate *α*-bromohydrazones through aziridination of a brominated alkene, which may then be thermally rearranged to generate the hydrazone.[12] To generate a "nitrenoid species," a combination of *N*-aminopthalimide and (diacetoxyiodo)benzene was used. The nitrene was generated through oxidation of *N*-aminophthalimide when the acetate ion was present to form *N*-acetoxyaminophthalimide, the reactive aziridinating agent.[13] This metal-free method generated aziridines from commercially available brominated olefins in 3 to 4 hours while stirring in dichloromethane (DCM), in yields from 36-90%. These aziridines may then thermally rearrange to form *α*-bromohydrazones (Scheme 7).

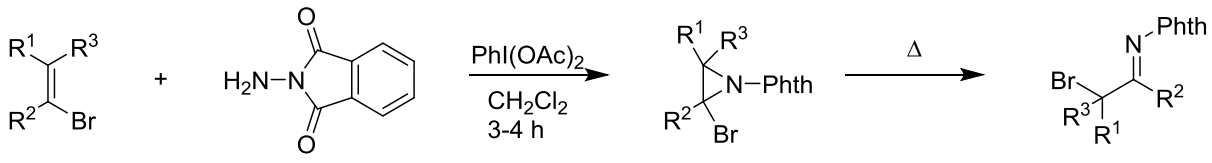

Scheme 7. Aziridination and subsequent rearrangement to form *α*-bromohydrazones.[12]

An electrochemical approach to synthesising aziridines was employed by Yudin in 2002.[14] Nitrene transfer from *N*-aminopthalimide to olefins was successful through use of platinum electrodes, in combination with triethylamine and acetic acid, to synthesise aziridines (Scheme 8). Utilising a working potential of +1.80 V provided aziridines in yields from 42 to 93%. This method was advantageous as anhydrous and inert atmospheres were not required and electron-poor and electron-rich olefins were able to form the desired aziridine.

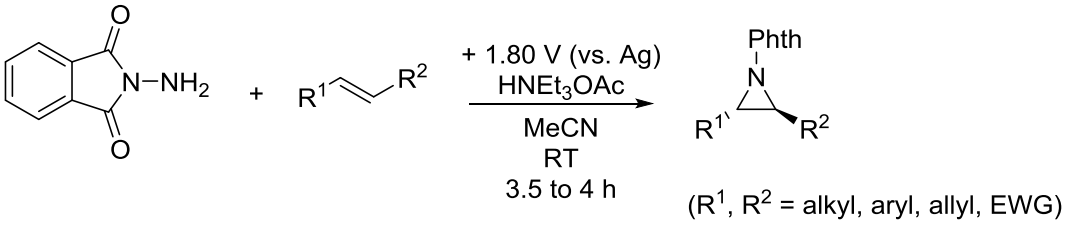

Scheme 8. Electrochemical aziridine synthesis developed by Yudin.

Metal-assisted aziridination protocols were also developed. Vyas *et al*. reported the use of bromamine-T (TsNBrNa, **2**, Figure 6) as a preferable nitrene source for aziridination in 1998 to use in conjunction with CuCl.[15] They later reported the use of bromamine-T with a polymer supported manganese (II)-complex for aziridination.[16] The recyclable Mn catalyst achieved yields of up to 70% when reacted with linear and cyclic alkenes. Palladium (II) chloride has also been used for the formation of aziridines from simple and electron deficient alkenes by Antunes *et al*.[17] In combination with bromamine-T, $PdCl_2$ was used to assist in the generation of aziridines in acetonitrile at room temperature. Yields from 20 to 81% were achieved utilising this methodology.

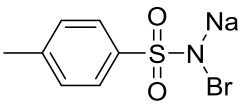

2

Figure 6. Bromamine-T nitrene source.

Colantoni *et al*. demonstrated unusual selectivity during their aziridinations of substituted 2,2,2-trifluoroethyl-*β*-dicarbonyl compounds.[18] Calcium oxide was used in conjunction with nosylcarbamates to form the 3-membered ring (Scheme 9). Formation of the aziridine was unaffected by the leaving group (Y) on the trifluoroethyl compounds, as morpholines, alcohols, and piperazines were all tolerated. Fluorenylmethyloxycarbonyl

(Fmoc), carboxybenzyl (Cbz), and ethyl ester substituted nosylcarbamates all generated the final aziridine in yields from 58 to 78%. However, changing the substitution to a *tert*-butoxycarbonyl (Boc) generated an isocyanate, supporting the suggested mechanism that the reaction took place *via* a nitrene.

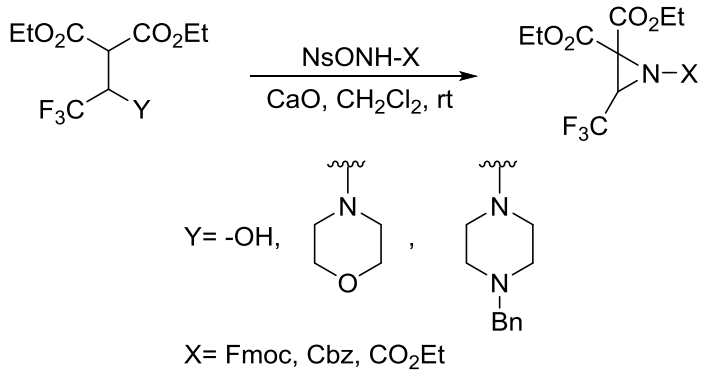

Scheme 9. Synthesis of aziridines from 2,2,2-trifluoroethyl-*β*-dicarbonyl compounds.

A common method to generate triplet and singlet nitrene species is through the decomposition of azides by thermal or photochemical means. Singlet nitrenes are able to react stereospecifically, while triplets are unselective with 1,2-disubstituted alkenes.[19] Unsubstituted azides reacted with 1,2-disubstituted alkenes under thermal or photochemical conditions generate a 1,2,3-triazoline, which then eliminates N_2 to yield the aziridine (Scheme 10). This method however, is not selective and the triazoline species may be isolated prior to converting to aziridine in a separate reaction.[19]

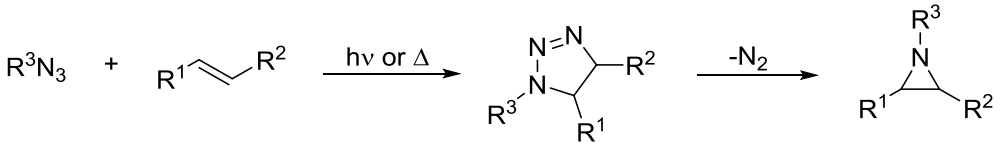

Scheme 10. Generation of an aziridine through the decomposition of 1,2,3-triazoline.[19]

1.2.2. Synthesis via *Cyclisations*

Carbene addition to imines is another method of aziridination, involving a two-step addition-elimination mechanism. Williams and Johnston employed Bronsted acid catalysis to synthesise *cis*-aziridines *via* an aza-Darzens mechanism.[20] Ethyldiazoacetate was used as the carbene source to react with Schiff base in the presence of trifluoromethanesulfonic acid in ethanenitrile. Aziridines were obtained in yields of 40 to 89%, with a *cis:trans*

ratio up to >95:5. This was the first report of proton catalysis to synthesise aziridines from imines and diazoesters.

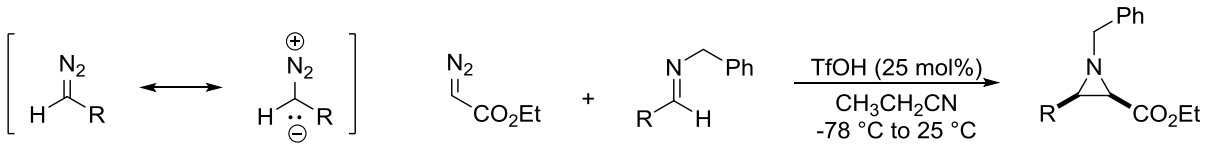

Scheme 11. Carbene formation and synthesis of *cis*-aziridines under acid catalysed conditions.[20]

Sulfilimines and *α*-bromoenolates may also be reacted, following the aza-Darzens mechanism, to form *N*-sulfinyl-substituted aziridines. Advantages of this method developed by Davis, involved the ability to further oxidise the *N*-sulfinyl to activate the aziridine ring for ring-opening reactions, or the ability to obtain the *NH*-aziridine through cleaving the sulfinyl group under basic or mildly acidic conditions.[21]

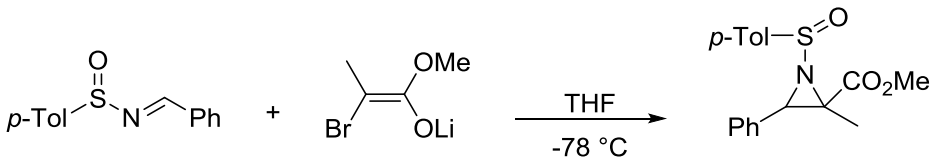

Scheme 12. Synthesis of *N*-sulfinyl aziridine by an aza-Darzens analogous method.

Ring-closing reactions of azidoalcohols are an additional method of synthesising aziridines. An azidoalcohol may be formed through opening of an epoxide with an azide nucleophile (Scheme 13). The subsequent step involves use of trialkyl or triarylphosphines to form an oxazaphospholidine which then forms the *NH*-aziridine upon heating in acetonitrile. Under these reaction conditions, the stereocentres are consistently inverted resulting in no difficulty with regiochemistry.[19]

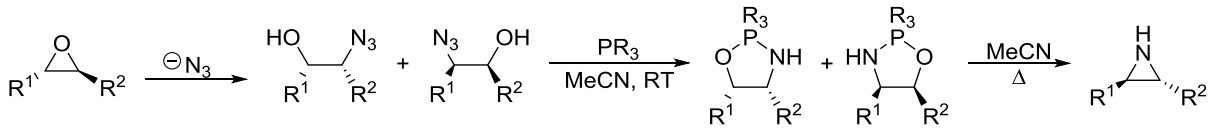

Scheme 13. Synthesis of *NH*-aziridines through formation of an azidoalcohol.[19]

Aziridines are readily synthesised from 1,2-aminohalides and 1,2-aminoalcohols. Gabriel first described the two-step synthesis of aziridines from 1,2-aminohalides in 1888.[22] Chlorination of an ethanolamine with thionyl chloride resulted in the 1,2-aminohalide which then cyclised when exposed to basic conditions. Wenker went on to describe an additional aziridine synthesis in 1935 (Scheme 14), which involved reaction of mono-ethanolamine (**3**) and 96% sulfuric acid at 250 °C to first generate *β*-aminoethyl sulfuric acid (**4**). The *β*-aminoethyl sulfuric acid was then distilled with aqueous basic solution to give pure aziridine (**5**).[23]

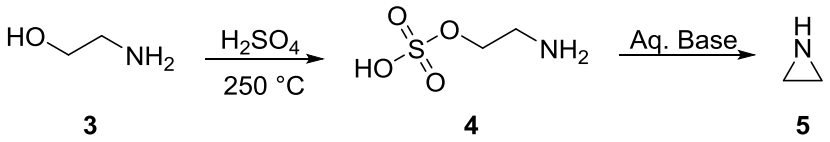

Scheme 14. Wenker aziridine synthesis.

Che *et al*. also described a similar aziridinating system involving (diacetoxyiodo)benzene, *N*-aminophthalimide or *N*-benzoxazolone, and potassium carbonate in DCM at room temperature. These reacted with a variety of alkenes and provided aziridines in 45-99% yield.[24] Che also described another protocol using aryl iodide as a mediator as an alternative to (diacetoxyiodo)benzene.[25] This system utilised *meta*-chloroperoxybenzoic acid (*m*-CPBA) as the oxidant, in the presence of *N*-aminophthalimide as the nitrogen source, and potassium carbonate in DCM at room temperature. It was important to note that lack of aryl iodide in the reaction resulted in the formation of an epoxide and the nitrogen source was recovered. The hypervalent iodine species was generated through oxidation of the aryl iodide by *m*-CPBA. This reactive intermediate, aryl-λ^3–iodane, formed the reactive aziridination species with the *N*-aminophthalimide and added to the olefin to create the aziridine (Scheme 15). The 12 hour room temperature reaction was able to form the aziridines in 49-94% yield, with the aryl iodide being recoverable for reuse. Aryl iodide even outperformed (diacetoxyiodo)benzene when aziridinating halogenated styrenes and *trans*-olefins.

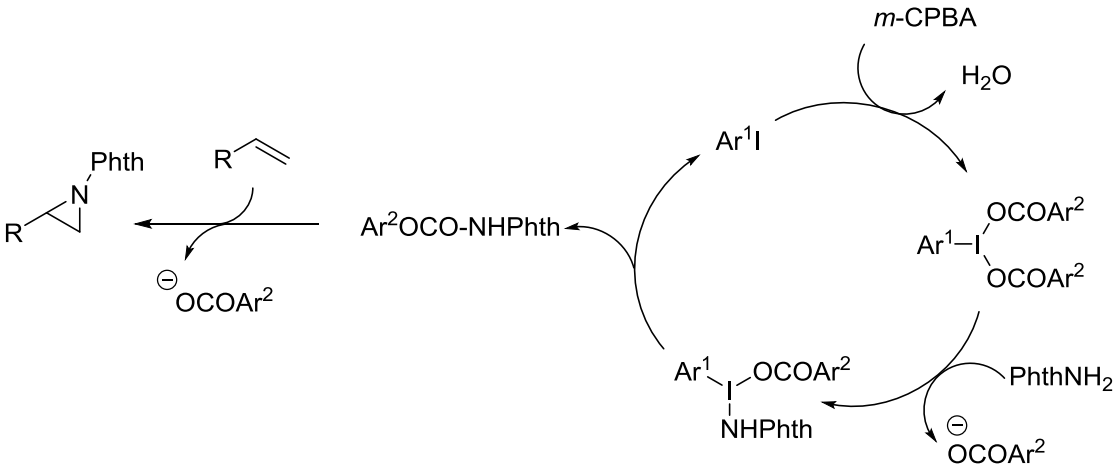

Scheme 15. Mechanism proposed by Che for the aziridination of alkenes using aryl iodides.[25]

Further building upon Yudin's and Che's work, Zhdankin *et al*. also used *N*-aminophthalimide as the nitrene source, along with tetrabutylammonium iodide catalytically and *m*-CPBA as the oxidant.[26] Similar to Che's work, it was found that the lack of an iodine reagent resulted in the preferential formation of epoxides over aziridines. The addition of tetrabutylammonium iodide, potassium carbonate, and *N*-aminophthalimide at 40 °C in ethyl acetate resulted in aziridine yields from 16% for cyclohexenone, and up to 80% for 4-fluorostyrene. Through multiple control experiments it was found that the active species was most likely hypoiodous acid (**6**), a product of the oxidation of the tetrabutylammonium iodide by *m*-CPBA. The alkene (**7**) then reacted with the acid to form an iodonium ion (**8**), which was followed by its opening at the benzylic position by *N*-aminophthalimide. *β*-Iodo-*N*-aminophthalimide (**9**) formed and cyclised to generate the aziridine (**10**) and an iodide anion (Scheme 16). The catalytic cycle continued with this iodide anion.

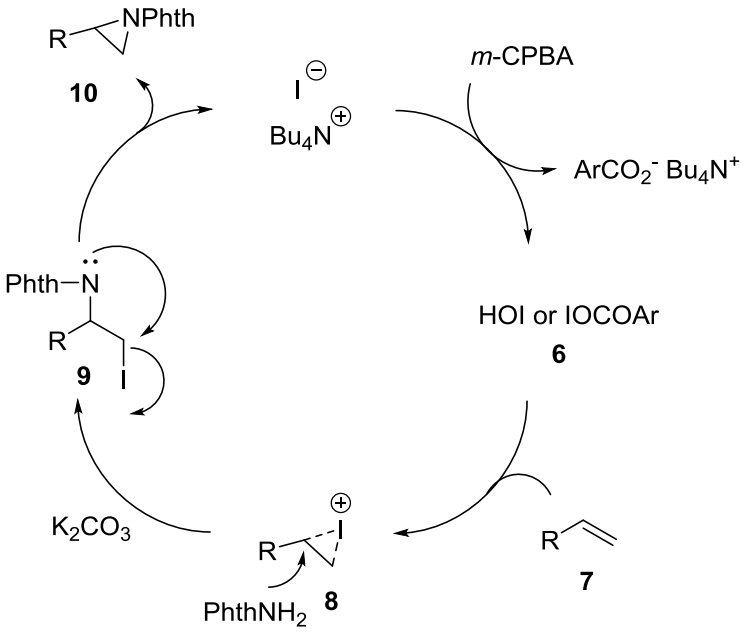

Scheme 16. Aziridination mechanism proposed by Zhdankin.[26]

Fan *et al*. explored using oxidative cyclisation of *β*-amino dicarbonyl compounds formed through *α*-amidoalkylation of activated methylenes.[27] The [1,3] oxidative cyclisation was successful when using iodosylbenzene (PhIO) and tetrabutylammonium iodide (Bu_4NI) to yield the aziridine, with a side product being the [1,5] oxidative cyclisation product, oxazoline (Scheme 17). This mild method was able to yield the aziridines in ten minutes at room temperature in tetrahydrofuran (THF), ranging from 46 to 93% yield. However, when Bu_4NI was not present in the reaction, no product was formed as a reactive iodine (III) species was required for the reaction to proceed. The yields were greatly affected by electronics, as it was found that electron-withdrawing substituents at R^1 led to higher yields of aziridines compared to electron-donating substituents. Oxazolines were preferentially formed when the *β*-amino dicarbonyl compound was electron rich for R^2 and R^3. When determining the reaction mechanism, it was found that the aziridine could not be converted to oxazoline and *vice versa*, using PhIO and Bu_4NI.

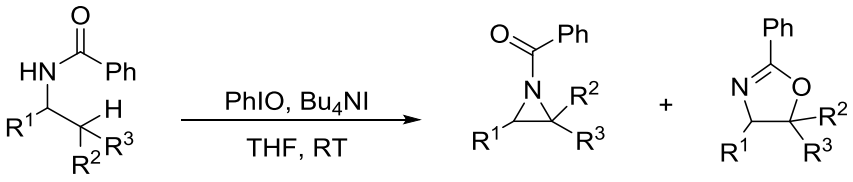

Scheme 17. Synthesis of aziridines and oxazolines by Fan.[27]

Houk and Armstrong also studied the use of oxaziridines (**11**) and diaziridines (**14**) for nitrogen transfer to alkenes (Scheme 18).[28-30] It was found that *N*-silyl, *N*-trifluoroacetyl, and *N*-alkyl oxaziridines and diaziridines would be useful *NH*-transfer reagents. The activation energy for the aziridination of alkenes by oxaziridines was similar in energy to that of epoxidation by organic oxidants. Diaziridines were also found to have low activation energies, capable of yielding aziridines from electron-rich and electron-deficient alkenes.

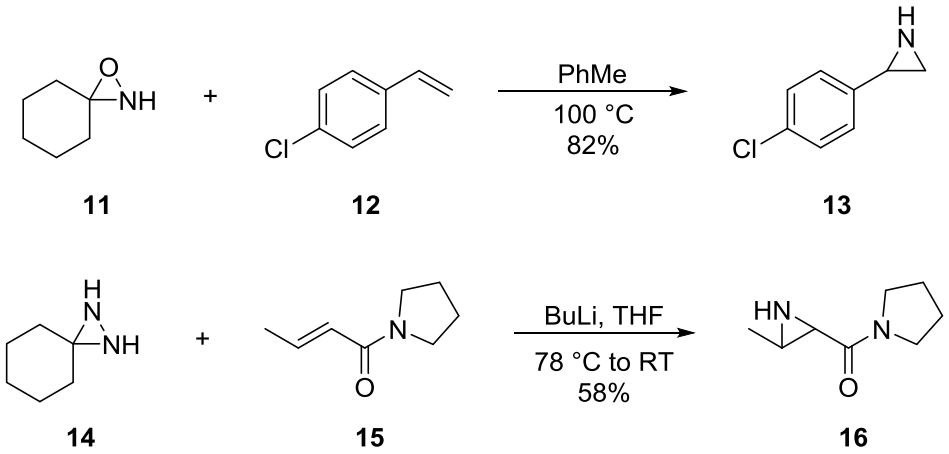

Scheme 18. Oxaziridines and diaziridines studied for the aziridination of alkenes by Houk and Armstrong.[28-30]

1.2.3. Synthesis via *Imines*

Imines may also be transformed to aziridines, as reported by Fan *et al.*[31] In their work, *N*-tosylimine was converted to an aziridine utilising an activated methylene compound, potassium *tert*-butoxide, (diacetoxyiodo)benzene, and tetrabutylammonium bromide in acetonitrile from 0 to 30 °C. The activated methylene reacted with the imine to form an enolate after proton transfer, which then reacted with AcOBr. The AcOBr was formed through exchange of the ligands between $PhI(OAc)_2$ and Bu_4NBr, which underwent reductive elimination to form the bromonium ion. The aziridine then formed through an intramolecular nucleophilic attack and elimination of bromine (Scheme 19). Yields up to 89% were reported when using this method, where R was alkyl or aromatic.

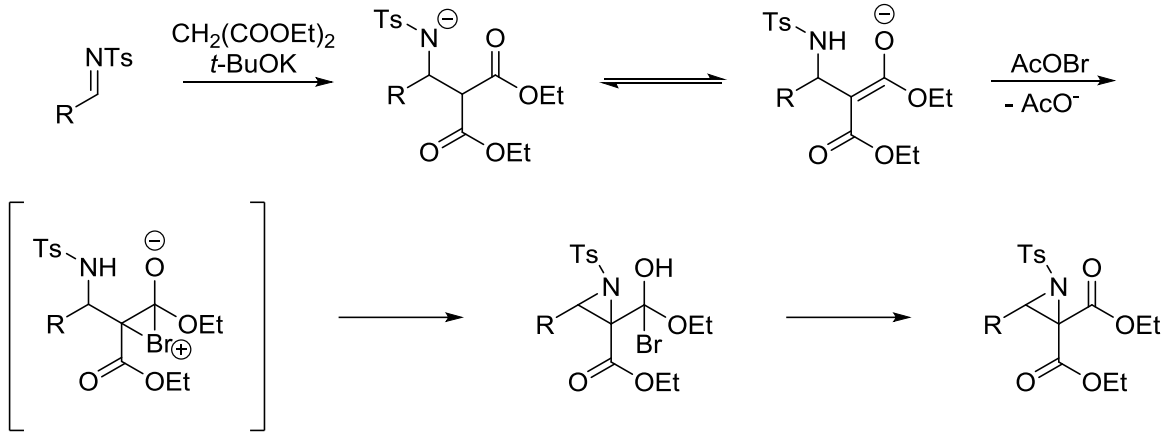

Scheme 19. Proposed mechanism by Fan *et al*. in the aziridination of an *N*-tosylimine.[31]

Azirines, cyclic unsaturated imines, are precursors to aziridines when undergoing addition reactions.[19] The oldest known azirine synthesis is known as the Neber reaction, presented in 1926, where 2-(*O*-tosyl)oximino carbonyl compounds undergo cyclisation to form the azirine.[32] Davis later proposed the conversion of tosylated aziridine (**17**) to an azirine (**18**) through loss of its tosyl group in the presence of lithium diisopropylamide (LDA) and water.[33] The azirine was then reacted with methylmagnesium bromide to yield the *NH*-aziridine (**19**) from 75 to 80% (Scheme 20).

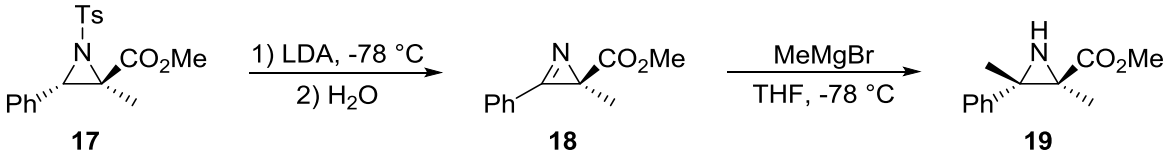

17 **18** **19**

Scheme 20. Davis' synthesis of *NH*-aziridines from azirines.

Additional methods to synthesise aziridines from azirines have also been proposed. Lemos *et al*. demonstrated that azirines were intermolecular radical acceptors.[34] Alkyl and aryl iodides were reacted with azirines in the presence of triethylborane to yield *NH*-aziridines in yields up to 89%.

1.2.4. Ylide Mediated Synthesis

Bismuthonium ylides were utilised to synthesise aziridines from imines by Matano *et al* in 1995.[35] They were easily generated through formation of a (2-oxoalkyl)-triphenylbismuthonium compound (**20**) from the reaction of a silyl enolate and triphenylbismuth difluoride with boron trifluoride diethyl ether (Scheme 21). Ylide **21** was

generated by reacting **20** with base, which then readily reacted with an imine to give the desired acyl aziridine (**22**). Stereochemical control was achieved through altering the base in the reaction, where potassium *tert*-butoxide or potassium hexamethyldisilazide yielded more of the *trans* product, while a combination of sodium hexamethyldisilazide with an additive of hexamethylphosphoramide or tetramethylethylenediamine reversed the stereoselectivity to the *cis* isomer. Yields of up to 91% were achieved with *cis*:*trans* ratios up to > 99:1. It was proposed the selectivity was due to the imine, and potential differences in the coordinations of the metal cations from the base with the additives.

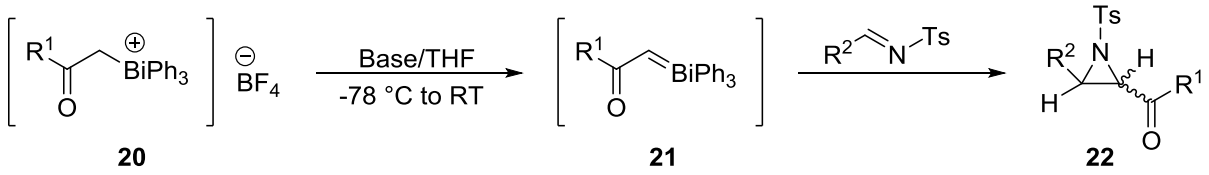

Scheme 21. Synthesis of tosylated aziridines from imines using bismuthonium ylides.[35]

Yadav also used a tertiary amine catalyst to synthesise aziridines from imines.[36] The catalyst was combined with phenacyl bromides to generate functionalised aziridines. The ammonium ylide was generated by reaction of phenacyl bromide with 1,4-diazabicyclo[2.2.2]octane (DABCO), *in situ*, in a one-pot synthesis with sodium carbonate and the imine (Scheme 22). Advantages of this procedure included the lack of necessity in preparing and isolating the ylides prior to use, as they were generated *in situ*. The *trans*-tosylated aziridines were synthesized in yields from 78 to 92% yield in high stereoselectivities up to 94:5 (*trans*/*cis*). Imines with alkyl or aromatic substituents with electron-withdrawing and electron-donating groups yielded product. Phenacyl bromides with electron-rich and electron-deficient aromatics were also used to successfully synthesise the aziridines.

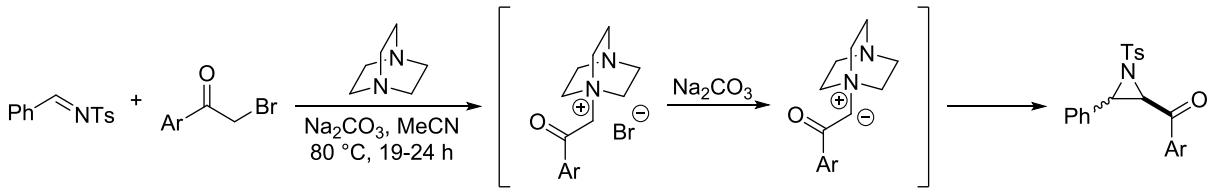

Scheme 22. Synthesis of tosylated aziridines through an ammonium ylide generated *in situ*.

The Corey-Chaykovsky aziridination reaction forms an aziridine through the addition of a sulfur ylide to an imine. An aziridine was formed in 91% yield by reacting dimethylsulfoxonium methylide (**24**) with benzalaniline.[37] The sulfur ylide was generated by deprotonating trimethyloxosulfonium iodide (**23**) with a base, such as sodium hydride (Scheme 23).

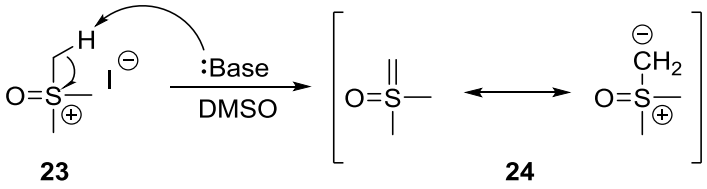

Scheme 23. Synthesis of dimethylsulfoxonium methylide developed by Corey and Chaykovsky.

Ikeda first described the use of aminimides, *N-N* ylides, for the direct aziridination of chalcones to form *NH*-aziridines in 1980.[38] The aminimide was easily prepared by reacting dimethylhydrazine with methyloxirane in 2-propanol at 50 °C for 3 hours. A solution of chalcone (**26**) in benzene was then added to the aminimide (**25**) and the aziridine (**27**) formed after 4 hours in 67 to 89% yield (Scheme 24). The substrate scope was limited to four chalcones, but was effective with electron-withdrawing substituted aryls. These initial experiments helped identify the utility of tertiary amines to promote aziridination.

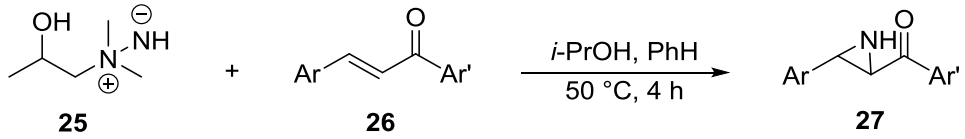

Scheme 24. Direct aziridination of chalcones proposed by Ikeda utilising an aminimide.

In order to improve upon substrate scopes and yield, an additional direct method for forming *NH*-ketoaziridines was developed by Xu.[39] The aziridination reagent, *N,N'*-diamino-1,4-diazoniabicyclo-[2.2.2]octane dinitrate (**28**), was synthesised through a literature procedure where DABCO and hydroxylamine-*O*-sulfonic acid were reacted in the presence of calcium oxide and calcium nitrate.[40] Reaction of **28** with chalcone using sodium hydride (NaH) in isopropanol (*i*-PrOH)/benzene at 0 °C provided the aziridine in 95% yield. The substrate scope was tested using a variety of chalcones, however, it was not successful with aliphatic *α,β*-unsaturated ketones or nitro-substituted chalcones (15-

17% yield). Halogens and other electron-donating groups on either aromatic ring of the chalcone yielded aziridine from 76 to 99%. In order to determine the mechanism of this reaction, the aziridination of styrene and other olefins were attempted. The lack of conversion to the desired product indicated the reaction did not go *via* a nitrene transfer to an alkene, but rather was a nitrogen ylide adding to the *α,β*-unsaturated ketone. Reaction of **28** with NaH formed the diamine imide, which then reacted by Michael addition with the chalcone. Collapse of the enolate created the aziridine (**31**) through cleavage of the *N-N* bond, releasing tertiary amine **32** (Scheme 25). One drawback of this method was the competing decomposition of **28** to DABCO, resulting in an excess of the reagent being required. This reaction also generally yielded the *trans*-aziridine.

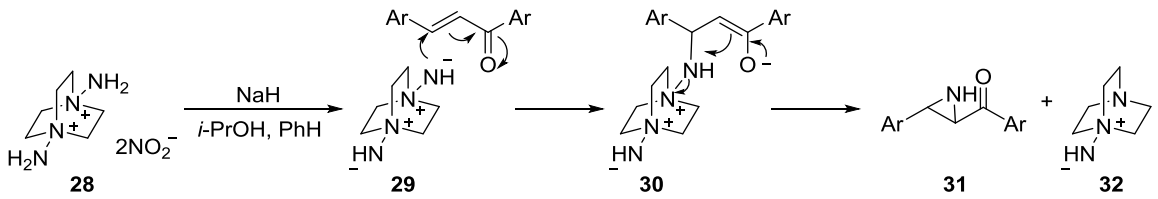

Scheme 25. Mechanism of aziridination proposed by Xu.[39]

Building upon the work of Xu, a straightforward synthesis was introduced in 2006 by Armstrong.[41] A hydrazinium iodide salt was synthesised using *N*-aminomorpholine and iodomethane in THF in yields up to 77%. This salt was then used in the aziridination of *trans*-chalcone with potassium *tert*-butoxide (*t*-BuOK) in dimethyl sulfoxide (DMSO) (Scheme 26). The reaction took place in 5 minutes and gave 61% yield.

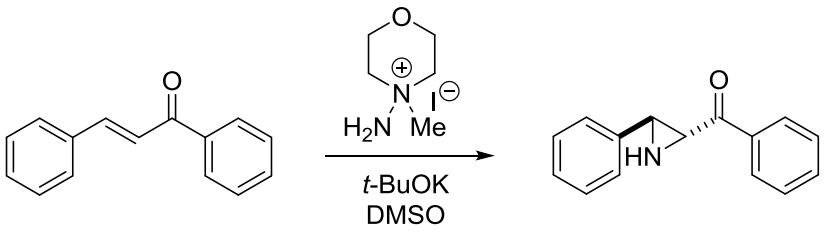

Scheme 26. Aziridine synthesis developed by Carbery and Armstrong.

Armstrong *et al*. also synthesised nitrate salt **33** from *N*-methylmorpholine using hydroxylamine-*O*-sulfonic acid, barium hydroxide, and barium nitrate in water. While this salt successfully made the aziridine with sodium hydroxide in acetonitrile, the reaction took 18 hours but provided 95% yield. Both methods were easily applicable to a wide variety of chalcones containing electron-donating and withdrawing groups. The nitrate salt

performed better with electron-deficient aryls, while the iodo salt was more suitable for the electron-rich aryls.

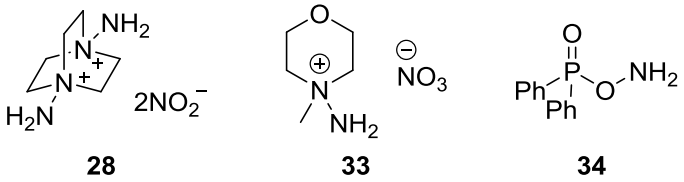

28 **33** **34**

Figure 7. Nitrogen sources employed by Xu (**28**) and Armstrong (**33** and **34**).

Armstrong *et al*. discovered further uses for tertiary amines to promote aziridination of *trans*-chalcone.[42] In the presence of *O*-(diphenylphosphinyl)hydroxylamine ($DppONH_2$, **34**) as the nitrogen source, a tertiary amine, and sodium hydroxide in acetonitrile, aziridination took place at room temperature after 9 hours (Scheme 27). Support for the mechanism *via* the formation of an *N*-*N* ylide was confirmed through observation of the inhibition of the reaction when removing the tertiary amine, or replacement with a secondary amine. The tertiary amines employed were *N*-methylmorpholine, *N*-methylpyrrolidine, or quinuclidine. This procedure successfully promoted aziridination with both electron-rich and electron-poor aromatics and alkyl enones. Selecting the appropriate combination of amine and solvent (MeCN, DCM, or dimethylformamide (DMF)) allowed the reactions to take place in 6 to 40 hours with yields varying from 32 to 97%, with the *trans*-aziridine preferentially formed >95:5.

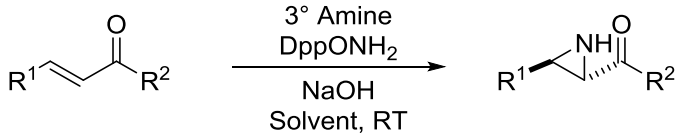

Scheme 27. Aziridine formation presented by Armstrong where R^1 and R^2 are aromatic or alkyl substituents.

The aziridination system developed by Armstrong was further expanded to dienes. Unlike previous reports by Xu and Ito, which used copper complexes and lithiated aziridination reagents, respectively, Armstrong was able to achieve selective aziridination without the use of metals.[43-45] *α,β,γ,δ*-Unsaturated ketones were used as the substrates for the optimised conditions involving *N*-methylmorpholine and a solution of *t*-BuOK in DCM, or NaH isopropanol conditions (Scheme 28).[45] Following stirring of the *N*-methylmorpholine and $DppONH_2$ for 30 minutes at room temperature, the substrate was

added with base and left to stir overnight. The vinyl aziridines were obtained in yields of 30 to 83%. The basic conditions were altered based on the presence of electron-deficient and alkyl groups, where the *t*-BuOK solution provided higher yields. Furfuryl and thiophenyl substituents were also tolerated. This method selectively yielded vinyl *NH*-unsubstituted *trans*-aziridines with diastereoselectivity of > 95:5.

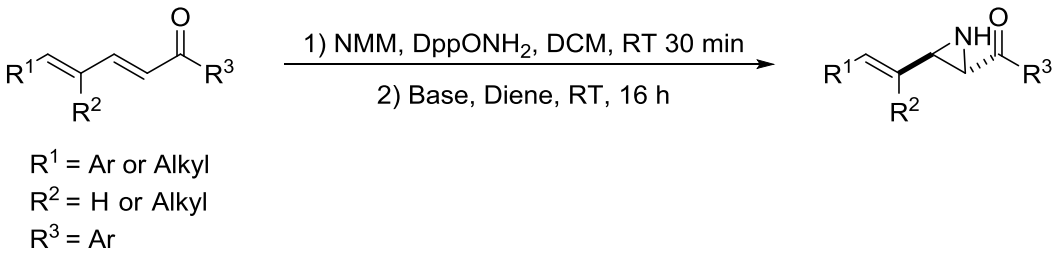

Scheme 28. Conditions developed by Armstrong using *N*-methylmorpholine (NMM).[45]

Additional methods were developed in 2015 by Samimi which expanded upon the use of amines to promote aziridination. Samimi proposed the use of 1-aminopyridinium iodide to synthesise *NH*-ketoaziridines from chalcones.[46] This mechanism was proposed to also proceed *via* an aminimine/nitrogen ylide. Reaction of 1-aminopyridinium and potassium carbonate with the substrate in refluxing THF, provided the *NH*-ketoaziridines after 7 hours in yields from 52 to 74%. This one-pot reaction was compatible with both electron-donating and electron-withdrawing substituted aryls on the chalcones.

Shen also presented the use of tertiary amines in conjunction with a nitrogen source to generate an aminimide *in situ* to promote aziridination of chalcones. In this case, *O*-mesitylenesulfonylhydroxylamine (MSH, **35**) was used as the nitrogen source to react with *N*-methylmorpholine in the presence of cesium hydroxide monohydrate (Figure 8).[47] Both the tertiary amine and base were required, as no aziridine formation was observed when either was lacking from the reaction. This methodology was applicable to chalcones containing electron-withdrawing and electron-donating substituents, with yields ranging from 49 to 85%. Wang *et al*. also identified an additional efficient nitrogen source, *O*-(2,4-dinitrophenyl)-hydroxylamine (**36**). Combining *N*-methylmorpholine with **36** and sodium hydroxide in DMF generated aziridines from a variety of *α,β*-unsaturated ketones regardless of their substituents.[47] Yields from 35 to 95% were obtained.

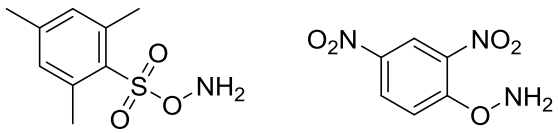

35 **36**

Figure 8. Nitrogen sources used by Shen (**35**) and Wang (**36**).

1.3. Photochemical Syntheses of Aziridines

Aziridines may also be synthesised photochemically. When methylpyridinium chloride was irradiated at 254 nm in an aqueous basic solution a bicyclic aziridine, 6-methylazabicyclo-[3.1.0]hex-3-en-2-*exo*-ol, was generated by Kaplan and Wilzbach in 1972.[49] Generation of this product was previously reported by Lwowski in 1968, however, the photochemical reaction was intermolecular between cyclopentadiene and carbethoxynitrene in DCM.[50] Ling expanded upon this work by altering the pyridinium salt used for the formation of aziridine by photoelectrocyclisation (Scheme 29).[51] Further studies demonstrated that nucleophilic solvents, such as water and methanol, incorporated into the pyridine ring. This protocol would allow highly substituted cyclopentene rings to be formed by varying the initial pyridinium salt.

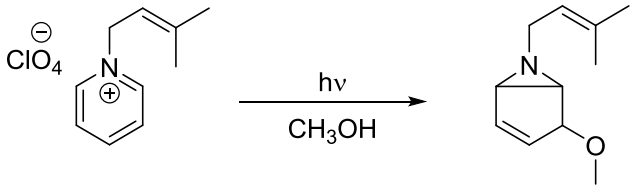

Scheme 29. Photochemical initiation to form an aziridine from pyridinium salts by Ling.[51]

Nitrene formation through photolysis was another common method to generate aziridines. Morita made use of dibenzothiophene *N*-substituted sulfilimines as the nitrene source, where its S-N bond was cleaved upon irradiation with wavelengths above 300 nm (Scheme 30). By reacting this newly formed nitrene with an olefin, aziridines were formed in yields up to 66%.[52] The nitrene was substituted with tosyl or Boc groups, and both effectively formed aziridines. Additionally, the dibenzothiophene was recoverable allowing the material to be recycled to make more nitrene precursor.

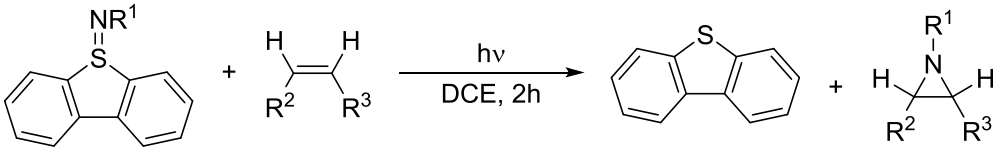

Scheme 30. Aziridine synthesis through reaction between an olefin and nitrene, generated through photolysis of dibenzothiophene sulfilimine.[52]

Similar work was performed by Furukawa utilising diphenylsulfilimine as the nitrene source.[53] The nitrene source was reacted with olefin in benzene to yield the

aziridine, without the use of light. Aziridine formed in yields up to 46%, with the exception of *trans*-chalcone yielding 73% aziridine but requiring reflux for 24 hours.

NH-aziridines were synthesised photochemically from alkylamino-2-cyclohexene-2-ones by Cossy and Pete in 1980 (Scheme 31).[54] Using their model substrate benzylamino-2-cyclohexene-2-one (**31**) in ether and irradiating at 313 nm, they obtained the *cis* and *trans* isomers in a 1:1 mixture in 40% yield. The mechanism suggested by the author involved the formation of an azomethine ylide upon irradiation, which then cyclised to form the aziridine.

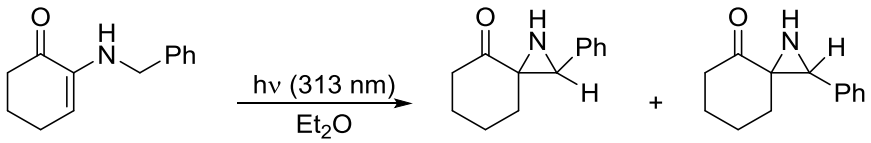

37 **38** **39**

Scheme 31. Photochemical synthesis of *NH*-aziridines by Cossy and Pete.

1.4. Reactions of Aziridines

Samimi described a deamination process for ketoaziridines, converting either the *cis* or *trans* unsubstituted or substituted aziridines to *trans*-alkenes.[55] This methodology used mild conditions, as only triphenylphosphine and iodine were required while refluxing in DCM (Scheme 32). All *trans*-2-aroyl-3-aryl unsubstituted aziridines gave the *trans*-chalcones in high isolated yields from 81-93% within 2.5 hours. The reaction was unaffected by electron-donating and electron-withdrawing groups on the aromatic rings. When expanding the substrate scope to *cis* or *trans*-substituted aziridines, the yields improved to 88 to 97% of the *trans*-alkene, regardless of substituents on the aryl rings.

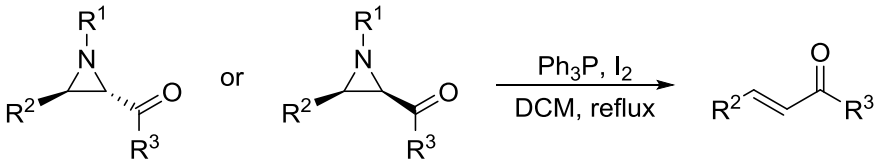

Scheme 32. Deamination procedure by Samimi where R^1 is H or CH_2Ph.

A ring-opening, ring-expansion procedure was developed by Samimi where the reagent selected in the initial acylation step affected whether a ring-opening or ring-expansion would occur (Scheme 33).[56] Reaction of *NH*-ketoaziridine (**40**) with di-*tert*-butyl dicarbonate in the presence of nickel (II) chloride and sodium iodide led to the formation of *tert*-butyl-1,3-diaryl-3-oxopropylcarbamates (**42**). The reaction was regioselective, where ring-opening occurred α to the carbonyl. The reaction tolerated electron-withdrawing substituents on the aryl groups, providing yields from 56 to 78%. Replacing di-*tert*-butyl dicarbonate with benzoyl chloride and triethylamine resulted in ring-expansion, and oxazolines (**44**) were obtained in yields up to 77%. Samimi also developed a synthesis of *trans*-4-benzoyl oxazolines in a one-pot procedure utilising $K_5[PW_{11}ZnO_{39}]\cdot 23H_2O$ as a catalyst in the presence of benzoic acid and *N*,*N*'-dicyclohexylcarbodiimide (DCC).[57] The procedure involved the acylation of an *NH*-ketoaziridine, followed by ring-opening of the aziridine and a C-O bond formation. The reaction took place in acetonitrile and provided the oxazolines in 71-85% yield.

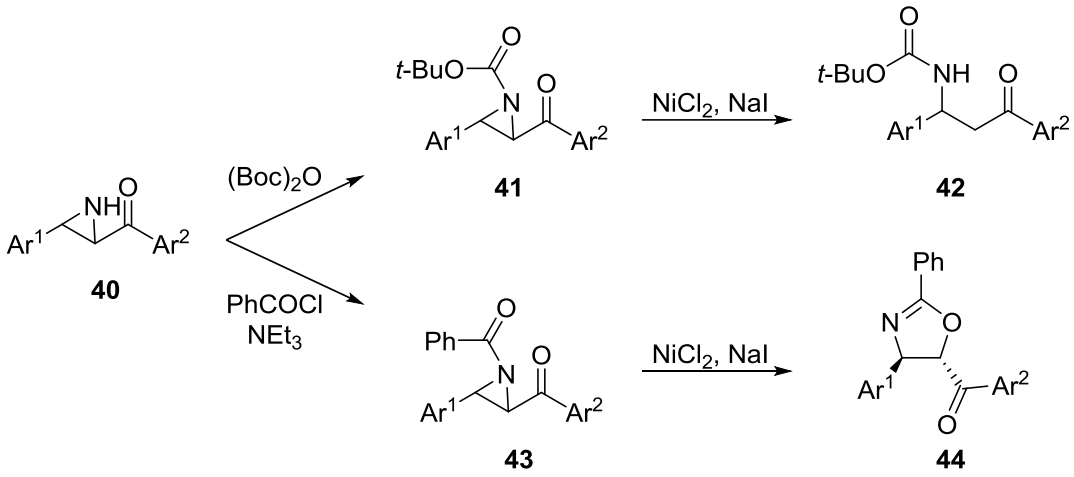

Scheme 33. Divergence in ring-opening and ring-expansion of *NH*-ketoaziridines through the selection of acylating reagent.[56]

NH-Ketoaziridines were employed by Wang in the synthesis of 3-pyrrolines, biologically active molecules, by their reaction with an alkyne (**46**) and sulfonyl azide (**45**) in the presence of copper (I) iodide (Scheme 34).[58] This one-pot reaction proceeded by a copper-catalysed cycloaddition between the alkyne and azide to form a Cu-triazolyl species (**47**) (Scheme 34). Release of N_2 yielded a ketenimine (**48**) which was then attacked by the aziridine (**49**) and cyclised to form 1-aza-bicyclo[3.1.0]-hexane (**51**) . This product was then dehydrated (**52**) and ring-opened to the pyrroline (**53**). The yields obtained were between 53 and 78%. It was found that aromatic sulfonyl azides enhanced the yield of the reaction, while alkyl-substituted alkynes decreased the yield. This was postulated to be due to the lack of stability of the ketenimine.

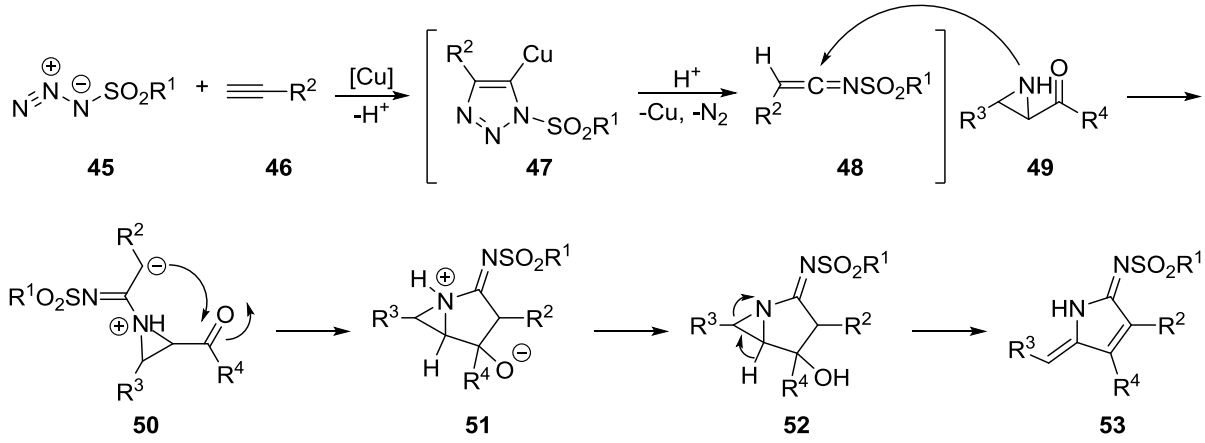

Scheme 34. Proposed mechanism for the synthesis of 5-arylidene-2-imino-3-pyrrolines by Wang.[58]

Samimi reported the use of *N*-bromosuccinimide (NBS) to brominate an *NH*-ketoaziridine, which would then rearrange to form 2,5-diphenyloxazole under thermal conditions.[59] Once brominated, the aziridine ring would selectively open at the C-C bond, allowing for easy rearrangement to form the oxazole in 1 hour when refluxing in 1,4-dioxane (Scheme 35). Electron-rich and electron-deficient aryls on the ketoaziridine were well tolerated, providing yields from 75 to 94%. Exceptions involved when both aryls were electron-61deficient or Ar^1 was *meta*-nitro substituted. In these cases, no product was formed. When the reaction temperature was changed to 15 °C, only the brominated aziridine was obtained, demonstrating thermal conditions were critical to this reaction.

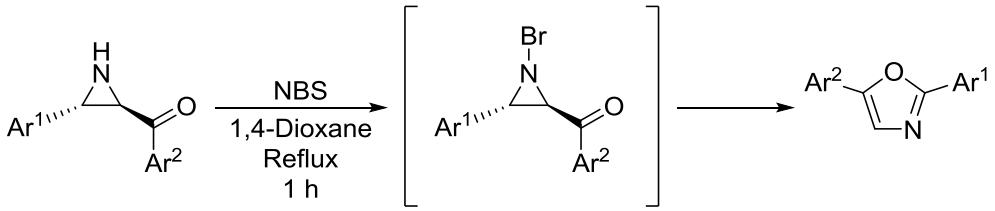

Scheme 35. Synthesis of 2,5-diphenyloxazole through brominated ketoaziridine intermediate.[59]

Coldham demonstrated the use of an aza-Wittig rearrangement to synthesise piperidines from substituted aziridines.[60] The Wittig rearrangement involves a [2,3]-sigmatropic rearrangement of allylic ethers, forming a new carbon-carbon bond, while an aza-Wittig rearrangement involves a [1,2]-sigmatropic shift of allylic tertiary amines. *NH*-Ketoaziridines were alkylated with *tert*-butyl-2-bromoacetate, in the presence of base, to

yield the alkylated aziridine (**54**) (Scheme 36). When reacting the alkylated aziridine under Wittig conditions using a phosphonium ylide, the olefination led to a [2,3]-sigmatropic rearrangement. This resulted in formation of only the *cis*-diastereomer (*cis*-**55**) of an unsaturated piperidine in yields from 55 to 66% when the reaction was performed at room temperature. However, when the reaction took place at 40 °C, the *cis* to *trans* ratio shifted to 71:29. The ratio could further be altered to 58:41 by changing the solvent from dimethoxyethane (DME) to DMSO.

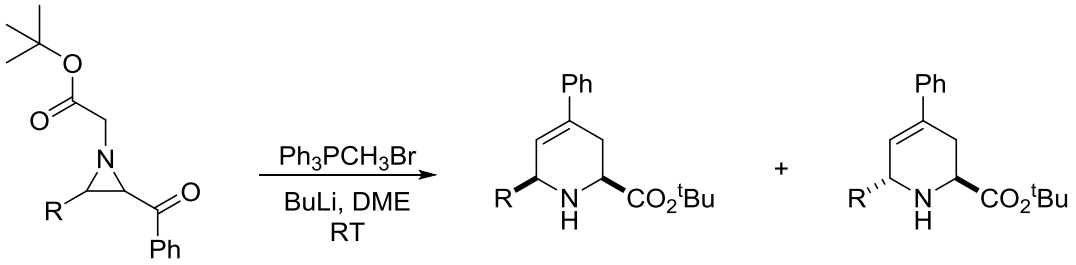

54 *cis*-**55** *trans*-**55**

Scheme 36. Aza-Wittig rearrangement of substituted aziridines by Coldham *et al*., where R was an alkyl substituent.[60]

A Payne rearrangement involves the isomerisation of 2,3-epoxy alcohols. This was extended to aza-Payne rearrangements of epoxides with free amines to form aziridines and alcohols, and *vice versa*. An aza-Payne rearrangement of an aziridinol, followed by a haloamination in a one-pot reaction was developed by Schomaker *et al* (Scheme 37).[61] Aziridinols were first synthesised through reaction of tosylated aziridine aldehydes with Grignard reagents in yields up to 96%. Use of dimethylsulfoxonium methylide as a base mediated the aza-Payne rearrangement, allowing the haloamination to then proceed and form the epoxide substituted pyrrolidines (**59**) at room temperature in DMSO. Decreases in yield were observed when the alkynes (**56**) contained alkyl- or silyl-substituents, which was proposed to be due to the alkyne being unable to stabilize a negative charge on the carbon next to the site of formation of the new C-N bond. Yields were obtained up to 82% for the functionalised pyrrolidines.

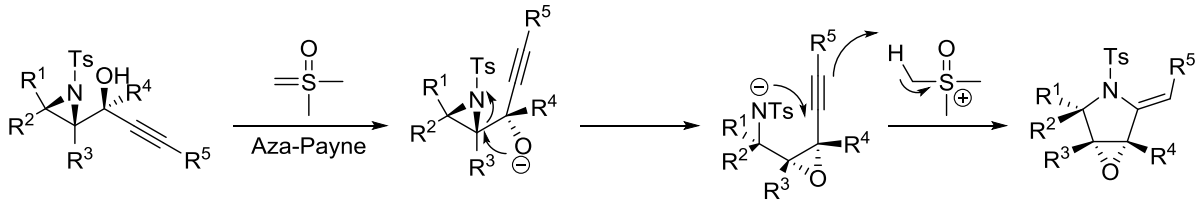

Scheme 37. Proposed mechanism for the aza-Payne/haloamination method by Schomaker *et al.*[61]

Wenkert and McPhail reported the thermal conversion of aziridines to pyrrolidines in 1985.[62] They proposed the [3+2] cycloaddition of an azomethine ylide with an olefin. Previously synthesised 2-alkenoyl-3-phenylaziridines and 2-alkenoylaziridines were heated to 80 °C in order to form the bicyclic product. When studying the mechanism, they found *cis*-aziridines would readily transform to the bicyclic products due to the azomethine ylide conformation (Scheme 38). However, *trans*-aziridines formed the *W*- or *U*-ylide configurations, where R substituents were on the same sides, preventing them from forming product directly. The ylide formed from the *trans*-aziridine would first have to isomerise to the *S* azomethine ylide before it would be able to form the product.

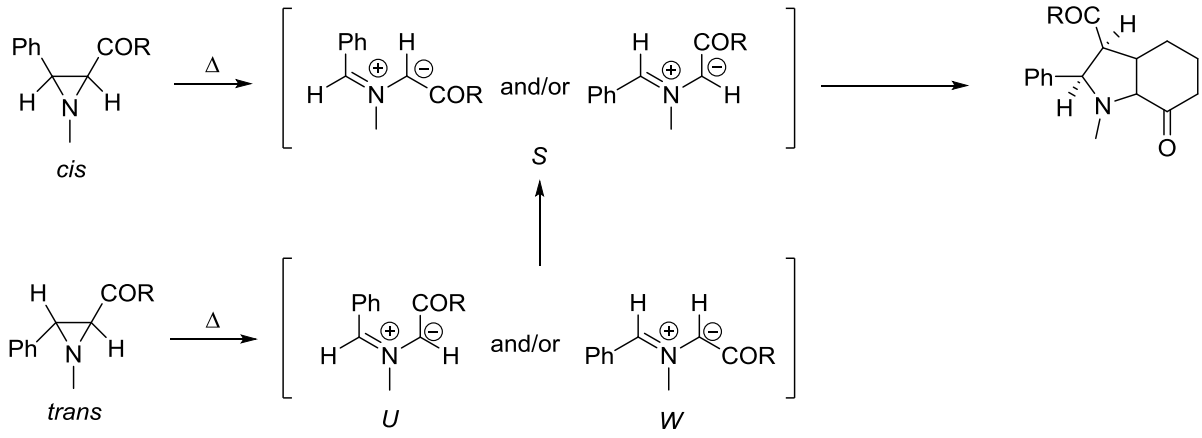

Scheme 38. [3+2] Cycloaddtion of azomethine ylides to form bicyclic systems.[62]

1.5. Kinetic Resolutions

1.5.1. Chiral DMAP use in Kinetic Resolutions of Alcohols

The utility of 4-dimethylaminopyridine (DMAP) was initially reported in the 1960s by two research groups, Litvinenko and Kirichenko in 1967 and Steglich and Höfle in 1968.[63,64] Litvinenko and Kirichenko demonstrated that DMAP was 150,000 times more reactive than triethylamine, and 6,000 times more reactive than pyridine in the benzoylation of benzyl alcohol (Scheme 39).[63] In Steglich and Höfle's studies, they discovered that DMAP was far more reactive than pyridine in the acylations of tertiary alcohols. *Tert*-butanol and 1-methyl-1-cyclohexanol were not acylated when using pyridine, however, using 1 equivalent of DMAP promoted the acylation of 1-methyl-1-cyclohexanol in 10 hours at room temperature.[64]

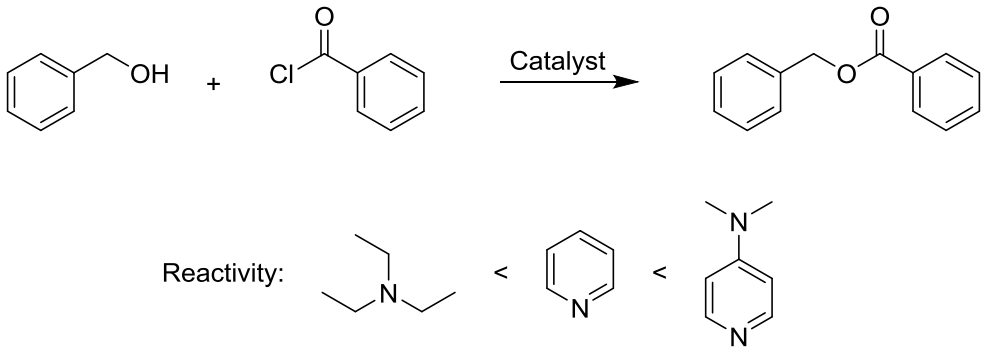

Scheme 39. Acylation of benzoyl chloride.

DMAP's capabilities cover a broad range of chemistry, and great efforts have been made in the use of chiral analogues for the kinetic resolution (KR) of alcohols. KR was described by IUPAC in 1996 as "the achievement of partial or complete resolution by virtue of unequal rates of reaction of the enantiomers in a racemate with a chiral agent (reagent, catalyst, solvent, etc.)."[65] Nonezymatic kinetic resolutions were initially tested and successful using chiral DMAP variants with secondary alcohols.

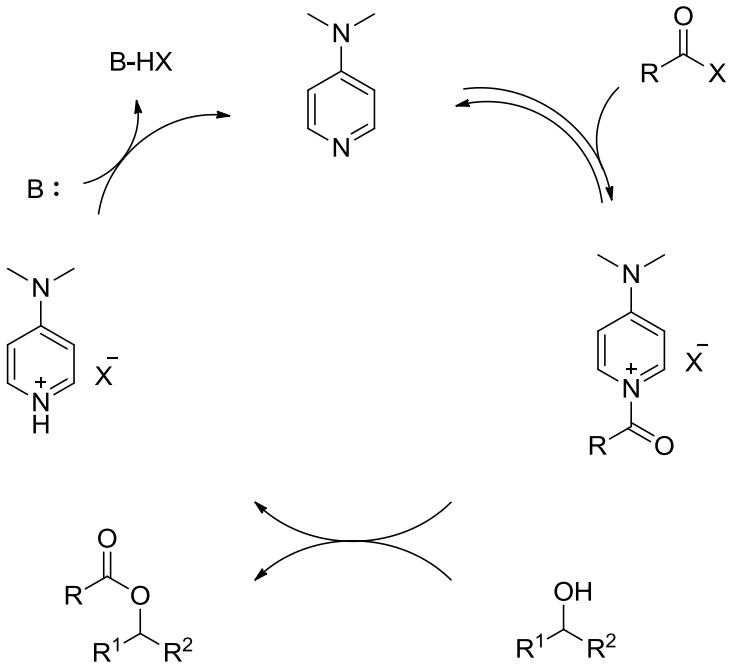

Scheme 40. Mechanism for the acylation of secondary alcohols with DMAP.

As shown in Scheme 40, DMAP first forms an acylpyridinium salt. Upon introduction of the secondary alcohol, the acyl group transfers to the alcohol, leaving the protonated catalyst. An additional base, such as triethylamine, then deprotonates DMAP to regenerate the catalyst, and the catalytic cycle may continue. Using a chiral DMAP would allow the stereochemistry to be determined during the acylation step, allowing one alcohol enantiomer to be selectively acylated.

1.5.2. Kinetic Resolution of Amines

A relatively unexplored area involves the KR of amines. While also being polar and able to hydrogen bond, these abilities are reduced for an amine when compared to an alcohol. However, amines have greater nucleophilicity, making them a greater challenge. Very basic amines are easily acylated without the need of a catalyst, resulting in background reactions.[66] The first report of *N*-acylation was by Murakami in 1998.[67] In this report, chiral 2-acetylamino-2'-diacetylamino-1,1'-binaphthyl **60** was used to selectively acylate 1-(1-naphthyl)ethylamine. *Ee v*alues up to 48% were obtained. Atkinson *et al* then reported the use of 3-diacylaminoquinazolin-4(3*H*)-ones for the kinetic resolution of amines.[68] Using 1 equivalent of catalyst and 2 equivalents of amine yielded acylated material with up to 95% *ee*.

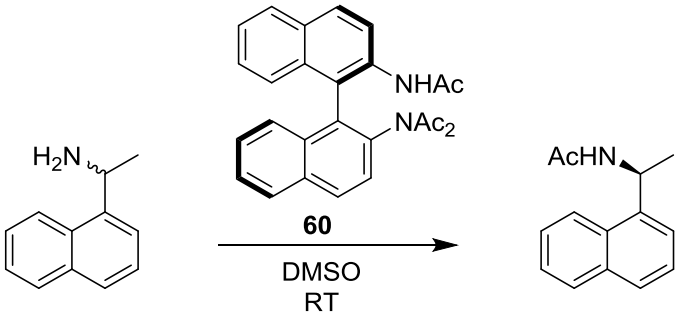

Figure 9. First reported *N*-acylation by Murakami.

Arai and Fu reported the first efficient KR of amines in 2001.[69] This was achieved by using *O*-acylated azlactone (**62**) as the acylating agent, as it was found to react more readily with the catalyst than the benzylic amine. When attempting acylation of racemic 1-phenylethylamine, an *s*-factor of 2.8 was seen. Altering the aromatic ring of the substrate indicated that electron donating and withdrawing groups did not affect selectivity when at the *para* position. However, placement of a methoxy on the *meta* position, increased selectivity to 22.

In 2008, Arp and Fu expanded the substrate scope to indolines.[70] When applying the previously developed method for the acylation of benzylic amines, indolines did not acylate due to their less nucleophilic nature. Manipulation of the catalyst (**61**) played an important role in selectivity. Methylation of the 3- and 5- positions of the phenyls on the bottom ring increased the selectivity. When increasing the groups to ethyls, the selectivity dropped once again. Having had previous success with halide counterions, lithium bromide was added with 18-crown-6 ether resulting in *s* = 23. Smaller crown ethers and lack of lithium bromide both decreased selectivity. This acylation also required the use of *O*-acylated azlactone, in place of commercial sources, as an acylating agent.

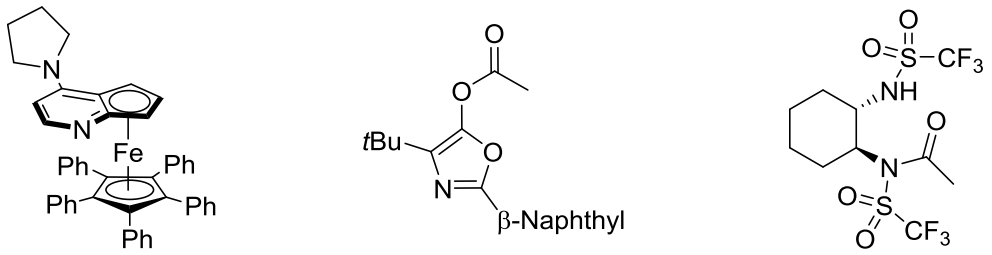

61 **62** **63**

Figure 10. Arp and Fu's catalyst **(61)** and acylating agent (**62**), and Wagner and Mioskowski's (**63**) catalyst for the KR of amines.

Further development on the acylation of primary amines was carried out in 2004 by Wagner and Mioskowski.[71] Catalyst **63** had the unique quality of solvent tuneability where the solvent allowed selection of which stereoisomer would acylate. In addition to this, the selectivities were the highest reported at the time and the reactions reached 50% conversion. Solvents with low permittivity demonstrated selectivity towards the *R* enantiomer of 1-phenylethylamine, while dipolar nonprotic solvents favoured the *S* enantiomer. Using 1,3-dimethyltetrahydro-2-pyrimidinone as the solvent, acylated amine was obtained with $s = 30$.

Birman was able to expand the scope of his 2,3-dihydroimidazo-[1,2-*a*]pyridine (DHIP)-based catalysts for their application to the acylation of amines.[72] 4-Phenyl-2-oxazolidinone was chosen as the initial acylation candidate due to previous studies indicating the importance of π-cation and π-π interactions. 2-Phenyl-7-chloro-1,2-dihydroimidazo[1,2-*a*]quinoline (Cl-PIQ) was the catalyst of choice for these reactions, as it was capable of promoting successful *N*-acylation providing *s*-factors up to 70. In accordance with previous studies, selectivity was improved when the phenyl group on the substrate was changed to a naphthyl. An even larger impact on selectivity was observed with catalyst **64**, termed BTM. Acylated products were obtained with *s*-factors from 50 to 520.

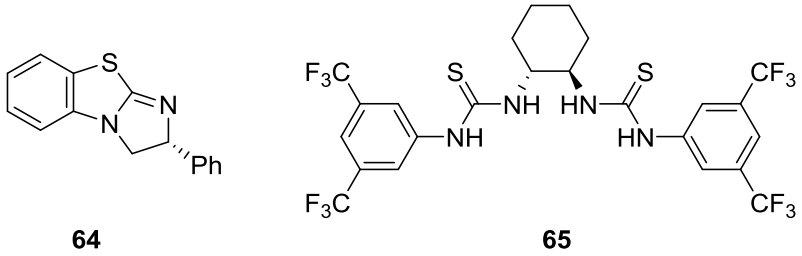

64 **65**

Figure 11. Birman's BTM catalyst and Seidel's "chiral promoter."

In 2009 Seidel reported the use of simple acylating agents combined with a "chiral promoter" to acylate primary amines.[73] The concept was that an achiral pyridinium salt would become chiral when bound to a chiral anion, resulting in a chiral ion pair. DMAP was used in 20 mol% to form the salt with benzoic anhydride. Seidel's thiourea catalyst **65** was used to induce chirality in the chiral ion pair. This concept proved successful as *s*-factors up to 24 were observed.

Another strategy to enhance the selectivity of DMAP was reported by Carbery incorporating DMAP into a helical structure, resulting in helical aminopyridine (**66**).[74] Adaptation of DMAP to a helical scaffold allowed desymmetrisation for its use in asymmetric catalysis. The reactivity and selectivity were increased due to the fixed conformation, where a naphthyl ring contributed π-density and prevented racemisation. Pendant ethyl groups assisted in increasing the solubility of the catalyst. *tert*-Amyl alcohol was found to be the best solvent when acylating secondary aryl alcohols with anhydrides. Using these conditions, **66** provided *s*-factors of up to 116. Modelling studies showed π-stacking of the aryl substrate and catalyst, with minimization of steric interference between the DMAP methyl and electrophile, which both contributed greatly to the selectivity.

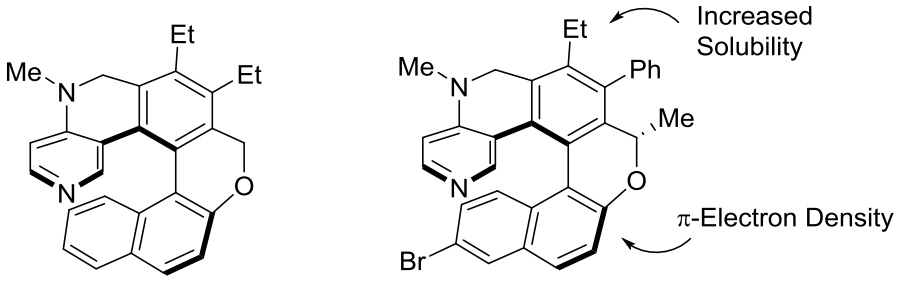

Figure 12. First and second generation of HeAP.

The 2nd generation of helical aminopyridine (HeAP, **67**) was later developed.[75] Synthesis of the 1st generation required unstable intermediates, as well as resolution of the racemic material by HPLC. The catalyst was further improved by incorporating a bromide on the naphthalene unit, which solved the issue of unstable intermediates and also allowed the capability of later functionalization of the catalyst. The new synthesis was resolution free and scaleable. The 2nd generation HeAP was used to acylate 1-naphthylethanol to ensure reactivity and selectivity were retained. An *s*-factor of 33 was achieved for the alcohol, the same value acquired for the 1st generation, thus demonstrating properties were retained. It was proposed to use this HeAP catalyst for the KR of amines.

1.6. Photochemistry of Ketoaziridines

Ketoaziridines readily undergo photochemical processes, as described by Padwa. These changes involve 1,5-hydrogen atom shifts, azomethine ylide formation through ring-opening, and cleavage of C-N bonds resulting in deamination. In 1966, Padwa and Hamilton reported on the photodeamination of 2-benzoylaziridines (Scheme 41).[76] A 450 Watt mercury lamp was used, in conjunction with a Pyrex filter to remove wavelengths below 280 nm, to irradiate **68** for 3 hours in 95% ethanol. This reaction yielded three products: *trans*-chalcone (**69**), *cis*-chalcone (**70**), and *N*-cyclohexylhydroxylamine (**71**). A possible mechanism to form the olefins was suggested to proceed *via cis-trans* photoisomerisation of the starting aziridine before undergoing deamination. However, when irradiating the *cis*-isomer of **68** in ethanol, **68** was not obtained and only acetophenone and *N*-cyclohexylbenzalimine were observed, thus ruling out the possibility of photoisomerisation. The *cis*-isomer was also found to react more slowly. Padwa and Hamilton suggested the *trans*-isomer underwent an intramolecular hydrogen transfer to form an enol, which then rearranged to generate a carbonyl compound. The formation of *cis* and *trans*-olefins in polar solvent suggested the solvent participated in the isomerisation to form both olefin isomers.

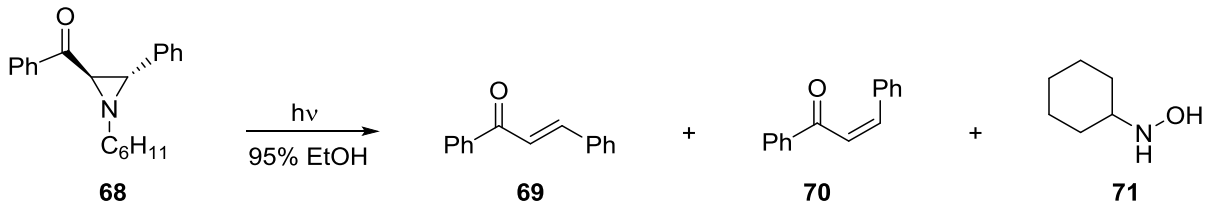

68 **69** **70** **71**

Scheme 41. Photochemical products of *trans*-l-cyclohexyl-2-phenyl-3-benzoylaziridine.

Further photochemical investigations by Padwa took place on *trans-N-tert*-butyl-2-phenyl-3-benzoylaziridine (**72**).[77] Irradiating **72** in pentane using a mercury lamp with a Pyrex filter generated two major products, 2,5-diphenyloxazole (**73**) and (*β-tert*-butylamino)-*trans*-benzalacetophenone (**74**) in 38 and 41% yields, respectively (Scheme 42). Two other minor products were observed as *N-tert*-butylbenzalimine (**75**, 6%) and benzaldehyde (**76**). Formation of 2,5-diphenyloxazole was the result of C-C bond cleavage yielding a 1,3-dipole intermediate, followed by subsequent rearrangement to a 2,3-dihydrooxazole, and oxidation to the oxazole. In order to understand the formation of **74**, deuterium labelling experiments were performed. These led to the conclusion that a 1,5-

hydrogen transfer occurred prior to ring-opening for the *trans*-isomer. This conclusion was further supported by reaction of the *cis*-isomer of **72**, where oxazole was the main product (51%) and **74** was not isolated, as ring-opening and closing to the 5-membered ring was able to occur without hydrogen transfer taking place.

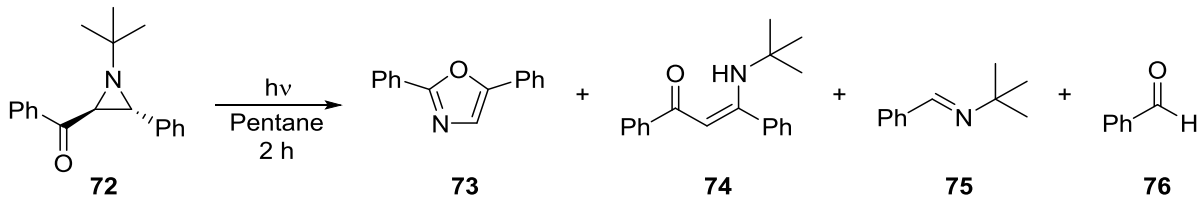

72 **73** **74** **75** **76**

Scheme 42. Photochemical reaction of **72** by Padwa.

Previous reports by Padwa claimed *NH*-ketoaziridine (**77**) was photochemically unreactive.[76] The lack of reactivity was proposed to be due to the H-bonding between the carbonyl oxygen and the hydrogen on the nitrogen. This affected the energy levels of the excited state, preventing the formation of oxazole from occurring when **77** was irradiated. Thus, there was no "direct route" to 2,5-diphenyloxazole, as stated by Padwa.[76]

George studied the substituent effect on ring-opening of aziridines through their photooxygenations.[78] Aziridines in benzene were irradiated with a 450 Watt medium pressure mercury lamp in the presence of Rose Bengal, in order to generate singlet from triplet oxygen, while oxygen gas was bubbled through the system (Scheme 43). Irradiation of *trans*-2-phenyl-3-benzoylaziridine (**77**) formed an azomethine ylide which then added to the singlet oxygen to form a five-membered ring, followed by formation of a diradical intermediate. This species then rearranged to form two products, benzoic acid and benzamide.

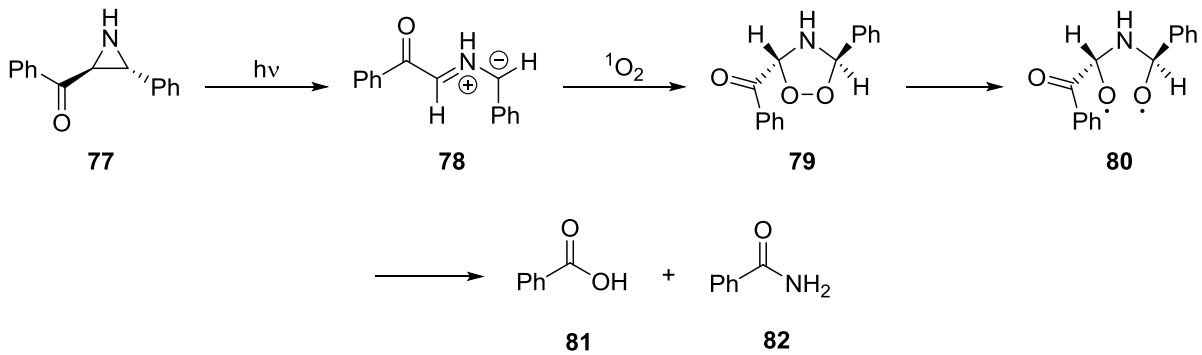

77 **78** **79** **80** **81** **82**

Scheme 43. Photooxygenation of **77** by George.

The influence of *N*-substitution on the photochemical behaviour of diphenylaziridines was studied by Hammer (Figure 13).[79] Aziridines were irradiated at 253.7 nm in cyclohexane, diethyl ether, and acetonitrile. Hammer found that when the nitrogen was substituted with a cyano group (**83**), the *trans*-diphenyl aziridine readily isomerised to the *cis*-isomer and then rearranged to form (*E*)-*N*-(1,2-diphenylethylidene)cyanamide. The yield of this product was also increased with increasing solvent polarity. When altering the *N*-substitution to ethoxy methanone (**84**), irradiation led solely to isomerisation. A mixture of 10 and 90% *trans*- and *cis*-isomers was generated, independent of solvent and the isomer used. Decreasing the electronegativity of the substituent to an *N*,*N*-dimethylformamide (**85**) also allowed for photo-induced isomerisation, as well as fragmentation, resulting in isolation of 3-benzyl-1,1-dimethylurea.

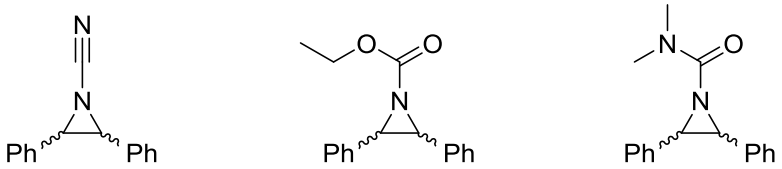

83 **84** **85**

Figure 13. Diphenylaziridines used by Hammer to study the photochemical effects of *N*-substituents.

Previous work by Trozzolo *et al*. in 1979 studied the photochromism of *N*-benzyl substituted aziridines, as shown in Figure 14.[80] These investigations demonstrated phenyl- or benzoyl-substituents on the aziridine ring were required for photochromism. Their presence resulted in a colour change upon flash photolysis when in either solid-state or glassy solution. This reversible colour change was due to the formation of an azomethine ylide. Addition of electron-withdrawing or electron-donating groups to the aryl rings aided stabilisation of the azomethine ylide, allowing the colour change to persist longer and the ability to withstand higher temperatures. Use of methoxy- or nitro-substituents in the *para* position on the aryl rings caused a red-shift in the absorption spectra. Once photolysed, the aziridine displayed a λ_{max} of 475 nm in ethanol at 77 K. When substituting the phenyl ring with a nitro-group, and the benzoyl group with a methoxy-substituent, the result was a blue colour following photolysis and a λ_{max} of 600 nm (**87**). When interchanging the nitro- and methoxy-groups, a red colour was obtained with a λ_{max} of 490 and 540 nm (**88**).

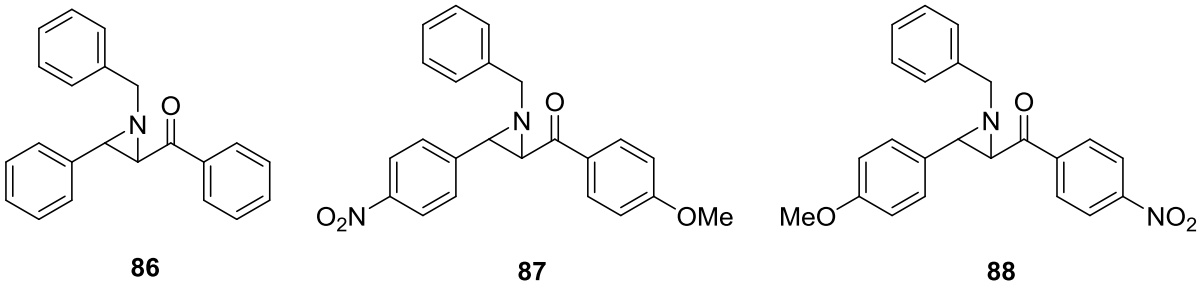

86 **87** **88**

Figure 14. Aziridines used in the photochomism study by Trozzolo *et al*.

George was also heavily involved in the investigation of ketoaziridines and their photochemistry. In 1986 a study was published involving the photochemical behaviour of 2-aryl-3-benzoylaziridines and 2,3-benzoylaziridines in solution, where flash lamp and laser photolysis were utilised (Figure 15).[81] Formation of azomethine ylides for these aziridines was monitored through low temperature photolysis at 77 K in ether-*iso*pentane-ethanol (EPA) glass. As observed by Trozzolo, George also noticed a colour change (pink to orange) upon irradiation attributable to the azomethine ylide, which dissipated when melting the glass. Compound **77** did not show any colour change. Steady-state irradiation at 315 nm revealed a slight red-shift for the absorption of the ylide generated from *trans*-isomer **89a** (494 nm) in relation to the *cis*-**89b** (490 nm). However, the opposite trend was noticed for the dibenzoylaziridines where the *trans*-**90a** (484 nm) was blue-shifted when irradiated at 366 nm, relative to its *cis*-isomer **90b** (492 nm) irradiated at 335 nm. When **77** was irradiated at 335 nm, a band system was observed between 300 to 400 nm with a λ_{max} of 368 nm. This azomethine ylide differed in that it was described as a "permanent photoproduct" by George, as melting and re-cooling the EPA glass did not affect the absorption band.

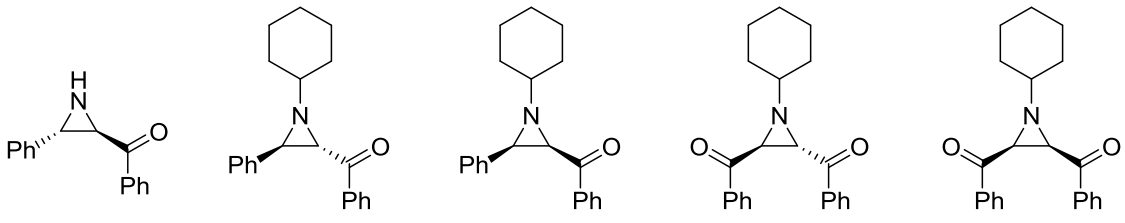

77 **89a** **89b** **90a** **90b**

Figure 15. 2-Aryl-3-benzoyl- and 2,3-dibenzoylaziridines studied by George.

Further studies on the substrates were performed using laser flash photolysis at 337.1 nm. Compounds **89a** and **89b** were irradiated in benzene and the absorbances were measured. These revealed a broad absorbance maxima from 470-475 nm with decays

ranging from 1.5-3.5 μs. George also attributed these absorbance bands to azomethine ylides due to their similar spectral features with those seen during steady-state photolysis. When continually pulsing the laser to allow for longer irradiation of **89a** in deoxygenated benzene, development of a species with a λ_{max} of ~350 nm was formed as a photoproduct. Irradiation of **90a** and **90b** revealed a transient species with a λ_{max} of 480 nm, which decayed only 15 to 30% over 150 μs. An additional species was seen at 360-400 nm with a shorter lifetime than the major species at 480 nm. Additional quenching studies with trifluoroacetic acid were performed and revealed a difference in reactivity between **89a** and **89b**, with the former reacting 4 to 6 times more slowly. For the dibenzoylaziridines, *cis*-**90b** was less reactive than **90a**. The difference in reactivity between the two isomers for both the 2-aryl-3-benzoyl and 2,3-dibenzoylaziridines indicated the ylides formed differed in structure.

The azomethine ylides were thought to be generated from C-C bond scission of the aziridine ring. Due to the lack of differences in the spectra, it was not possible to distinguish between the structural differences in the azomethine ylides derived from each isomer of **89a,b** and **90a,b**. Decay of the ylides was thought to be thermal in nature, where they were either: converted to the other isomer of the parent aziridine through conrotatory ring closure (**I**), formed oxazolines through cyclisation (**II**), or formed a ketocarbene and Schiff base through fragmentation (**III**). George proposed the 1,4-migration of the *N*-substituent to the oxygen of the carbonyl, a 1,4-diphenylbutadiene derivative (**IV**), as the source of the absorbance featured observed from 320-360 nm (Figure 16).[81]

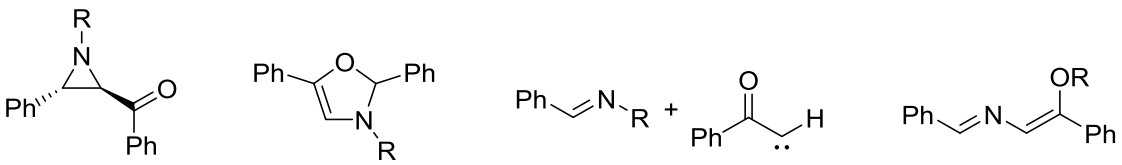

Figure 16. Potential ylide decay products proposed by George.

In the laser flash photolysis of **77** in benzene, a strong absorbance was measured with a λ_{max} of 360 nm. It was said to not decay over 150 μs, leading George to refer to this absorbance as a "permanent photoproduct." An additional shoulder was also observed from 400-500 nm. Following a single laser pulse on the sample, rapid growth of the 360 nm species was observed simultaneously with decay of a species at 450-550 nm. The ylide

formed from the irradiation of **77** was considered to be a minor product contributing to the shoulder seen at higher wavelengths. This ylide may then undergo a 1,4-proton transfer to form photoenol (**92**), attributed to the "permanent product" (Figure 17). The major route to **92** was suggested to be due to the proton transfer occurring in the triplet state of a biradical formed by irradiation (**93**), followed by ring-opening. Confirmation of a long-lived biradical species was confirmed through its oxidation by paraquat (4,4´-dimethylbipyridiniumdication, PQ^{2+}).

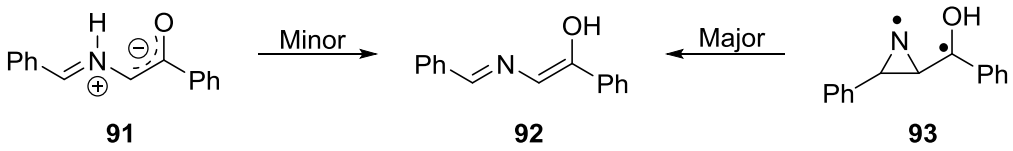

Figure 17. Formation of photoenol **92** through ylide (**91**) and biradical (**93**) pathways.

George continued his studies on *N*-benzoyl aziridines, where it was found that the benzoyl group on the nitrogen was initially photoexcited, as it was farthest away from the C-C bond in the aziridine ring.[82] Aziridines **94a-c** underwent steady state photolysis at 300 nm on 2-methyltetrahydrofuran (MTHF) glass at 77 K (Figure 18). All three aziridines generated yellow coloured azomethine ylides upon irradiation with λ_{max}'s of 484 (**94a**), 450 (**94b**), and 412 (**94c**) nm. As seen in George's previous work, **94a** was considerably red-shifted in comparison with **94b**, indicating the two isomers generate geometrically different ylides.

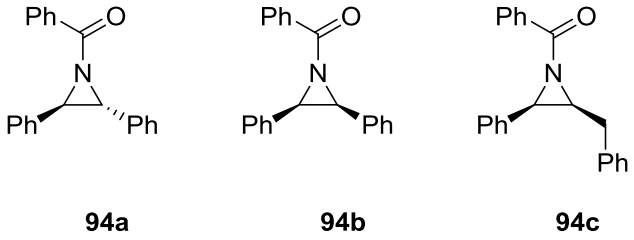

Figure 18. *N*-Benzoylaziridines studied by George.

Laser photolysis studies at 308 nm were also performed on **94a-c** in nonpolar aromatic and polar solvents; methanol and acetonitrile. The species observed at 440 and 610 nm decayed more rapidly in the polar solvents, 20 μs *vs*. 4.8 to 6 sμ. The wavelengths were assigned to the azomethine ylide, thus the shorter lifetimes may be the result of solvent interaction/trapping by the ylide. Trapping studies with dimethylacetylenedicarboxylate (DMAD) further confirmed the generation of azomethine

ylides as a pyrroline derivative was formed by **94b**. The transient absorbances observed at 440 and 610 nm for **94a** and **94b**, and those at 400 and 580 nm for **94c**, were assigned as biradical species due to C-N cleavage. Spectral features were lacking in similarity between **94a,b** and **94c**, suggesting they did not form similar species. Structural differences must also be present between **94a** and **94b**, as their reactions in trifluoroacetic acid (TFA) quenching studies were not identical.

These studies revealed similar behaviour to *C*-benzoylaziridines, as they also underwent C-N and C-C bond cleavages. Breaking of the C-N bond yielded biradicals, while C-C bond scission resulted in formation of the azomethine ylide. *N*-Benzoylaziridine derived azomethine ylides also displayed peak maxima within 400-500 nm in solid and solution states. However, the additional maxima observed between 580 and 610 nm was less strongly observed in the lower temperature studies. Ylides from both classes also exhibited slow reactivity with DMAD.

George continued his studies in 1996 with steady-state irradiations of the model aziridines using a Hanovia 450 W medium-pressure mercury lamp under steady-state conditions.[83] *Trans*-1-cyclohexyl-2,3-dibenzoylaziridine (**95a**), *cis*-1-cyclohexyl-2,3-dibenzoylaziridine (**95b**), *trans*-1-benzyl-2,3-dibenzoylaziridine (**95**c), and *trans*-2-phenyl-3-benzolyaziridine (**77**) were investigated. It was found that **95a**, and **95b**, both generated (*Z*)-1-(cyclohexylamino)-1,2-dibenzolyethylene after 4 and 4.5 hours of irradiation in benzene, respectively, in addition to starting material. However, when irradiating **95** for 4 hours in benzene, (*Z*)-1-(benzylamino)-1,2-dibenzoylethylene (**98**) was obtained as the major product, with small amounts of benzaldehyde (**76**) and *trans*-1,2-dibenzoylethylene (**100**). A significant difference was observed when irradiating **77**, as a mixture of products were obtained: benzaldehyde (**76**), dihydropyrazine (**106**), benzamide (**82**), acetophenone (**103**), dibenzoyl-3,6-diphenylpyrazine (**107**), 2,5-diphenylpyrazine (**110**), and staring material.

Mechanisms for the formations of these products were also proposed by George, as shown in Scheme 44. The products yielded by **95a** and **95c** were the result of scission of the C-N bond, caused by radical triplet formation generating a biradical. An intramolecular hydrogen abstraction may then take place and provide dienol (**97**), which then formed product **98**. The same mechanism was proposed for **95c**, where hydrolysis of an intermediate (**99**) resulted in benzaldehyde and *trans*-1,2-dibenzoylethylene.

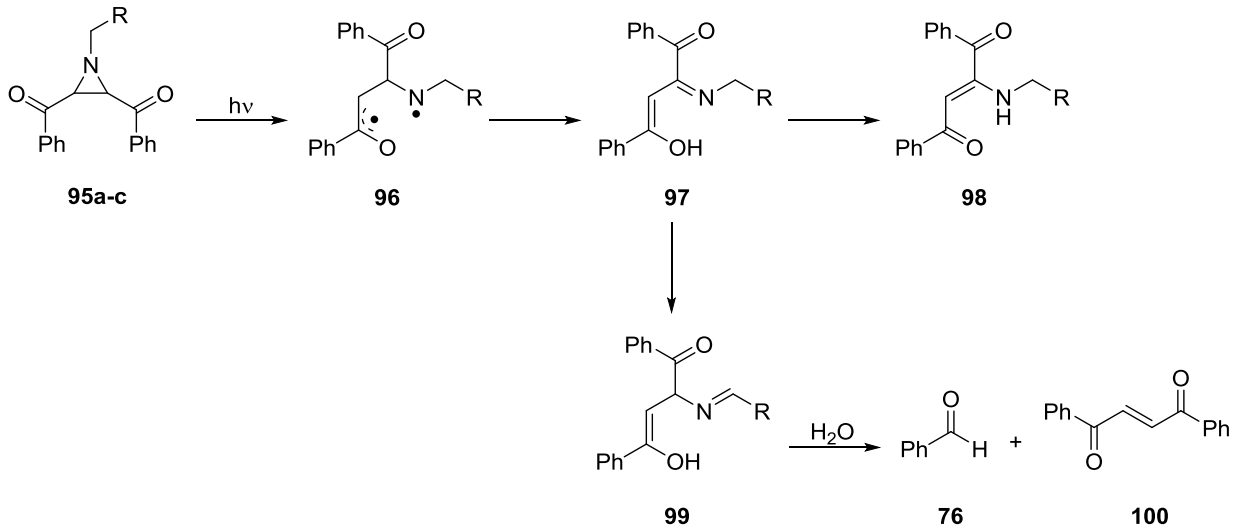

Scheme 44. Mechanistic pathways for steady state irradiation products from 2,3-dibenzoylaziridines.[83]

Two pathways were suggested for the reaction of **77** (Scheme 45). Following irradiation to the excited state, a proton may be removed then undergo a C-N bond scission. This would yield **102**, which may then hydrolyse to form benzamide (**82**) and acetophenone (**103**). Alternatively, ring-opening of **77** led to an azomethine ylide (**104**) resulting in further products from dimerisation of the ylide to form **105** which then forms dihydropyrazine (**106**). Oxidation of **106** through air exposure during work-up would yield pyrazine (**107**). Proton transfer from the nitrogen to the carbonyl formed an enol (**108**) which may then cleave to form benzaldehyde (**76**) and phenacylamine (**109**). The 2,5-diphenylpyrazine (**110**) isolated could be derived from the dimerization of phenacylamine.

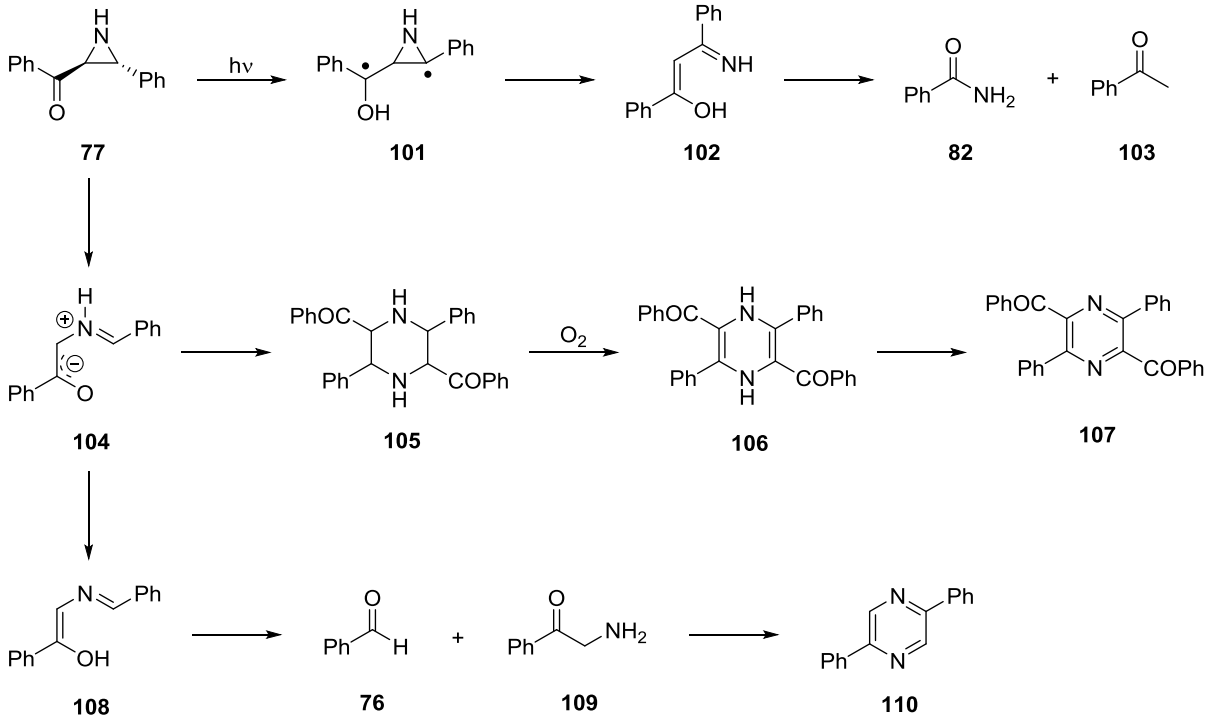

Scheme 45. Mechanism proposed by George on the photochemical products formed from **77** during steady-state irradiation.[83]

Trapping studies with DMAD were also carried out on **94a** and **94b** with their irradiations taking place in acetonitrile. Reactions of both aziridines yielded *cis*-3-pyrroline as major products in 62 and 54% yield, respectively. It was proposed that **94a** first formed the *trans*-3-pyrroline, but may then isomerise to the more thermodynamically stable *cis*-3-pyrroline during work-up involving solvent evaporation and a Florisil column. The formation and amounts isolated of the products supported the hypothesis of azomethine ylide formation during irradiation. The ability to isolate these 3-pyrrolines also suggested photoinduced C-C bond scission.

Huisgen *et al*. also studied the formation of azomethine ylides from *cis*- and *trans*-1-(*p*-methoxyphenyl)aziridine-2,3-dicarboxylates by photolysis in 1971.[84] Both *cis* and *trans*-isomers were irradiated for 5 seconds in dioxane using a medium pressure mercury arc lamp at room temperature. A yellow colour appeared following irradiation, then faded after ~20 seconds. Addition of diethyl fumarate to the coloured solution resulted in an immediate loss of colour. Due to these experiments, it was thought the azomethine ylide caused the yellow colour.

Chapter 2: Kinetic Resolutions of Aziridines

Table of Contents

2.1. Kinetic Resolutions

Due to the nitrogen atoms of aziridines having more sp^2 character and the adjacent electron-withdrawing carbonyl, the nucleophilicity of the nitrogen centre would be reduced. These combined properties led to the selection of aziridines as promising substrates for the KR of amines, which was the initial focus of this project. As previous work on the KR of 2° alcohols was successful using a helical DMAP based catalyst developed by Carbery, reaction conditions were in place to begin studying the resolution of aziridines.[74]

2.2. Selectivity and *ee* Determination

In kinetic resolutions enantiomers react at different rates when interacting with a chiral catalyst. This is the result of two diastereomeric transition states. The free energies of these transition states define the rate constants for conversion, k_{fast} for the fast reacting enantiomer and k_{slow} for the slow reacting enantiomer. The ratio of k_{fast} / k_{slow} is equal to selectivity (*s*).[85]

$$C = \frac{ee}{ee + ee'}100 \qquad S = \frac{k_{fast}}{k_{slow}} = \frac{In[(1-C)(1-ee)]}{In[(1-C)(1+ee)]}$$

ee = enantiomeric excess measured for the starting material

ee'= enantiomeric excess measured for the product

C = conversion

Equation 1. Calculation of *s* based on the ratio of k_{fast} / k_{slow}.

Conversion (*C*) must first be determined to obtain the *s*-factor. This may be calculated from the *ee* values of recovered starting material and product when the reaction is 1st order. Using the above equation (Equation 1), the values may be substituted for the variables. The threshold for a synthetically useful reaction has a selectivity of 10 or above, which is the result of 62% conversion where the unreacted starting material has an *ee* above 90%.[66]

2.3. Aziridine Synthesis

In order to access the aziridine substrate, an iodoaminomorpholine salt **112** was first synthesised. Morpholin-4-amine was methylated with iodomethane to acquire the desired crystalline solid. Following recrystallization, the salt was isolated in 92% yield (Scheme 47). It was then carried on to form the aziridine.

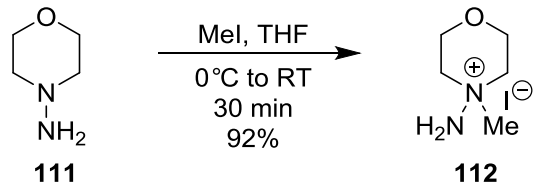

Scheme 47. Synthesis of 4-amino-4-methylmorpholin-4-ium iodide.

Trans-chalcone (**69**) was reacted with **112** and *t*-BuOK to yield **77** in 83% yield (Scheme 48). These reaction conditions were taken from the method developed by Armstrong and Carbery.[41] This procedure stated a reaction time of 10 minutes; however, it was found that extending the reaction time to 45 minutes yielded more product. No additional modifications were made, as the reaction consistently produced product in good yield, and was chosen to make the aziridine substrates.

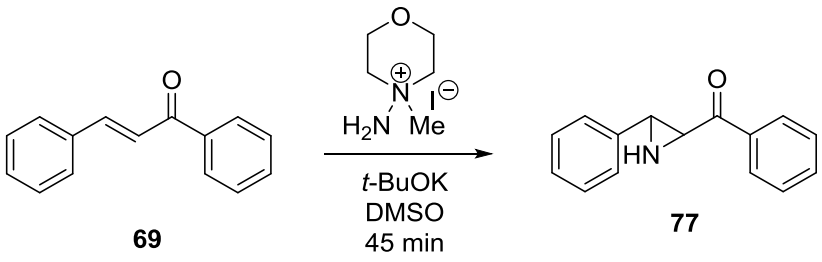

Scheme 48. Synthesis of phenyl(3-phenylaziridin-2-yl)methanone (**77**).

2.4. Aziridine Reactions with HeAP

Initial studies were attempted utilising the previous successful conditions for the KR of 2° alcohols using HeAP.[74] Initial conditions required 0.5 mol% catalyst loading, triethylamine (0.75 eq.), and isobutyric anhydride (0.75 eq.) in *t*-amyl alcohol at 0 °C. A noticeable reduction in reactivity for the aziridines was demonstrated, as only 25% conversion was observed by HPLC after 47 hours. Following this observation, attempts to optimise the reaction conditions were made.

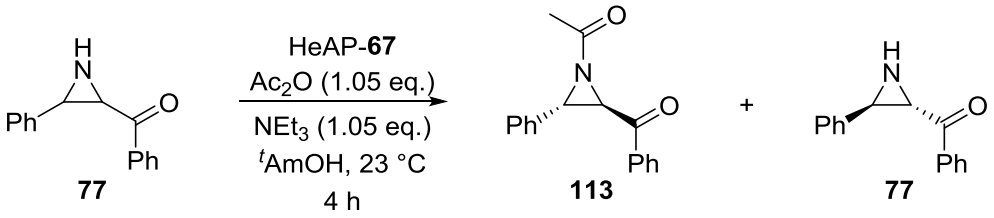

Scheme 49. General acylation scheme for **77** using Ac_2O.

Catalyst loading was the first variable studied in the acylation of **77** (Table 1). A slight increase in *s*-factor to 1.3 from 1.1 was observed when increasing the amount of catalyst from 0.5 mol% to 5 mol%. Observable *ee*'s for the acylated and starting material were also noted; however, reducing the catalyst loading below 2 mol% also lowered *ee*. This data suggested 2 mol% was the optimal catalyst loading. It was also noted that the highest conversion was observed at the lowest catalyst loading of 0.5 mol%, which was potentially indicative of a background reaction taking place.

Table 1. Effects of catalyst loading on the acylation of **77** with acetic anhydride.

HeAP (mol %)	**C (%)**	**113 *ee* (%)**	**77 *ee* (%)**	***S***
0.5	66	3.0	5.2	1.1
1	57	1.4	3.5	1.1
2	36	6.4	11.5	1.2
5	31	4.8	10.3	1.3

*Reaction conditions used as shown in Scheme 49. Conversion was calculated based on *ee*.

Temperature was also taken into account. Using a 1:1 mixture of *t*-amyl alcohol and DCM, a reaction containing aziridine (1.0 eq.), triethylamine (1.0 eq.), and HeAP (2 mol%) was cooled to -48 °C. Acetic anhydride (1.0 eq.) was added to this solution and the

reaction was left to stir 4 hours. *Ee*'s of 3% and 12% were obtained for **113** and starting **77**, respectively, reaching a conversion of 7.4% and *s* = 2.6.

To determine the impact of a potential background reaction, the acylation was run altering two variables (Table 2). One reaction removed HeAP, while triethylamine was removed from the other, leaving the remaining conditions unchanged. When removing triethylamine from the reaction, the conversion decreased to 31% while the *ee* of **113** showed an increase with a negligible change in selectivity. Removal of HeAP decreased the selectivity and *ee*'s significantly, as expected. While a minimal amount of selectivity and *ee* were observed in the initial experiments, this study demonstrated that HeAP did affect selectivity and *ee*, thus conditions required optimisation for further improvement. Having discovered the reaction did not require triethylamine, subsequent reactions were run without base.

Table 2. Effects of catalyst and triethylamine on the acylation of **77** with acetic anhydride.

HeAP (mol %)	**Ac_2O (Eq.)**	**NEt_3 (Eq.)**	**C (%)**	**113 *ee* (%)**	**77 *ee* (%)**	***S***
2	1.05	1.05	36	6.4	11.5	1.2
2	1.0	--	31	12.2	9.1	1.3
-	1.0	1.0	41	--	--	--

*Reaction conditions modified from those shown in Scheme 49. Conversion was calculated based on *ee*.

Acylation was then attempted using higher loadings of catalyst. HeAP (0.5 eq.) and acetic anhydride (0.5 eq.) were stirred in *t*-amyl alcohol for 1 hour. A solution of aziridine in *t*-amyl alcohol was then added and the reaction was left to stir at 23 °C for 4 hours. As anticipated, selectivity increased to 8.7 with a product *ee* of 48% and 41% conversion. While the highest selectivity and *ee* values were observed, the catalyst loading was deemed too demanding for it to be a viable option.

Sterically hindered anhydrides were used to determine if enhanced selectivity was achievable. Anhydrides (1 eq.) were reacted with **77** over 4 hours. Isobutyric anhydride demonstrated a slight improvement for the *ee* of the acylated product, however, a 10% decrease in conversion was also measured. While the standard equation to determine *s*-factors is based on the conversion obtained from *ee* values, this equation assumes the reaction is 1st order. An *s*-factor was unable to be calculated for this reaction, as a negative value was obtained. This observation suggested the reaction was not 1st order with respect

to the nucleophile being resolved. It was proposed that the reaction in general may not be 1st order, therefore any *s*-factors obtained were not true values. Benzoic anhydride was also used for acylation, but did not yield product (Table 3).

Table 3. Acylation of aziridine with varying anhydrides.

Anhydride	**Anhydride (Eq.)**	**C (%)**	**Acylated *ee* (%)**	**77 *ee* (%)**	***S***
Ac_2O	1.0	31.0	12.2	9.1	1.3
$(^{i}PrCO)_2O$	1.0	10.0	13.1	2.7	-
Bz_2O	1.0	-	-	-	-

*Reaction conditions used as shown in Scheme 49, altering the anhydride used. Conversion was calculated based on *ee*.

2.5. Kinetic Studies

2.5.1. HPLC Analysis

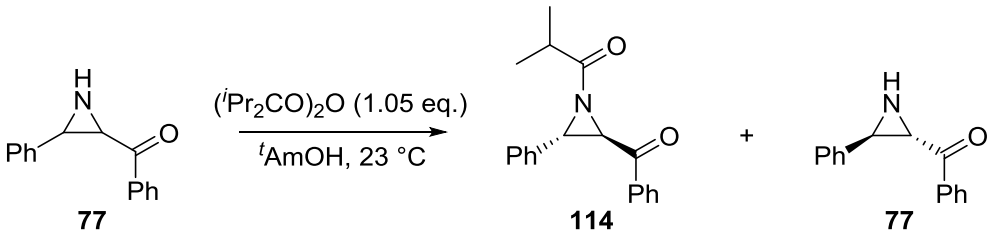

Scheme 50. General reaction scheme for the acylation of **77** with isobutyric anhydride.

Following preliminary acylations taking place over 4 hours, kinetic studies were performed to monitor the rate of conversion. Reactions were run taking 0.1 mL aliquots by syringe, which were then quenched with 1 mL of methanol. The aliquots were then analysed by HPLC using a ChiralPak IA column with 95:5 hexane/isopropanol with a flow rate of 1.5 mL per minute. UV absorbance peak areas were measured at 210 nm. In addition to measuring *ee*'s to obtain *s*-factors, concentrations were calculated. This was accomplished by acquiring a response factor (RF) of the starting material. Known concentrations of starting material or product with naphthalene were injected into the HPLC in triplicate and peak values were used to calculate the RF (Equation 2). Following identification of the response factor, data was converted into concentrations and plotted.

$$RF = \frac{\left(\frac{Product\ Area}{Product\ Concentation}\right)}{\left(\frac{Standard\ Area}{Standard\ Concentration}\right)}$$

Equation 2. Equation used to calculate RF.

As isobutyric anhydride exhibited higher *ee*'s, it was chosen as the standard electrophile for initial acylation studies. For comparison, DMAP (2 mol%) was used as the catalyst and samples were taken at 1, 2, 3, 5, 10, 15, 30, 60, 90, 180, and 240 minutes. Beginning with 0.0453 mmol of aziridine, the reaction reached only 22% conversion after 4 hours when using DMAP. While the increase in acylated material followed a linear progression, the starting material did not decrease to indicate consumption, which was unexpected (Figure 19). As the product increased, a decrease in starting material at a rate similar to product formation should have been observed.

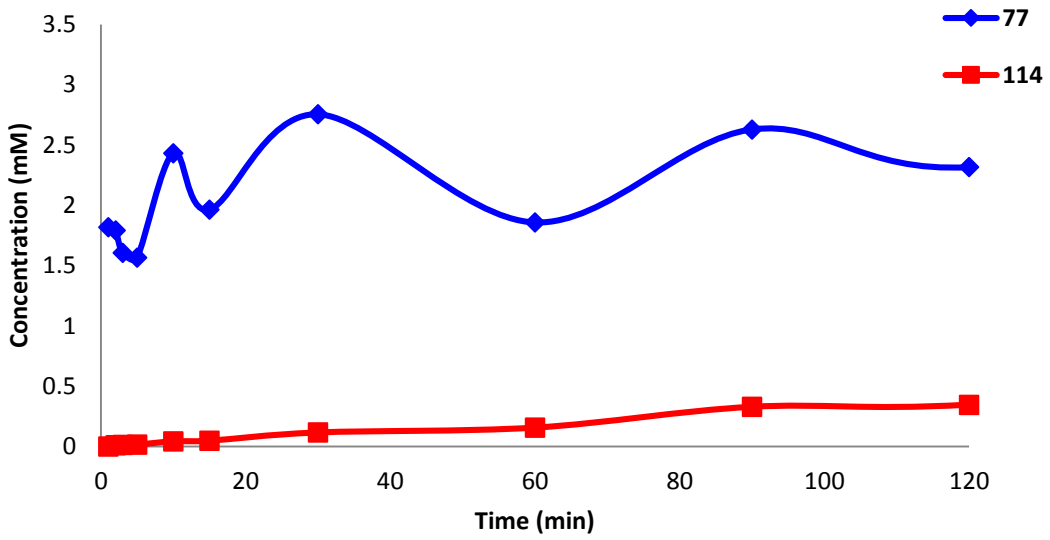

Figure 19. Acylation of 2.5 mM **77** with 1.0 eq. isobutyric anhydride using DMAP.

Selectivity was evaluated by acylating aziridine using 2 mol% HeAP. Following 30 minutes, the reaction showed consumption of starting material, followed by an increase at 60 minutes, then further consumption as the reaction progressed (Figure 20). This was indicative of high reactivity as the starting material concentration dropped 69% within the first 30 minutes of the reaction. As expected, the acylated material increased as the starting material concentration decreased. However, the unexpected decrease in product after its formation and increase in starting material, suggested reaction reversibility.

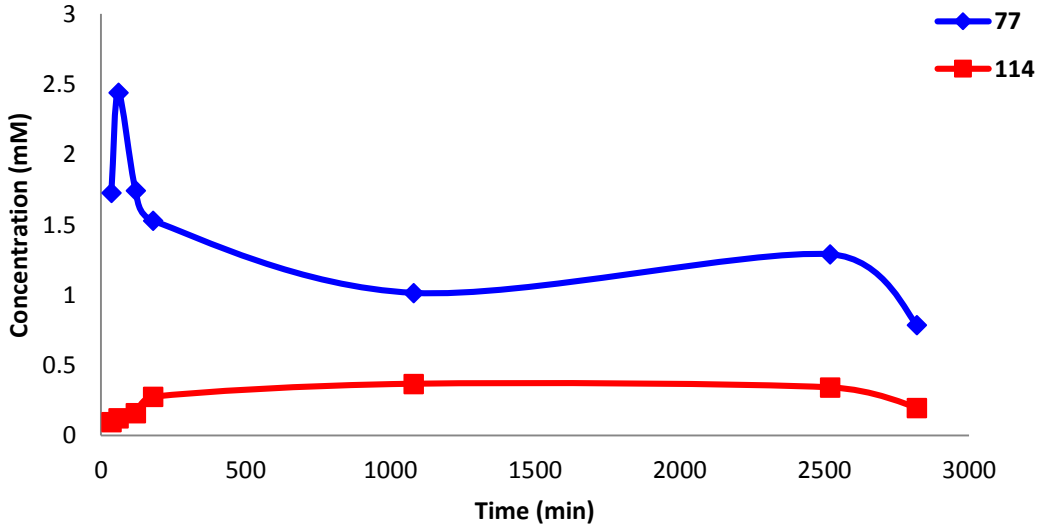

Figure 20. Acylation of 2.5 mM **77** with 1.0 eq. isobutyric anhydride using HeAP.

In addition to the concentration of starting material fluctuating by vast amounts, a similar observation was made with respect to *ee* (Table 4). *E*e was observed within the first minute of the reaction at 46%. This number continued to vary between 36 and 48% for 90 minutes, but later fell to 16% after 120 minutes. At 240 minutes, the value then increased to 48%. This variation was consistently observed with isobutyric anhydride acylations using HeAP. While aziridines demonstrated *ee*, their unforeseen reactivity resulted in refocusing efforts to discover the influence on the odd behaviours observed.

Table 4. HPLC measured *ee* of **77** acylated with isobutyric anhydride at room temperature.

Time (min)	114 *ee* (%)
1	46
2	36
5	40
10	41
15	43
30	43
60	42
90	48
120	16
240	48
1470	50

The possibility of a background reaction was explored by running a reaction without catalyst and acylating with acetic anhydride, as no selectivity was expected. Acylating in the presence of triethylamine yielded a different result from the reactions involving catalysts (Figure 21). Starting material and acylated product both showed a steady increase prior to a plateau, which then continued to increase. This behaviour was unexpected as an increase in product should result in a decrease in starting material. As both starting material and product demonstrated increases, the next variable was to omit the triethylamine and to determine its effect on the reaction.

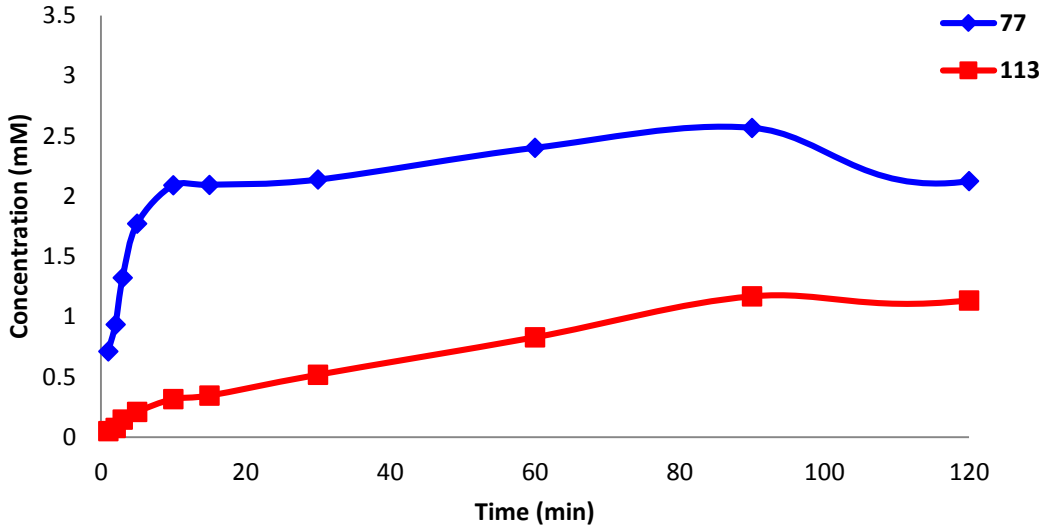

Figure 21. Acylation of 2.5 mM **77** with acetic anhydride in the presence of triethylamine.

The next study involved reacting aziridine and anhydride in *t*-amyl alcohol while monitoring conversion. It was discovered that base was not required for the acylation of **77** with acetic and isobutyric anhydrides. Initial reaction conversions were monitored by ^{1}H NMR. Acylation with acetic anhydride was found to reach full conversion after 6 days, while acylation with isobutyric anhydride reached approximately 86% after 4 days.

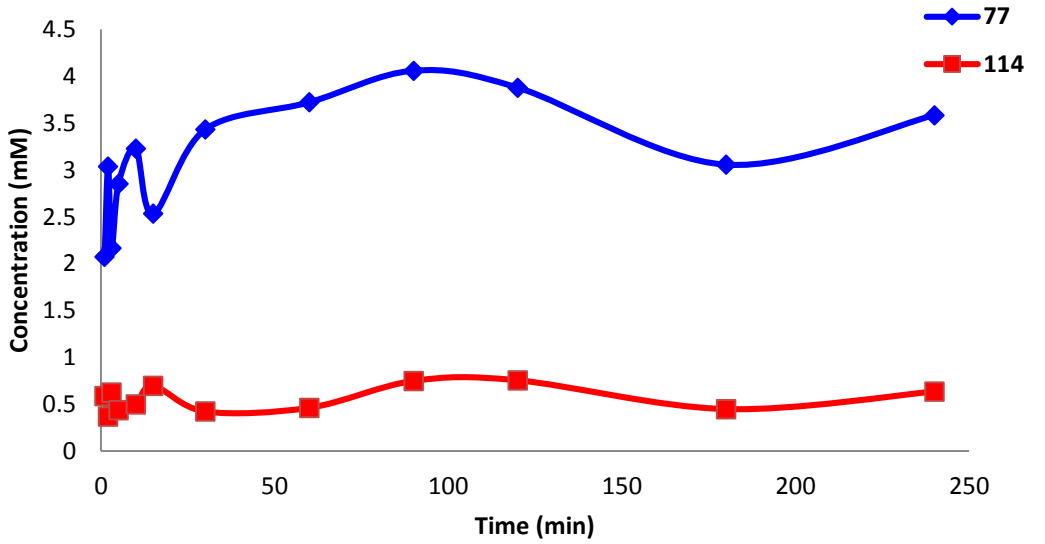

Figure 22. Acylation of 2.5 mM **77** with isobutyric anhydride, without base or catalyst.

Following the same HPLC sampling protocol, the reaction dynamics were further explored through acylation of **77** with isobutyric anhydride. The product and starting

material continued to fluctuate in concentration, showing an increase in product with a decrease in **77** and vice versa, indicating reaction reversibility. This was observed over the course of the reaction from 1 to 240 minutes (Figure 22). While this was somewhat seen in the reactions with HeAP, the behaviour was more well-defined when base and catalyst were not present.

Reactions with acetic anhydride were further investigated through more frequent sampling. Aliquots were taken at 1, 2, 3, 5, 10, 15, 30, 60, and 90 minutes. The results from this reaction revealed multiple fluctuations where the starting material increased while the product decreased, and vice versa (Figure 23). This behaviour mimicked that observed with isobutyric anhydride; however, the fluctuations were more pronounced when acylating with the simpler anhydride. As this behaviour was unexpected, it warranted further investigation.

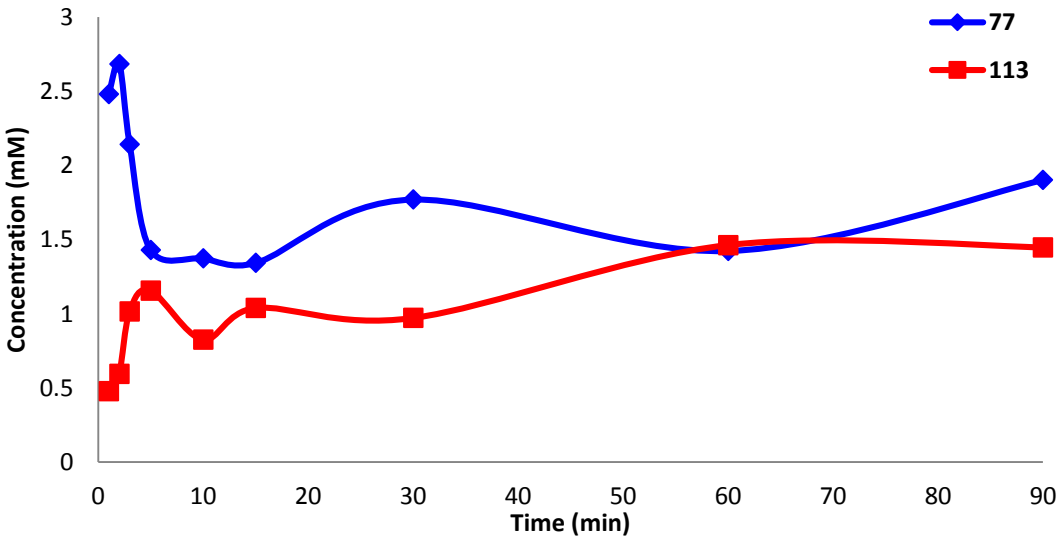

Figure 23. Acylation of 2.5 mM **77** with acetic anhydride.

The acylation mechanism taking place in this study, shown in Scheme 51 occurs through the nitrogen lone pairs attacking the carbonyl on the anhydride creating the carbon-nitrogen bond. Collapse of the negative charge eliminates the acetate ion, which then removes the proton from the nitrogen to yield the acylated aziridine.

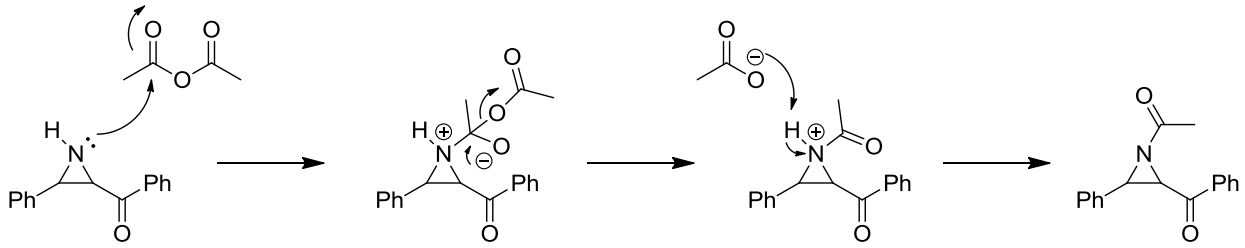

Scheme 51. Proposed reaction mechanism for the acylation of aziridine with acetic anhydride.

As increased sampling appeared to affect the fluctuations, the next area to explore was the effect of sampling. In order to determine if sampling frequency increased the fluctuations observed, samples were taken every 15 seconds during the first 10 minutes of the reaction. These samples were analysed using a Zorbax Eclipse XDB-CN column and UV absorbance data was measured at 230 nm. Due to *ee* no longer being the focus of the investigation, the cyano column allowed for decreased analysis times. Samples were run in 95:5 hexane/isopropanol, with a flow rate of 1.0 mL per minute.

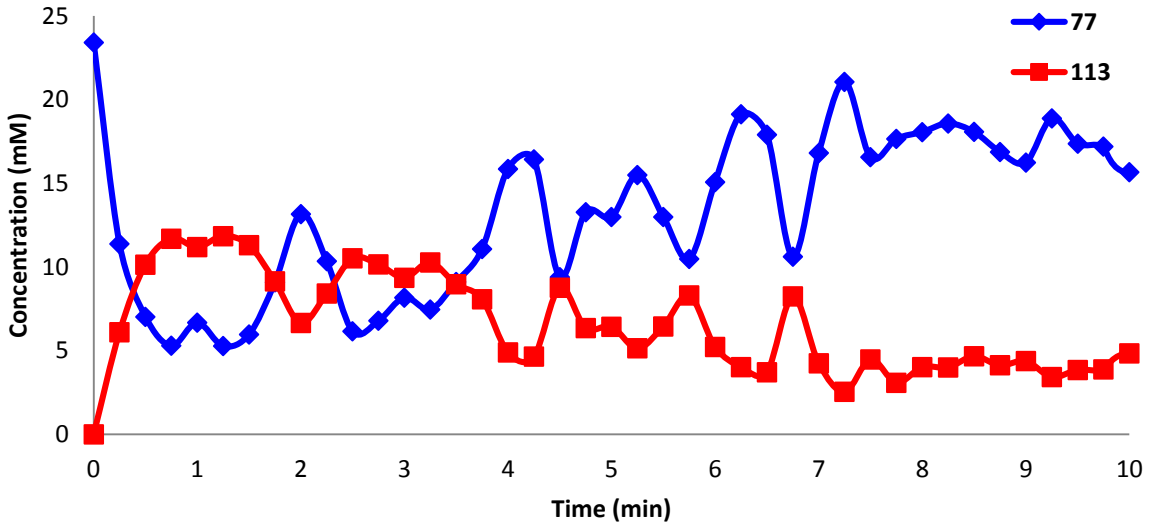

Figure 24. Acylation of 23.4 mM **77** with acetic anhydride over 10 minutes.

HPLC analysis revealed that increasing the sampling frequency did impact the fluctuations observed in the reaction. As shown in Figure 24, the mirroring between starting material and product was still seen, with more fluctuations present due to increased sampling. At 15 seconds, a dramatic decrease was measured in the concentration of the starting material, indicating the high reactivity of the aziridine. The product continued to

vary in concentration, in accordance with the starting material. Additionally, it was noticed that the concentration of the acylated and starting materials did not combine to yield the starting concentration of **77**, indicating an additional product may be present.

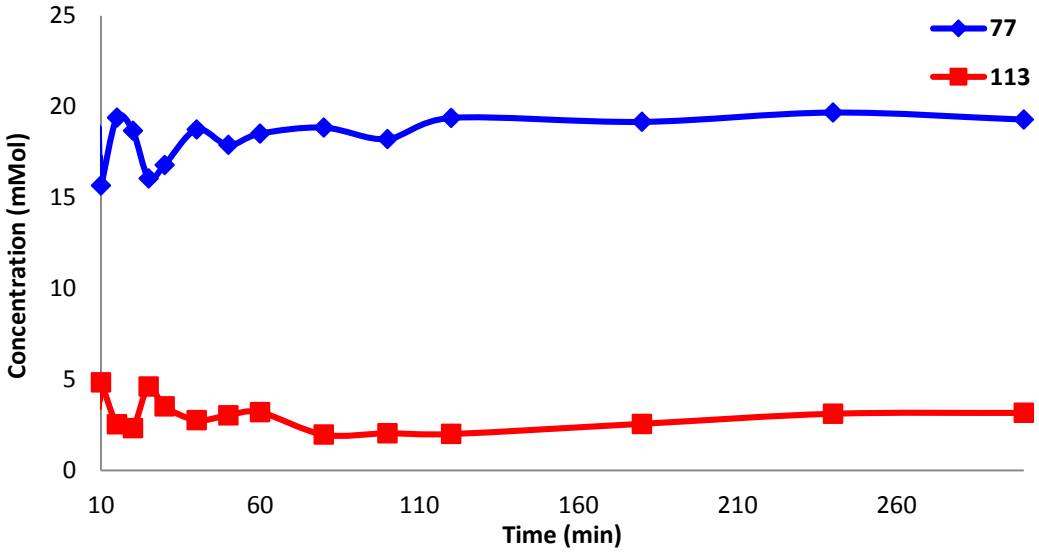

Figure 25. Expansion of Figure 24 showing 10 to 360 minutes.

The trend was still detected when monitoring the reaction from 10 to 360 minutes. However, as the reaction progressed the variations dampened over time. As previous reactions suggested reversibility, a plausible mechanism involved the acylation and deacylation of the aziridine, which may be in part contributing to the observed variations (Scheme 52).[1]

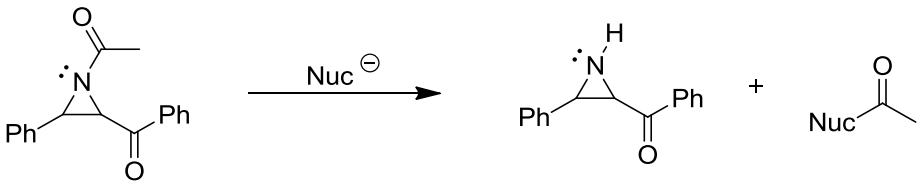

Scheme 52. Deacylation of aziridine.[1]

The possibility of an oscillating reaction taking place was considered due to the observed fluctuations. In order for a chemical oscillation to occur, the temporary changes in state are separate from thermodynamic equilibrium; multiple kinetic variables take part in the process, they affect the rates of change for each other in spite of being set as independent; and they are non-linear kinetically, containing self-catalysed and self-inhibited mechanisms.[86] As demonstrated, the reactions do not reach a state of equilibrium

and are in a constant state of flux. Both starting material and product are linked with regards to concentration and the reactions are non-linear when studying the kinetics. Additional HPLC experiments, as shown in Figure 26, demonstrate reproducibility of this general fluctuating behaviour with symmetry between **77** and **113**.

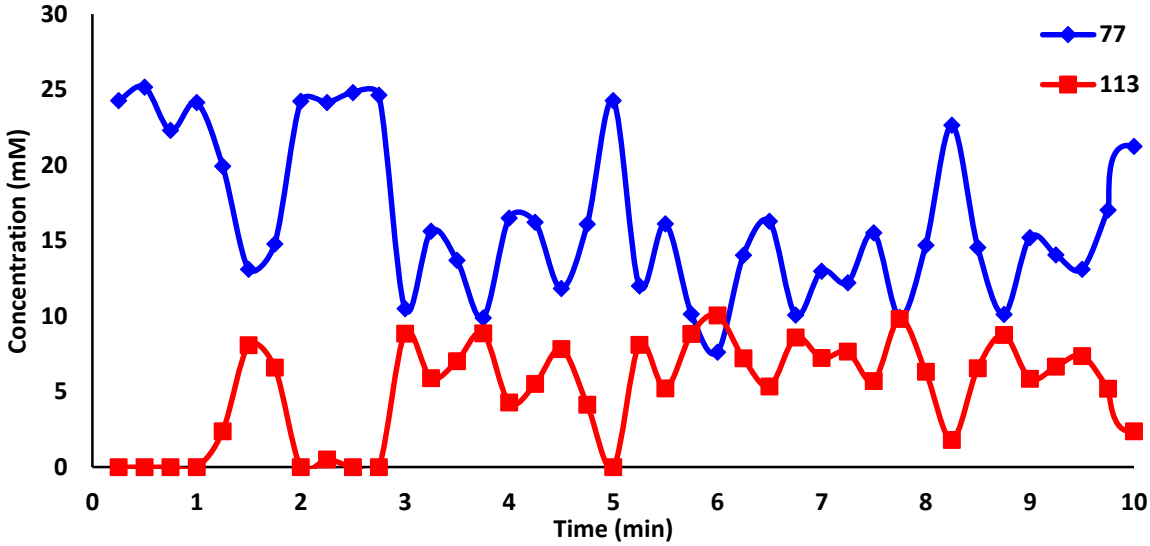

Figure 26. Additional acylation experiments of 23.4 mM **77** with acetic anhydride over 10 minutes.

Additional experiments were performed to measure the effects of the acyl donor and the solvent polarity on the observed fluctuations. Acetyl chloride was used as the electrophile under the previous reaction conditions. This reaction verified the oscillations were independent of the acyl donor, with a faster progression towards equilibrium over 10 minutes. Changing the solvent to ones with a hydroxylic component, such as water and methanol, also demonstrated complex behaviour.

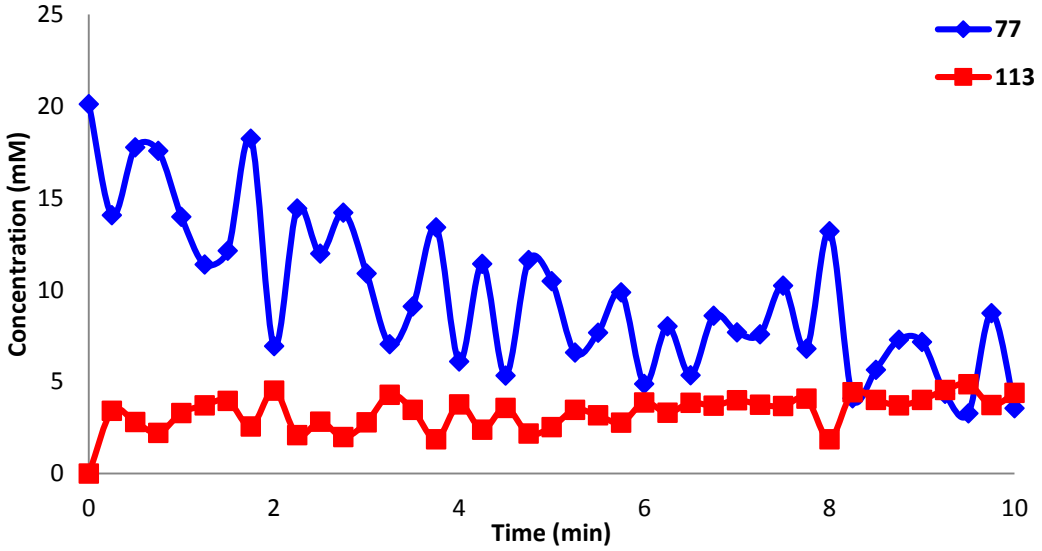

Figure 27. Acylation of **77** using acetyl chloride with reaction monitoring over 10 minutes.

While fluctuations were pronounced in water (Figure 28), the starting material was not fully soluble, which may account for the concentration of aziridine being greater than the zero time point. As the starting aziridine was insoluble, it is possible the acylated material may also be insoluble in water, reducing the observed oscillations. Methanol, which was initially used to quench the reaction during the initial studies, still demonstrated oscillatory behaviour when used as the reaction solvent (Figure 29).

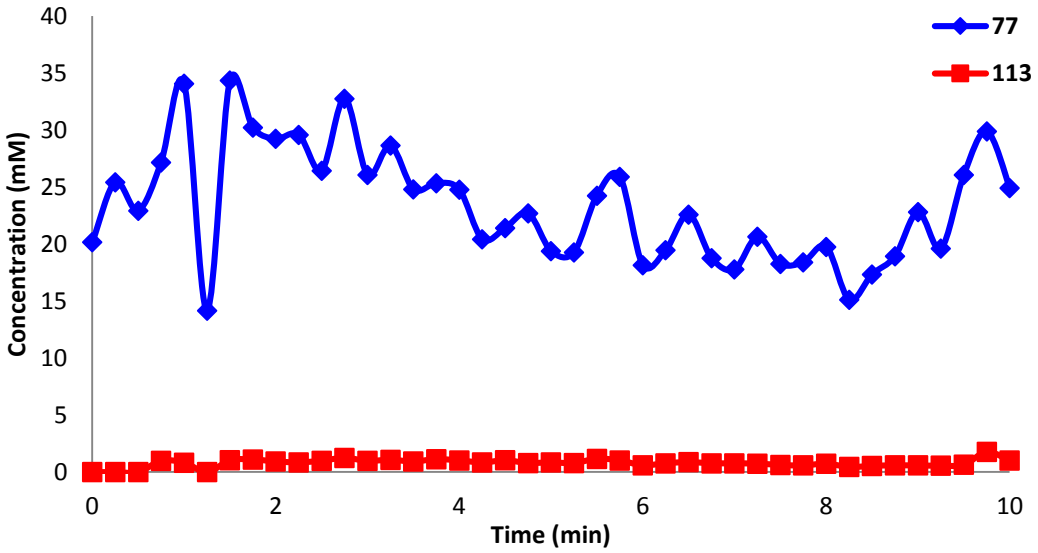

Figure 28. Acylation of **77** in H_2O with acetic anhydride.

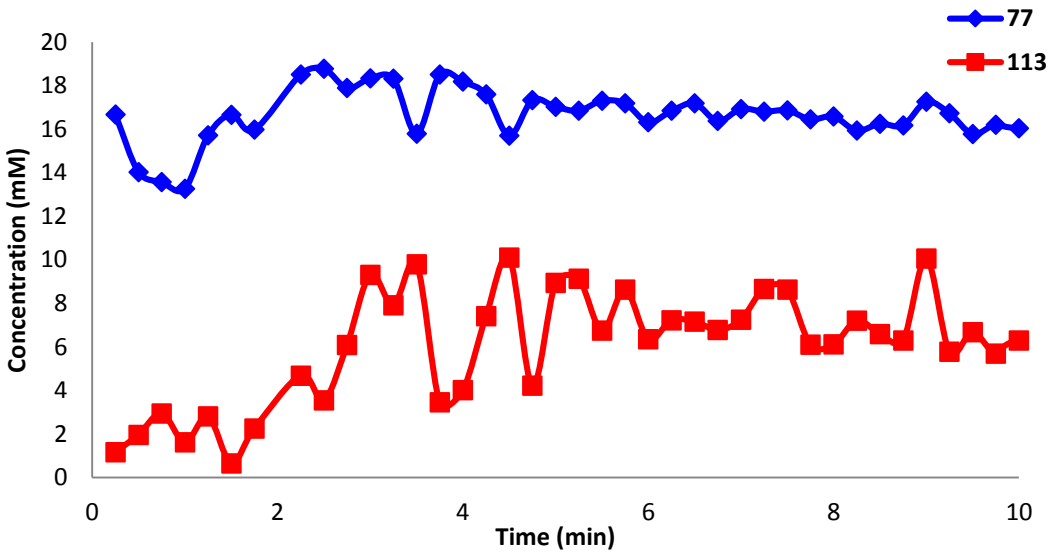

Figure 29. Acylation of **77** in methanol with acetic anhydride.

A noticeable difference was observed when changing to a less polar solvent, dichloromethane (Figure 30). The consumption of starting material was markedly slower, along with the formation of product. Fluctuations observed in the acylated product were minimal, suggesting a hydroxylic solvent aided reaction progression and also amplified observed changes in concentrations.

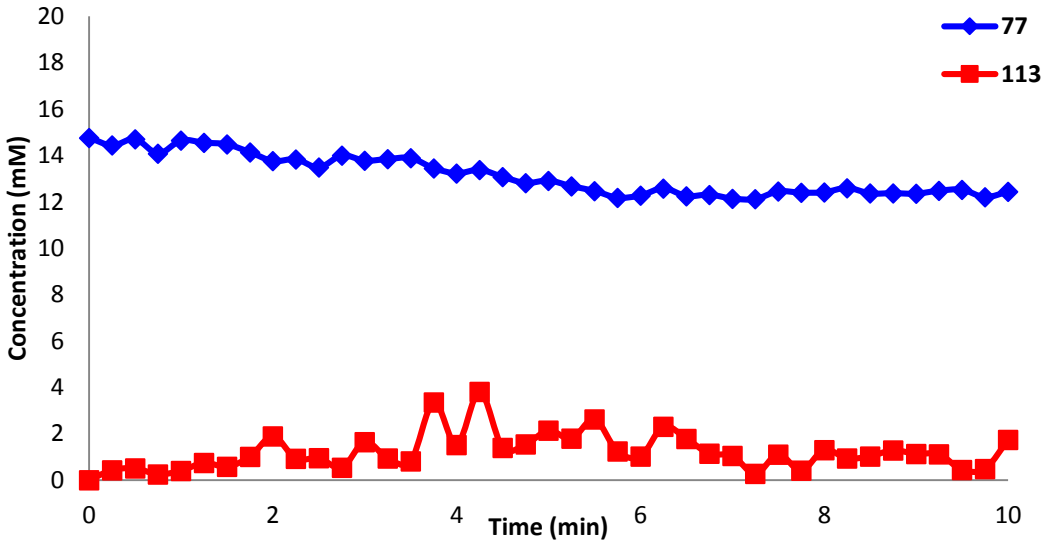

Figure 30. Acylation of **77** with acetic anhydride in DCM.

2.5.2. ^{1}H NMR Analysis

In addition to HPLC studies, ^{1}H NMR was attempted to monitor the reactions noninvasively in real time. Having previously observed the dependence of the reaction on a hydroxylic solvent, *tert*-butanol was selected. Solutions of 45 mM **77** in deuterated *tert*-butanol (*t*-BuOD) were studied. DCM (5 mol% relative to **77**) was used as an internal standard. The region from 8 ppm to 2 ppm was scanned to eliminate solvent peaks. A multiacquisition programme was run with 6 scans per experiment taking approximately 31 seconds per acquisition.

Initial studies were run on aziridine and internal standard in *t*-BuOD in order to determine any noise within the NMR signal and starting material fluctuations. DCM concentrations were also monitored to ensure the internal standard baseline was consistent. Background measurements demonstrated minimal fluctuation in the starting material and stability in the DCM. The aziridine ring protons were averaged to show one set of data points due to their equivalence.

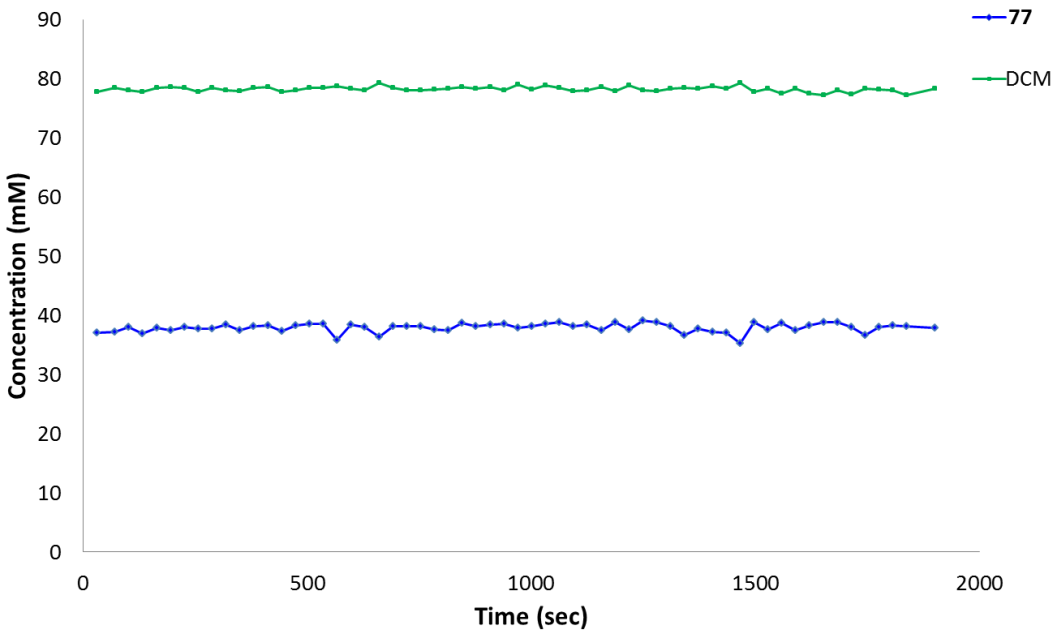

Figure 31. ^{1}H NMR study performed on Bruker Avance 400 (400 MHz) measuring **77** and DCM concentrations over 31 minutes.

Isobutyric anhydride was selected initially due to its distinct methine septet signal. However, the reaction rate was slow and ring proton peaks could not be measured for the

product. While the septet signal was measured, the changes observed in the integration were most likely due to the anhydride's diffusion through the sample. In order to better compare with the HPLC studies, acetic anhydride was then used.

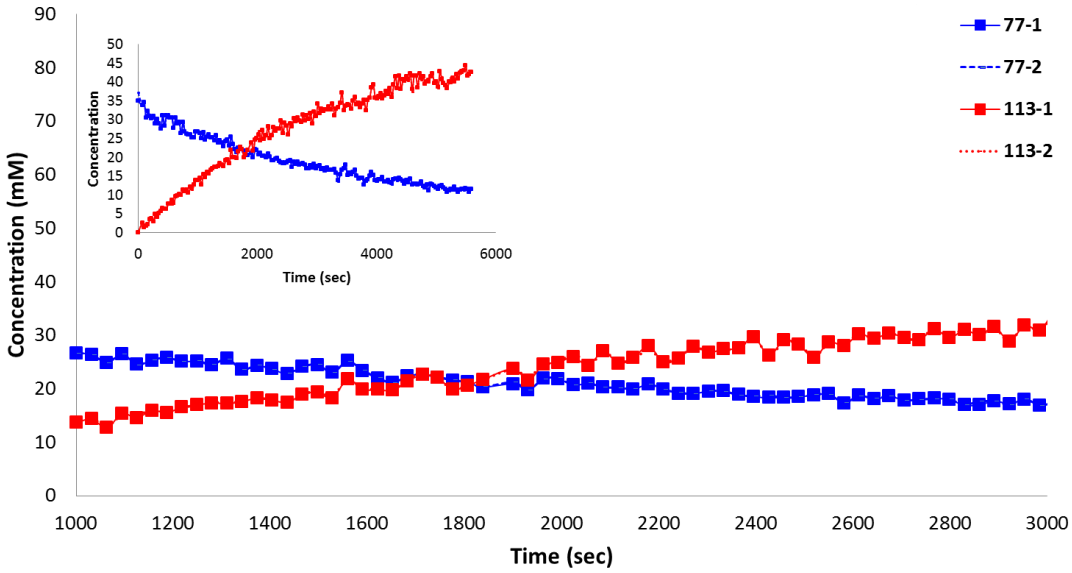

Figure 32. ^{1}H NMR study performed on Bruker Avance 400 (400 MHz) measuring concentration of the starting material and acylated aziridine, with inset showing reaction progress.

Reactions with acetic anhydride generated product within the first minute, allowing for improved analysis and comparison with HPLC data. All integrations were converted to concentrations based on the internal standard, as shown in Figure 32. Both aziridine ring protons from the starting material and product were integrated, demonstrating minor fluctuations in concentration throughout the reaction. The reaction plot, shown in Figure 32, shows starting material and product when their ratio reached 50/50 and demonstrated negligible changes in concentration.

It must be noted that the system was not directly comparable to HPLC data. *In situ* ^{1}H NMR was noninvasive as physical sampling was not required during the analysis of the reaction taking place. Furthermore, methanol was not utilised to quench the reaction, as in HPLC. This variable was quite significant as the MeOH was stopping the reaction at the specified time points, allowing the oscillations to be observed. The lack of MeOH quench for the NMR experiments may be causing the reduction in the observable oscillations.

Additionally, HPLC traces were acquired at several sampling times and at faster rates than those achieved by NMR. In order to obtain a cleanly resolved spectrum, multiple scans were required by NMR, thus shorter time points were unable to be collected.

2.5.3. Stopped-Flow UV

Due to the sensitivity of the reaction and the desire to further probe the reaction mechanism, the next investigation involved stopped-flow UV measurements. Under these conditions, faster measurements are taken 1 ms after the initial mixing of aziridine and acetic anhydride as solutions in *t*-AmOH. In addition to being a noninvasive technique, this instrumentation would also allow for more data points to be collected. The studies demonstrated reaction rates for a solution of aziridine and anhydride, in addition to just aziridine in solution (Figure 33). Unexpectedly, a reaction appeared to have taken place when only aziridine was present in the cell. Addition of anhydride appeared to inhibit the reaction which was observable with only **77** present. This observation suggested a photochemical sensitivity of **77**.

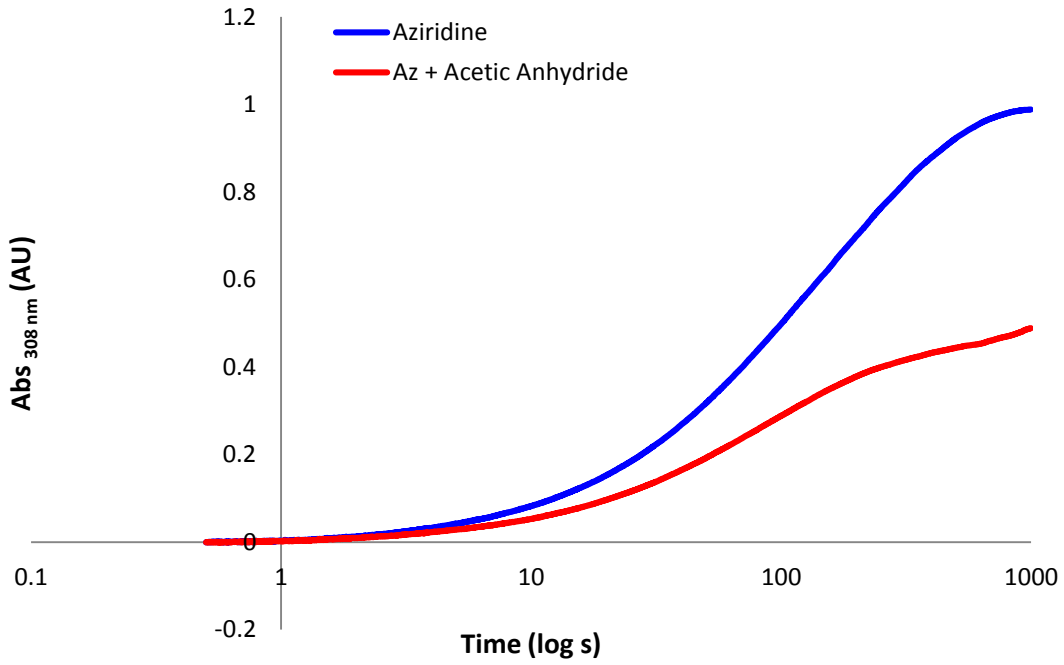

Figure 33. Stopped-flow UV absorbance data measured at 308 nm for aziridine in *t*-AmOH, and aziridine with acetic anhydride in *t*-AmOH. Slit widths set to 3 nm.

In order to further investigate the unexpected behaviour of aziridine in *t*-AmOH, measurements were taken over 1000 seconds at varying slit widths. The results revealed a slit width dependence, demonstrating a reaction was taking place when exposed to UV light. Increasing the intensity of light led to an increased reaction rate, suggesting photochemistry was taking place in the solution of *NH*-ketoaziridine (Figure 34).

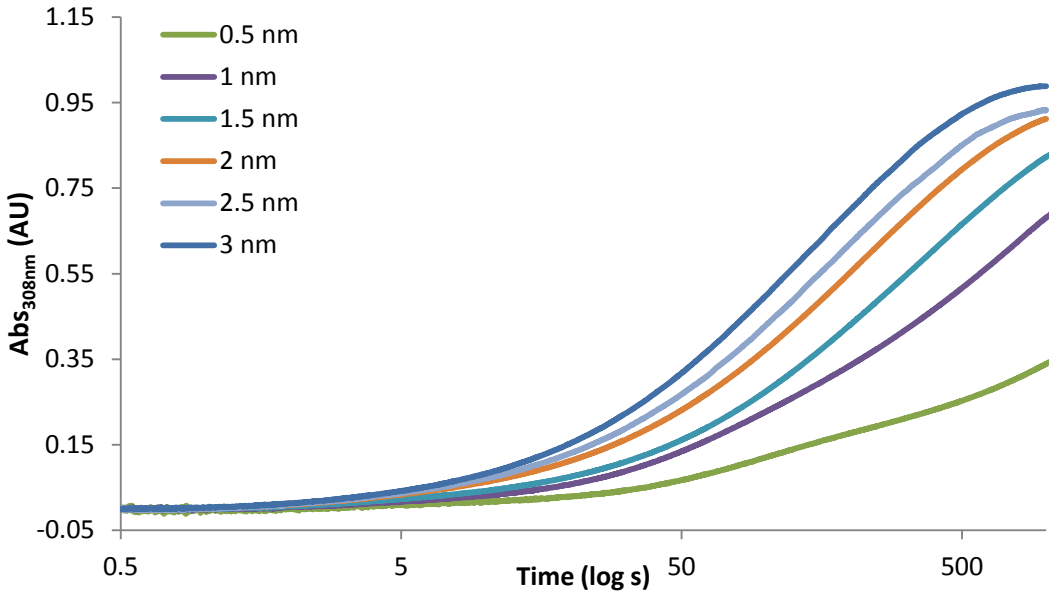

Figure 34. Stopped flow UV data of aziridine in *t*-AmOH monitoring the effects of increasing the slit width, demonstrating the presence of a photochemical reaction.

2.6. Conclusions and Future Work

Attempts were made to develop a catalytic kinetic resolution of aziridines. These studies revealed a background reaction was dominant, preventing resolution of **77**. Further investigation into the kinetics of these reactions with HeAP and DMAP revealed fluctuations in *ee*'s and conversions, along with constant variations in starting material and product concentrations. Control reactions with triethylamine demonstrated a linear reaction progression with respect to starting material and product. Investigation into background reactions further studies which revealed the aziridine readily reacted with, and was acylated by acetic and isobutyric anhydrides, thus preventing the HeAP from being able to properly resolve the two enantiomers.

The reaction between aziridine and anhydrides was studied using HPLC and ^{1}H NMR. HPLC analysis clearly demonstrated fluctuations in both starting material and product concentrations, resulting in considering the possibility of the reaction being a chemical oscillator. The fluctuations observed were present in other hydroxylic solvents, but were not seen when using less polar solvents, such as DCM. Changes observed when reacting aziridine with acetic anhydride and comparing to the internal DCM standard were negligible when studied by ^{1}H NMR. A normal reaction progression was demonstrated, thus not revealing any complex dynamics were taking place without the addition of methanol.

HPLC clearly demonstrated the inhibition of fluctuations through the addition of basic additives or less polar solvents. A potential mechanism for an oscillating reaction is presented in Scheme 53. Acylation of **77** would yield *N*-acyl aziridinium (**115**), which may then form **113** or deacylate to regenerate **77**. Deprotonation of **115** would result in **113**, which may form enol **116**. The enol may then lead to enol acetate (**117**) through reaction of **116** with acetic anhydride. This would generate a positive-feedback loop in the system, as **117** would be an intermediate acting as an acyl transfer agent, and suggests the acylation of the aziridine may be autocatalytic.[87] As aziridine reacts, a negative-feedback loop may introduced to the system through deacylation of *N*-acyl aziridine (**113**) by an acetate anion or acetic acid.[88,89]

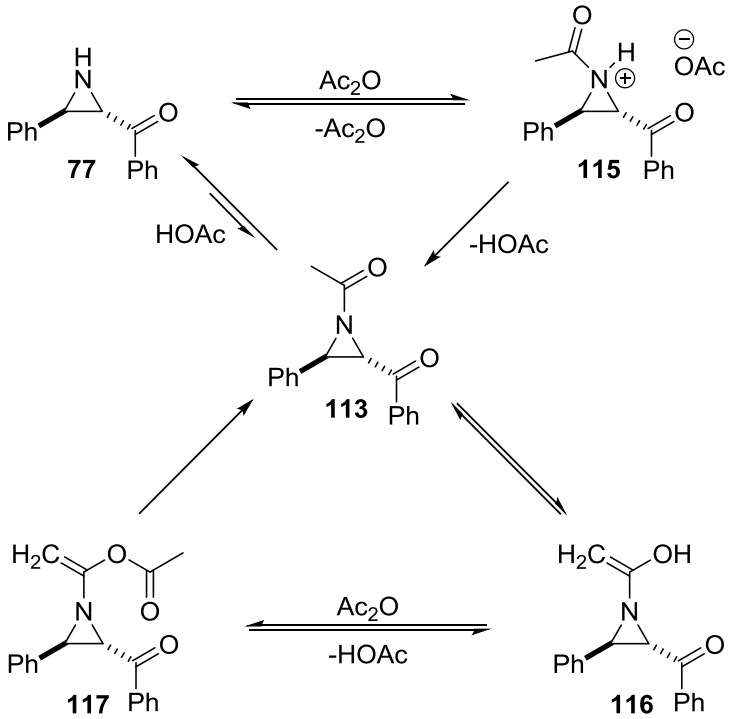

Scheme 53. Proposed potential oscillatory mechanism for the acylation of aziridine **77**.

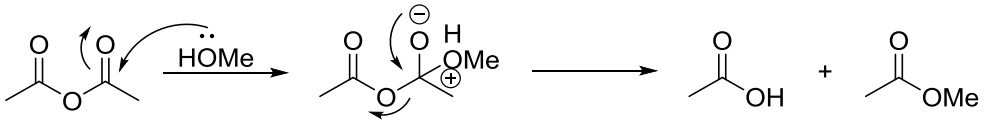

Scheme 54. Methanol quench of acetic anhydride.

While the proposed mechanism could potentially lead to an oscillating reaction, it does not take into account the effect of the methanol quench of anhydride used for acylation. As shown in Scheme 54, methanol would generate acetic acid and an ester in the presence of acetic anhydride. If the reaction were generating **117**, addition of methanol to quench unreacted anhydride would also quench **117**, generating the desired product **113** (Scheme 55). Additionally, the acetic acid generated may potentially affect the stability of the product or starting aziridine **77**.

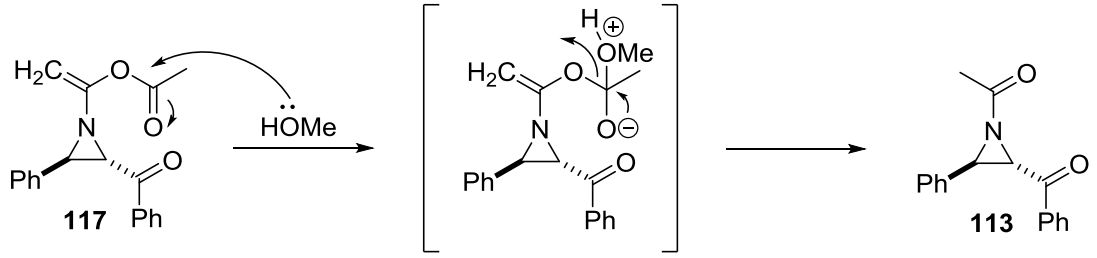

Scheme 55. Methanol quench of **117** yielding **113**.

Comparing the HPLC data with that obtained by ^{1}H NMR would indicate a sensitivity to the addition of methanol which may affect the ratio of substrate and product concentrations. As the HPLC data was acquired following the quench, it may not be indicative of an oscillating reaction taking place prior to methanol addition. Additional experiments would be required to ascertain the cause of the observed fluctuations. As acetic acid is generated in the reaction, the stability of the aziridine and product in acid should be studied. In order to determine if the acylated aziridine is behaving as an acyl transfer agent, cross-over experiments combining acylated aziridine with an *NH*-aziridine of a different structure could be performed to establish if acyl transfer is taking place.

Final investigations using stopped-flow UV revealed further unexpected behaviour. Anhydride appeared to inhibit the reaction taking place when aziridine was exposed to UV light. The slit width dependence of aziridine in *t*-AmOH revealed the molecule was photochemically reactive, in addition to the complexity of the previously presented oscillatory type behaviour. Due to the interest in the photochemical reactivity, focus was redirected to this area in order to determine the mechanism and the photochemical product.

Chapter 3: Aziridine Photochemistry- Spectroscopic Studies

Table of Contents

3.1. Photochemistry of Aziridines

Previously shown in Chapter 2 Figure 34, aziridine (**77**) demonstrated a slit width dependence when observing a solution of aziridine by stopped-flow UV and measuring the absorbance at 308 nm. Increasing the slit widths showed an increase in absorbance and observed rate, demonstrating an intensity dependence which suggested the occurrence of a photochemically initiated process (Figure 35). A linear relationship was observed for the rate where using a 5 nm slit widths provided a rate which was 12 times faster than that observed at 0.5 nm slit widths. The photochemical reaction taking place did not show full conversion, indicating more time was required to reach a saturation point. While stopped-flow UV provided evidence of this unexpected activity, its typical use is for monitoring faster occurring reactions, as it allows for the point following 1 ms of mixing to be measured. Due to this, fluorescence was then utilised since it would allow wavelength and intensity selectivity. Additional variables, such as concentration, time, and oxygen dependence were investigated offering a more complete study of the system.

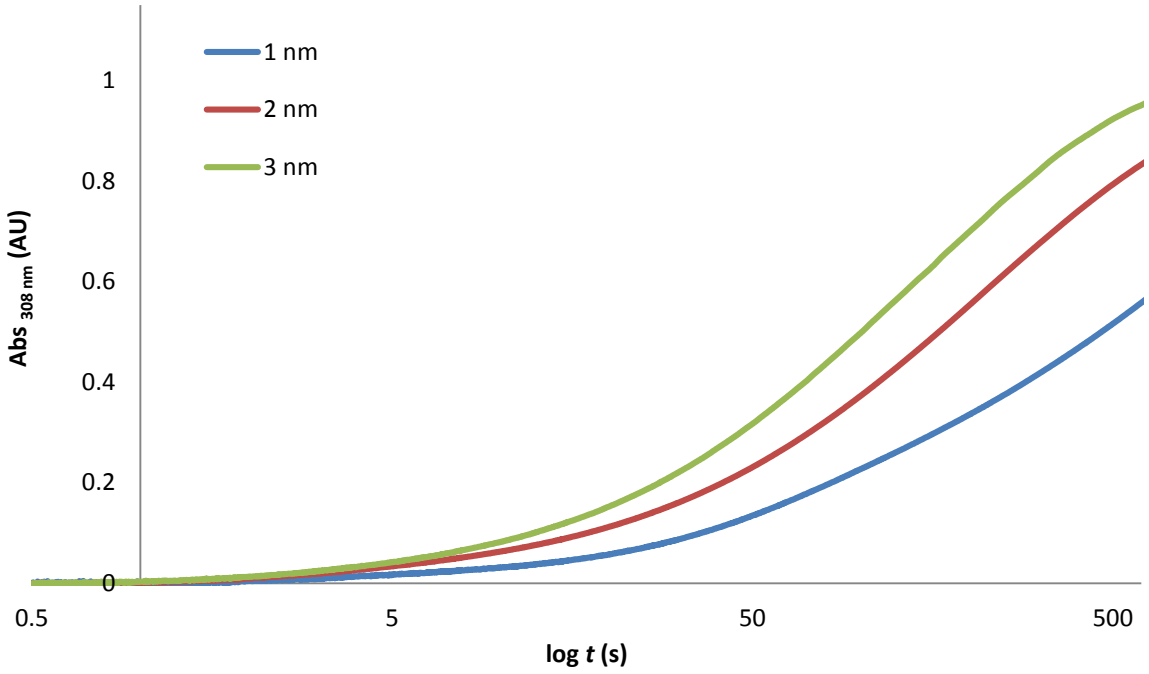

Figure 35. Stopped flow UV data demonstrating slit width dependence at 1, 2, and 3 nm of the photochemical reaction taking place for aziridine (**77**).

3.2. Formation of the Azomethine Ylide

3.2.1. Wavelength Dependence

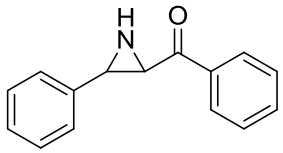

77

Figure 36. Aziridine under photochemical study.

An investigation of wavelength dependence of the photochemical reaction of **77** was carried out to determine which wavelengths were most effective for inducing the photochemical change. A fluorimeter was used to irradiate a 93 μM sample of **77** in *t*-AmOH. This concentration was used as it provided an absorbance within the detector limits and allowed monitoring of absorbance changes. Initial studies involved irradiation at 250 nm based on the λ_{max} absorbance for **77**, as shown in Figure 37. Initial irradiations were performed at 10 and 30 minutes. Following 10 minutes of irradiation, a series of new apparently separate absorbance features formed, centred at ~360 nm. A decrease in the λ_{max} at 250 nm was also observed. An additional effect from this irradiation was observed, where the shoulder of the main aziridine peak around 275 nm also decreased. However, longer irradiation at 30 minutes led to a smaller increase in the peak at 360 nm but a larger decrease in the shoulder at 275 nm. The peak centred at 360 nm may also contain multiple species as it displayed multiple features, as shown in Figure 37.

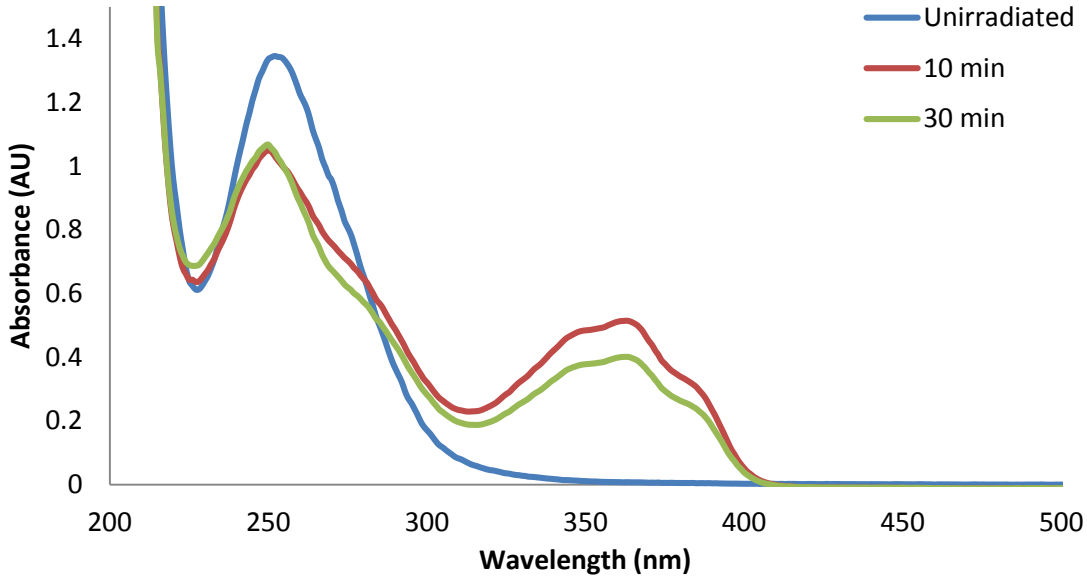

Figure 37. Irradiation of **77** in *t*-AmOH at 250 nm for 10 and 30 minutes at 93 μM.

Wavelength dependence was further investigated by irradiating above 300 nm. Initial measurements were taken after 5 minutes of irradiation. Irradiation at 350 and 380 nm induced no change in the λ_{max} of 250 nm, nor was the species at 360 nm observed. Decreasing the wavelength to 320 nm did provide the 360 nm feature; however, the formation was minimal in comparison with the irradiation at 250 nm.

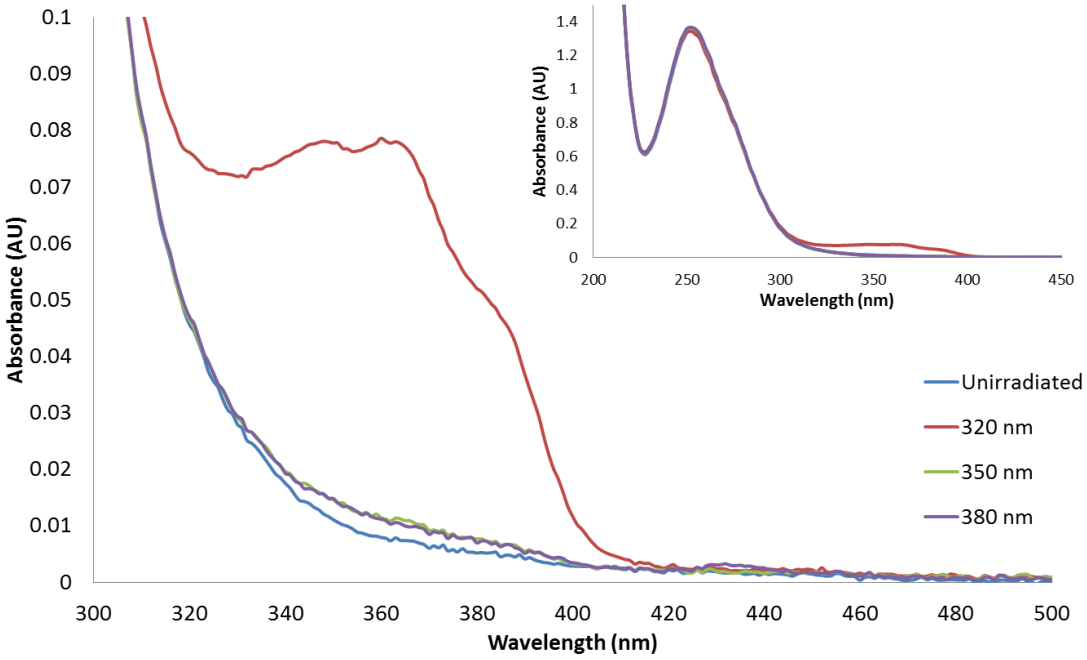

Figure 38. Irradiation of **77** at varying wavelengths for 5 minutes in *t*-AmOH at 93 µM. Inset showing full absorbance spectrum from 200 to 450 nm.

Following initial experiments with *t*-AmOH, it was found that the solvent created spectral background noise resulting in a need to reconsider the solvent. *t*-AmOH absorbs around 300 nm making it an non-ideal solvent for UV and fluorescence studies as aziridine absorbs within this region.[90] Acetonitrile was selected since it does not have a significant absorption above 220 nm, which was the area of interest in this study.[91]

3.2.2. Concentration Dependence

Additional studies were carried out on determining the concentration dependence of the photochemical reaction. A range of concentrations were studied, from 22 µM up to 4.48 mM of aziridine in acetonitrile using a fluorimeter as the excitation source. Irradiations took place at 250 nm for 30 minutes, and the growth of the 360 nm peak was monitored by UV absorbance. Irradiations taking place at the lowest concentrations of 22 and 45 µM led to minimal formation of the 360 nm peak (Figure 39). However, increasing the concentration to 72 µM led to the highest formation of the new species after 30 minutes.

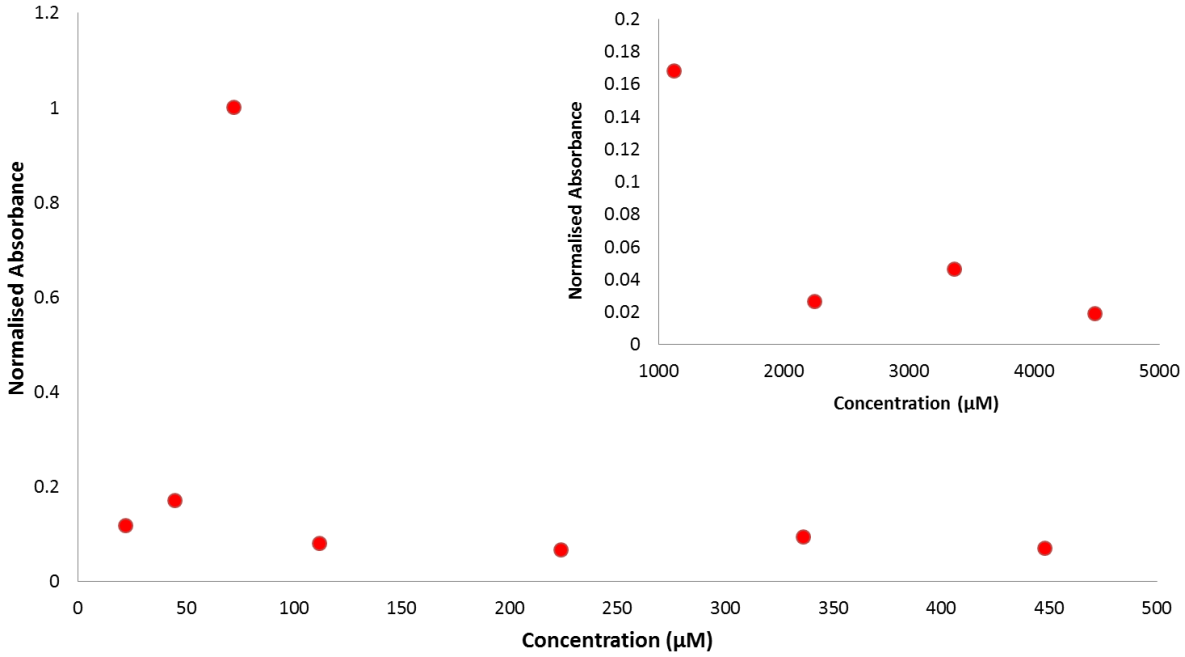

Figure 39. Normalised absorbance vs. concentration for the peak centred at 360 nm following 30 minutes of irradiation at 250 nm of **77**. Inset showing concentrations from 1120 µM to 4480 µM.

When increasing the concentration significantly to 4.48 mM, the 360 nm peak was not observed (Figure 39). While the 250 nm peak appeared to have grown, the 0 minute point overlapped with the 30 minute trace, demonstrating the inconsistency with the UV absorbance measurement at this higher concentration. Additionally, no 360 nm peak was observed at concentrations of 2.24 and 3.36 mM. Due to the solution being too concentrated, the absorbing molecules prevent the excitation light from being uniform throughout the solution. This inner filter effect would lead to only a small amount of molecules being excited, inhibiting the photochemical change. Another possibility is "collisional quenching."[92] The fluorophores reach an excited state when irradiated, but then return to the ground state upon contact due to this being a short range interaction. The molecules do not undergo a permanent change, thus no photochemical reaction takes place.

Aziridine **77** clearly displayed a concentration sensitivity, with inhibition of the photochemical reaction taking place at higher concentrations. Low concentrations of 22 and

45 µM displayed small amounts of the new photochemical species, with the highest amount observed at 72 µM. Due to this observation, remaining experiments were performed on concentrations of 72 µM in MeCN.

3.2.3. Time Dependence

As the optimum concentration had been identified, a time dependence study was also completed. The experiments were carried out on a fluorimeter and the absorbance of the sample was measured. Initial experiments revealed a lack of growth in the 360 nm peak when the sample was not continuously irradiated. It appeared that once this peak formed, it could not be re-excited to generate more of the 360 nm species. This information suggested an irreversible photochemical change was taking place. It was not possible to irradiate, measure the absorbance, and then re-irradiate the same sample. A new sample was prepared for each time point to monitor the continuous irradiation measurements at the specified times.

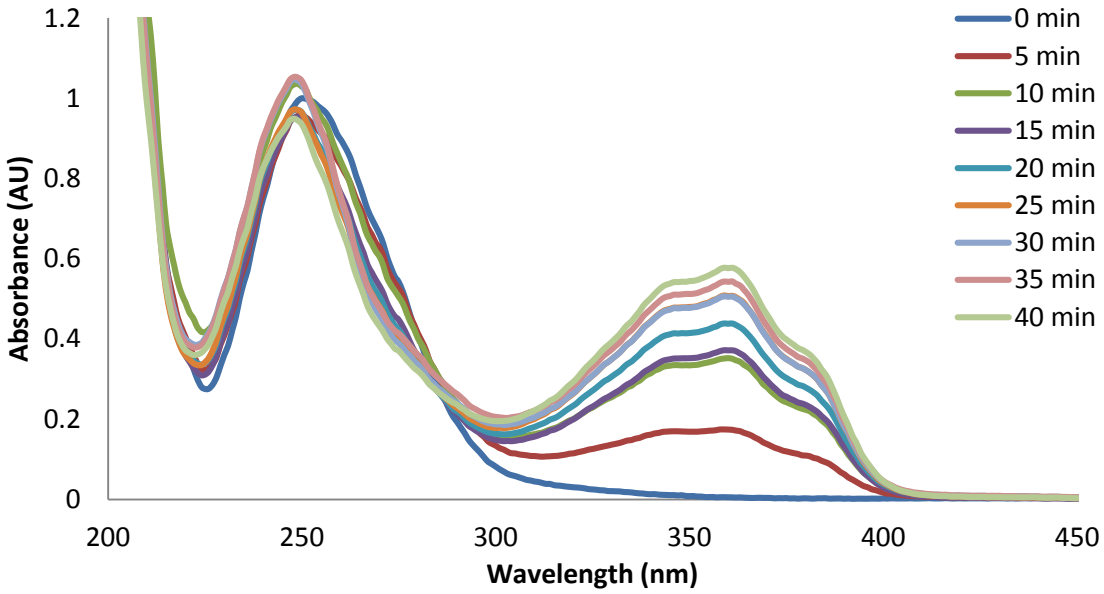

Figure 40. Normalised absorbance spectrum of 72 µM **77** in MeCN following irradiation at 250 nm with 15 nm fluorimeter excitation slit widths at various time points.

As shown in Figure 40, the highest amount of the 360 nm peak was formed after 40 minutes. Previously mentioned was the reduction in the 250 nm peak, with an isosbestic point

present around 285 nm. The final time of 40 minutes showed a blueshift, a shift to lower wavelengths, of the shoulder of the main aziridine peak, being pulled in around 275 nm.

In accordance with previous literature findings, the sample underwent a colour change to yellow following irradiation. Based on previous experimental work carried out by Huisgen, it was suggested that the formation of the new feature was an azomethine ylide (Figure 41). This was based on the photolysis of *cis*- and *trans*-1-(*p*-methoxyphenyl)aziridine-2,3-dicarboxylates, where diethyl fumarate was added following 5 minutes of irradiation causing the yellow colour to disappear from the solution.[84] Additional low-temperature photolysis studies by George on **77** on EPA glass at 77 K, also observed a spectral feature with a λ_{max} of 368 nm and proposed it was the azomethine ylide. Based on the literature and the spectral similarities of the λ_{max} in both cases, it may be hypothesised that the 360 nm feature was attributed to an azomethine ylide.

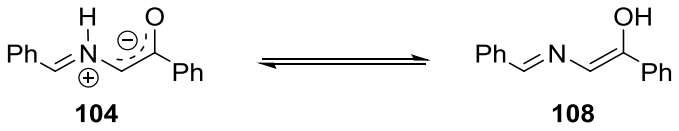

104 **108**

Figure 41. Azomethine ylide, suggested by Huisgen and George, responsible for the 360 nm peak.

3.2.4. Decay Monitoring

Studies were then performed to monitor the decay of this newly generated spectral feature. Following irradiation of a 72 μM solution of aziridine in MeCN at 250 nm for 30 minutes in the presence of oxygen, the absorbance was measured every 30 minutes over 72 hours. The highest 360 nm peak was observed immediately following irradiation, and decayed 30 minutes later. This decay continued until 1770 min, where it reached its lowest absorbance. However, the 360 nm peak then began to increase in absorbance until the final measurement at 4290 min (Figure 42). Additionally, an isosbestic point was observed at 270 nm. Plotting the absorbance of the 360 nm peak over time further confirmed the decay of this feature. A plateau was reached around 1500 minutes, followed by a steady growth (Figure 43).

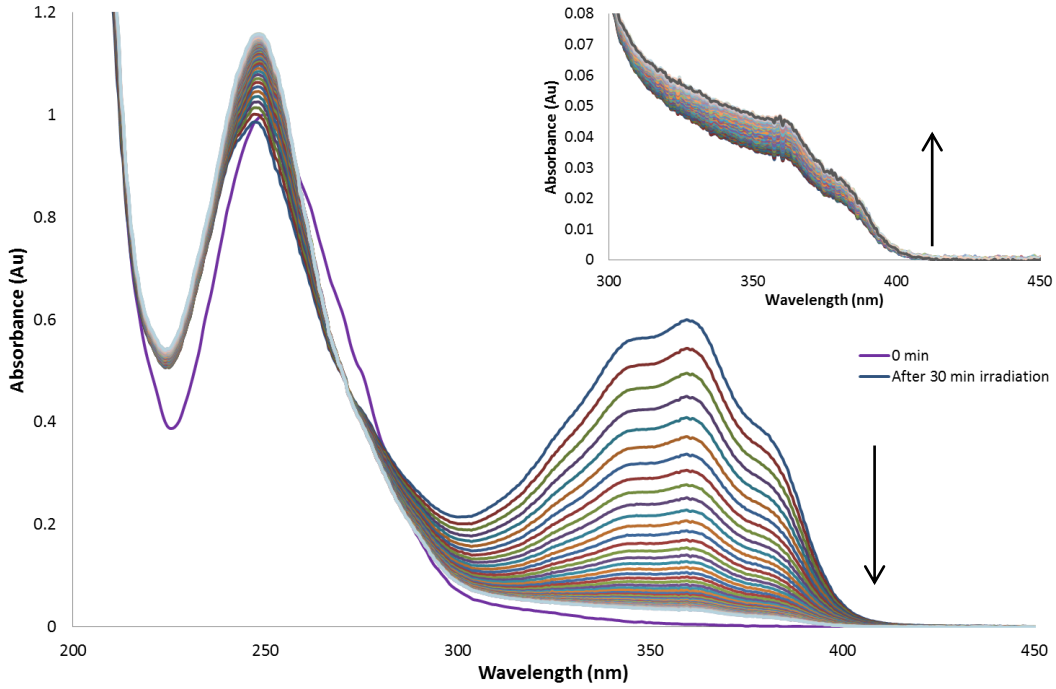

Figure 42. Monitoring of the decay of the 360 nm peak. Maximum absorbance of the 360 nm peak was observed immediately following 30 minutes of irradiation at 250 nm. Inset plot shows the regrowth of the feature being monitored from 1770 to 4290 minutes.

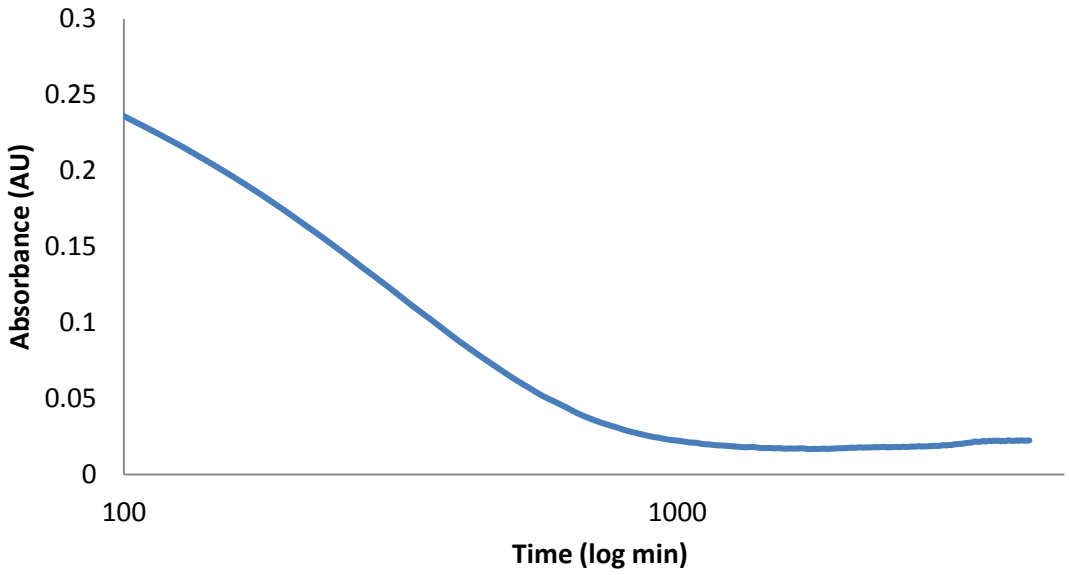

Figure 43. Plot of the absorbance of the 360 nm peak over 72 hours.

3.3. Initial Fluorescence Studies

In order to further characterise **77** and determine its spectroscopic features, fluorescence studies were undertaken. A 3D experiment was carried out to obtain an excitation-emission profile. As it was not possible to characterise the molecule in its ground state, due to its sensitivity to UV light, the experiment led to continuous irradiation of the sample. The emission was monitored at excitation wavelengths from 200 to 350 nm in 5 nm increments. The 3D experiment required that the aziridine be monitored in its excited state following 30 minutes of irradiation at 250 nm. Data was processed to remove 2nd order transmission, i.e. peaks double the excitation wavelength. The wavelengths 20 nm and below the excitation wavelength were subtracted in addition to the MeCN background.

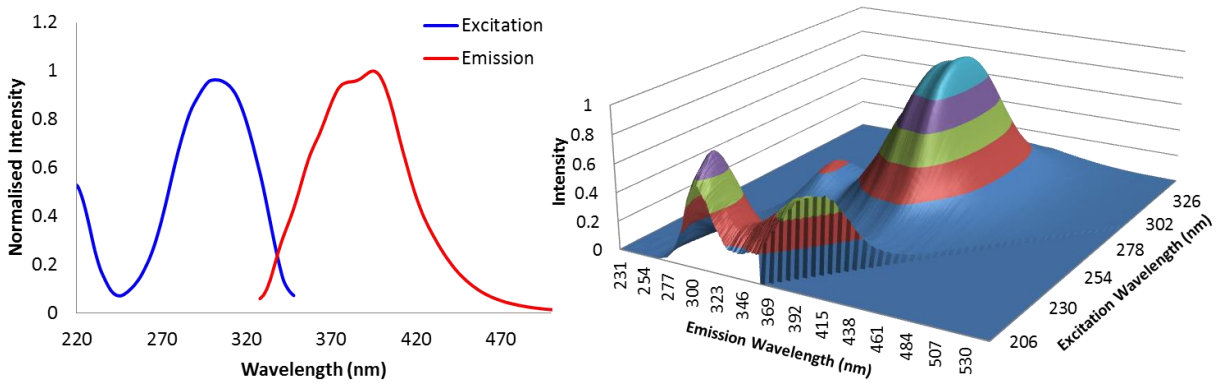

Figure 44. Excitation and emission peak maxima of **77** from the normalised excitation-emission 3D spectrum of **77.** Excitation and emission slit widths were set to 6 nm. Excitation spectrum obtained at λ_{em} 385 nm and emission obtained at λ_{ex} 310 nm.

The 3D plot of **77** showed the excitation at 215 nm led to an emission at 375 nm, resulting in a Stokes shift of 160 nm (Figure 44). Emission at 385 nm provided an excitation spectrum with a λ_{max} centred at 300 nm. The emission maximum was observed at 395 nm with an excitation wavelength of 310 nm. As an emission maximum was observed at λ_{ex} 310 nm, a time based experiment was performed monitoring the emission at this wavelength over time. The samples were irradiated at 250 nm prior to measuring the emission profiles at 310 nm over the specified times.

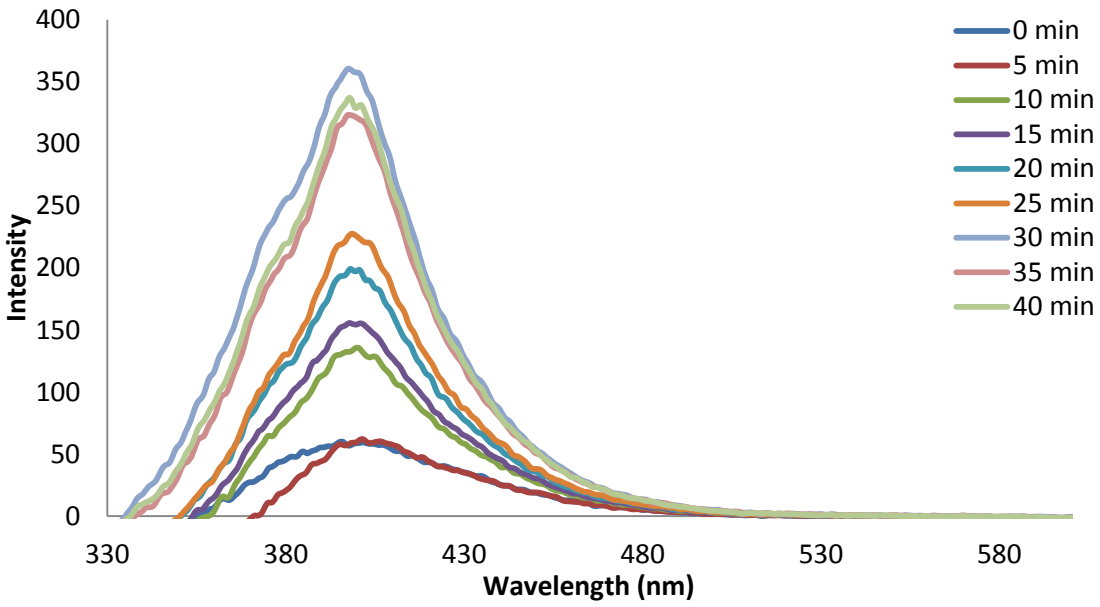

Figure 45. Emission spectra monitoring of **77** with an excitation wavelength of 310 nm following irradiations at the specified times.

An emission at 400 nm was observed when excitation took place at 310 nm (Figure 45). An additional shoulder was also seen around 375 nm for spectra from 10 to 40 minutes, potentially indicative of an additional species contributing to the emission. With increasing irradiation time, emission increased with a maximum observed at 30 minutes. No change in emission was measured between 0 and 5 minutes, therefore, irradiation of the sample under 10 minutes did not allow for the photochemical reaction to generate enough of the emitting species.

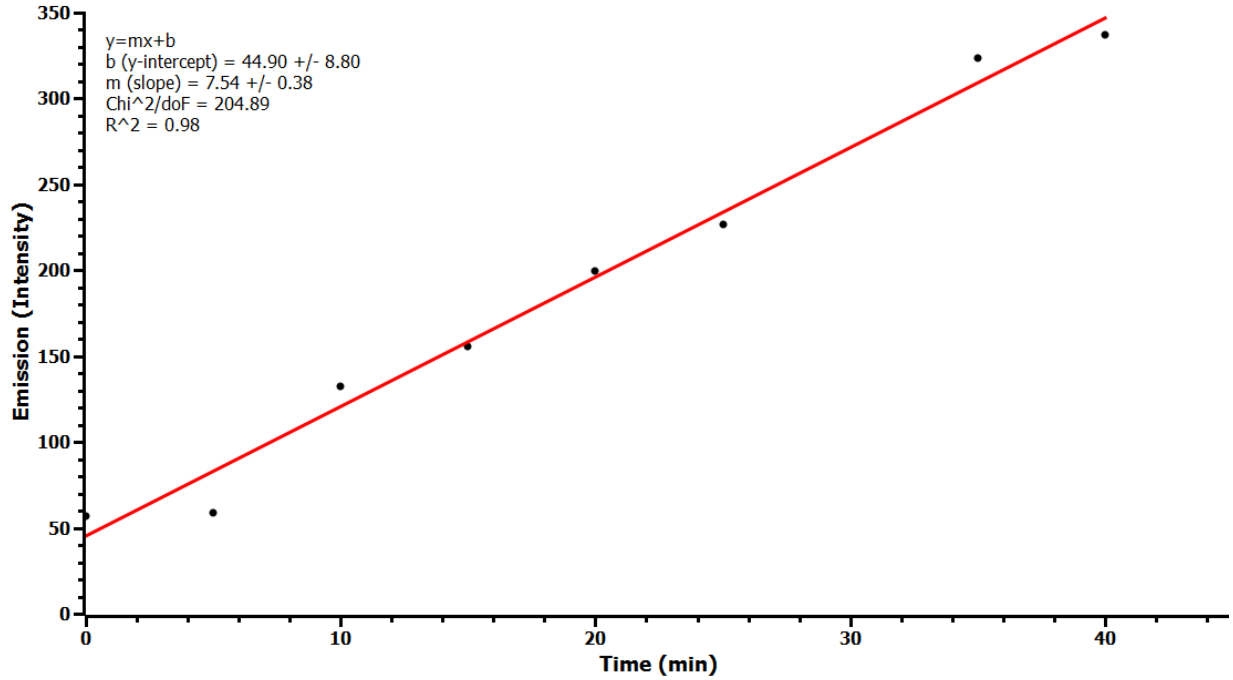

Figure 46. Emission versus time monitoring the growth of the emission band at 400 nm.

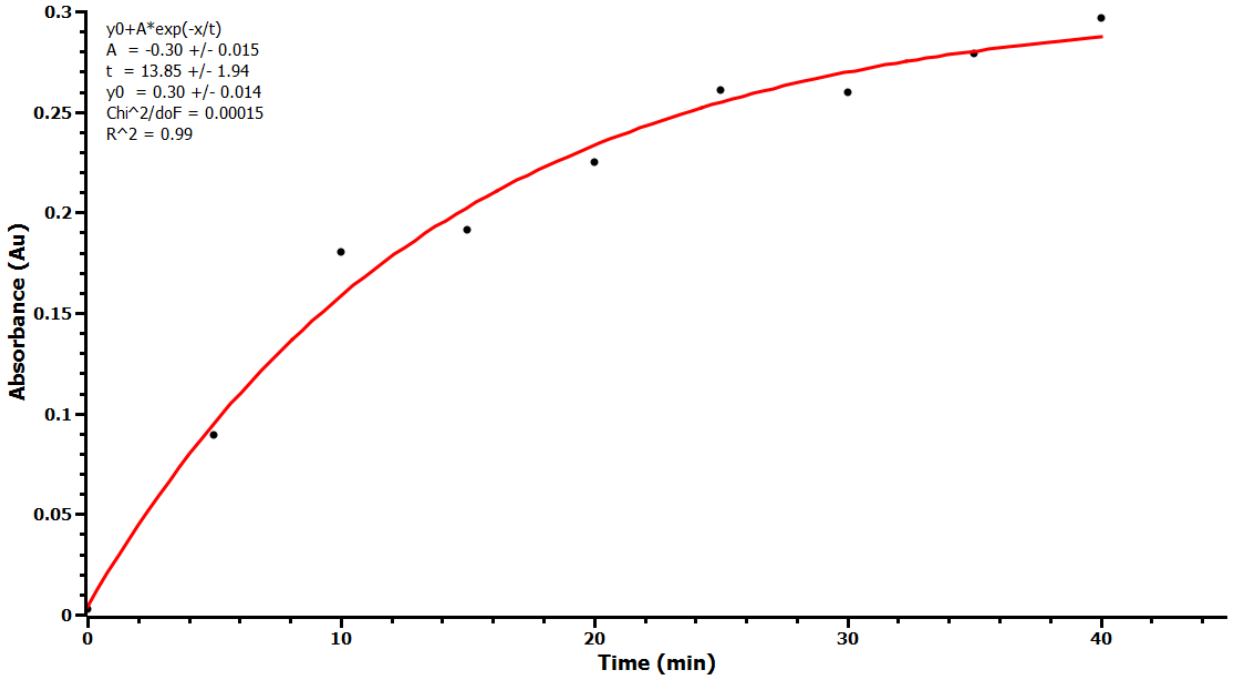

Figure 47. Absorbance versus time monitoring for the formation of the 360 nm peak.

Plotting the emission versus time to derive a rate for the formation of the emission at 400 nm revealed a linear growth (Figure 46). Comparison of the emission band with the 360 nm peak growth demonstrated that the latter fitted an exponential decay (Figure 47). The absorbance data revealed a point of saturation in formation of the 360 nm feature was possible, but had not yet been reached. From this information it may be said that the emission and absorbance rates were not coupled. Both data sets fit different rate equations and provided different rates. Thus it may be suggested that the same processes were not taking place and the lifetimes of different species were being measured. Additionally, as shown in section 3.5, not all aziridine derivatives formed new absorbance features upon irradiation.

3.4. Product Formation

3.4.1. Computational Studies

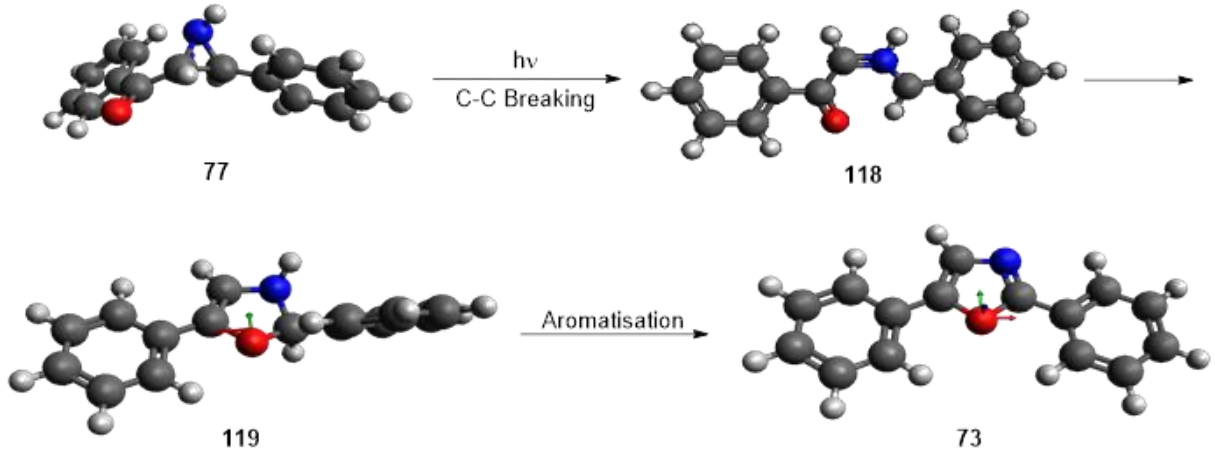

Figure 48. Computational TD-DFT study of the photochemical mechanism of **77** in the gas phase.

As a new species had been observed by fluorescence, additional insight was desired in order to identify the product was being formed by the irradiation of **77**. Computational time dependent density functional theory (TD-DFT) calculations were carried out by Dr. Rachel Crespo-Otero at the University of Bath, modelling the aziridine to be studied in the gas phase (Figure 48). The calculations suggested that upon irradiation, the C-C bond of the aziridine ring was broken and a biradical intermediate (**118**) was formed (Figure 48). As **118** was lower in energy than its precursor, it was more stable. The energy gap for **118** was also small between its ground state (S_0) and first excited singlet state (S_1), resulting in the emission not being visible. This intermediate may then undergo a conformational change, as shown in Scheme 56, and then may form a carbon-oxygen bond to form the 5-membered ring (**119**). Aromatisation as the driving force would yield 2,5-diphenyloxazole (**73**).

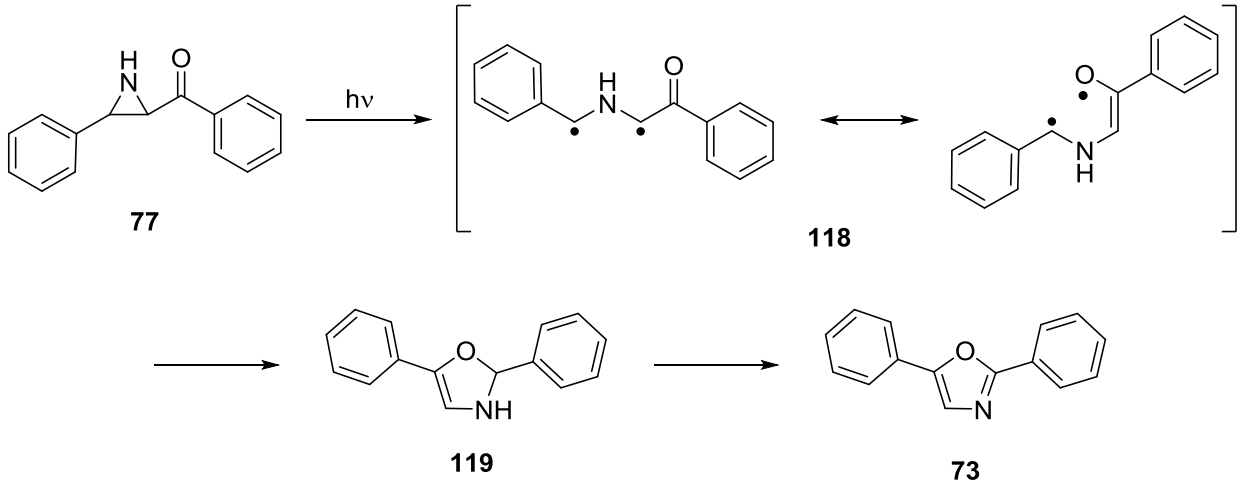

Scheme 56. Schematic of Figure 48.

3.4.2. Verification of Product through Fluorescence

Computational studies suggested the final product of the photochemical reaction yielded a commercially available product (**73**). Characterisation of **73** by fluorescence allowed comparison with irradiated aziridine. A 3D excitation-emission spectrum showed an emission maximum at 380 nm, while excitation maxima were at 220 and 300 nm (Figure 49). Excitation at 215 nm led to emission at 375 nm with a Stokes Shift of 160 nm, the same observed for **77** following irradiation at 250 nm. This experiment was performed with 2.5 nm excitation and emission slit widths, due to the oxazole having a strong emission.

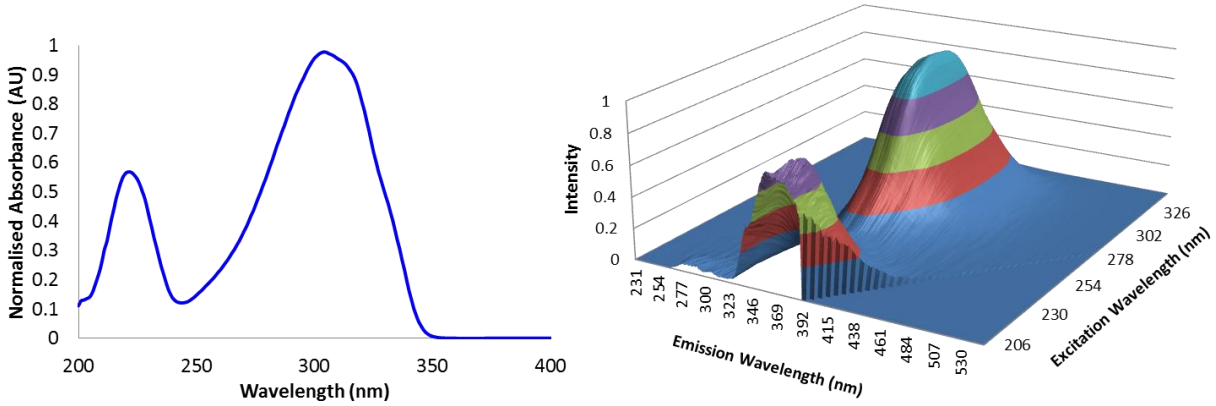

Figure 49. Normalised absorbance and excitation-emission 3D spectrum of 0.09 µM of **73** in MeCN with 2.5 nm fluorimeter slit widths.

Comparison of the absorbance profile of **73** with the excitation profile of irradiated **77** provided evidence which supported the computational data. The excitation and absorbance spectra would match if the compounds were the same or structurally similar. Overlaying the absorbance spectrum of oxazole with the excitation spectrum of the irradiated aziridine, as shown in Figure 50, revealed nearly identical spectra. This was a strong indication that 2,5-diphenyloxazole was formed from the irradiation of aziridine **77**. Additional data (*vide infra*) was collected by GC-MS and HPLC confirming the presence of 2,5-diphenyloxazole in the photochemical reaction.

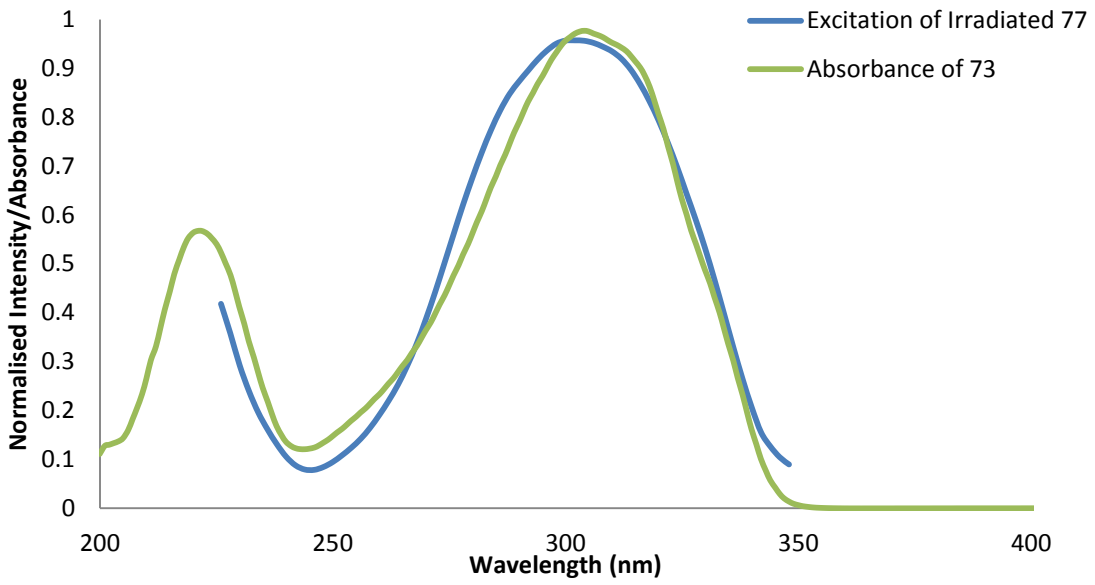

Figure 50. Overlay of the normalised absorbance of 90 µM 2,5-diphenyloxazole in MeCN with the normalised excitation spectrum of 72 µM aziridine in MeCN. The excitation spectrum was collected from 218 nm to 350 nm following a 30 minute irradiation at 250 nm.

3.4.3. Magnetic Field Effect (MFE) Studies

Due to the proposed biradical intermediate, and confirmation of the presence of radicals through a photochemically initiated polymerisation using aziridine (*vide infra*, Chapter 4.2.1), magnetic field effects were investigated. The biradical intermediate could potentially be a radical pair (RP), an intermediate with a short lifetime containing 2 radicals generated at the same time with unpaired electron spins. These spins may be antiparallel, a singlet state (↑↓, S) or parallel, a triplet state (↑↑, T).[93] Singlet RP's are reactive, while triplet pairs are not due to their parallel spins. Transitions between singlet and triplet states are typically forbidden, however, the application of a magnetic field will allow the transitions to take place should a RP be present.[94] It is possible to generate RP's through homolytic bond cleavage, hydrogen atom transfer, and electron transfer. In photoexcited molecules, intersystem crossing usually takes place prior to any reaction, therefore RP's generated photochemically are in a pure triplet state and cannot react until some S-T mixing occurs.[95]

When influenced by a magnetic field, a reaction rate and yield may be altered. The magnetic field would affect the singlet to triplet interconversion due to the spin angular

momentum of the radical pair being changed. Every radical encounter has a 3 in 4 chance of being in the triplet state, therefore 75% of these encounters are nonreactive. However, if there is a mechanism to induce the singlet and triplet interconversion, such as a magnetic field, the reaction may take place before the radicals diffuse apart.

Magnetic fields of differing strength affect RP's differently, as shown in Figure 51. In the presence of a strong magnetic field, greater than 1 T, the $T_{\pm}$ levels are separated from T_0 and S states, preventing interconversion between these levels and $T_{\pm}$. However, T_0 and S may still interconvert due to unpaired electrons experiencing different local magnetic fields. This is also the result of hyperfine coupling, as unpaired radicals are coupled to magnetic nuclei. A low field, under 0.1 mT, may induce mixing of S and $T_{\pm}$, resulting in a mixture of products. The radical pairs would need lifetimes of 100 nanoseconds or more in a low field scenario. Fields from 10 mT to 1 T are considered mid-field, while the Earth's field is approximately 0.05 mT.[96] Mid-fields inhibit mixing of the S and $T_{\pm}$ states due to the $T_{\pm}$ states having separated in energy and unable to convert to the S state. In comparison, fields over 1 mT increase yield as they would allow for more S-T_0 mixing to take place.

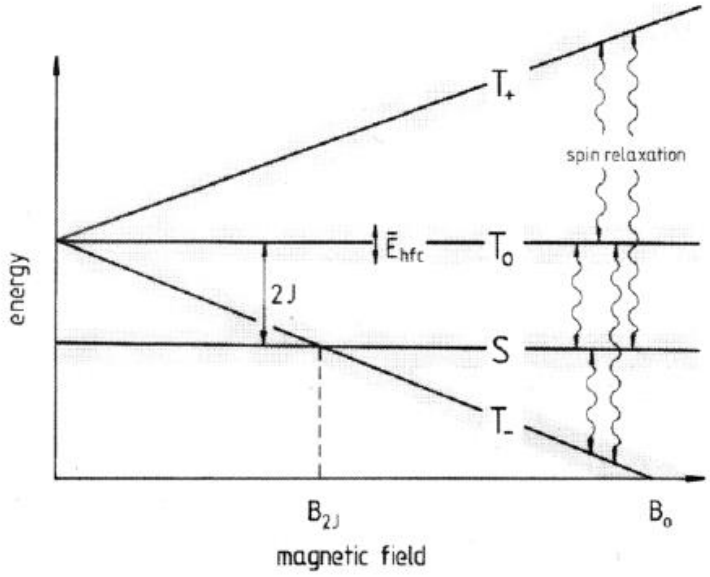

Figure 51. Energy diagram demonstrating the electronic spin states of a RP in the presence of a magnetic field. The average bandwidth due to hyperfine coupling is represented by $\bar{E}_{hfc}$, while the exchange integral is *J*. Figure reproduced from Ulrich and Steiner.[97]

Steady state irradiations in the presence of a magnetic field were carried out. Samples were irradiated using a fibre optic cable from the fluorimeter as an irradiation source. An optical table was designed to hold the sample and magnets in a fixed geometry to ensure there was minimal variation between measurements (Figure 52). Following irradiation of 86 μM solutions of aziridine in MeCN at 250 nm for 1 hour, absorbance and emission spectra were obtained to monitor for any differences. Temperature was also taken into account and kept at 23 °C. Measurements were repeated 4 to 5 times and the data averaged in order to determine if a field effect was present. The magnetic field was measured with a gaussmeter and was 60.5 mT.

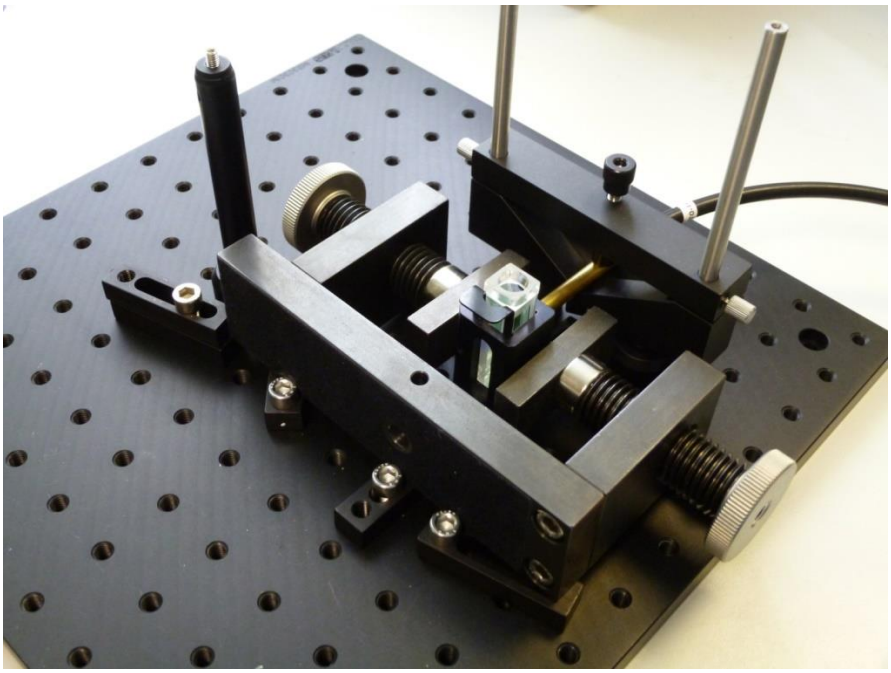

Figure 52. Optical setup utilised for steady-state magnetic field effect studies.

An initial absorbance study monitoring formation of the 360 nm peak revealed a slight effect may have been present. A reduction in the absorbance by the 360 nm peak was observed in the presence of the 60.5 mT field. In this study, it appeared the zero field and applied field UV traces fell just within error. The emission spectra comparing the irradiations in the presence of a field and without, showed a slight increase in emission which did not

overlap with the error. This would suggest more oxazole was formed in the presence of a field, consistent with the trend of increased emission with reduction of the 360 nm absorbance (*vide infra*, Chapter 3.6). However, further confirmation was desired and the experiment was repeated.

Repetition of the MFE study under the same conditions revealed a variable level of observed absorbance at 360 nm. Absorbance measurements showed more of the 360 nm peak was formed in the presence of a magnetic field, which fell outside the error for the no field measurement (Figure 53). Emission measurements were inconclusive as field and no field measurements fell within error, as shown in Figure 54. Consistency was observed, however, in that the emission following irradiation in the presence of a field decreased while the 360 nm absorbance increased.

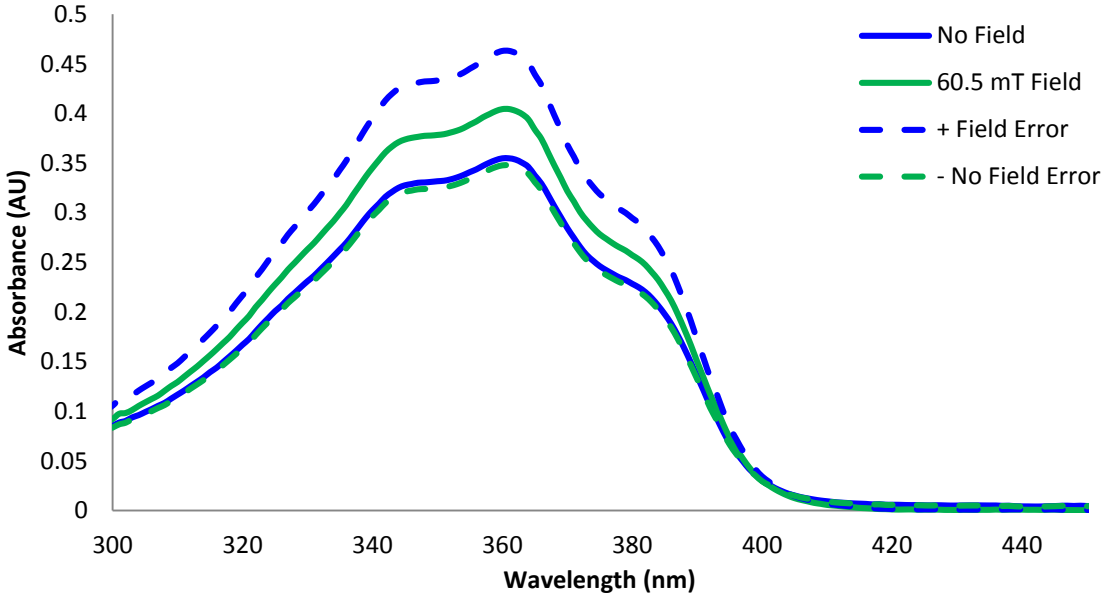

Figure 53. UV absorbance measurements from the repeat MFE study of **77** following irradiation in the presence of a 60.5 mT magnetic field and no field. Error was calculated based on standard deviation.

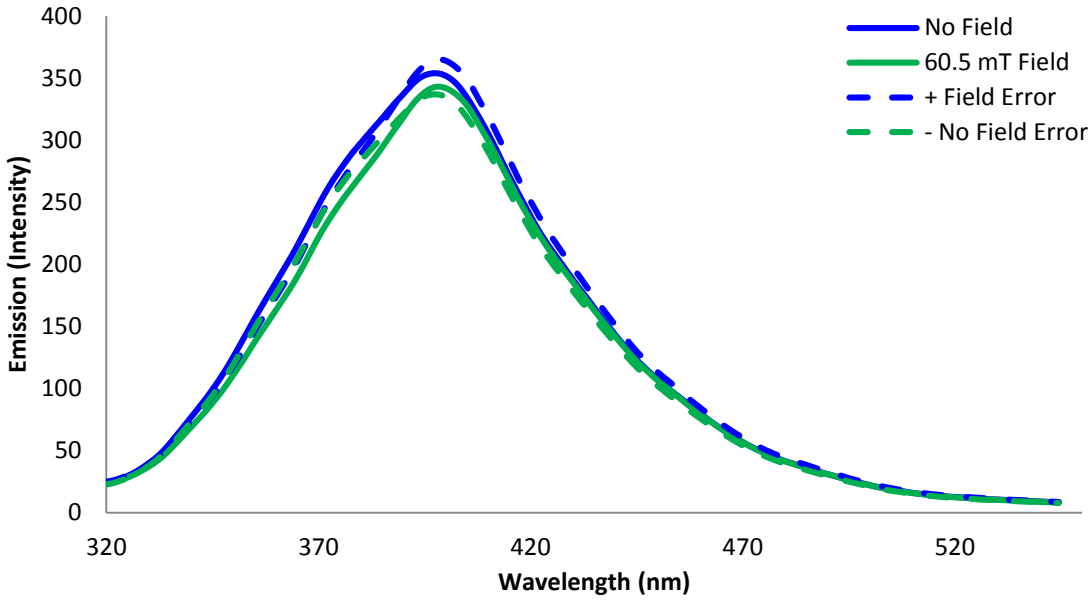

Figure 54. Emission measurements, λ_{ex} 220 nm, from the repeat MFE study of **77** following irradiation in the presence of a 60.5 mT magnetic field and no field. Error was calculated based on standard deviation.

As preliminary steady-state data suggested an MFE may be present, further investigations using transient laser absorption were carried out in collaboration with the Manchester Institute of Biotechnology. An Nd-Yag laser was used at 266 nm for photolysis of the sample in the presence of a magnetic field, with absorbance measured at 430 nm due to it giving the most signal. In order to help prevent the radicals from diffusing apart before they were able to react, the solvent system was altered to MeCN/cyclohexanol (20:80 by volume). This would increase the viscosity, which would slow down the radicals to improve the chances of measuring an MFE.

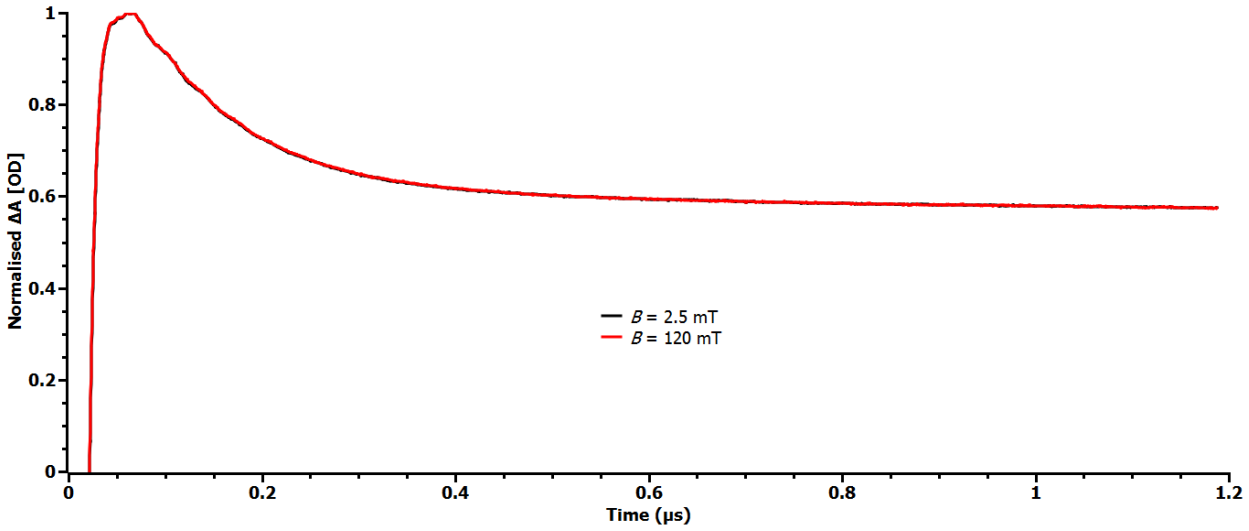

Figure 55. Transient absorption time traces following excitation at 266 nm of 150 μM **77** in MeCN/cyclohexanol (20:80), observing at 430 nm.

Initial tests indicated there was an MFE, however, fluctuations in the laser excitation signal were present. The measured signal from the sample was within the noise limit, making it difficult to determine if there was a clear MFE. Compensating for the excitation fluctuations, the amplitudes of the data sets were scaled to one another resulting in no observable differences, as shown in Figure 55. In order to improve upon these studies, a new setup was designed for future experiments to alleviate these issues. Improvements involve using mirrors instead of lenses and less surfaces. Therefore, rather than losing 40% of the laser beam intensity, only 20% would be lost as 4 surfaces would be used instead of 8. A reference measurement would also be taken of the excitation signal from the laser.

Based on the data presented in the steady-state and transient state, results were inconclusive with regards to an MFE. Should a magnetic field not affect a reaction rate or yield, an effect is not present. The only situation where this is not the case, is if back electron transfer to the starting material is possible. In this situation, rapid electron transfer initiation is required, such as through use of a laser. However, laser studies did not allow an MFE to be observed; suggesting back electron transfer was not a valid mechanism, therefore it was not proposed for **77**. This may be due to the lifetime of the RP's not being long enough to experience an effect from a magnetic field. Additionally, some photochemical reactions

undergo an electron transfer reaction with an excited triplet state, which would typically be affected by a field. However, if radical escape is the dominant mode, the recombination of radicals would have a minor effect. In order to increase the possibility of observing an MFE, viscosity would need to be further increased or the temperature lowered.[97]

3.5. Synthesis of Aziridine Derivatives

The steady state MFE studies were designed with the idea of being able to generate more oxazole through adjusting the magnetic field. It was proposed that increasing the amount of the azomethine ylide formed through application of a magnetic field, it may be possible to increase the conversion and yield of **73**. As these results were inconclusive, another alternative was to alter the electronic character of the aryl rings on the aziridine to determine if this would aid in increasing the oxazole yield. Functional groups were installed early on in the synthesis through an aldol condensation to form the chalcone, which would then undergo aziridination using the method described in the previous chapter. The aziridine would then be irradiated to generate the oxazole (Scheme 57).

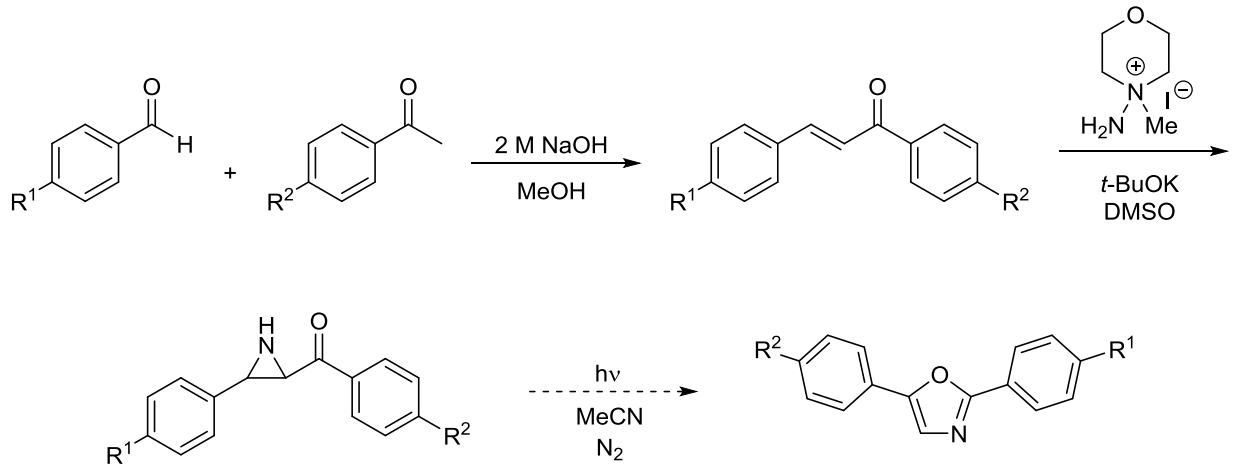

Scheme 57. Synthetic route to synthesis aziridine derivatives and oxazoles.

Aziridines **120**-**128**, as shown in Table 5, were synthesised to determine the effect of electron-donating and electron-withdrawing groups on the aryl rings. Following their syntheses, they were subjected to the same conditions as aziridine **77**. Irradiations were conducted at 250 nm on a fluorimeter for 30 minutes, with a concentration of 72 µM in MeCN. The UV absorbances were measured in addition to obtaining 3D excitation-emission spectra.

Table 5. Synthesised aziridine derivatives.

Compound	R^1	R^2	Yield (%)
120	Me	H	66
121	OMe	H	62
122	NO_2	H	40
123	Cl	H	57
124	H	Me	31
125	H	OMe	38
126	H	NO_2	45
127	H	Cl	42
128	Br	Br	38

Aziridine **124** showed two main absorbance peaks at 210 and 260 nm (Figure 56). Similar to **77**, **124** formed a new peak following irradiation with a λ_{max} of 365 nm. The peak at 260 nm decreased in absorbance and showed a slight blueshift. The new 365 nm feature also had multiple smaller peaks within, indicative of multiple species. The 3D excitation-emission spectrum showed similarities to the parent aziridine with emission maxima at 300 and 400 nm when excitation wavelengths were 218 and 318 nm, respectively (Figure 57). The emission profile was similar to that of 2,5-diphenyloxazole, where an emission band was observed between 340 and 450 nm. When changing the methyl group to R^1, compound **120** revealed similar properties. The UV absorbance spectrum of unirradiated **120** had a λ_{max} of 250 nm, and also formed a new feature at 365 nm following irradiation. UV absorbance was also measured following the 3D spectrum and showed a decrease in the 365 nm peak. A slight difference was observed for its excitation-emission profile, where the emission maxima were 300 and 378 nm when excitation wavelengths were 218 and 312 nm, respectively. However, the general profile was similar to that of **124** and provided an emission and excitation profile similar to 2,5-diphenyloxazole.

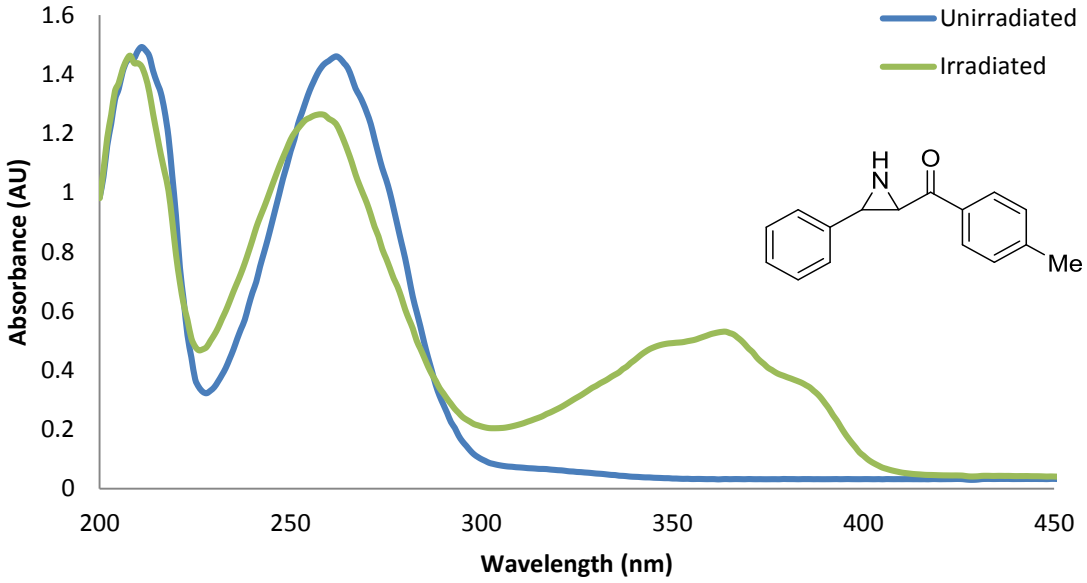

Figure 56. Absorbance spectrum of **124** following 30 minutes of irradiation at 250 nm.

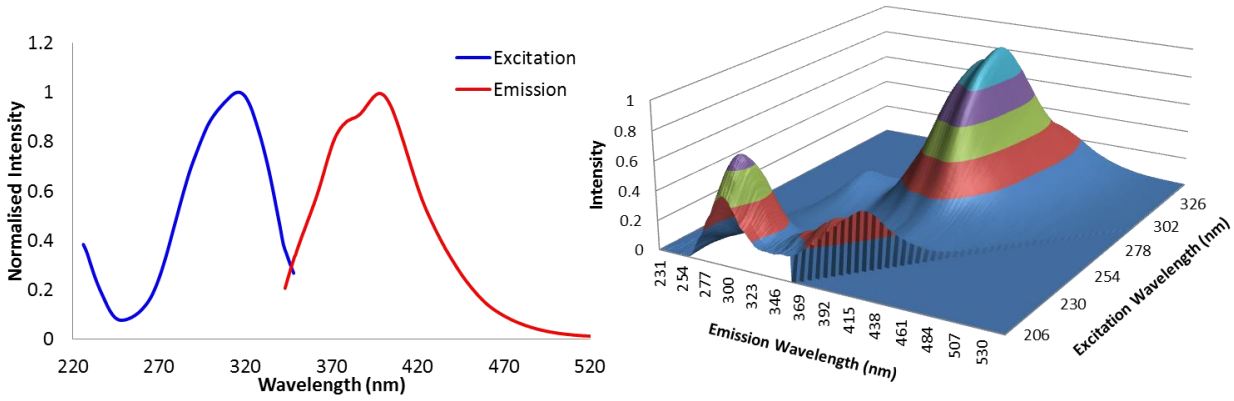

Figure 57. Excitation and emission peak maxima of **124** from the normalised excitation-emission 3D spectrum of **124.** Excitation and emission slit widths were set to 6 nm. Excitation spectrum obtained at λ_{em} 398 nm and emission obtained at λ_{ex} 318 nm.

Introduction of a methoxy-substituent on either aryl ring was also investigated. Substitution on R^1 did not lead to a new peak upon irradiation, however, the 3D excitation-emission spectrum showed the strongest similarity to 2,5-diphenyloxazole and strong emission intensity, resulting in the slit widths being lowered from 8 to 6 nm in order to prevent

saturation of the detector. The emission maximum was 370 nm, when irradiated at 222 and 310 nm. The UV absorbance had a λ_{max} of 273 nm, with no effect observed following irradiation (Figure 58).

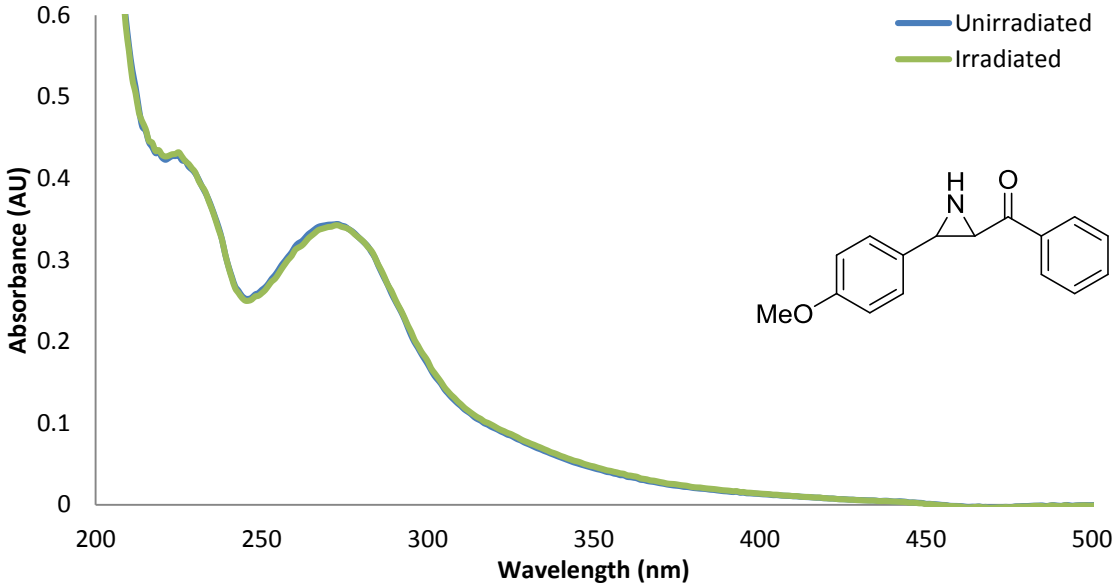

Figure 58. UV absorbance of **121** before and after irradiation.

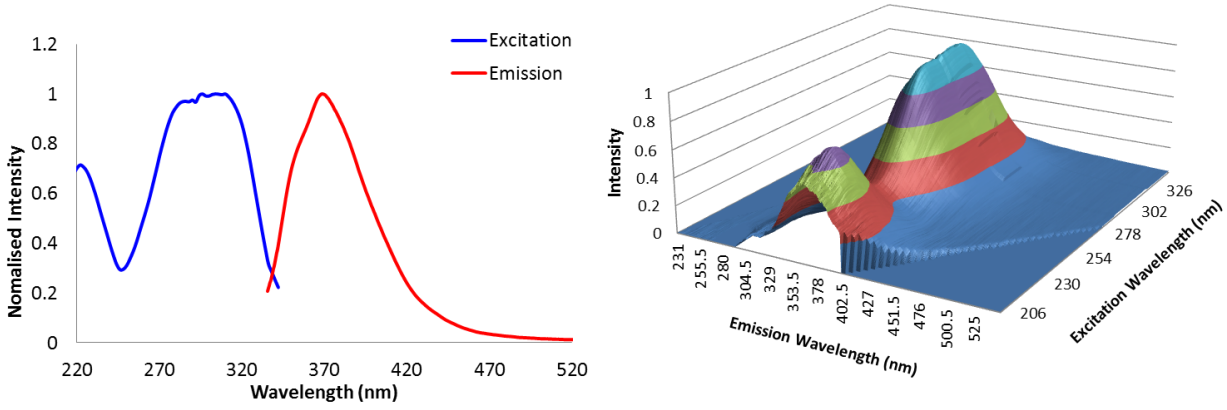

Figure 59. Excitation and emission peak maxima of **121** from the normalised excitation-emission 3D spectrum of **121.** Excitation and emission slit widths were set to 6 nm. Excitation spectrum obtained at λ_{em} 370 nm and emission obtained at λ_{ex} 310 nm.

Placement of a methoxy group for R^2 (**125**) yielded very different results when compared to **121**. In this case, 30 minutes of irradiation at 250 nm did form a new peak at 370 nm, and significantly reduced the absorbance of the λ_{max} at 286 nm (Figure 60). Following the 3D scan, the absorbance of the new peak decayed while the λ_{max} broadened and shifted slightly to 282 nm with an additional shoulder visible around 250 nm, indicative of a new species forming. The 3D emission-excitation spectrum displayed emission bands at 206 and 406 nm when excitation wavelengths were 310 and 326 nm, respectively. The emission bands were also indicative of oxazole formation.

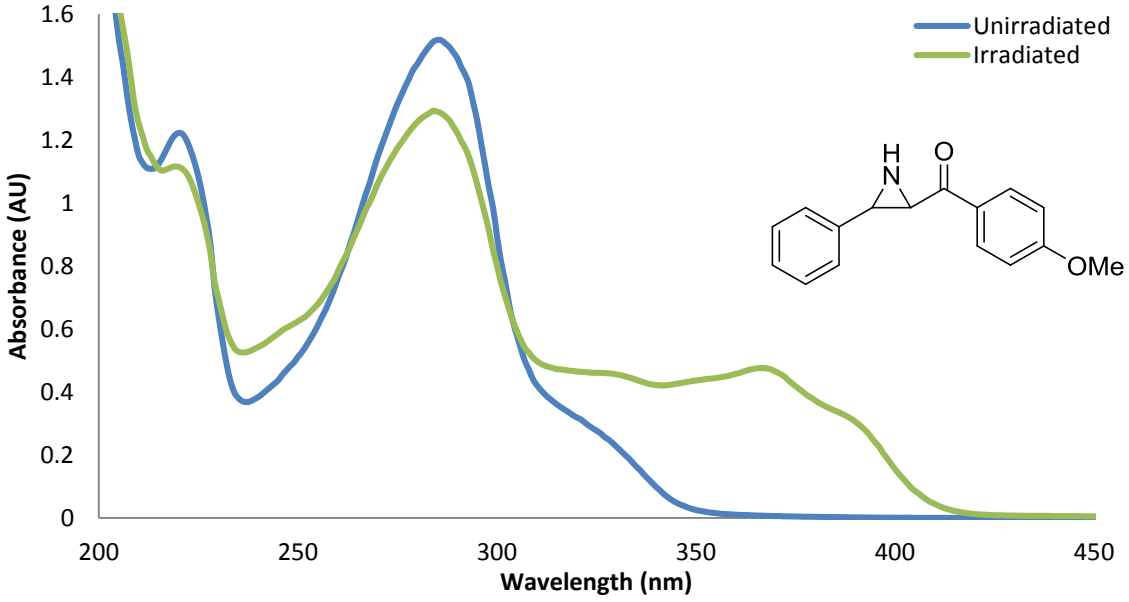

Figure 60. UV absorbance of **125** before and after irradiation.

Investigations of electron-withdrawing groups demonstrated the strong effect of a nitro group on both rings. Substitution for R^1, compound **122**, showed λ_{max}'s at 255 and 278 nm. Following irradiation, a new peak formed at 400 nm without any additional spectral features (Figure 61). No change in this peak was observed when the absorbance was measured after the 3D excitation-emission spectrum. The excitation-emission profile displayed an emission maximum of 367 nm when irradiated at 212 nm.

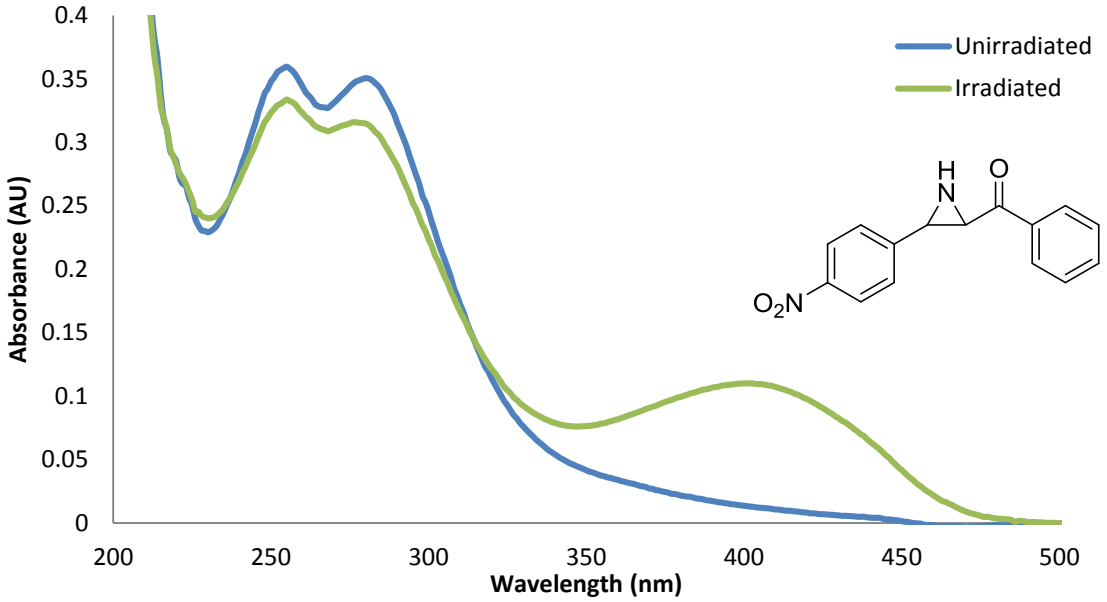

Figure 61. UV absorbance of **122** before and after irradiation.

Moving the nitro-group to R^2 (**126**) led to an absorbance spectrum with a λ_{max} of 272 nm (Figure 61). Upon irradiation, a new peak was also observed at 390 nm. However, this peak showed an increase in absorbance after the 3D spectrum was obtained, indicating the new species had yet to reach saturation and was sensitive to the various excitation wavelengths. The excitation-emission spectrum was similar to **122**, with a blueshift of the emission band to 318 nm when irradiating at 210 nm (Figure 62). Additionally, the nitro-substituted compounds were measured at 8 nm slit widths and had low emission intensities compared with the obtained spectra measured at 6 nm for the other substrates. Both nitro-substituted aziridines did not display a characteristic excitation-emission spectrum similar to oxazole, suggesting these compounds may not undergo the same mechanism and were not able generate diaryloxazoles. The lack of diaryloxazole formation may be due to the strongly electron-withdrawing nature of the nitro-substituent, which deactivates the ring preventing product formation.

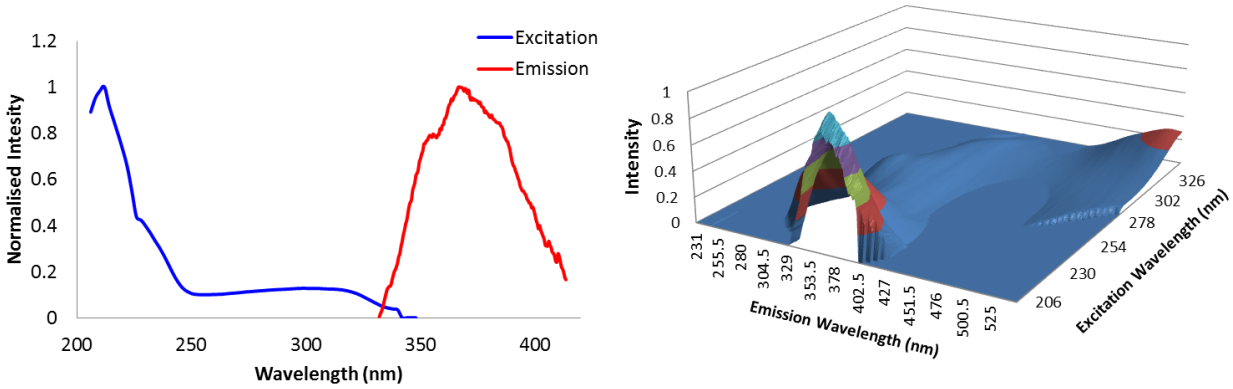

Figure 62. Excitation and emission peak maxima of **122** from the normalised excitation-emission 3D spectrum of **122.** Excitation and emission slit widths were set to 8 nm. Excitation spectrum obtained at λ_{em} 365 nm and emission obtained at λ_{ex} 212 nm.

Changing the electron withdrawing group to a halogen gave similar results to the methyl substituted aziridines. A difference in 10 nm was observed between the two *para*-chlorinated aziridines, where R^1 and R^2 gave λ_{max} values of 250 and 260 nm, respectively (Figure 63). Both compounds formed a new species at 365 nm upon irradiation, with decreased absorbance of their respective λ_{max} values. The excitation-emission profiles were similar for compounds **123** and **127**. Emission maxima were observed at 305 and 405 nm when excitation took place at 216 and 312 nm, respectively for **123**. Excitation of **127** at 214 nm led to emission at 299 nm, while excitation at 312 nm provided an emission of 400 nm (Figure 64). Comparing the emission and excitation profiles of the two chlorinated aziridines with 2,5-diphenyloxazole showed similar spectral features, indicative of **123** and **127**'s ability to form oxazole.

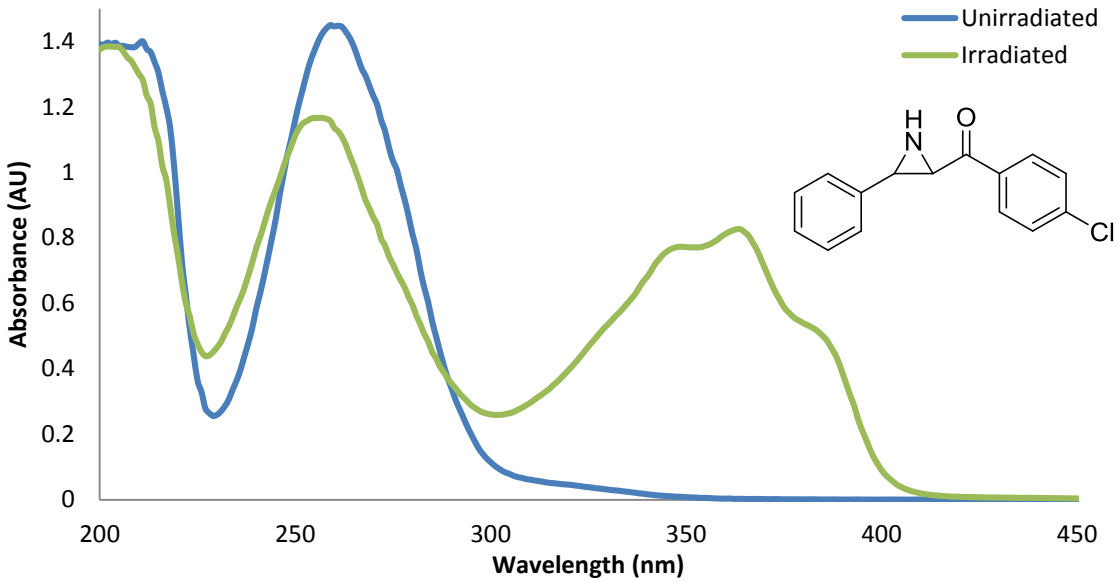

Figure 63. UV absorbance of **127** before and after irradiation.

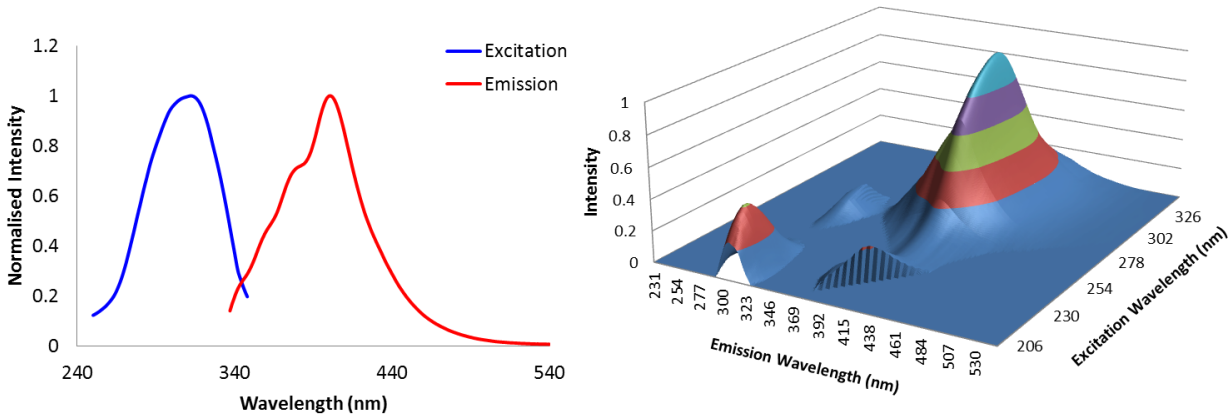

Figure 64. Excitation and emission peak maxima of **123** from the normalised excitation-emission 3D spectrum of **123.** Excitation and emission slit widths were set to 6 nm. Excitation spectrum obtained at λ_{em} 400 nm and emission obtained at λ_{ex} 312 nm.

Introduction of a halogen on both rings was also studied. A λ_{max} of 264 nm was observed for compound **128**. Irradiation led to the formation of a new peak at 370 nm, which was no longer visible by UV following the 3D spectrum acquisition (Figure 65). A slight decrease in the λ_{max} absorbance was also seen as a result of the irradiation. Due to the peak

shape, it may also be assumed that the new absorbance feature at 370 nm contained more than one species.

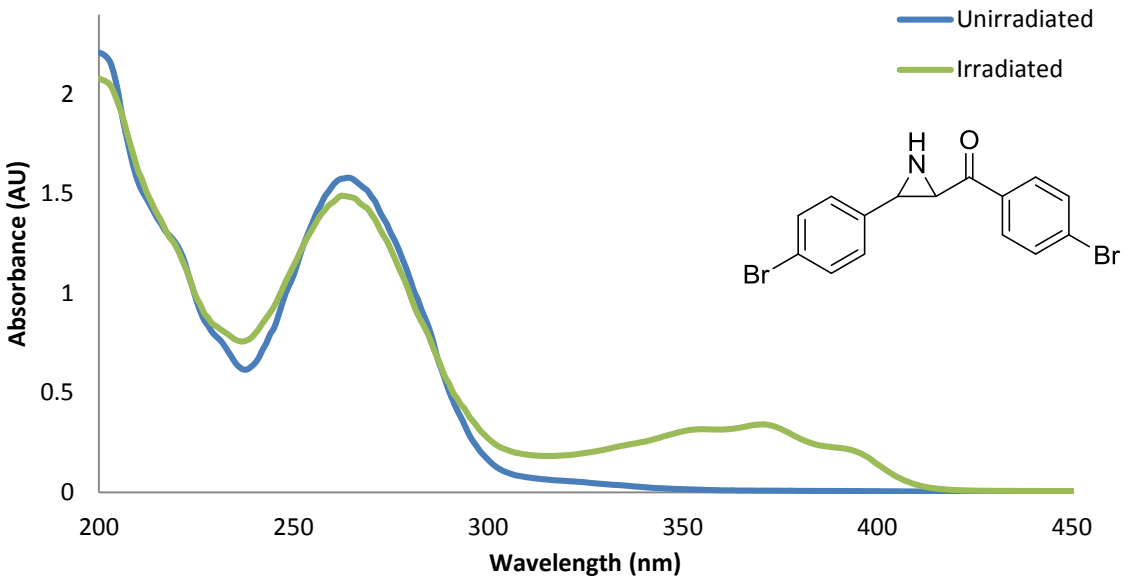

Figure 65. UV absorbance of **128** before and after irradiation.

When obtaining the excitation-emission profile of **128**, a strong emission was measured resulting in reduction of the slit widths. Two main emissions were observed at 350 and 375 nm, when excitation wavelengths were 230 and 324 nm, respectively (Figure 66). The emission profile suggested no additional species were present as the excitation wavelengths all led to the same emission. In addition to the excitation-emission spectrum having a similar profile to 2,5-diphenyloxazole, the emission intensity also indicated the aziridine formed oxazole, due to its high emission intensity at low concentrations.

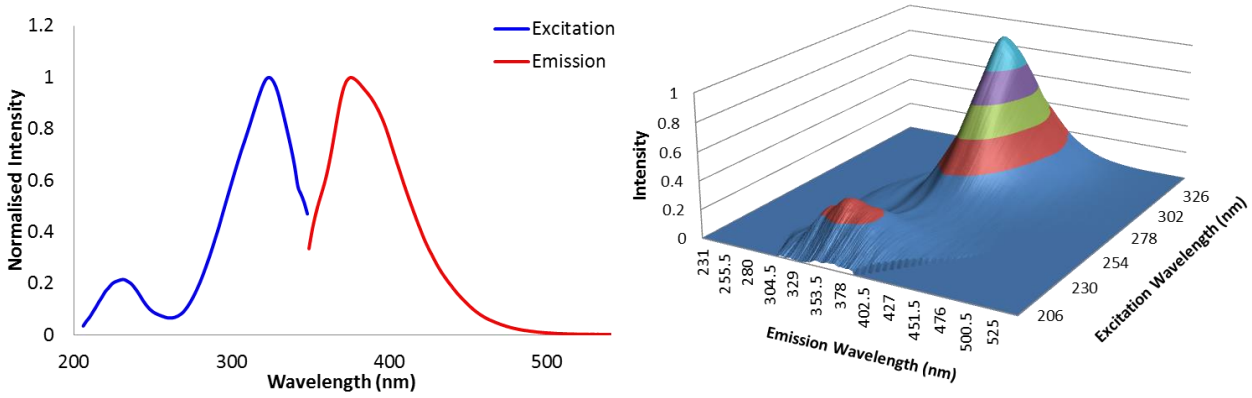

Figure 66. Excitation and emission peak maxima of **128** from the normalised excitation-emission 3D spectrum of **128.** Excitation and emission slit widths were set to 6 nm. Excitation spectrum obtained at λ_{em} 375 nm and emission obtained at λ_{ex} 324 nm.

Aromatic substitution effects on aziridine photochemistry were confirmed with spectroscopic measurements. As the new peak formed by irradiation was assumed to be an azomethine ylide, it was suggested that the new absorbance features from the irradiated aziridines were intermediates which formed diaryloxazoles. Generally, most electron-donating and electron-withdrawing groups assisted in the formation of oxazole, with starting aziridine still present. However, addition of a methoxy group on R^1 showed a strong effect where no intermediate peak was observed following irradiation and full conversion to oxazole appeared to have taken place. A strong electron-withdrawing group, NO_2, showed significant inhibition of the formation of oxazole. This may be due to a nitro-group's ability to reduce the fluorescence quantum yield, as quantum yield indicates the how efficiently absorbed photons are used by the molecule.[98] While the quantum yield was not measured for these compounds, it may still be proposed that this reduction in photon efficiency resulted in the nitro-substituted aziridines inability to make oxazoles efficiently, in comparison to the other substituted aziridines. The dibrominated aziridine also demonstrated the ability to readily form oxazole. This may be due to the heavy atom effect, where the probability of intersystem crossing is increased by increasing spin orbit coupling.[98] When increasing the spin orbit coupling, mixing takes place between states of different multiplicities, making forbidden transitions more accessible.

3.6. Mechanistic Studies

The hypothesis that the new azomethine ylide/360 nm feature, generated by irradiation, was the intermediate leading to diaryloxazole formation was investigated by an excitation wavelength variation experiment. The experiment was designed to form the new feature through irradiation at 250 nm, and was followed by direct excitation of the azomethine ylide by irradiating at 340, 360, and 380 nm. A 150 μM solution of **77** in MeCN was first irradiated for 33 minutes at 250 nm with excitation and emission slit widths at 15 and 10 nm, respectively. The same sample was then irradiated for 1 hour at 340 nm. The process was repeated, irradiation at 250 nm followed by irradiation at a higher wavelength, for excitations at 360 and 380 nm. Monitoring of the emission intensity during the direct excitation of the 360 nm peak demonstrated an increase in intensity when the excitation wavelength was increased. The absorbance was measured following both excitations for comparison (Figure 67). It was found that the 360 nm peak showed the opposite relationship, where increasing wavelength led to a decrease in absorbance. The higher excitation wavelength led to the consumption of the azomethine ylide, which was observed by a decrease in absorbance and an increase in emission, indicating more oxazole was present in the solution.

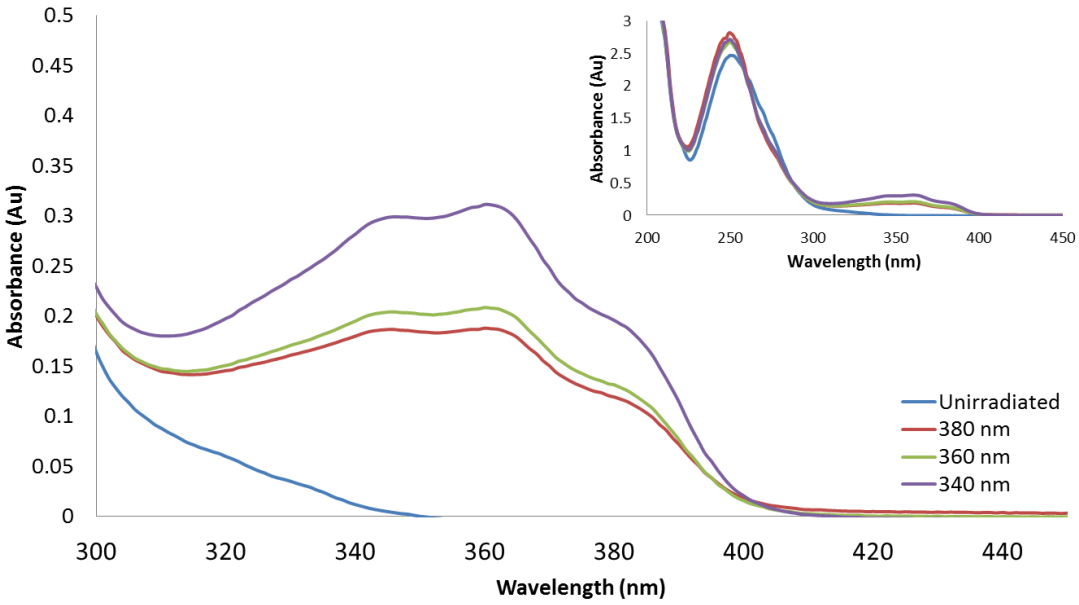

Figure 67. UV absorbance measurements of 150 µM **77** in MeCN following irradiation at 340, 360, and 380 nm after an initial 250 nm irradiation. Inset showing full absorbance spectrum.

Previous results demonstrated decreased absorbance of the 360 nm feature and increased emission when λ_{ex} was 380 nm. As the observed emission of 2,5-diphenyloxazole is around 380 nm, an autocatalytic mechanism for 2,5-diphenyloxazole formation was suggested. A 150 µM solution of **77** in MeCN was irradiated at 300 nm for 1 hour, another wavelength found to form 2,5-diphenyloxazole. This was compared with the irradiation of the same solution doped with 2 mol% of 2,5-diphenyloxazole. The emission was monitored at 380 nm for both solutions. The sample with only aziridine emitted at an intensity around 17 and steadily dropped until a plateau was reached. The emission curve then began to increase (Figure 68). This demonstrated the solution had absorbed enough light to build up an accumulation of an emitting species, indicated by the plateau, which was then beginning to emit light from the formed oxazole.

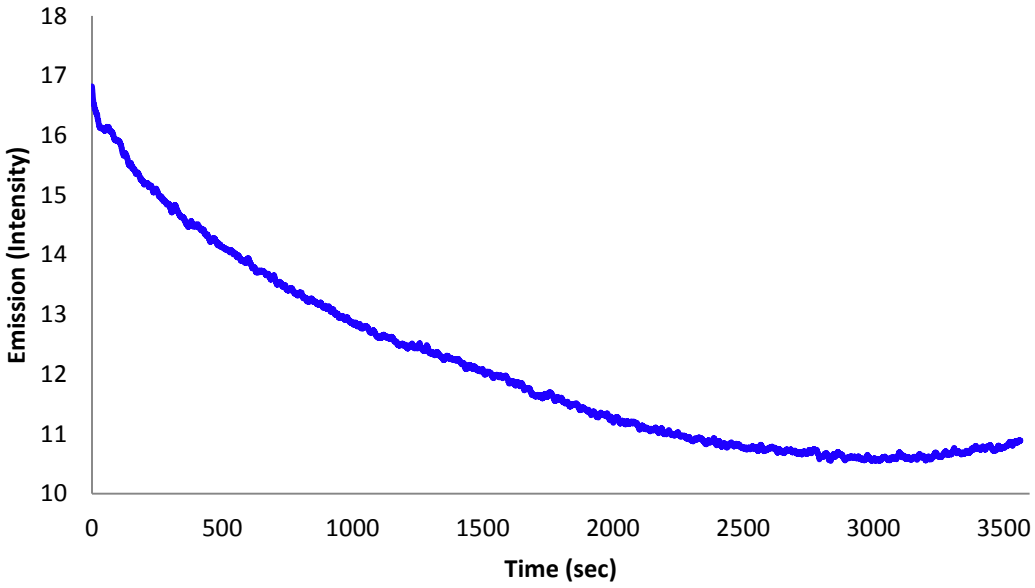

Figure 68. Irradiation of 150 μM **77** in MeCN at 300 nm for 1 hour with excitation and emission slit widths of 15 and 2.5 nm, respectively.

When doping the aziridine solution with 2 mol% 2,5-diphenyloxazole, a drop in emission was observed. Under the same irradiation conditions, the emission decreased from 700 to 200 in intensity (Figure 69). This suggested the emission from the oxazole was being absorbed by the aziridine in solution, in order to make more oxazole. Had the doping with oxazole not affected the photochemical reaction, only the emission from the oxazole would have been observed, thus the drop in emission confirms it was being absorbed by the aziridine. The two experiments showed similar decay rates, as both were absorbing the emitted light from 2,5-diphenyloxazole. From other experiments (*vide infra*, Chapter 4) it was shown a small amount of 2,5-diphenyloxazole was formed. As only 2 mol% was used for the autocatalytic experiments, approximately 3 μM of 2,5-diphenyloxazole, the amounts present in both systems may be similar, causing the similarity in rates of decay.

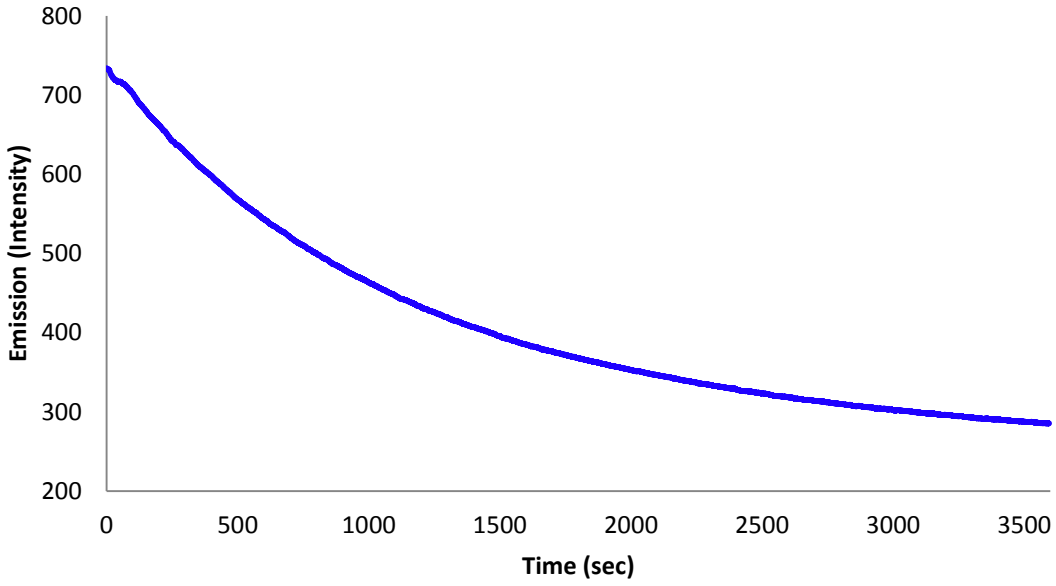

Figure 69. Irradiation of 150 µM **77** doped with 2 mol% oxazole in MeCN at 300 nm for 1 hour with excitation and emission slit widths of 15 and 2.5 nm, respectively.

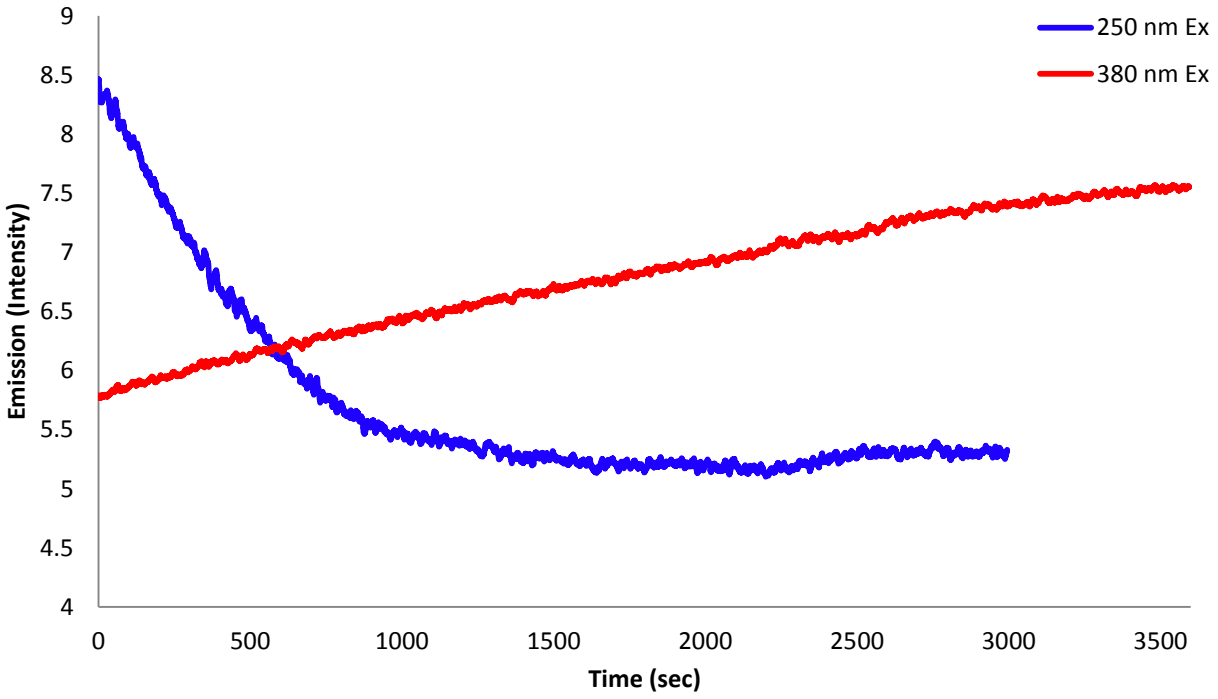

Figure 70. Emission monitoring at 400 nm of the irradiation of 150 µM **77** in MeCN at 250 nm for 50 minutes, followed by 1 hour at 380 nm. Excitation and emission slit widths of 15 and 5 nm were used, respectively.

A further experiment was carried out to confirm the mechanism was autocatalytic. The purpose of this experiment was to input the wavelength of light emitted by oxazole in order to determine if this was the driving force in generating more product. For this experiment a sample of 150 μM **77** was irradiated at 250 nm for 50 minutes, as this wavelength generates the 360 nm species. This was followed by irradiation at 380 nm for 1 hour, the emission wavelength of 2,5-diphenyloxazole. The 250 nm irradiation showed a decrease in emission, as the aziridine absorbed the excitation light (Figure 70). Subsequent irradiation at 380 nm displayed an increase in the observed emission, indicative of more oxazole being formed. An additional experiment was carried out by irradiating the **77** at 380 nm for 1 hour (Figure 71). This wavelength did not increase the emission intensity, supporting the requirement of the intermediate species to be formed in order to make 2,5-diphenyloxazole.

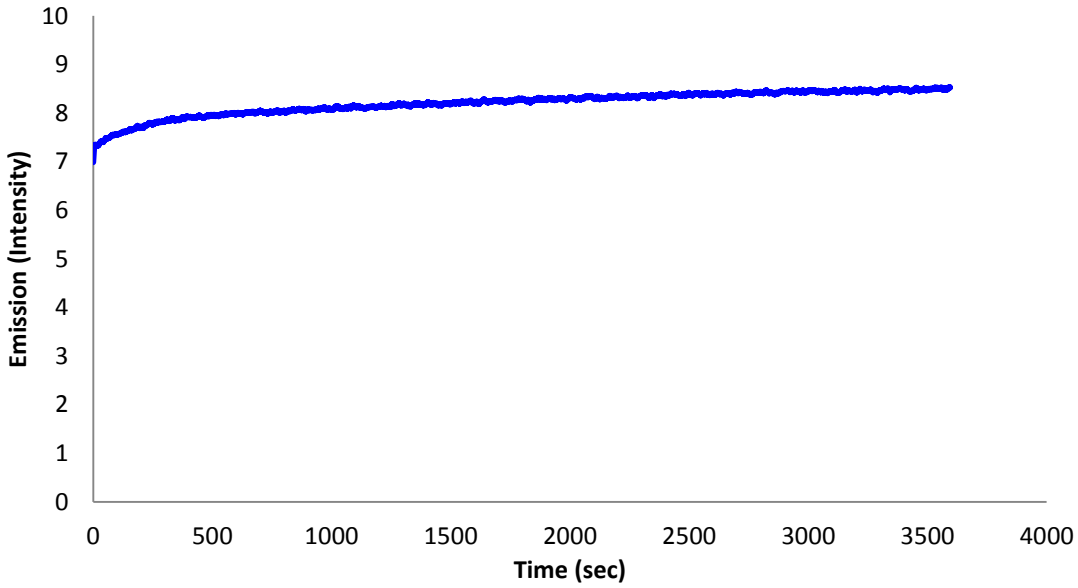

Figure 71. Emission monitoring at 400 nm of the irradiation of 150 μM **77** in MeCN at 380 nm for 60 minutes, showing minimal increase in emission intensity. Excitation and emission slit widths of 15 and 5 nm were used, respectively.

The proposed autocatalytic mechanism is summarised in Scheme 58. Irradiation of **77** led to formation of an azomethine ylide (**104**). Continued irradiation allowed **104** to cyclise and form **73**. Once formed, **73** emits predominantly at 380 nm. As shown in Figure 67, the azomethine ylide was consumed and generated more **73** when irradiated at 380 nm.

Therefore, it may be suggested that an autocatalytic cycle was present where the emission from **73** allows more conversion of **104** to 2,5-diphenyloxazole.

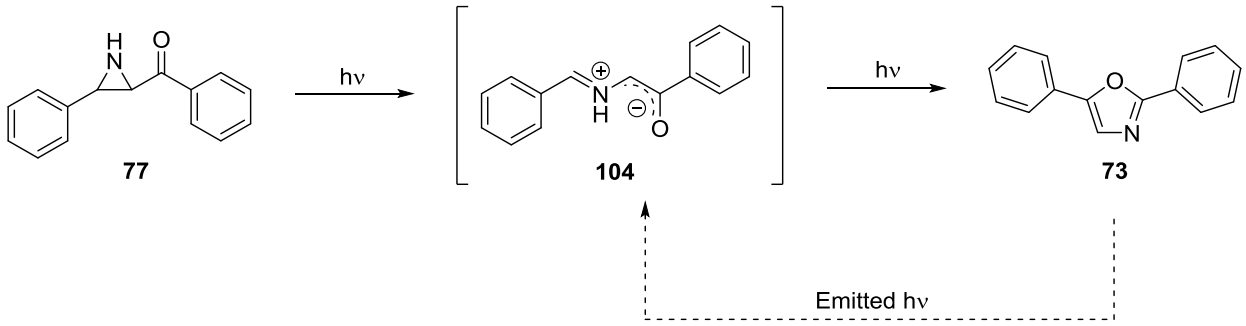

Scheme 58. Proposed autocatalytic cycle for the formation of 2,5-diphenyloxazole.

3.7. Conclusions

Irradiation of **77** demonstrated the formation of an azomethine ylide with an absorbance centred at 360 nm. Generation of this species demonstrated wavelength, concentration, and time dependencies. The decay of this species was also monitored and showed an initial decay followed by growth in absorbance after 29 hours. Formation of the azomethine ylide revealed an exponential growth which was not coupled to the observed linear growth of the fluorescence band centred at 400 nm.

Fluorescence studies supported the TD-DFT calculations through confirming the formation of 2,5-diphenyloxazole **73** by *NH*-aziridine **77**. These studies also demonstrated the photochemical reactivity of aziridine derivatives and their ability to form 2,5-diphenyloxazole. Electron-donating and electron-withdrawing substituents proved to affect the formation of diaryloxazoles, with the formation appearing to be inhibited by nitro-substitution.

A photochemical mechanistic model was proposed with a potential to apply to a synthetic route. Irradiation of **77** using 250 then 380 nm, supported the hypothesis of an autocatalytic mechanism and the potential to use two wavelengths to generate more product on a synthetic scale. Combination of wavelengths assisted in the consumption of the azomethine ylide which led to more observed emission, the result of more **73** being formed. Magnetic field effects were also investigated, which were potentially observed under steady-state conditions. Additional work to optimise the conditions for MFE studies would be required.

Chapter 4: Photochemical Batch Reactor Studies

Table of Contents

4.1. Photoreactor Studies

4.1.1. Initial Studies

Having carried out experiments on a small scale spectroscopically, the scalability of the reaction was then investigated for synthetic utility. Initial studies used a medium pressure 400 W mercury lamp in an immersion well photochemical reactor, as shown in Figure 72. Emission from this lamp consists of a wide range of lines with the most prominent being at 313, 366, 405, and 550 nm.[99]

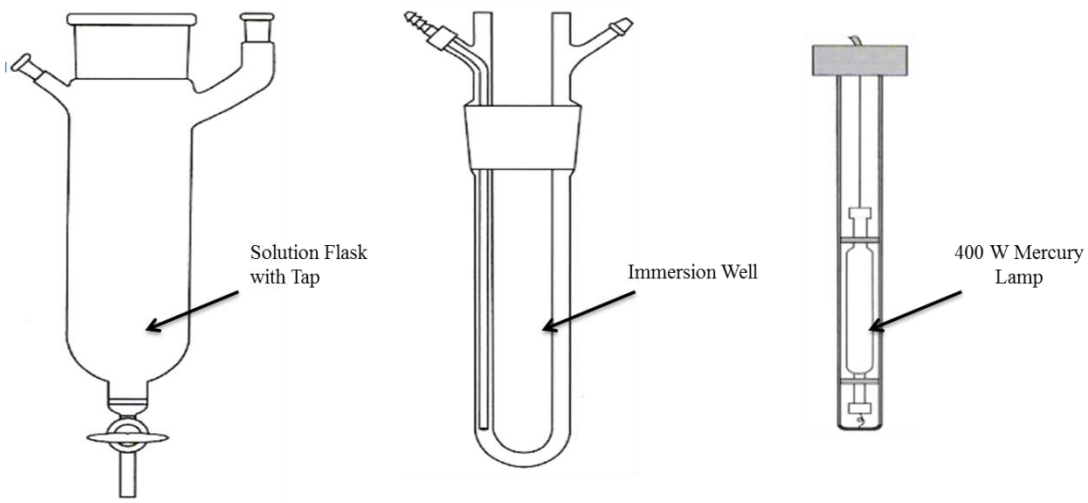

Figure 72. Photochemical reactor setup used for scale-up.

A non-degassed solution of 135 μM *NH*-ketoaziridine **77** in MeCN was irradiated while aliquots were taken every 30 seconds for 3 minutes. This was done to monitor the formation of the azomethine ylide/360 nm peak using this setup. The maximum absorbance was obtained at 2.5 minutes (Figure 73). The absorbance of the 250 nm peak was also increased by 1 absorbance unit during the course of the reaction. Despite the 360 nm peak still being formed on a larger scale, the ratio between the 360 and 250 nm peaks was not as large as that observed in spectroscopic studies. Spectroscopic measurements provided a 360/250 nm peak ratio of 0.62, while the photoreactor only reached a maximum of 0.11.

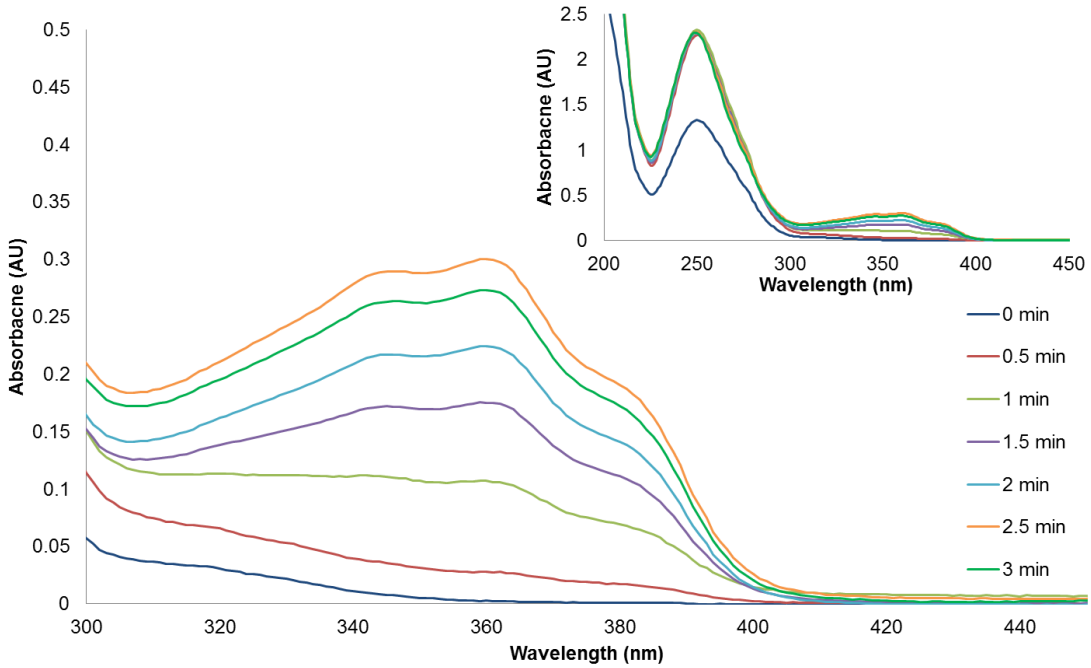

Figure 73. Initial studies measuring the absorbance of a solution of **77** irradiated in a large scale photoreactor.

Longer irradiation times of the solution revealed three isosbestic points at 213, 238 and 281 nm, as also observed in spectroscopic measurements (Figure 74). The 360 nm peak reached a maximum at 2 minutes, which was then followed by a decrease in absorbance for the next time point. The peak at 250 nm grew until 3 minutes, as previously observed, then decreased in absorbance over 15 minutes. As the peak decreased, it also shifted to a lower wavelength creating a new peak around 230 nm. From this data it may be supported that a new product was being formed as new spectral features were observed.

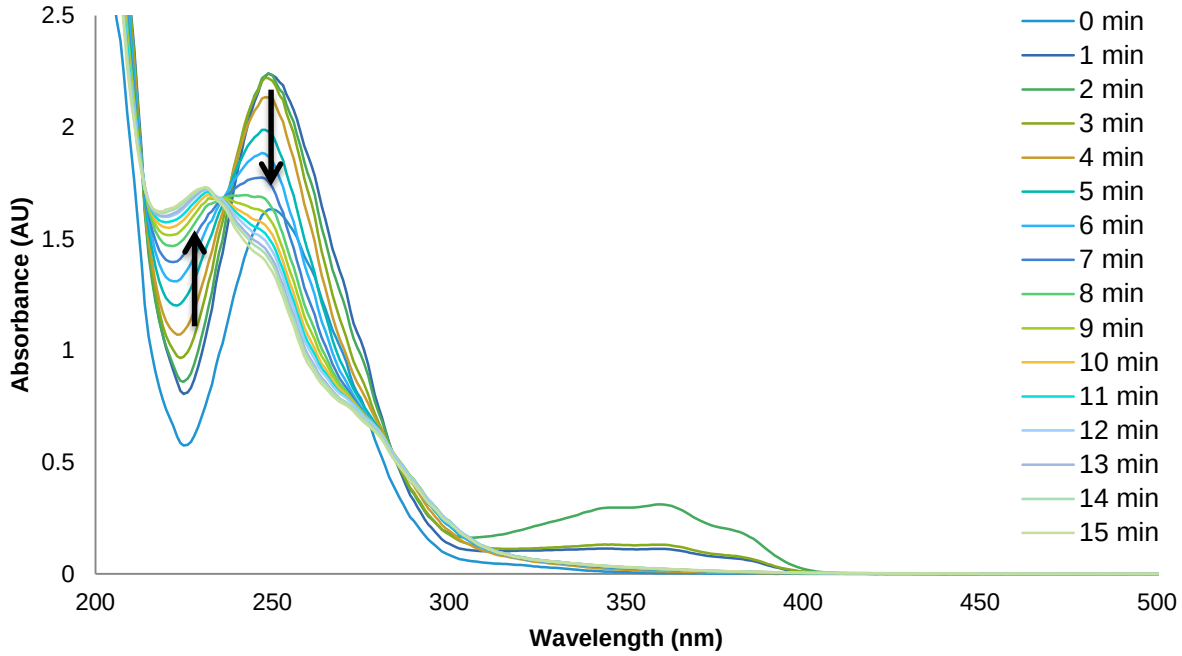

Figure 74. Absorbance measurements taken over 15 minutes from the photoreactor showing a shift in the 250 nm peak, indicating a new product was formed.

In addition to UV analysis, ^{1}H NMR spectra were also obtained following irradiation. While UV traces allowed for some characterisation, NMR results were more complex, as shown in Figure 75. Aziridine appeared to have been consumed, as the characteristic NH and CH ring protons were not visible. While aromatic and aldehyde proton peaks were visible, no other structural features could be distinguished by NMR, only a complex reaction mixture. A solution of 2,5-diphenyloxazole (**73**) was subjected to the same conditions in the photoreactor to determine if the proposed product was stable under the same conditions. The oxazole irradiation also showed a complex NMR spectrum, indicating a lack of stability when subjected to the same irradiation environment.

Comparing the two independent irradiations of aziridine and oxazole suggested that the mercury lamp was too powerful and causing fragmentation of the molecules. Analysing the irradiated aziridine solution by TLC showed over 8 compounds were present in the solution, with no spot corresponding to the oxazole. In order to optimise the reaction, multiple variables were investigated. As the molecules appeared to be sensitive to the lamp intensity, and based on wavelength spectroscopic studies, a lower intensity and wavelength specific lamp was proposed. Initial experiments were also exposed to oxygen,

which was also thought to be affecting the reaction. Subsequent experiments were carried out investigating these variables.

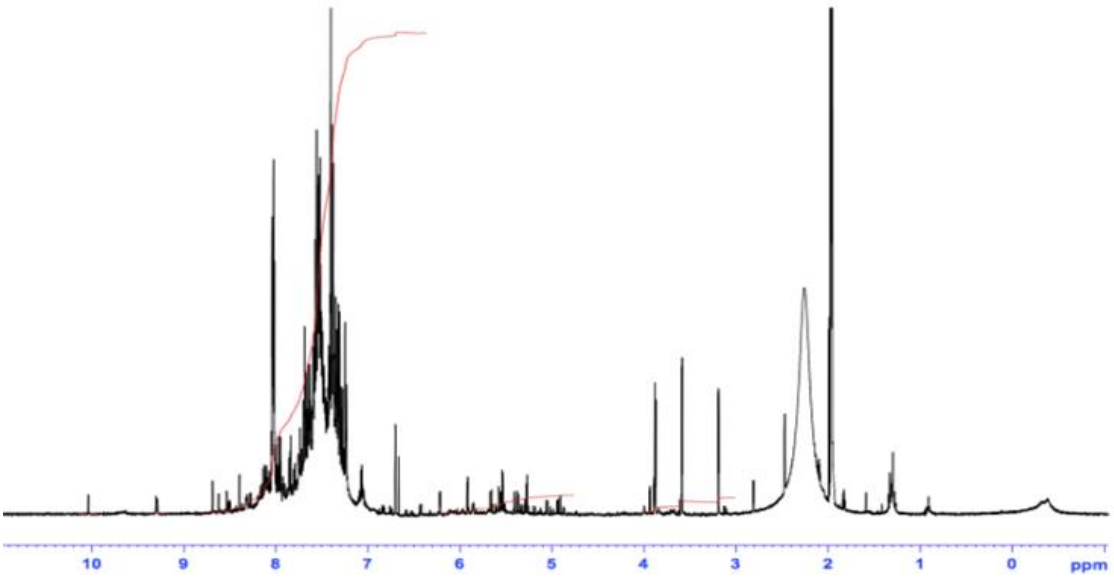

Figure 75. ^{1}H NMR spectrum of irradiated sample of 135 µM aziridine (**77**) following 15 minutes with a medium pressure mercury lamp.

4.1.2. Lamp and Oxygen Studies

A UVC lamp was provided by Dr. Luke Elliot from the University of Bristol. The Philips 36 W UVC PL-L lamp emits predominantly around 254 nm with a power of 12 W. Using this low pressure mercury lamp, it would be possible to test whether the 400 W medium pressure lamp previously used was fragmenting the molecule. In order to determine the effect of oxygen, degassed and non-degassed MeCN were used. Oxygen was an important variable to monitor, as it has the ability to quench excited states. Organic solvents which have been equilibrated with air may have 0.002 to 0.003 M amounts of oxygen, an amount high enough to quench 90% of long-lived triplets.[99]

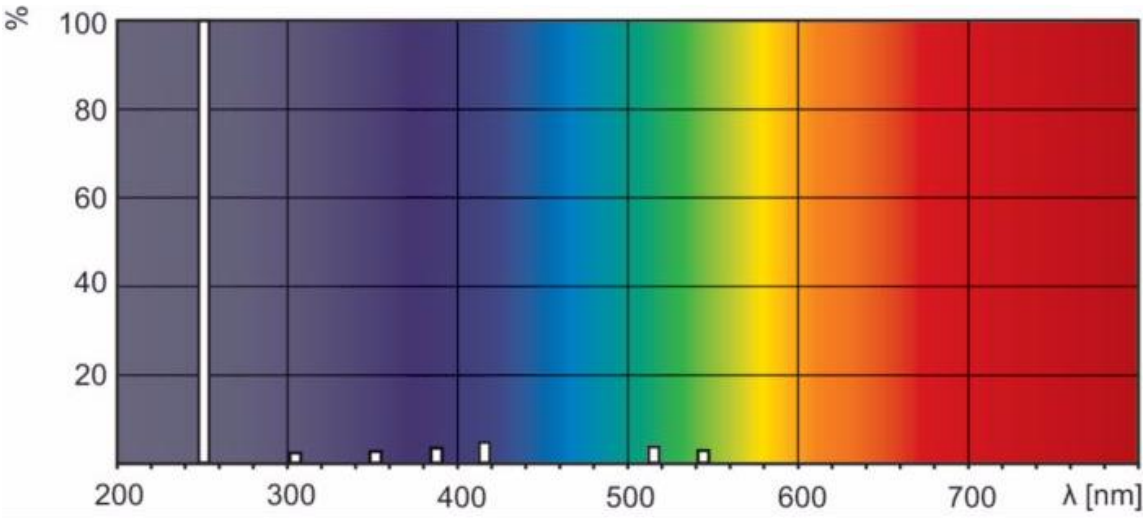

Figure 76. Wavelength distribution of the Philips 36 W UVC PL-L lamp used for these studies. Image reproduced from Philips.[100]

Initial studies showed non-nitrogen purged reactions had more defined NMR spectra, as compared to the 30 minute N_2 purged reactions. However, it was still not possible to extract meaningful structures from this data. Further investigations were carried out by stopped-flow fluorescence irradiating at 300 nm and measuring the emission over 3 hours, with slit widths at 5 nm, to identify whether purging the solution with nitrogen led to a more efficient reaction. Irradiation of the sample at 300 nm in the presence of oxygen revealed two reaction rates, indicating two processes were taking place (Figure 77). The rate of k_2 with a positive amplitude refers to the initial decay taking place in the observed emission. The second process took place at nearly half the rate and was approaching saturation. When purging the sample with nitrogen prior to irradiation, the data fitted a single exponential, suggesting one process was occurring (Figure 78). The rate was nearly 8 times slower when no oxygen was present in the system. Additionally, the reaction was not close to approaching saturation. As both plots contained negative amplitudes of similar values, it may be suggested that both reflect the same process, with oxygen increasing the rate.

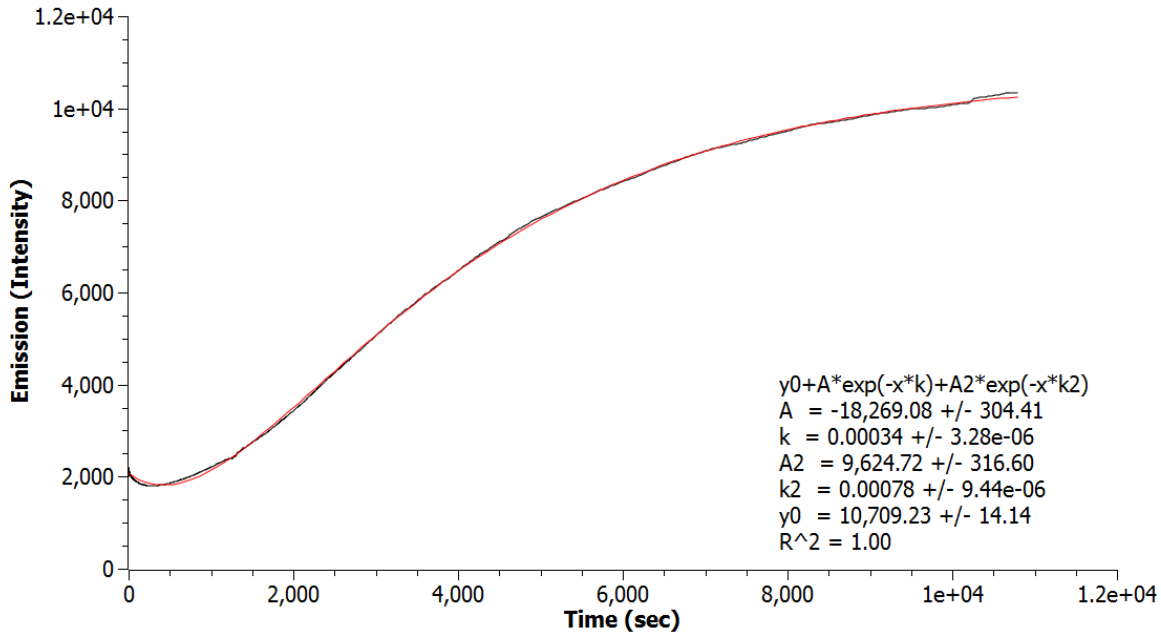

Figure 77. Relative emission measured by stopped-flow fluorescence from the irradiation at 300 nm of a 150 µM solution of **77** in MeCN when exposed to air.

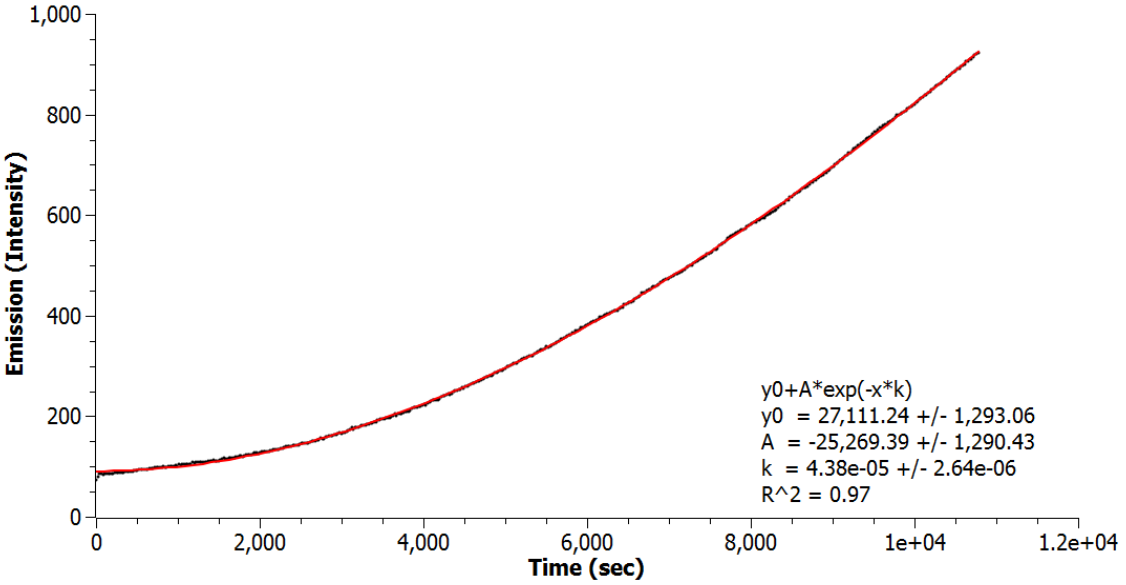

Figure 78. Relative emission measured by stopped-flow fluorescence from the irradiation at 300 nm of a 150 µM nitrogen purged solution of **77** in MeCN.

4.1.3. Analysis of Batch Reactions

4.1.3.1. GC-MS Analysis

While it was confirmed that nitrogen purging led to a single process being measured, a comparison was conducted using GC-MS as an analytical method. One obstacle was the concentration of the solution being irradiated. Spectroscopic characterisation showed low substrate concentrations led to higher conversion of starting material. However, this would have required large amounts of solvent to obtain small mass of product making lower concentrations synthetically unviable, for example 13 mg in 400 mL of MeCN was 150 µM. Experiments were carried out at 240 µM, as UV absorbance showed the 360 nm feature was still produced at this concentration in the reactor. A GC-MS run of a 30 minute reaction demonstrated **73**, benzaldehyde (**76**), benzonitrile (**129**), and acetophenone (**103**) were all present in the reaction mixture when comparing the mass spectra to the National Institute of Standards and Technology (NIST) database.

Table 6. Concentrations obtained by GC-MS of oxazole and side-products found during the UVC irradiation of 240 µM of **77** under air.

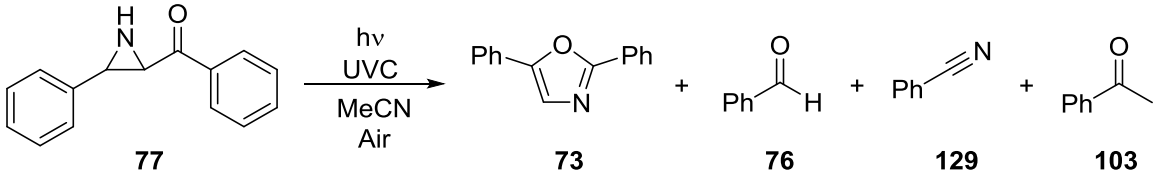

77 **73** **76** **129** **103**

Time (min)	Benzaldehyde [µM]	Benzonitrile [µM]	Acetophenone [µM]	Oxazole [µM]
1	23	0	0	52
3	30	7	6	9
4	39	7	0	12
5	30	9	5	0

Following acquisition of calibration curves, reactions were carried out under air and nitrogen to determine the effects on the amounts of 2,5-diphenyloxazole, benzaldehyde, benzonitrile, and acetophenone formed. A calibration curve was also generated for **77**; however, it was only observed in the initial aliquots prior to irradiation. The solution was irradiated in the photoreactor using a UVC lamp with 1 mL aliquots taken at regular time intervals. Following irradiation, the solution was yellow in colour. Within the first

minute, 52 µM of **73** and 23 µM of benzaldehyde were observed (Table 6). The amount of **73** decreased to 12 µM at 4 minutes and was no longer visible after 5 minutes. The amount of benzaldehyde and benzonitrile increased with the decrease in **73** concentration, in addition to the presence of a low amount of acetophenone. It may be suggested that **73** was unstable under these irradiation conditions, and continued irradiation of **73** led to fragmentation of the molecule into benzaldehyde, benzonitrile, and acetophenone. A peak was also observed at 4 minutes with a retention time of 14.24 minutes which was attributed to benzamide when compared with the NIST database. Additionally, the presence of benzaldehyde was suggestive of a Norrish Type I reaction, which involves cleavage of a bond α to a carbonyl to generate a radical (Scheme 59).[98]

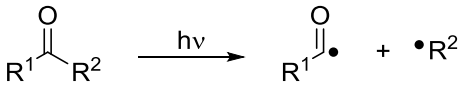

Scheme 59. General scheme for a photochemical Norrish Type I reaction.

The reaction was then carried out using the same conditions following 20 minutes of nitrogen purging. Within the first minute, 65 µM of **73** had formed, in addition to benzaldehyde and benzonitrile at 28 and 8 µM, respectively (Figure 79). As with previous reactions, the solution was yellow in colour after irradiation. Following the first minute, concentration of **73** continued decreasing throughout the reaction, with a final concentration of 8 µM after 1 hour of irradiation. After 5 minutes acetophenone was observed in conjunction with high amounts of benzaldehyde and a larger amount of benzonitrile. The highest amount of benzaldehyde seen was 71 µM at 10 minutes. This carried on decreasing throughout the remainder of the reaction. As the concentrations of benzonitrile and acetophenone continued increasing while **73** decreased, in agreement with the air exposed reaction, it may be suggested that continued irradiation led to fragmentation of the molecule into the two components. An additional observation was the increased stability of the oxazole during irradiation while under nitrogen, as the reaction under air no longer displayed 2,5-diphenyloxazole at 5 minutes. As previously mentioned, this lack of stability suggested the reaction was oxygen sensitive due to the presence of long-lived triplet excited states. These triplet states may be due to the presence of the aromatic ketone in the ketoaziridine, as photochemistry of aromatic ketones is governed by triplet-state processes due to their intersystem crossing being efficient. The combination of forming triplet states efficiently, having a small energy gap between the singlet and triplet

states, and absorbing at longer wavelengths makes aromatic ketones useful as triplet sensitisers.[98]

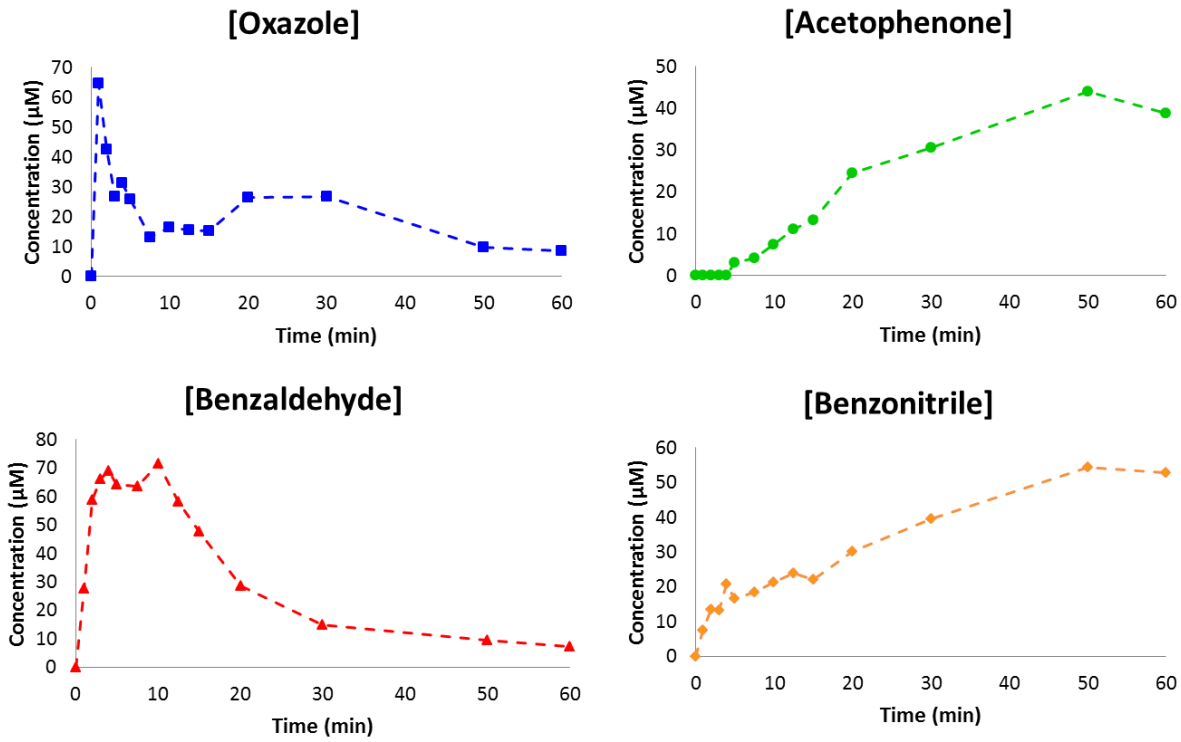

Figure 79. GC-MS analysis plots monitoring the concentrations of 2,5-diphenyloxazole (**73**), benzaldehyde (**76**), acetophenone (**103**), and benzonitrile (**129**) vs. time for the UVC irradiation of **77** under nitrogen.

In order to confirm the fragmentation of 2,5-diphenyloxazole was taking place with continued irradiation, a 240 µM solution of **73** in MeCN was irradiated with UVC light for 3 hours under nitrogen. Analysis of the final reaction mixture showed benzaldehyde and acetophenone, with the majority of the sample being 2,5-diphenyloxazole. When comparing to the previous irradiations with the medium pressure lamp, a power dependence may be suggested as the UVC lamp did not completely fragment the molecule. As benzaldehyde and acetophenone were still observed in the reaction mixture, it may be proposed that the oxazole formed in the aziridine reactions did fragment with continued irradiation.

A control experiment was carried out to compare Padwa's previous research on the photochemical reactivity of *tert*-butyl substituted aziridine (**72**).[77] Synthesis of **72** was carried out by reacting *trans*-chalcone with 5 equivalents of freshly distilled *tert*-butyl

amine and 1 equivalent of iodine in diethyl ether over 72 hours. The purified compound was recovered in 30 % yield (Scheme 60).

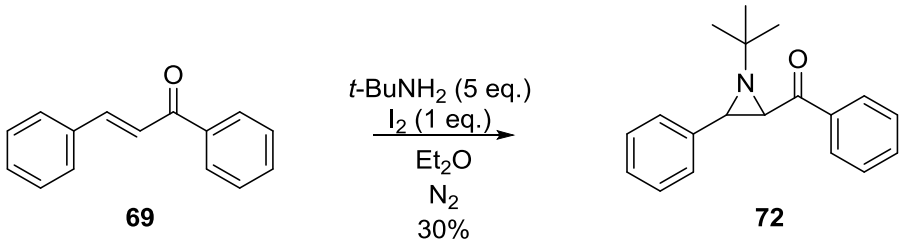

Scheme 60. Synthesis of t-butyl-substituted aziridine (**72**).

Padwa's conditions involved 2 hours of irradiation of 3.22 mM **72** in pentane using a mercury lamp with Pyrex filter. Using a UVC lamp and nitrogen purged 240 µM solution of **72** in MeCN, the sample was irradiated for 1 hour and samples were taken for GC-MS analysis throughout. The main compounds observed were 2,5-diphenyloxazole (**73**), benzaldehyde (**76**), benzamide (**82**), *N*-(*tert*-butyl)benzamide (**130**), and imine (**75**) (Scheme 61). The highest amount of **73** was observed at 50 minutes with a concentration of 55 µM. Imine **75** was first observed at 2 minutes, with the highest peak area observed at 60 minutes.

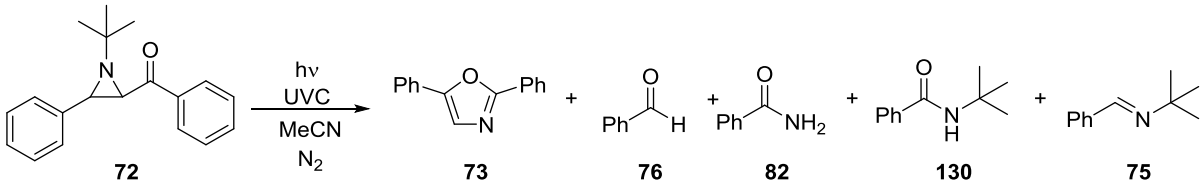

Scheme 61. UVC irradiation of **72** and identified product by GC-MS.

Samimi *et al*. described the thermal conversion of bromine and chlorine *N*-substituted ketoaziridines into 2,5-diphenyloxazoles.[59] *N*-Chlorosuccinimide (NCS) was used to chlorinate **77** in dimethoxyethane and water (80:20). (1-Chloro-3-phenylaziridin-2-yl)(phenyl)methanone (**131**) was isolated in 57% yield. A 240 µM nitrogen purged solution of **131** in MeCN was irradiated with a UVC lamp over 1 hour, with samples taken throughout for GC-MS analysis. Results showed benzaldehyde within the first minute, along with **73**. However, benzonitrile and acetophenone were not observed until 50 minutes into the reaction. The concentration of benzaldehyde peaked at 10 minutes at 24 µM, while **73** was 27 µM. Concentrations of both compounds continued dropping

throughout the remainder of the reaction. It may be concluded that substitution of the nitrogen with chlorine did not allow for a more efficient photochemical reaction to take place, and a bulkier substituent, such as *tert*-butyl, led to higher conversion of **72** to **73**.

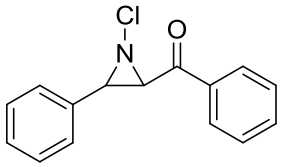

131

Figure 80. (1-Chloro-3-phenylaziridin-2-yl)(phenyl)methanone (**131**) subjected to UVC irradiation.

In addition to the reactions of *N*-substituted aziridines, reactions were carried out with but-2-ynedioic acid in order to trap the proposed azomethine ylide intermediate.[84] A solution of **77** and but-2-ynedioic acid (**132**) (1:1) was irradiated under nitrogen with a UVC lamp for 5 minutes (Scheme 62). The reaction time was chosen as the 360 nm intermediate and oxazole form within the first minute. Following irradiation, the solution was colourless, which had not been previously observed when irradiating aziridine without the alkyne. The reaction mixture was concentrated to an orange oil. Benzaldehyde and acetophenone proton peaks were visible; however, no other diagnostic peaks, such as the carboxylic acid proton, were observed. This suggested the reaction may have led to fragmentation due to a longer irradiation time, preventing the formation of 2-benzoyl-5-phenyl-2,5-dihydro-1H-pyrrole-3,4-dicarboxylic acid (**133**).

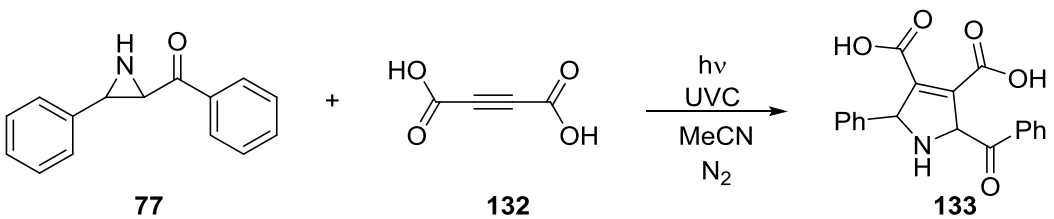

77 **132** **133**

Scheme 62. Photochemical reaction of **77** with but-2-ynedioic acid (**132**) carried out in order to trap the photochemical intermediate.

4.1.3.2. HPLC Analysis

Analysis of the photochemical reactions was also carried out by HPLC using 1 mL aliquots from the irradiations of 240 μM aziridine **77** in MeCN under nitrogen. A ChiralPak IA column using 98:2 hexane/isopropanol with a flow rate of 1.5 mL per minute

was used and UV absorbance peak areas were measured at 270 and 290 nm. A solution was irradiated for 1 minute using a UVC lamp and analysed by HPLC. As previously suggested, the 360 nm peak associated with the azomethine ylide intermediate led to 2,5-diphenyloxazole. When the sample taken from the 1 minute reaction was first irradiated, the 3D UV absorbance spectrum for the peak at 5.21 minutes showed a 360 nm absorbance feature identical to previous spectroscopic data (Figure 81). The sample was left to stand for 1 hour before reanalysing by HPLC. Analysis no longer displayed the peak at 5.21 minutes, but instead a peak at 6.14 minutes was seen with an absorbance profile similar to that of 2,5-diphenyloxazole (Figure 81). HPLC analysis of a pure sample of 2,5-diphenyloxazole revealed the retention times were the same (Figure 82). This study supported the hypothesis of the 360 nm peak being the intermediate leading to **73**.

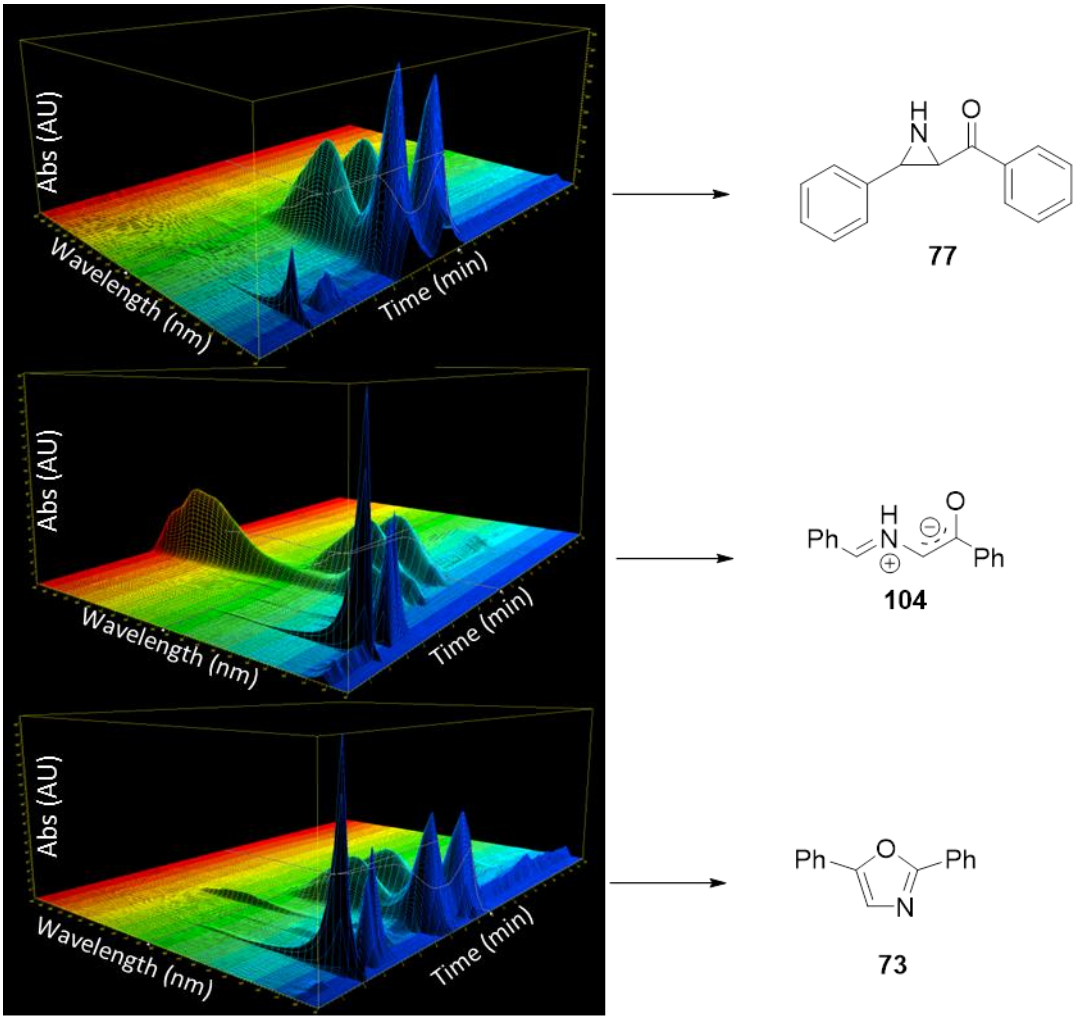

Figure 81. 3D UV Absorbance data obtained by HPLC showing **77**, and the 360 nm intermediate's (**104**) conversion into 2,5-diphenyloxazole (**73**).

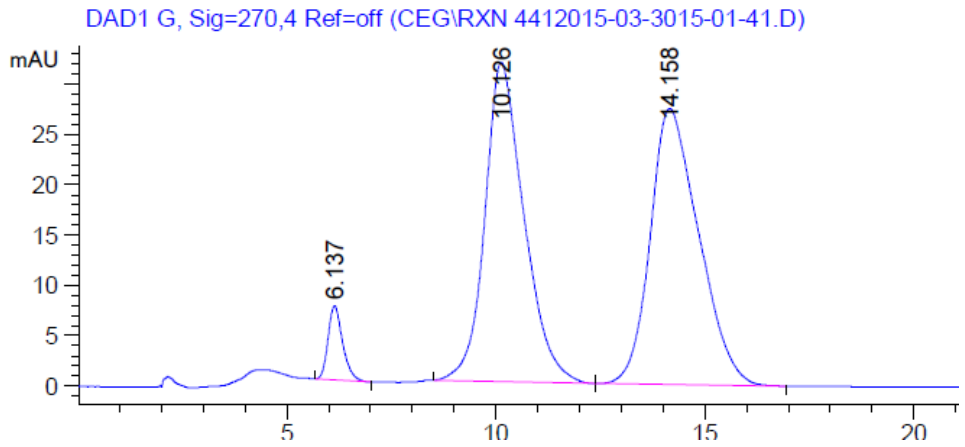

Figure 82. HPLC analysis of a 1 minute UVC irradiation of 240 µM **77** showing **73** at 6.14 minutes and racemic **77** at 10.13 and 14.16 minutes.

As shown in the previous excitation-emission profile (Chapter 3, Figure 49), **73** emits strongly at a concentration of 3 µM in MeCN, as only 2.5 nm slit widths could be used while acquiring spectra. Based on the previous spectroscopic data, it was suggested the reaction led to low yield. As shown by GC-MS data from the photoreactor, the maximum concentration of **73** observed was 65 µM for the reaction of a 240 µM solution of aziridine under nitrogen after 1 minute. This concentration would lead to approximately 6.5 milligrams for a 450 mL reaction, causing difficulties in isolating the desired product. Attempts were made to isolate the oxazole using semi-prep HPLC, however these were unsuccessful. In order to determine ways to optimise the reaction, further investigations regarding the mechanism were undertaken.

4.2. Mechanistic Studies

4.2.1. Photoinitiated Polymer Synthesis

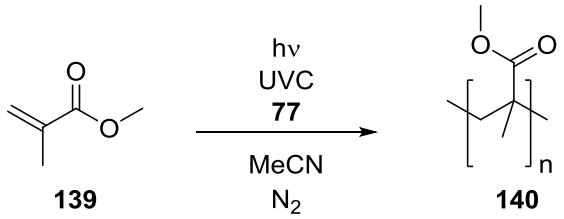

Scheme 63. Polymerisation of MMA (**139**) using **77** as a photoinitiator.

A biradical mechanism was previously proposed in Chapter 3. Investigation into **77**'s ability to photoinitiate a polymerisation would help support the generation of radicals. Additionally, it was suggested the degree of polymerisation by **77** could be compared with a known photoinitiator which underwent cleavage into radical fragments (Scheme 64). This would assist in determining whether biradicals were present, or if the molecule was producing radical fragments.

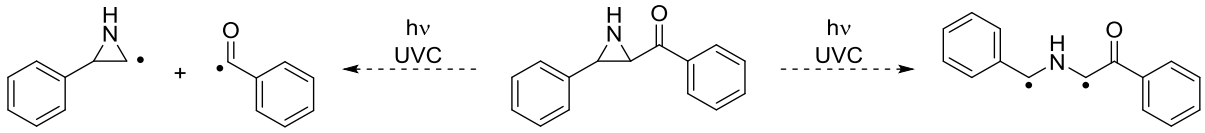

Scheme 64. Potential photoinitiated radicals formed by **77** under study.

Attempts were made to use **77** as a photoinitiator for the polymerisation of methyl methacrylate (**139**) (MMA) (Scheme 63). Initial experiments were carried out in the photoreactor using nitrogen purged solutions of 4-methoxyphenol inhibited MMA in MeCN. The solutions were irradiated with UVC light for 10 to 90 minutes, as shown in Table 7. Reactions were then concentrated to remove MeCN, followed by addition of methanol until polymer precipitated from solution. The poly-dispersity index (PDI) was measured by gel permeation chromatography (GPC) to determine the uniformity of the length of the polymer chains. The initial 10 minute run led to a PDI of 1.71 and a polymer molecular weight of 360,000. Using the same concentration of **77** but increasing the irradiation time to 1 hour led to a lower molecular weight polymer with a higher PDI, indicative of less control in the polymerisation. The most improved conditions were when the concentration of **77** was 0.22 mM, where irradiation for 1 hour resulted in a molecular weight of approximately 700,000 and a PDI of 1.19. A slight increase in the percentage

recovery was also observed. A control experiment was also carried out where MMA was irradiated in the absence of **77** and no polymer was formed.

Table 7. Polymerisation reactions using **77** as a photoinitiator to synthesise polymethyl methacrylate.

Entry	77 (mg)	Concentration of 77 (mM)	Irradiation Time (min)	Polymer (mg)	Recovery (%)	Polymer MW (kDa)	PDI
1	11.22	0.11	10	28.31	0.028	360	1.71
2	27.92	0.12	60	10.63	0.011	171	2.06
3	11.35	0.22	60	27.85	0.056	~700	1.19
4	2.41	2.39	90	2.23	0.039	331	1.58

Additional experiments took place after removal of the inhibitor from MMA. Inhibitor was removed by washing the MMA with 1 M NaOH and distilled water, followed by drying with magnesium sulfate.[101] The **77** concentration was kept to 0.11 mM and MMA at 100.15 g, with nitrogen purging while irradiating for 2 hours. The MeCN was removed *in vacuo* and MeOH was added until polymer precipitated from the solution. This yielded 420.71 mg of poly-methyl methacrylate (PMMA). A comparison was also performed with a known polymer photoinitiatior, 2-methyl-4′-(methylthio)-2-morpholinopropiophenone (**141**), under the same concentrations and irradiation conditions on MMA without inhibitor. The reaction yielded 3.36 g of product.

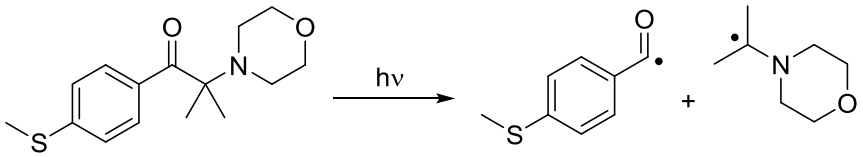

141 **142** **143**

Scheme 65. Photolytic decomposition of **141** into its radical fragments used for comparison polymerisation studies.[102]

Comparison of the two polymerisations demonstrated the reduced ability of **77** as a photoinitiator. As the formation of the two radical fragments by **141** allowed the increased formation of PMMA, it may be suggested that **77** does not undergo the same photolytic decomposition due to a reduced amount of polymer formed. The polymerisation data supports the formation of a biradical species upon irradiation, since the two radicals would

be in close proximity being on the same molecule, reducing their ability to interact with more molecules of MMA to initiate polymerisation.

4.2.2. Transient Laser Studies- Collaboration with Manchester Institute of Biotechnology

In order to gain more information about the photochemical reaction and its intermediates and lifetimes, transient absorption studies were performed. In addition to the MFE studies carried out in collaboration with the Manchester Institute of Biotechnology, transient absorption data was acquired for 150 µM solutions of **77** in MeCN by Dr. Roger Kutta. A xenon lamp was used with an excitation wavelength of 266 nm and absorbances were measured. In order to improve the signal-to-noise, an average of 100 shots were taken for the spectra obtained. The data showed a broad absorbance between 350 to 600 nm, with λ_{max}'s of 350 and 475 nm. The feature at 475 nm decayed around 50% within the first 100 ns while the 350 nm species increased. Deconvolution of the data showed 3 intermediates were present with lifetimes of 57 ns, 1.2 µs, and 4.5 µs. The experiment was repeated with an expanded time window to 500 ns. An additional feature was observed with a lifetime longer than the 500 ns window. Based on these studies, it was suggested that 4 species may be involved in the photochemical transformation.

A sample was irradiated by 300 laser shots at 266 nm (Figure 83-A). The UV-Vis absorbance was measured and showed the aziridine had converted into a new spectrum with a 4.5 nm blue shift in the λ_{max} to 245 nm. The sample was placed in the dark for several minutes then re-examined, and did not show any changes in the absorbance spectrum, demonstrating an irreversible photochemical change into a new compound had taken place.

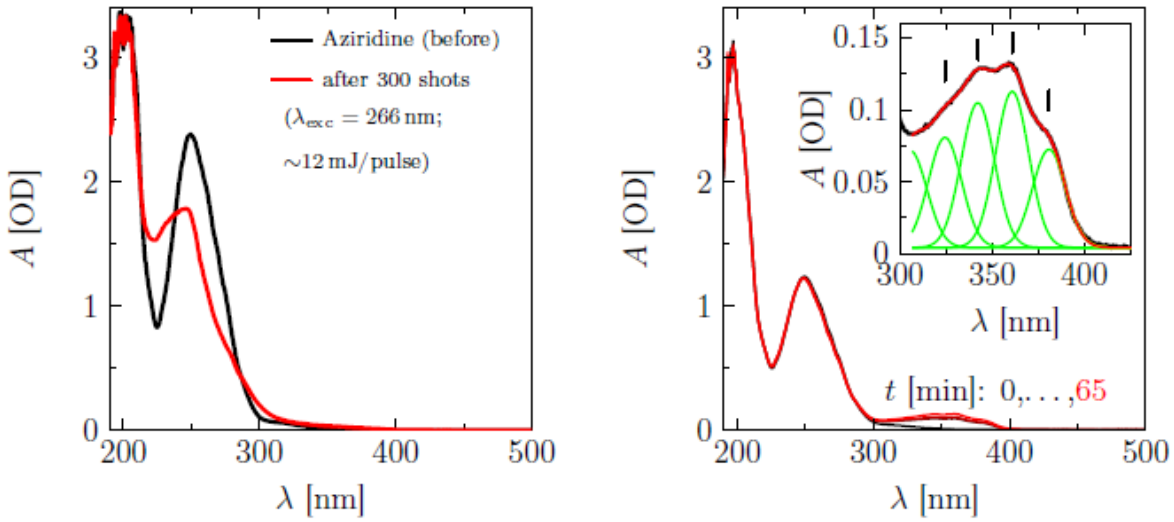

A **B**

Figure 83. A) Absorbance data acquired after 300 laser shots showing the irreversible photochemical change. B) Absorbance data monitoring of the 360 nm species; inset showing Gaussian fittings. *Figures provided by Dr. Roger Kutta.

The previous experiment was repeated; however, only a single shot was used to irradiate the sample at 266 nm (Figure 83-B). The λ_{max} of **77** was still observed in addition to the 360 nm species. This new feature continued to grow up to 1 hour before it began to decay. This species was fitted to 5 Gaussians with energy separations of ~1500 cm^{-1}. It was suggested that the energy separation may be attributed the vibronic progression of the extended π–system of the azomethine ylide. Vibrational fine structures may be visible in absorption spectra for highly conjugated molecules, showing the transitions from the ground electronic state (v = 0) to a vibrational level in the excited electronic state (v = 0, 1, 2, 3, etc.).[98] This has been observed for anthracene, where the transitions from the lowest vibrational levels of S_0 to higher vibrational levels in S_1 were observed (Figure 84).[92]

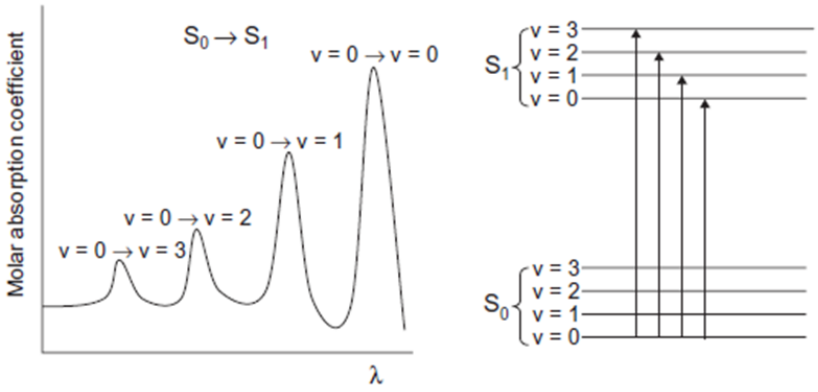

Figure 84. Absorption spectrum of anthracene in benzene showing the vibrational fine structure and the vibronic transitions from S_0 to S_1. Image reproduced from Principles and Applications of Photochemistry by Brian Wardle.[98]

4.2.3. Power Dependence Studies

As previous data obtained from lamp studies suggested a power dependence was present, further investigation took place utilising various irradiation sources. Irradiation sources, shown in Table 8, were compared using a 150 µM solution of **77** in MeCN. When using a fibre optic cable in conjunction with the fluorimeter as the irradiation source, a third of the power was lost at 250 nm. This was previously noted as the accumulation of the 360 nm species took 2 hours when using the fibre optic cable, compared to 30 minutes with the fluorimeter alone when irradiating at 250 nm.

Table 8. Power measurements of irradiation sources used in spectroscopic studies. Measurements were obtained using a Thorlabs PM100A power meter.

Irradiation Source	Power at 250 nm (mW)	Power at 300 nm (mW)
Fluorimeter	0.163	0.122
Fibre Optic from Fluorimeter	0.048	0.007
Stopped-Flow Lamp	0.165	0.540

In the presence of air, irradiation with a stopped-flow lamp at 300 nm showed a small initial lag phase. This was followed by a steady increase in emission with a plateau beginning as the curve was approaching saturation, as shown previously in Figure 77. However, when using the fluorimeter as an irradiation source, the first rate was slower, suggesting more time was required to accumulate the intermediate which then formed the oxazole (Figure 85). At 17 minutes, the sample irradiated with the stopped-flow lamp was

no longer absorbing light and was beginning to emit. Emission was not observed until approximately 30 minutes for the fluorimeter irradiated sample. The data confirmed the presence of a power dependence as the stopped-flow lamp was over 4.4 times more powerful at 0.540 mW compared to the fluorimeter lamp at 0.122 mW when the irradiation wavelength was 300 nm.

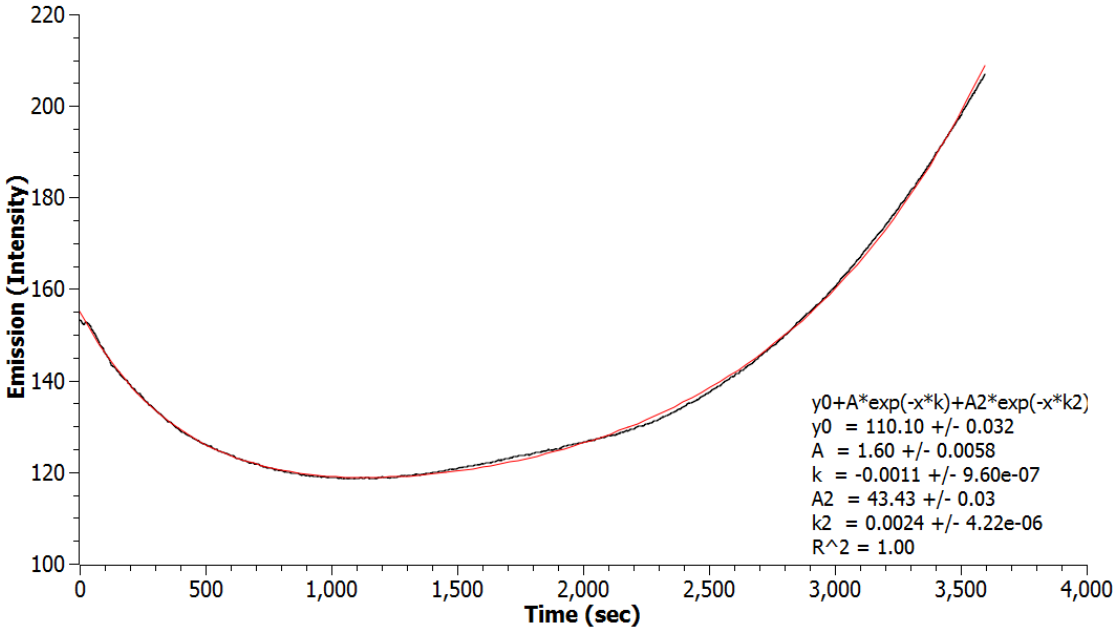

Figure 85. Emission monitoring at 380 nm of 150 µM solution of **77** in MeCN over 60 minutes when irradiating at 300 nm. Slit widths were set to 15 and 7 nm for excitation and emission, respectively.

4.3. Enantiopure Studies

Single enantiomer studies were carried out on **77** as previous reaction data analysed by HPLC showed an *ee* of ~5% for the remaining starting **77**, suggesting one enantiomer may have been reacting more readily. Enantiomers were isolated by HPLC using a ChiralPak IA semi-prep column using 95:5 hexane/isopropanol and a flow rate of 3 mL per minute. Using a polarimeter, the specific rotations were obtained for each enantiomer providing values of +300 deg·mL·g^{-1}·dm^{-1} and -330 deg·mL·g^{-1}·dm^{-1} for *(2S,3R)*-**77** and *(2R,3S)*-**77**, respectively (Figure 86). Measurements were recorded in chloroform at concentrations of 10.9 mM. Structure configuration was confirmed with the literature.[103]

(2*S*,3*R*)-**77** (2*R*, 3*S*)-**77**

Figure 86. Isolated enantiomers of **77** using semi-prep HPLC.

4.3.1. HPLC Studies

Once isolated, the individual isomers were subjected to UVC irradiation and spectroscopic studies. UVC irradiations took place in the photoreactor at a concentration of 240 µM in MeCN over 10 minutes. Aliquots were taken every minute from the nitrogen purged reactions and analysed by HPLC on a ChiralPak IA column using 95:5 hexane/isopropanol with a flow rate of 1.5 mL per minute. Peak area was measured by UV absorbance at 290 nm at retention times of 6.20, 7.15, and 9.36 min for **73**, *(2S,3R)*-**77**, and *(2R,3S)*-**77**, respectively.

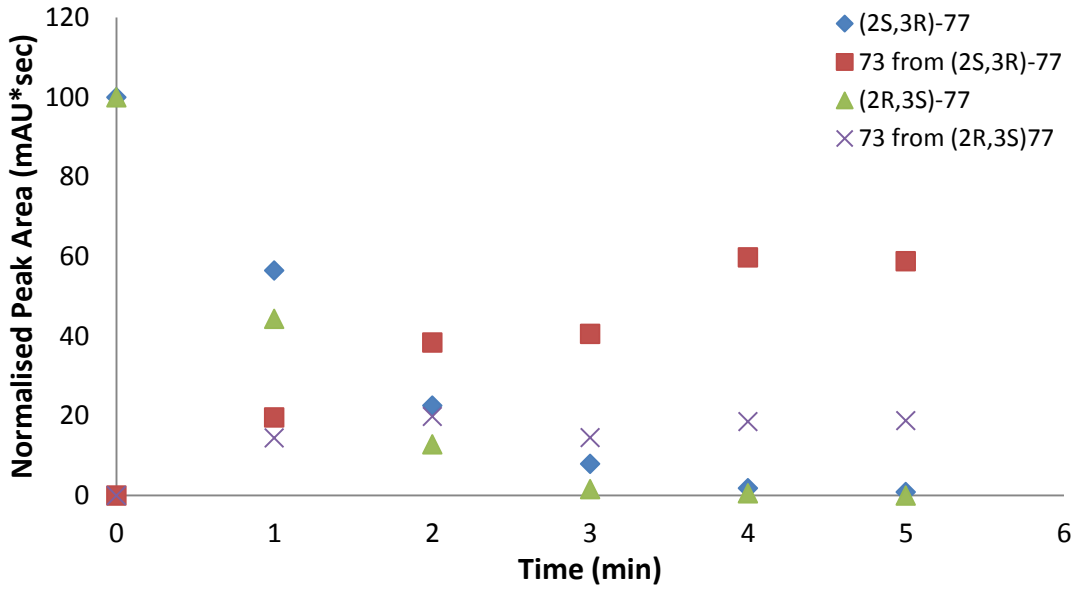

Figure 87. Plot of normalised peak area vs. time for single enantiomer reactions in the photoreactor using a UVC lamp.

UVC irradiation revealed more **73** was formed by the *(2S,3R)*-**77** enantiomer (Figure 87). Within the first minute, both *(2S,3R)*-**77** and *(2R,3S)*-**77** had formed oxazole; however, the amount generated by *(2R,3S)*-**77** peaked at 2 minutes and stayed constant throughout the remainder of the reaction. While irradiating *(2S,3R)*-**77**, the amount of **73** continued growing throughout the reaction, with the highest amount visible at 4 minutes. *(2R,3S)*-**77** appeared to be consumed more rapidly, as no starting material was observed after 4 minutes, whereas some *(2S,3R)*-**77** remained at 5 minutes. The largest peak area was observed for oxazole when irradiating *(2S,3R)*-**77**, with a peak area of 1134 mAU*sec, compared to 266 mAU*sec for *(2R,3S)*-**77**. The experiment was performed in triplicate and provided reproducible results. All three experiments showed *(2S,3R)*-**77** yielded more 2,5-diphenyloxazole within 5 minutes.

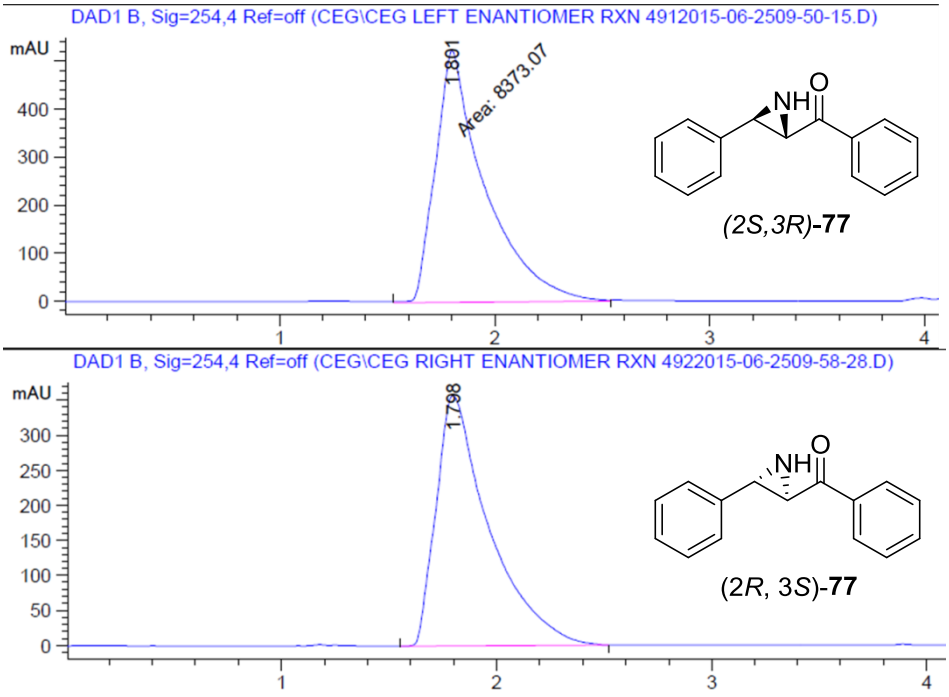

Figure 88. HPLC traces obtained on a nonchiral column for *(2S,3R)*-**77** and *(2R,3S)*-**77** showing retention times of 1.801 and 1.798 min, respectively.

In order to eliminate the possibility of impurities and also confirm the two enantiomers were otherwise spectroscopically identical, multiple analyses were performed. HPLC analysis was carried out on a non-chiral Zorbax Eclipse XDB-CN column using 95:5 hexane/isopropanol with a flow rate of 1.5 mL per minute. The UV absorbance was measured for each enantiomer at 254 nm (Figure 88). Similar retention times of 1.801 and 1.798 minutes for *(2S,3R)*-**77** and *(2R,3S)*-**77** were observed. NMR was also used to characterise *(2S,3R)*-**77** and *(2R,3S)*-**77**. Comparison of ^{1}H and ^{13}C NMR revealed the same spectra for both enantiomers, thus confirming their similarity and lack of impurities (Figure 89).

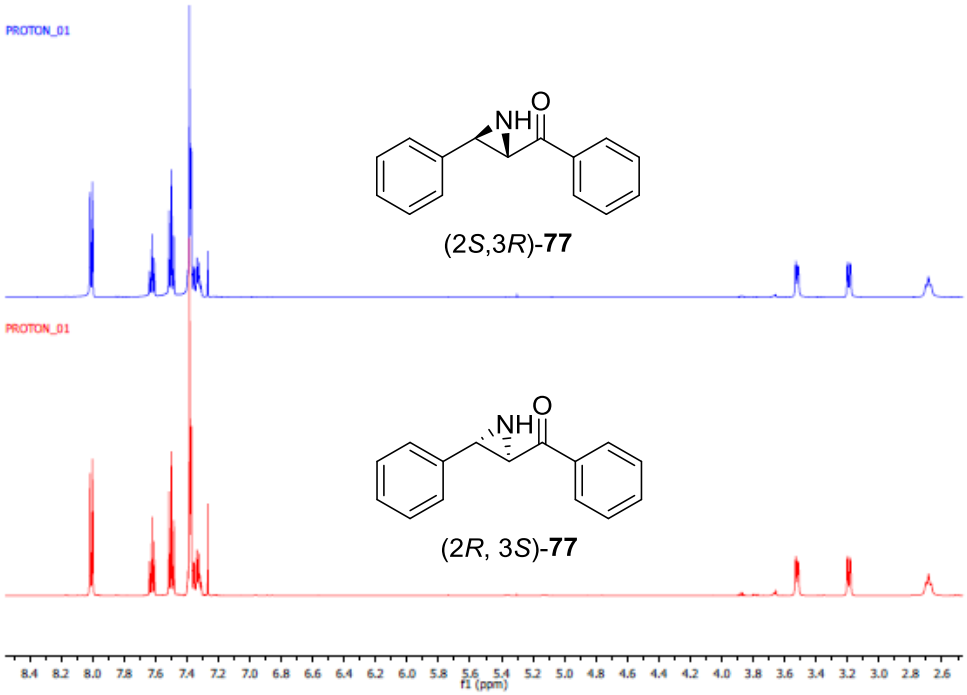

Figure 89. ^{1}H NMR spectra of *(2S,3R)*-**77** and *(2R,3S)*-**77** obtained on an Agilent 500 MHz NMR in $CDCl_3$.

Circular dichroism (CD) spectroscopy was used to analyse the single enantiomers. Solutions of *(2S,3R)*-**77** and *(2R,3S)*-**77** in MeCN with a concentration of 72 µM were analysed by CD using a 5 mm path length cuvette (Figure 90). The normalised spectra demonstrated mirroring of the two enantiomers, further confirming their assignments were accurate and that a racemic mixture was not present.

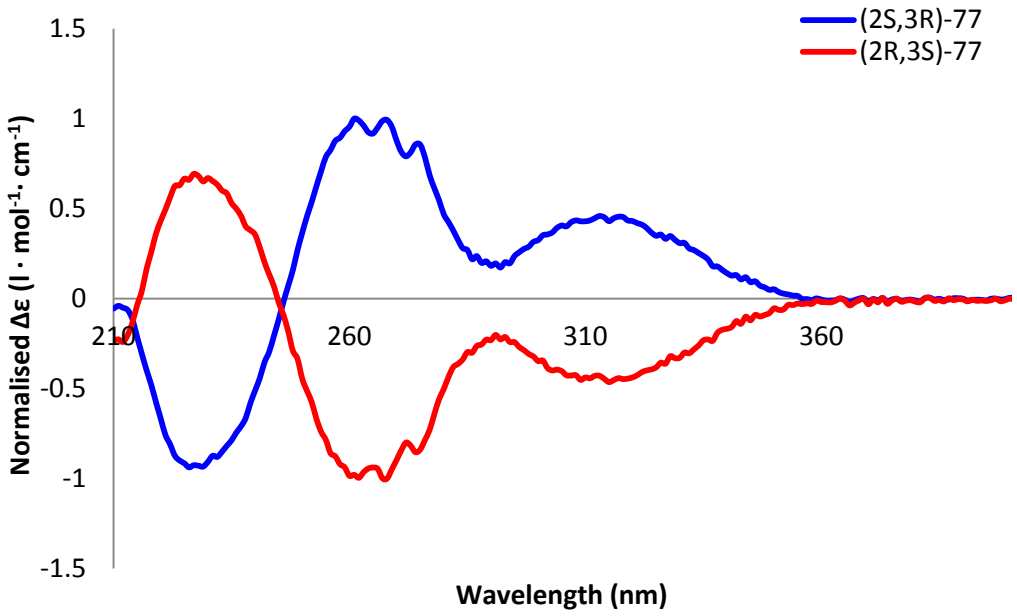

Figure 90. Normalised CD spectra of 72 µM *(2S,3R)*-**77** and *(2R,3S)*-**77**.

Photochemical results for the single enantiomer reactions were reproducible as confirmed by HPLC. Additional characterisation of the unirradiated enantiomers by HPLC and NMR demonstrated similar retention times and chemical shifts. CD characterisation also verified proper separation of the two enantiomers which underwent irradiation. Further spectroscopic measurements were carried out by stopped-flow fluorescence for *in situ* reaction monitoring to obtain reaction rates.

4.3.2. Stopped-Flow Fluorescence Studies

Irradiations were carried out at 300 nm using stopped-flow fluorescence with 5 nm slit widths on 150 µM MeCN solutions of *(2S,3R)*-**77** and *(2R,3S)*-**77** over 3 hours. The data from both enantiomers fit two exponentials, indicative of two processes taking place. The first rate with negative amplitudes for both enantiomers accounts for the initial decay in the system, which was previously shown to be oxygen dependent (Figure 77). This rate was slower for *(2S,3R)*-**77**, at 0.00022 s^{-1}, compared to 0.00032 s^{-1} for *(2R,3S)*-**77**. However, k_2 for *(2S,3R)*-**77** became 1.5 times faster at 0.00077 s^{-1} for the second process taking place (Figure 91 and Figure 92).

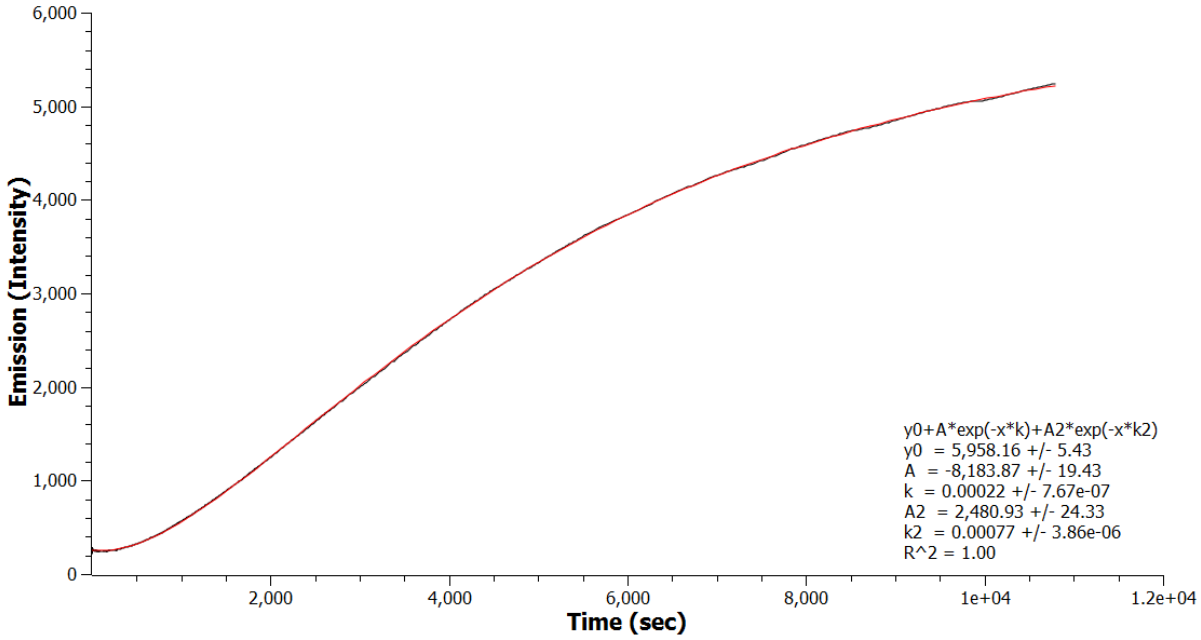

Figure 91. Stopped-flow fluorescence of *(2S,3R)*-**77** monitoring the emission over 3 hours.

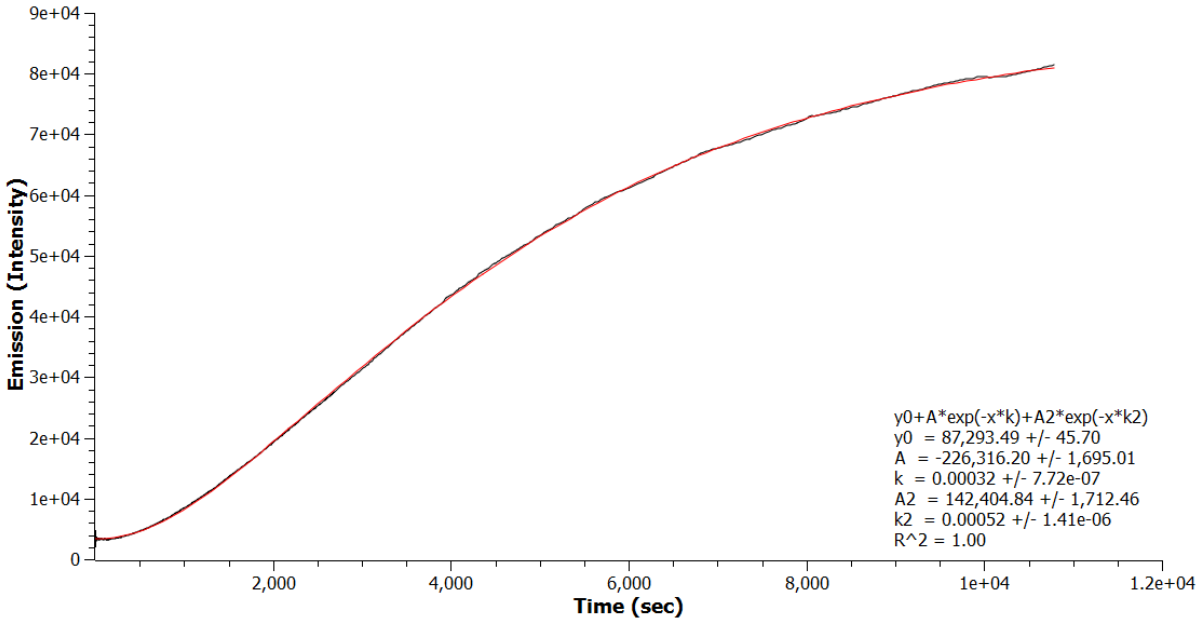

Figure 92. Stopped-flow fluorescence of *(2R,3S)*-**77** monitoring the emission over 3 hours.

The data from the racemic irradiation also fitted two exponentials, as previously shown in Figure 77. The first rate was 0.00034 s^{-1}, while *(2R,3S)*-**77**'s was 0.00032 s^{-1}. When looking at k_2, the rates of the racemic mixture and *(2S,3R)*-**77** were identical at 0.00078 s^{-1}. Based on this data, it may be hypothesised that *(2R,3S)*-**77** was the dominant enantiomer contributing to k_1, while *(2S,3R)*-**77** was dominant for k_2.

When compared with the HPLC reaction data using UVC irradiation, both experiments were consistent as they demonstrated the initial faster reaction rate of *(2R,3S)*-**77** converting to oxazole. While *(2S,3R)*-**77** formed more oxazole in the sampled reactions, stopped-flow data showed the reaction had not yet reached saturation, therefore, a final amount of 2,5-diphenyloxazole formed was not measured. As previously shown, the reaction is power dependant which would require longer irradiation times to achieve full conversion using the stopped-flow lamp.

4.3.3. Polarisation Studies

Previous studies by Rikken and Raupach suggested enantioselectivity in a photochemical reaction was possible with unpolarised light in the presence of a parallel magnetic field.[104,105] As MFE's on aziridines were previously carried out in Chapter 3, the work by Rikken and Raupach prompted observation of potential effects on the reaction using linearly polarised light. A linear polariser was used in conjunction with the stopped-flow lamp. Irradiation took place on 150 µM MeCN solutions of racemic **77**, *(2S,3R)*-**77**, and *(2R,3S)*-**77** over 3 hours monitoring the emission with 5 nm slit widths.

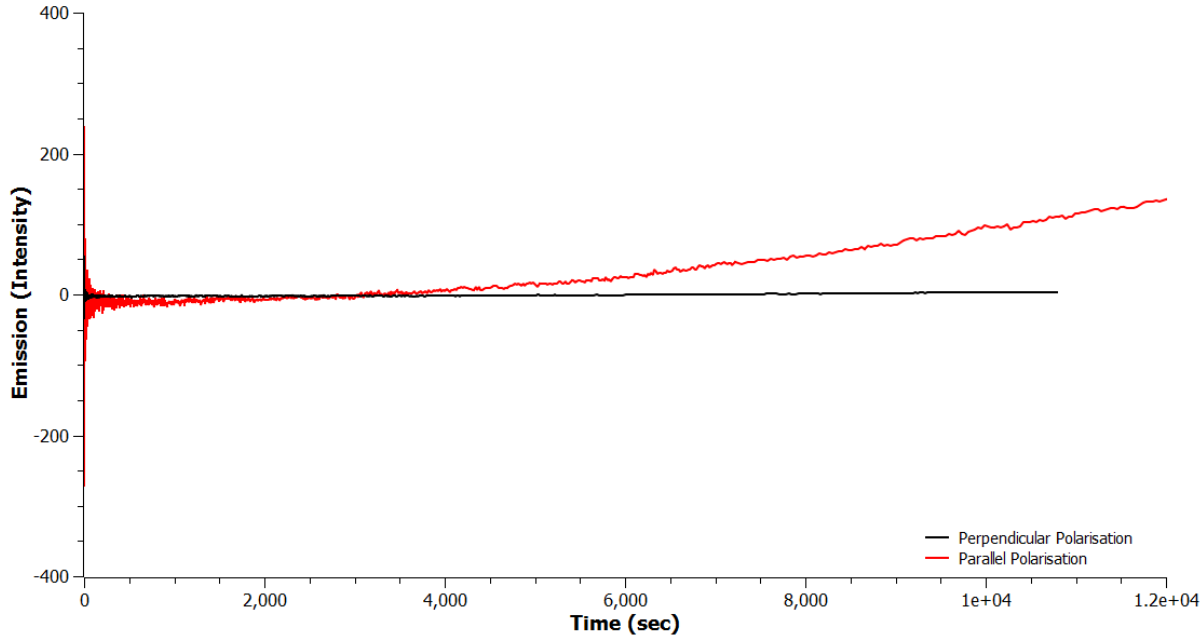

Figure 93. Stopped-flow fluorescence of *(2S,3R)*-**77** with linear polarisation applied at 300 nm.

A dramatic change in reaction rate was observed when irradiation took place with perpendicular or parallel polarisation. Irradiation of *(2S,3R)*-**77** showed reaction inhibition using parallel polarisation, with barely any observable emission when using perpendicular polarisation (Figure 93). When irradiating *(2R,3S)*-**77** with polarised light, the reaction was significantly inhibited but minimal difference was seen between perpendicular and parallel polarisation (Figure 94). The most striking measurement was the near total inhibition of the reaction of *(2S,3R)*-**77** with perpendicular polarisation. One thought for these unexpected results was a loss in lamp intensity due to the polarisation lens. A power meter was used to confirm there was no loss in lamp power with and without the polarisation lens.

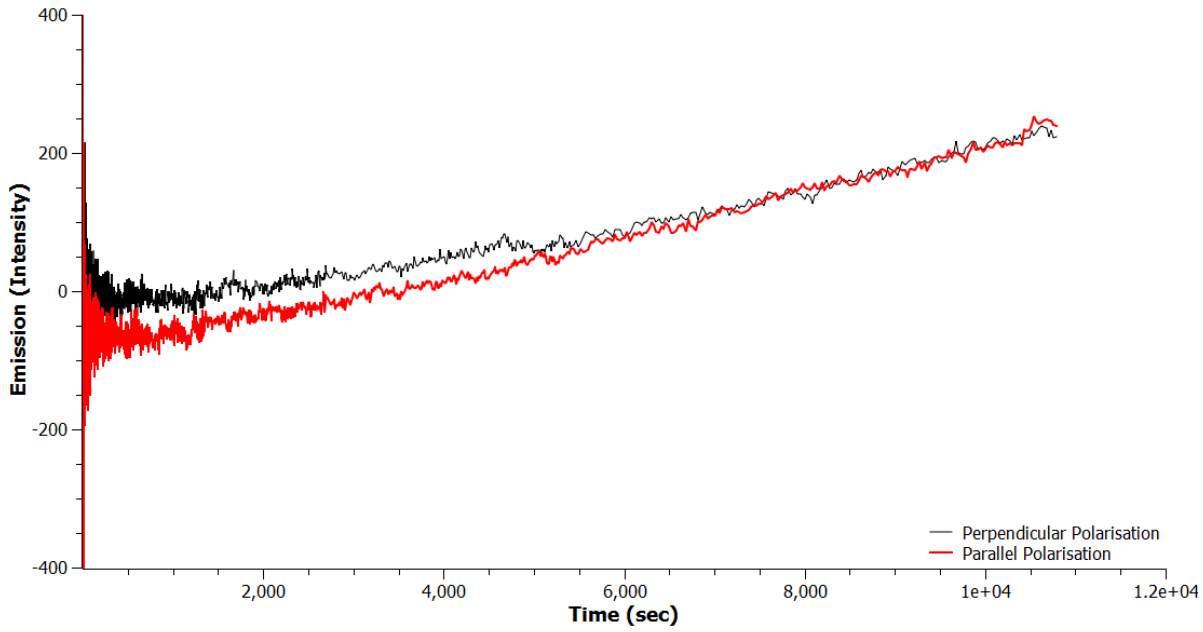

Figure 94. Stopped-flow fluorescence of *(2R,3S)*-**77** with linear polarisation applied at 300 nm.

Publications demonstrated the use of linearly and circularly polarised light for selectivity in photoreactions.[106–108] Chae, *et al*. studied photosensitive polyester liquid crystals and the effect of linearly polarised light. A selective photoreaction took place where the chromophores parallel to the direction of polarisation reoriented the polymer chains when exposed to linearly polarised light.[106] In another example, liquid crystalline polymethacrylate with 4-methoxybistolane side groups was synthesised by Kawatsuki *et al*. and irradiated with linearly polarised light at 365 nm. This induced reorientation of the molecules to lie parallel to the polarisation.[107] Additionally, Richardson *et al*. utilised dual wavelength circularly polarised light in the asymmetric synthesis of dihydrohelicenes.[108] A combination of circularly polarized light at 355 nm was used to form a helicene by ring-closure, followed by 532 nm light to ring-open the helicene to induce asymmetry. There have also been photoresolution experiments carried out on a chiral ketone, 8-(phenylmethylene)bicyclo[3.2.l]octan-3-one, by Zhang and Schuster.[109] Irradiation of the compound with circularly polarised light resulted in incomplete photoresolution, however with a measureable enantiomeric excess. Irradiating with unpolarised light then led to photoracemization.

Application of the knowledge obtained from the literature led to possible rationalisations for the lack of reactivity with linearly polarised light. Light is formed by

electromagnetic waves with undefined directions when unpolarised, and defined directionality when polarised. Linearly polarised light may be converted into circularly polarised light by passing it through a quarter wave plate which is 45° to the polarisation axis.[110] Optically active molecules rotate the plane of polarisation when linearly polarised light is passed through them. Two linear components perpendicular to each other are required to make circularly polarised light, thus removing one of the linear components prevents the ability to generate circularly polarised light. As the aziridine was only exposed to one component due to the parallel or linear polarisation, it was unable to make circularly polarised light, which may be preventing the photoreactivity. A potential way to test this hypothesis would be to irradiate the single enantiomers, as well as the racemic mixture, with either left or right circularly polarised light.

4.4. Photochemical Synthesis of a Natural Product- Texaline

Having confirmed **77** was capable of photochemically transforming into **73** by GC-MS, HPLC, and fluorescence, the next goal was to test the synthetic utility of this procedure. Texaline (**134**), a natural product isolated from *Amyris texana* and *Amyris elemifera*, was found to inhibit bacteria responsible for tuberculosis, leprosy, and respiratory infections caused by mycobacterium avium.[111] Previous syntheses have involved 5 steps, beginning with 3,4-(methylenedioxy)acetophenone (**135**).[112]

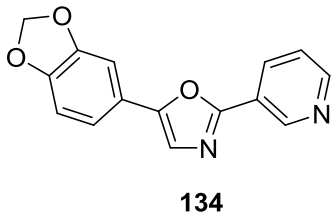

134

Figure 95. Structure of synthetic target texaline (**134**), a natural product.

The methods used in this study were altered to apply the route to the synthesis of **134** (Scheme 66). An aldol condensation between nicotinaldehyde (**136**) and **135** yielded the chalcone (**137**) in 54%, which then underwent aziridination using the iodoaminomorpholine salt to provide novel aziridine **138** in 50% yield. Irradiation of **138** with UVC light would then ideally allow the final product to be obtained.

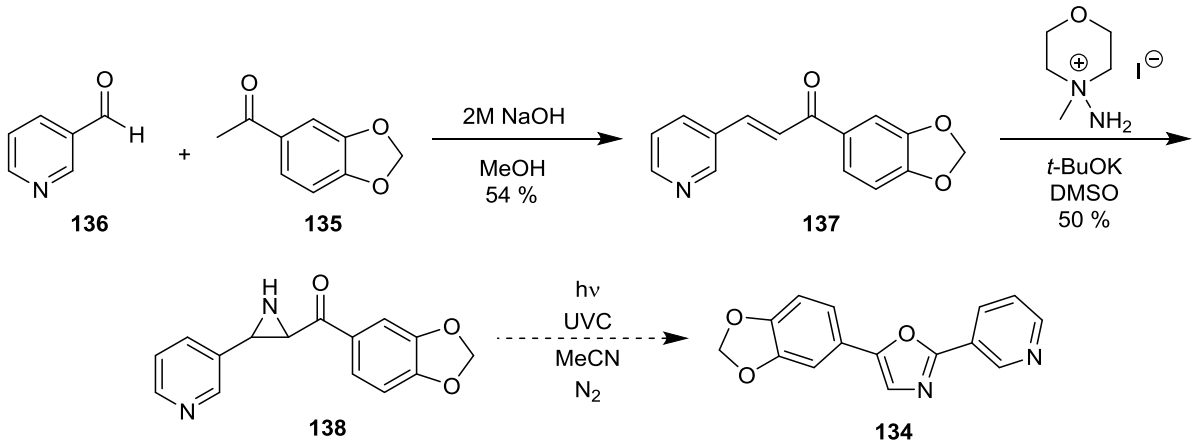

Scheme 66. Proposed synthesis of texaline (**134**).

Proof of concept was carried out on a 0.48 mM solution of **138**. Analysis was performed by GC-MS on 1 mL samples taken at 1, 5, 20, and 50 minutes, and peak areas were compared. As with previous reactions, the aldehyde, **136**, was observed after 1

minute. Analysis of the reaction at 5 minutes showed an increased amount of aldehyde, and the first amount of nicotinonitrile. At 20 minutes the mass ion peak of **134** was observed at 266 m/z, comprising the majority of the reaction mixture (Figure 96). In addition to texaline being formed after 20 minutes, the reaction mixture also contained **136**, nicotinonitrile, and **135**. Following 50 minutes, **136** and texaline decreased while nicotinonitrile and **135** increased in peak area. Compared with previous reactions, texaline appeared to be more stable under photochemical conditions, as less decomposition products were observed. This reaction was also slower as the oxazole product was not observed until 20 minutes, compared to the 1 minute taken previously for aziridine reactions.

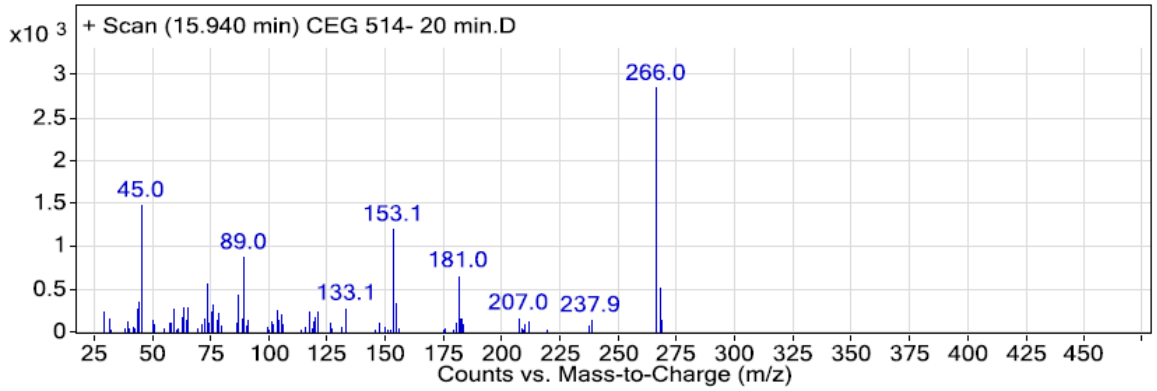

Figure 96. MS spectrum showing the mass ion peak of **134**, obtained from GC-MS analysis following 20 minutes of UVC irradiation of **138**.

Additional spectroscopic characterisation was carried out on a 72 µM solution of **138** in MeCN. Irradiation of **138** took place for 1 hour at 300 nm with slit widths of 15 nm for excitation and 7 nm for emission, due to it showing the highest emission and reaction rate at this wavelength, and an excitation-emission profile was obtained (Figure 97). A broad emission was observed at 420 nm with excitation at 338 nm. A λ_{max} of 338 nm with additional features at 255 and 290 nm was observed for **138**. While typical spectra for diaryloxazoles were not observed, it may not be discounted that texaline was formed on a spectroscopic scale. While the reaction in the photoreactor used a more powerful lamp and required 20 minutes to form **134**, it may be suggested that a small amount of texaline formed at 72 µM but would require longer irradiation times to allow for further conversion. While GC-MS confirmed the presence of the oxazole, it was not isolated for characterisation due to the low amount of material formed.

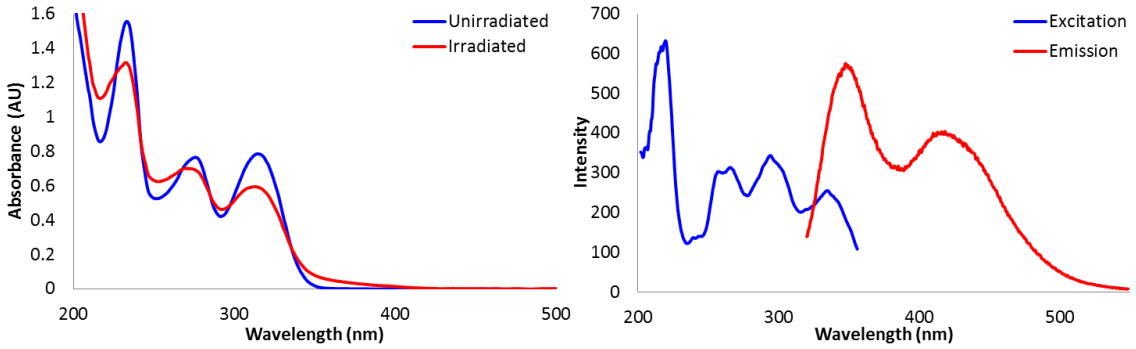

Figure 97. Absorbance of **138** unirradiated and after 30 minutes of irradiation at 250 nm. Emission profile at 338 nm and excitation profile at 420 nm at 4 nm slit widths following 60 minutes of irradiation at 300 nm.

4.5. Comparison with Previous Work

Previous work by Padwa stated aziridine **77** was photochemically unreactive as only starting material was recovered from the reaction.[76] Padwa's experiments involved use of a 450 W medium pressure mercury lamp to irradiate a 4.5 mM solution of **77** in 95% ethanol. A Pyrex filter was also used and the reaction was nitrogen purged. Starting material was the only component observed following 28 hours of irradiation. Contrary to Padwa's findings, this work confirmed and demonstrated the photochemical reactivity and sensitivity of **77**. Concentration and wavelength were found to be critical variables as too high a concentration did not yield product, and wavelengths of 300 nm and below were required for **77** to form the intermediate species which formed 2,5-diphenyloxazole. Using a UVC lamp for photoreactor irradiations demonstrated the aziridine reacted within the first minute of irradiation and was able to form 2,5-diphenyloxazole.

In order to further compare the similarities between the system used in this study and that used by Padwa, irradiation of **72** was also investigated. Irradiation of 3.2 mM of **72** took place in pentane using a 450 W medium pressure mercury lamp with Pyrex filter by Padwa.[77] The main products of this irradiation were 2,5-diphenyloxazole (**73**), (*β-tert*-butylamino)-*trans*-benzalacetophenone (**74**), *N-tert*-butylbenzalimine (**75**), and benzaldehyde (**76**). Using the UVC lamp from this study found that irradiating 240 µM of **72** in acetonitrile led to **73**, **76**, benzamide (**82**), *N*-(*tert*-butyl)benzamide (**130**), and imine **75**. Similarities were observed in that **73** and benzaldehyde were formed; however, wavelength and concentration may have played a role in fragmentation of the molecule resulting in the different products being observed. Use of a higher pressure mercury lamp with a Pyrex filter would most likely lead to the formation of the products observed by Padwa.

George also studied the irradiation of **77** under steady-state conditions and laser flash photolysis.[83] A solution of 5.7 mM **77** in benzene was irradiated for 4.5 hours using a 450 W medium pressure mercury lamp. The lack of Pyrex filter allowed for isolation of similar products as observed in section 4.1.3.1, such as benzaldehyde and acetophenone. However, George isolated pyrazine structures **106**, **107**, and **110**. These structures were the result of dimerisation of the ylide, which was not seen by this study under steady state conditions using the UVC lamp, lower concentrations, and shorter irradiation times.

Laser flash photolysis of **77** was carried out by George at 337 nm in benzene.[81] The presence of a "permanent photoproduct" was identified with a λ_{max} of 360 nm, being

described as permanent due to the lack of decay over 150 μs. Experiments carried out in collaboration with the Manchester Institute of Biotechnology used laser flash photolysis of **77** at 266 nm in acetonitrile. These studies revealed the λ_{max} of 360 nm observed grew for 1 hour before it began to decay. Species with lifetimes of 57 ns, 1.2 μs, 4.5 μs, and one longer than 500 ns were observed, indicating 4 species may be involved in the photochemical transformation. Thus the work performed at the Manchester Institute of Biotechnology revealed further complexity to the photochemical reaction of **77**, and identified the presence of multiple species.

4.6. Conclusions and Future Work

Photoreactor and spectroscopic studies revealed an oxygen sensitivity, power dependence, and wavelength dependence. Use of a lower wattage UVC lamp allowed for analysis of the reaction by GC-MS and HPLC, with less molecular fragmentation. Studies carried out in the presence of air and degassed solutions demonstrated formation of 2,5-diphenyloxazole within the first minute of the reaction. GC-MS data revealed benzaldehyde was formed during the initial stages of the reaction, with decomposition products being benzonitrile and acetophenone. Additionally, HPLC showed the 360 nm species converted into oxazole.

Studies were carried out to assist in corroborating the previously suggested radical mechanism. Photoinitiated polymerisation of MMA using a low loading of aziridine **77** generated PMMA, confirming the presence of radicals. Mechanistic studies at the Manchester Institute of Biotechnology revealed 4 species were most likely present during the reaction, with lifetimes of greater than 500 ns, 57 ns, 1.2 μs, and 4.5 μs.

This study has developed a chemical platform for oxazole synthesis and its derivatives, as demonstrated by the synthesis of texaline. Isolation of the enantiomers revealed an initial faster reaction rate of *(2R,3S)*-**77**, but a larger formation of oxazole by *(2S,3R)*-**77**. Additional unexpected results were the polarisation studies showing inhibition of the photochemical reaction, which has not been previously reported.

Future work would involve optimisation of the photoreaction on a larger scale, as the oxazoles formed were unable to be isolated for characterisation due to the low concentration and conversion of the reaction. One possibility would be to use a flow reactor, which would allow for lower concentrations to be used. A combination of wavelengths could also be attempted to generate the 360 nm species then irradiate this feature using higher wavelengths to drive the reaction to form oxazole. Single enantiomer reactivity may be further probed by using varying *ee*'s of **77** when irradiating. This would aid in determining whether a small initial difference in *ee* is capable of altering the overall autocatalytic effect. Further investigation into the reaction inhibition by polarisation would also be suggested. Experiments using circularly polarised light may be beneficial in determining the effect on reactivity.

Chapter 5: Materials and Methods

Table of Contents

General

All reactions were carried out under an inert nitrogen atmosphere, unless otherwise noted. Reagents were purchased from commercial suppliers: Fisher Scientific, Alfa Aesar, and Sigma Aldrich and were used without further purification. Reactions were monitored by thin layer chromatography (TLC) using pre-coated MN Alugram Sil G/UV254 silica gel aluminium backed plates. Plates were developed using standard techniques and UV 254 nm absorption was used to determine presence of materials. Purification was performed *via* flash chromatography using chromatography grade silica 60Å particle size 200-400 mesh from Sigma Aldrich using the solvent systems stated.

^{1}H and ^{13}C NMR were performed on a Bruker Avance 250 (250 MHz), Bruker 300 (300 MHz) or Agilent Technology 500 (500 MHz) at 303 K. Chemical shifts are reported in parts per million (ppm) relative to deuterated chloroform ($CDCl_3$) (δ = 7.27) and deuterated dimethyl sulfoxide (DMSO-d_6) (δ = 2.50). Coupling constants are reported in Hertz (Hz) and multiplicity is denoted as singlet (s), doublet (d), triplet (t), quartet (q), doublet of doublets (dd), doublet of triplets (dt), doublet of quartets (dq), septet (spt), multiplet (m), and broad (br). Mass spectra were acquired on a Bruker μTOF using electrospray ionisation (ESI) in positive or negative ionisation as stated. Infra-red spectroscopy was performed on a Perkin Elmer Spectrum 100 FT-IR instrument using thin-film. Spectra were measured in cm^{-1} and denoted as strong (s), medium (m), and weak (w).

5.1. Experimental for Chapter 2

4-Amino-4-methylmorpholin-4-ium iodide (112)

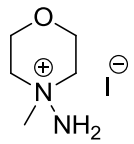

A solution of 4-aminomorpholine (100.0 mg, 0.98 mmol, 1.0 eq.) in THF (1 mL) was cooled to 0°C. Methyliodide (144.9 mg, 1.03 mmol, 1.05 eq.) was then added dropwise and the reaction mixture was left to stir for 10 minutes. The white precipitate was then filtered from solution and rinsed with diethyl ether and left to dry. Once dry, the solid was dissolved in a heated mixture of ethanol and methanol (3:1) and was left to cool to recrystallize the product. It was filtered from solution and washed with cold ethanol to give white crystals (239.0 mg, 92%). mp 168-171 °C. υ_{max} (film)/cm^{-1}: 3270 (m), 1456 (s), 1092 (s), 894 (s); ^{1}H NMR (250 MHz, DMSO-d6): δH 5.98 (s, 2H, NH_2), 4.00 (ddd, J = 13.1, 9.3, 3.0 Hz, 2H, CH_2), 3.89 (dt, J = 13.0, 3.3 Hz, 2H, CH_2), 3.60 (ddd, J = 12.6, 9.0, 3.5 Hz, 2H, CH_2), 3.44 (d, J = 13.1 Hz, 3H, CH_2), 3.37 (s, 3H, CH_3); ^{13}C NMR (75 MHz, DMSO-d6): δC 63.5, 61.3, 57.5. Data in accordance with the literature.[41]

Phenyl(3-phenylaziridin-2-yl)methanone (77)

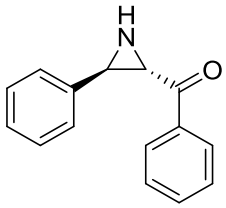

To a solution of *trans*-chalcone (73.9 mg, 0.36 mmol, 1.0 eq.) and **112** (95.2 mg, 0.39 mmol, 1.1 eq.) in DMSO (5 mL) potassium *tert*-butoxide (43.8 mg, 0.39 mmol, 1.1 eq.) was added over 2 minutes in 9 portions. The reaction was left to stir open to air at room temperature for 1.5 hours. The orange-brown solution was then quenched with diethyl ether (25 mL) and distilled water (25 mL). The product was extracted into diethyl ether and washed with distilled water (2 x 25 mL) and brine (1 x 25 mL). The ether layer was

then dried over magnesium sulphate, filtered and concentrated under reduced pressure. Product was purified by flash column chromatography, petroleum ether/diethyl either (4:1) to afford a white crystalline solid (65.4 mg, 83%). mp 98-99 °C. υ_{max} (film)/cm^{-1}: 3220 (m), 1658 (s), 1595 (m), 1010 (s), 695 (s); ^{1}H NMR (500 MHz, $CDCl_3$): δH 8.01 (d, J = 8.3 Hz, 2H, Ar), 7.63 (t, J = 7.3 Hz, 1H, Ar), 7.50 (t, J = 7.6 Hz, 2H, Ar), 7.36 (m, 5H, Ar), 3.52 (dd, J = 7.8, 2.0 Hz, 1H, CH), 3.19 (dd, J = 9.0, 2.2 Hz, 1H, CH), 2.69 (t, J = 8.3 Hz, 1H, NH); ^{13}C NMR (125 MHz, $CDCl_3$): δC 195.7, 138.5, 135.9, 133.8, 128.8, 128.8, 128.8, 128.8, 128.6, 128.4, 128.3, 127.9, 126.2, 44.1, 43.6; (ESI HRMS) m/z calcd. for $C_{15}H_{13}NOH$ 224.1075 and $C_{15}H_{13}NONa$ 246.0895 $(M+H)^+$, found 224.1071, $(M+Na)^+$, found 246.0908. Data in accordance with the literature.[41]

1-(2-Benzoyl-3-phenylaziridin-1-yl)-2-methylpropan-1-one (114)

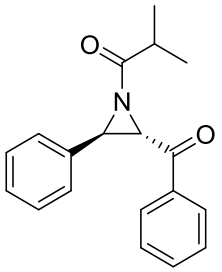

Triethylamine (0.09 mL, 0.67 mmol, 6.0 eq.) was added to a solution of **77** (25.4 mg, 0.11 mmol, 1.0 eq.) in DCM (2.5 mL), followed by isobutyryl chloride (0.06 mL, 0.56 mmol, 5.0 eq.). The solution was left to stir under nitrogen for 2 hours. The reaction was then reduced under pressure, redissolved in EtOAc, and salts were filtered from solution. The filtrate was then reduced under pressure. The product was purified by GRACE Reveleris [Ethyl Acetate/Petroleum Ether 0-10% (3 CV), 20% (2 CV), 30% (2 CV), 40% (2 CV), 50% (2 CV), 50-100% (7 CV)] and yielded a clear oil (20.5 mg, 61%). υ_{max} (film)/cm-1: 2925 (m), 1670 (s), 1449 (m), 698 (s); ^{1}H NMR (500 MHz, $CDCl_3$): δH 8.01 (dd, J = 8.3, 1.5 Hz, 2H, Ar), 7.61 (t, J = 7.3 Hz, 1H, Ar), 7.49 (t, J = 7.8 Hz, 2H, Ar), 7.37 (m, 5H, Ar), 4.12 (d, J = 2.0 Hz, 1H, CH), 3.91 (d, J= 2.0 Hz, 1H, CH), 2.62 (spt, J = 6.9 Hz, 1H, CH), 1.29 (d, J = 6.8 Hz, 3H, CH_3), 1.21 (d, J = 6.8, 3H, CH_3); ^{13}C NMR (125 MHz, $CDCl_3$): δC 192.4, 186.6, 136.6, 136.2, 134.3, 129.2, 129.1, 128.9, 128.8, 126.7, 126.7, 126.7, 48.1, 47.2, 36.9, 20.1, 19.1; (ESI HRMS) m/z calcd. for $C_{19}H_{19}NO_2Na$ 316.1314 $(M+Na)^+$, found 316.1300.

1-(2-Benzoyl-3-phenylaziridin-1-yl)ethan-1-one (113)

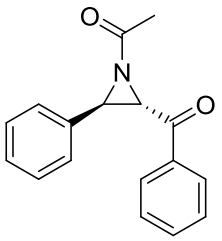

Triethylamine (0.09 mL, 0.67 mmol, 6.0 eq.) was added to a solution of **77** (24.9 mg, 0.11 mmol, 1.0 eq.) in DCM (2.5 mL), followed by acetyl chloride (0.04 mL, 0.56 mmol, 5.0 eq.). The solution was left to stir under nitrogen for 23 minutes. The reaction was then reduced under pressure, redissolved in EtOAc, and salts were filtered from solution. The filtrate was then reduced under pressure. The product was purified by GRACE Reveleris [Ethyl Acetate/Petroleum Ether 0-10% (3 CV), 20% (2 CV), 30% (2 CV), 40% (2 CV), 50% (2 CV), 50-100% (7 CV)] and yielded a pale yellow oil (16.2 mg, 55%). υ_{max} (film)/cm^{-1}: 2925 (s), 2855 (m), 1690 (s), 1450 (m), 713 (w); ^{1}H NMR (500 MHz, $CDCl_3$): δH 7.92 (d, J = 7.3 Hz, 2H, Ar), 7.55 (t, J = 7.4 Hz, 1H, Ar), 7.42 (t, J = 7.6 Hz, 2H, Ar), 7.30 (m, 5H, Ar), 4.09 (d, J = 2.1 Hz, 1H. CH), 3.78 (d, J= 2.3 Hz, 1H, CH), 2.13 (s, 3H, CH_3); ^{13}C NMR (125 MHz, $CDCl_3$): δC 192.0, 179.7, 136.1, 135.6, 134.1, 128.9, 128.8, 128.6, 128.5, 126.4, 126.3, 126.3, 48.1, 47.3, 24.4; (ESI HRMS) m/z calcd. for $C_{17}H_{15}NO_2Na$ 288.1000 $(M+Na)^+$, found 288.1014. Data in accordance with the literature.[113]

5.2. Experimental Data for Chapters 3 and 4

5.2.1. General Chalcone Synthesis

Acetophenone (1 mmol, 1 eq.) was stirred in 2M NaOH in MeOH (6 eq.) for 1 hour under nitrogen before adding aldehyde (1 mmol, 1 eq.) and leaving to stir at room temperature for 12 to 48 hours. Reactions were monitored by TLC using 20% ethyl acetate/petroleum ether as the eluent. 1M HCl was added until the reaction was neutral and precipitate appeared. The precipitate was filtered from solution, recrystallised from ethanol, and filtered to yield the crystalline solids.

(*E*)-1-Phenyl-3-(*p*-tolyl)prop-2-en-1-one (144)

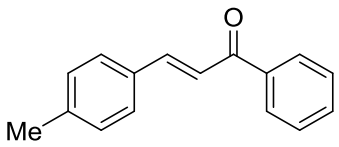

Acetophenone (1.2 mL, 10.0 mmol) and *p*-tolualdehyde (1.2 mL, 10.0 mmol) yielded a pale yellow crystalline solid (894 mg, 40%). mp 97-98 °C. υ_{max} (film)/cm^{-1}: 3023 (m), 1654 (s), 1594 (s), 1449 (m); ^{1}H NMR (300 MHz, $CDCl_3$): δH 8.04-8.01 (m, 2H, Ar), 7.81 (d, J = 15.8 Hz, 1H, C=H), 7.62-7.48 (m, 6H, Ar, C=H), 7.24 (d, J = 7.9 Hz, 2H, Ar), 2.41 (s, 3H, CH_3); ^{13}C NMR (75 MHz, $CDCl_3$): δC 190.7, 144.9, 141.1, 138.3, 132.7, 132.1, 129.7, 128.6, 128.5, 128.4, 121.0, 21.5; (ESI HRMS) m/z calcd. for $C_{16}H_{14}O_1H$ 223.1123 $(M+H)^+$, found 223.1024. Data in accordance with the literature.[114]

(*E*)-3-(4-Methoxyphenyl)-1-phenylprop-2-en-1-one (145)

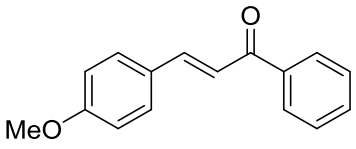

Acetophenone (2.4 mL, 10.0 mmol) and *p*-anisaldehyde (2.5 mL, 10.0 mmol) yielded a pale orange crystalline solid (3.30 g, 69%). mp 70-73 °C. υ_{max} (film)/cm^{-1}: 3016 (m), 2600 (m), 1656 (s), 1595 (s), 1510 (s), 1302 (s); ^{1}H NMR (300 MHz, $CDCl_3$): δH 8.04-8.01 (m,

2H, Ar), 7.80 (d, J = 15.6 Hz, 1H, C=H), 7.63-7.40 (m, , 6H, Ar, C=H), 6.95 (d, J = 8.7 Hz, 2H, Ar), 3.87 (s, 3H, CH_3); ^{13}C NMR (75 MHz, $CDCl_3$): δC 190.6, 161.6, 144.7, 138.4, 132.5, 130.2, 128.5, 128.4, 127.5, 119.7, 114.4, 55.4; (ESI HRMS) m/z calcd. for $C_{16}H_{14}O_2Na$ 261.0891 $(M+Na)^+$, found 261.0878. Data in accordance with the literature.[114]

(*E*)-3-(4-Nitrophenyl)-1-phenylprop-2-en-1-one (146)

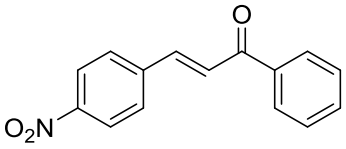

Acetophenone (58 µL, 0.5 mmol) and 4-nitrobenzaldehyde (76 mg, 0.5 mmol) yielded a pale orange crystalline solid (67 mg, 52%). mp 162-163 °C. υ_{max} (film)/cm^{-1}: 3076 (m), 2931 (m), 2842 (m), 1656 (s), 1511 (w), 1329 (s); ^1H NMR (300 MHz, $CDCl_3$): δH 8.29 (d, J = 8.9 Hz, 2H, Ar), 8.06-8.03 (m, 2H, Ar), 7.86-7.79 (m, 3H, Ar, C=H), 7.69-7.52 (m, 4H, Ar, C=H); ^{13}C NMR (75 MHz, $CDCl_3$): δC 189.7, 148.6, 141.5, 141.1, 137.5, 133.4, 129.0, 128.9, 128.6, 125.7, 124.3; (ESI HRMS) m/z calcd. for $C_{15}H_{12}NO_3$ 254.0817 $(M+H)^+$, found 254.0822. Data in accordance with the literature.[114]

(*E*)-3-(4-Chlorophenyl)-1-phenylprop-2-en-1-one (147)

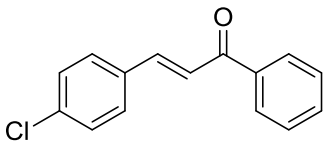

Acetophenone (1.12 mL, 10.0 mmol) and 4-chlorobenzaldehyde (1.44 g, 10.0 mmol) yielded a pale yellow crystalline solid (542 mg, 22%). mp 114-115 °C. υ_{max} (film)/cm^{-1}: 3010 (m), 1656 (s), 1590 (s), 1445 (m); ^1H NMR (300 MHz, $CDCl_3$): δH 8.04-8.01 (m, 2H, Ar), 7.77 (d, J = 14.7 Hz, 1H, Ar), 7.64-7.49 (m, 6H, Ar, C=H), 7.41 (d, J = 8.5, 2H, Ar); ^{13}C NMR (75 MHz, $CDCl_3$): δC 190.2, 143.3, 138.0, 136.4, 133.3, 132.9, 129.6, 129.2, 128.7, 128.5, 122.4; (ESI HRMS) m/z calcd. for $C_{15}H_{11}ONa$ 265.0396 $(M+Na)^+$, found 265.0374. Data in accordance with the literature.[114]

(*E*)-3-Phenyl-1-(*p*-tolyl)prop-2-en-1-one (148)

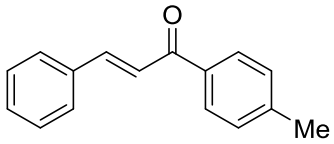

4'-Methylacetophenone (1.33 mL, 10.0 mmol) and benzaldehyde (1.02 mL, 10.0 mmol) yielded a pale yellow crystalline solid (529 mg, 22%). mp 55-56 °C. υ_{max} (film)/cm^{-1}: 3028 (m), 2970 (m), 1656 (s), 1595 (s), 1450 (m); ^{1}H NMR (300 MHz, $CDCl_3$): δH 7.95 (d, J = 8.1 Hz, 2H, Ar), 7.82 (d, J = 15.6 Hz, 1H, C=H), 7.66 (m, 2H, Ar), 7.55 (d, J =15.6 Hz, 1H, C=H), 7.43 (m, 3H, Ar), 7.32 (d, J = 7.9 Hz, 2H, Ar), 2.45 (s, 3H, CH_3); ^{13}C NMR (75 MHz, $CDCl_3$): δC 190.0, 144.4, 143.6, 135.6, 135.0, 130.4, 129.3, 128.9, 128.6, 128.4, 122.0, 21.7; (ESI HRMS) m/z calcd. for $C_{16}H_{14}O_1Na$ 245.0942 $(M+Na)^+$, found 245.0933. Data in accordance with the literature.[114]

(*E*)-1-(4-Methoxyphenyl)-3-phenylprop-2-en-1-one (149)

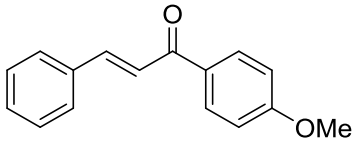

4-Methoxyacetophenone (1.5 g, 10.0 mmol) and benzaldehyde (1.02 mL, 10.0 mmol) yielded a white crystalline solid (1.72 g, 68%). mp 106-107 °C. υ_{max} (film)/cm^{-1}: 3055 (m), 2842 (m), 1652 (s), 1597 (s), 1256 (w), 951 (m); ^{1}H NMR (300 MHz, $CDCl_3$): δH 8.07-8.04 (m, 2H, Ar), 7.82 (d, J = 15.6 Hz, 1H, C=H), 7.66-7.64 (m, 2H, Ar), 7.56 (d, J = 15.6 Hz, 1H, C=H), 7.45-7.40 (m, 3H, Ar), 7.01-6.98 (m, 2H, Ar), 3.90 (s, 3H, CH_3); ^{13}C NMR (75 MHz, $CDCl_3$): δC 188.7, 163.4, 144.0, 135.0, 131.0, 130.8, 130.3, 128.9, 128.3, 121.8, 113.8, 55.5; (ESI HRMS) m/z calcd. for $C_{16}H_{14}O_2Na$ 261.0891 $(M+Na)^+$, found 261.0871. Data in accordance with the literature.[114]

(*E*)-1-(4-Nitrophenyl)-3-phenylprop-2-en-1-one (150)

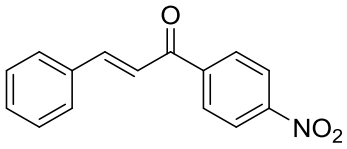

4-Nitroacetophenone (830 mg, 5.0 mmol) and benzaldehyde (0.51 mL, 5.0 mmol) yielded an orange crystalline solid (329 mg, 26%). mp 102-105 °C. υ_{max} (film)/cm^{-1}: 3021 (m), 2942 (m), 1661 (s), 1593 (s), 1518 (s); ^{1}H NMR (300 MHz, $CDCl_3$): δH 8.37 (d, J = 8.7 Hz, 2H, Ar), 8.16 (d, J = 8.7 Hz, 2H, Ar), 7.86 (d, J = 15.6 Hz, 1H, C=H), 7.69-7.66 (m, 2H, Ar), 7.53-7.45 (m, 4H. Ar); ^{13}C NMR (75 MHz, $CDCl_3$): δC 189.1, 149.3, 146.8, 143.0 134.2, 131.2, 129.4, 129.1, 128.7, 123.9, 121.24; (ESI HRMS) m/z calcd. for $C_{15}H_{11}NO_3H$ 254.0817 $(M+H)^+$, found 254.0821. Data in accordance with the literature.[115]

(*E*)-1-(4-Chlorophenyl)-3-phenylprop-2-en-1-one (151)

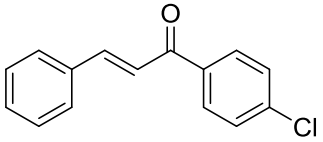

4-Chloroacetophenone (1.3 mL, 10.0 mmol) and benzaldehyde (1.02 mL, 10.0 mmol) yielded a pale yellow crystalline solid (700 mg, 29%). mp 97-98 °C. υ_{max} (film)/cm^{-1}: 3054 (m), 1659 (s), 1585 (s), 1600 (s), 1569 (s); ^{1}H NMR (300 MHz, $CDCl_3$): δH 8.00-7.97 (m, 2H, Ar), 7.83 (d, J = 15.6 Hz, 1H, C=H), 7.68-7.65 (m, 2H, Ar), 7.53-7.43 (m, 6H, Ar, C=H); ^{13}C NMR (75 MHz, $CDCl_3$): δC 189.2, 145.4, 139.2, 136.5, 134.6, 130.7, 129.9, 129.0, 128.9, 128.5, 121.4; (ESI HRMS) m/z calcd. for $C_{15}H_{11}OClNa$ 265.0396 $(M+Na)^+$, found 265.0370. Data in accordance with the literature.[114]

(*E*)-1,3-Bis(4-bromophenyl)prop-2-en-1-one (152)

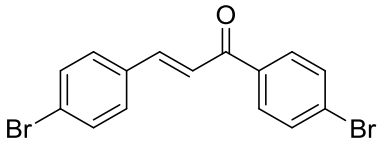

4-Bromoacetophenone (500 mg, 2.51 mmol) and 4-bromobenzaldehyde (464 mg, 2.51 mmol) yielded a pale yellow crystalline solid (677 mg, 74%). mp 186-187 °C. υ_{max} (film)/cm^{-1}: 3020 (m), 2970 (m), 1655 (s), 1601 (s), 1582 (s), 1560 (m); ^{1}H NMR (300 MHz, $CDCl_3$): δH 7.90 (d, J = 8.5 Hz, 2H, Ar), 7.76 (d, J = 15.6 Hz, 1H, C=H), 7.66 (d, J = 8.5 Hz, 2H, Ar), 7.59-7.50 (m, 5H, Ar); ^{13}C NMR (75 MHz, $CDCl_3$): δC 189.0, 143.9, 136.7, 133.5, 132.2, 132.0, 130.0, 129.8, 128.1, 125.1, 121.8; (ESI HRMS) m/z calcd. for $C_{15}H_{10}OBr_2Na$ 386.8996 $(M+Na)^+$, found 386.8976. Data in accordance with the literature.[116]

(*E*)-1-(benzo[*d*][1,3]dioxol-5-yl)-3-(pyridin-3-yl)prop-2-en-1-one (137)

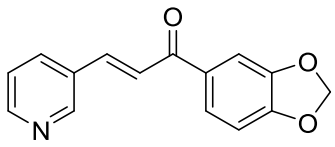

1-(Benzo[*d*][1,3]dioxol-5-yl)ethan-1-one (824 mg, 5.0 mmol) and nicotinaldehyde (0.47 mL, 5.0 mmol) yielded a pale yellow crystalline solid (693 mg, 54%). mp 135-136 °C. υ_{max}(film)/cm^{-1}: 2916 (m), 1656 (s), 1597 (s), 1585 (s), 1442 (s), 1247 (s); ^{1}H NMR (300 MHz, $CDCl_3$): δH 8.87 (d, J = 2.1 Hz, 1H, Ar), 8.64 (dd, J = 4.8, 1.6 Hz, 1H, Ar), 7.97-7.93 (m, 1H, Ar), 7.79 (d, J = 15.6 Hz, 1H, CH), 7.67 (dd, J = 8.2, 1.8 Hz, 1H, Ar), 7.56-7.54 (m, 2H, Ar, CH), 7.37 (dd, J = 8.1, 4.7 Hz, 1H, Ar), 6.92 (d, J = 8.1 Hz, 1H, Ar, 6.09 (s, 2H, CH_2); ^{13}C NMR (75 MHz, $CDCl_3$): δC 187.5, 152.0, 151.0, 149.9, 148.4, 140.3, 134.5, 132.4, 130.7, 124.8, 123.7, 123.4, 108.3, 107.9, 101.9; (ESI HRMS) m/z calcd. for $C_{15}H_{11}NO_3H$ 254.0817 $(M+H)^+$, found 254.0800.

5.2.2. General Aziridine Synthesis

To a solution of chalcone (0.36 mmol, 1.0 eq.) and **112** (0.39 mmol, 1.1 eq.) in DMSO (10 mg/mL of chalcone) potassium *tert*-butoxide (0.39 mmol, 1.1 eq.) was added over 5 minutes portion-wise. The reaction was left to stir open to air at room temperature from 0.5 to 1.5 hours, substrate dependant. The dark orange/brown solutions were then quenched with diethyl ether (25 mL) and distilled water (25 mL). The products were extracted into diethyl ether and washed with distilled water (2 x 25 mL) and brine (1 x 25 mL). The ether layer was then dried over magnesium sulphate, filtered and concentrated under reduced pressure. Products were purified by flash column chromatography on a GRACE Reveleris® X2 Flash Chromatography System, [Ethyl Acetate/Petroleum Ether 0-10% (3 CV), 20% (2 CV), 30% (2 CV), 40% (2 CV), 50% (2 CV), 50-100% (7 CV)].

Phenyl(3-(*p*-tolyl)aziridin-2-yl)methanone (120)

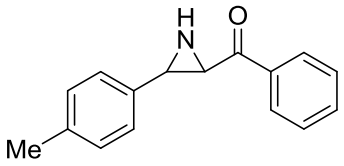

144 (400 mg, 1.69 mmol) was reacted using the general conditions and yielded a yellow crystalline solid (266 mg, 66%). mp 104-108 °C. υ_{max} (film)/cm^{-1}: 2917 (s), 2850 (m), 1690 (w), 1655 (s), 1593 (s), 1567 (s); ^{1}H NMR (250 MHz, $CDCl_3$): δH 8.05-8.00 (m, 2H, Ar), 7.76 (tt, J = 14.8, 7.4 Hz, 1H, Ar), 7.54-7.48 (m, 2H, Ar), 7.31-7.28 (m, 2H, Ar), 7.20 (d, J = 8.1 Hz, 2H, Ar), 3.52 (dd, J = 8.0, 2.3, 1H, CH), 3.18 (dd, J = 9.2, 2.3, 1H, CH), 2.69 (t, J = 8.5, 1H, NH), 2.39 (s, 3H, CH_3) ; ^{13}C NMR (75 MHz, $CDCl_3$): δC 195.8, 137.7, 135133.8, 129.2, 128.8, 128.3, 126.1, 44.2, 43.5, 21.2; (ESI HRMS) m/z calcd. for $C_{16}H_{15}NONa$ 261.1124 $(M+Na)^+$, found 261.1103. Data in accordance with the literature.[42]

(3-(4-Methoxyphenyl)aziridin-2-yl)(phenyl)methanone (121)

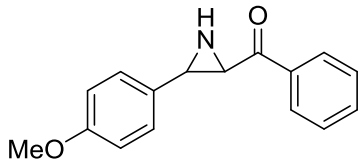

145 (500 mg, 0.42 mmol) was reacted using the general conditions and yielded a yellow oil (329 mg, 62%). υ_{max} (film)/cm^{-1}: 3256 (s), 3064 (m), 2840 (m), 1660 (s), 1611 (m), 1513 (s); ^{1}H NMR (300 MHz, $CDCl_3$): δH 8.01-7.99 (m, 2H, Ar), 7.62 (t, J = 7.4 Hz, 1H, Ar), 7.49 (t, J = 7.5, 2H, Ar), 7.33-7.28 (m, 2H, Ar), 6.93-6.88 (m, 2H, Ar), 3.82 (s, 3H, CH_3), 3.49 (d, J = 5.7, 1H, CH), 3.15 (d, J = 7.3, 1H, CH), 2.67 (t, J = 8.3 Hz, 1H, NH) ; ^{13}C NMR (75 MHz, $CDCl_3$): δC 195.7, 159.3, 135.9, 133.7, 130.3, 128.7, 128.2, 127.2, 113.9, 55.2, 44.1, 43.3; (ESI HRMS) m/z calcd. for $C_{16}H_{15}NO_2Na$ 276.1000 $(M+Na)^+$, found 276.0988. Data in accordance with the literature.[42]

(3-(4-Nitrophenyl)aziridin-2-yl)(phenyl)methanone (122)

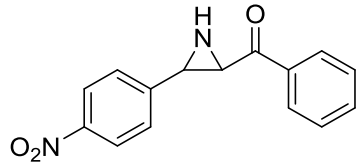

146 (100 mg, 0.40 mmol) was reacted using the general conditions and yielded an oily brown residue (48.2 mg, 40%). υ_{max} (film)/cm^{-1}: 3264 (m), 2925 (s), 2853 (m), 1663 (s), 1580 (s), 1514 (s); ^{1}H NMR (300 MHz, $CDCl_3$): δH 8.27-8.21 (m, 2H, Ar), 8.03-7.98 (m, 2H, Ar), 7.68-7.63 (m, 1H, Ar), 7.57-7.49 (m, 4H, Ar), 3.53 (s, 1H, CH), 3.27 (s, 1H, CH), 2.88-2.71 (br s, 1H, NH); ^{13}C NMR (75 MHz, $CDCl_3$): δC 194.8, 147.5, 147.8, 135.5, 134.2, 129.0, 128.3, 127.1, 123.8, 44.1, 42.3; (ESI HRMS) m/z calcd. for $C_{15}H_{12}N_2O_3H$ 269.0926 $(M+H)^+$, found 269.0916. Data in accordance with the literature.[42]

(3-(4-Chlorophenyl)aziridin-2-yl)(phenyl)methanone (123)

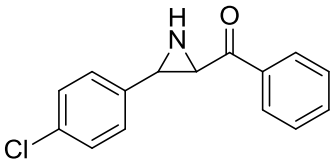

147 (300 mg, 1.24 mmol) was reacted using the general conditions and yielded a yellow crystalline solid (184 mg, 57%). mp 84-87 °C. υ_{max} (film)/cm^{-1}: 3263 (m), 2997 (m), 2253 (m), 1631 (s), 1443 (s), 1375 (s); ^{1}H NMR (300 MHz, $CDCl_3$): δH 8.01-7.98 (m, 2H, Ar), 7.64 (t, J = 7.3 Hz, 1H, Ar), 7.51 (t, J = 7.6, 2H, Ar), 7.36-7.30 (m, 4H, Ar), 3.47 (s, 1H, CH), 3.16 (s, 1H, CH), 2.70 (br s, 1H, NH); ^{13}C NMR (75 MHz, $CDCl_3$): δC 195.4, 136.9, 135.8, 134.0, 133.7, 128.9, 128.8, 128.4, 127.6, 44.1, 42.8; (ESI HRMS) m/z calcd. for $C_{15}H_{12}NOClNa$ 281.0578 $(M+Na)^+$, found 281.0526. Data in accordance with the literature.[48]

(3-Phenylaziridin-2-yl)(*p*-tolyl)methanone (124)

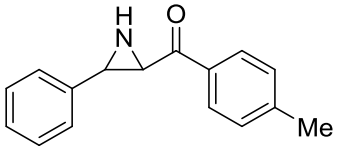

148 (250 mg, 1.05 mmol) was reacted using the general conditions and yielded a white crystalline solid (78.2 mg, 31%). mp 87-90 °C. υ_{max} (film)/cm^{-1}: 3224 (m), 3022 (m), 1660 (s), 1605 (s), 1413 (m); ^{1}H NMR (300 MHz, $CDCl_3$): δH ^{1}H NMR (300 MHz, $CDCl_3$): δH 7.91 (d, 2H, J = 8.3 Hz, Ar), 7.38-7.28 (m, 7H, Ar), 3.51 (s, 1H,CH), 3.17 (s, 1H, CH), 2.68 (br s, 1H, NH), 2.44 (s, 3H, CH_3); ^{13}C NMR (75 MHz, $CDCl_3$): δC 195.2, 144.9, 138.4, 133.4, 129.5, 128.5, 128.4, 127.8, 126.2, 43.9, 43.3, 21.7; (ESI HRMS) m/z calcd. for $C_{16}H_{15}NONa$ 260.1051 $(M+Na)^+$, found 260.1040. Data in accordance with the literature.[42]

(4-Methoxyphenyl)(3-phenylaziridin-2-yl)methanone (125)

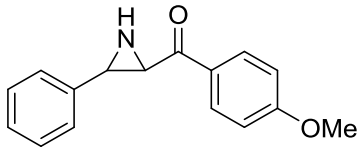

149 (250 mg, 0.99 mmol) was reacted using the general conditions and yielded a yellow solid (96.1 mg, 38%). mp 72-76 °C. υ_{max} (film)/cm^{-1}: 3262 (m), 2979 (s), 2844 (m), 1652 (s), 1592 (s), 1249 (s); ^{1}H NMR (300 MHz, $CDCl_3$): δH 8.00 (d, J = 8.9 Hz, 2H, Ar), 7.38-7.31 (m, 5H, Ar), 6.99-6.95 (m, 2H, Ar), 3.88 (s, 3H, CH_3), 3.48 (d, J = 1.9 Hz, 1H, CH), 3.16 (d, J = 1.5 Hz, 1H, CH), 2.68 (br s, 1H, NH); ^{13}C NMR (75 MHz, $CDCl_3$): δC 193.9, 164.1, 138.5, 130.6, 128.9, 128.5, 127.7, 126.1, 114.0, 55.5, 43.7, 43.1; (ESI HRMS) m/z calcd. for $C_{16}H_{15}NO_2H$ 254.1181 $(M+H)^+$, found 254.1168. Data in accordance with the literature.[42]

(4-Nitrophenyl)(3-phenylaziridin-2-yl)methanone (126)

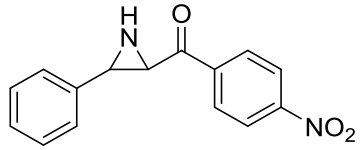

150 (100 mg, 0.37 mmol) was reacted using the general conditions and yielded an oily dark orange residue (48 mg, 45%). υ_{max} (film)/cm^{-1}: 3263 (m), 2925 (m), 1665 (s), 1599 (s), 1450 (s), 1253 (s); ^{1}H NMR (300 MHz, $CDCl_3$): δH 8.42-8.26 (m, 5H, Ar), 8.15 (m, 4H, Ar), 3.54 (d, J = 2.3, 1H, CH), 3.28 (d, J = 2.3, 1H, CH), 2.73 (br s, 1H, NH); ^{13}C NMR (75 MHz, $CDCl_3$): δC 195.4, 147.2, 131.1, 129.4, 128.7, 128.3, 126.2, 124.0, 123.5, 44.6, 43.4; (ESI HRMS) m/z calcd. for $C_{15}H_{12}N_2O_3Na$ 291.0746 $(M+Na)^+$, found 291.0722.

(4-Chlorophenyl)(3-phenylaziridin-2-yl)methanone (127)

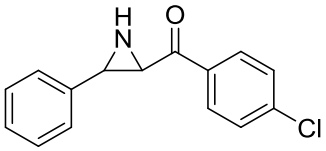

151 (250 mg, 1.03 mmol) was reacted using the general conditions and yielded a white crystalline solid (112 mg, 42%). mp 119-120 °C. υ_{max} (film)/cm^{-1}: 3267 (m), 3245 (m), 3031 (m), 1658 (s), 1589 (s), 1412 (s); ^{1}H NMR (250 MHz, $CDCl_3$): δH 7.97-7.92 (m, 2H, Ar), 7.49-7.44 (m, 2H, Ar), 7.39-7.29 (m, 5H, Ar), 3.47 (dd, J = 7.8, 2.1 Hz, 1H, CH), 3.20 (dd, J = 9.2, 2.2 Hz, 1H, CH), 2.69 (t, J = 8.4 Hz, 1H, NH); ^{13}C NMR (75 MHz, $CDCl_3$): δC 194.5, 140.3, 138.0, 134.1, 129.6, 129.1, 128.5, 127.9, 126.1, 44.0, 43.7; (ESI HRMS) m/z calcd. for $C_{15}H_{12}NONa$ 280.0505 $(M+Na)^+$, found 280.0472. Data in accordance with the literature.[42]

(4-Bromophenyl)(3-(4-bromophenyl)aziridin-2-yl)methanone (128)

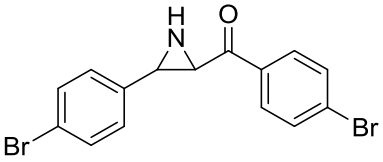

152 (200 mg, 0.55 mmol) was reacted using the general conditions and yielded a white crystalline solid (79 mg, 38%). mp 116-118 °C. υ_{max} (film)/cm^{-1}: 3000 (m), 2923 (m), 2854 (m), 1653 (s), 1600 (m), 1580 (s); ^{1}H NMR (300 MHz, $CDCl_3$): δH 7.75-7.70 (m, 2H, Ar), 7.54-7.49 (m, 2H, Ar), 7.39-7.34 (m, 2H, Ar), 7.17-7.10 (m, 2H, Ar), 3.29 (dd, J = 7.5, 2.0 Hz, 1H, CH), 3.03 (dd, J = 8.8, 1.7 Hz, 1H, CH), 2.57 (t, J = 8.8 Hz, 1H, NH); ^{13}C NMR (75 MHz, $CDCl_3$): δC 194.1, 137.2, 134.5, 132.2, 131.7, 130.4, 129.3, 127.8, 121.9, 44.0, 43.0; (ESI HRMS) m/z calcd. for $C_{15}H_{12}NOBr_2H$ 379.9286 $(M+H)^+$, found 379.9296.

Benzo[*d*][1,3]dioxol-5-yl(3-(pyridin-3-yl)aziridin-2-yl)methanone (138)

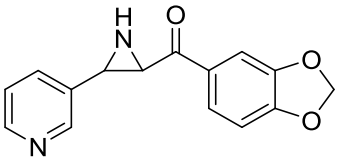

137 (200 mg, 0.59 mmol) was reacted using the general conditions and yielded an orange crystalline solid (105.8 mg, 50%). mp 118-120 °C. υmax(film)/cm^{-1}: 3270 (m), 2917 (m), 1645 (s), 1596 (s), 1498 (s), 1439 (s); ^{1}H NMR (300 MHz, $CDCl_3$): δH 8.63 (d, J = 1.9 Hz, 1H, Ar), 8.56 (dd, J = 4.7, 1.5 Hz, 1H, Ar), 7.69-7.59 (m, 2H, Ar), 7.46 (d, J = 1.7, 1H, A4), 7.3 (dd, J = 7.8, 4.8 Hz, 1H, Ar), 6.88 (d, J = 8.1 Hz, 1H, Ar), 6.08 (s, 2H, CH_2), 3.42 (dd, J = 7.5, 1.9 Hz, 1H, CH), 3.16 (d, J = 7.3 Hz, 1H, CH), 2.67 (t, J = 8.4 Hz, 1H, NH); ^{13}C NMR (75 MHz, $CDCl_3$): δC 193.0, 152.7, 149.1, 148.5, 134.1, 133.3, 130.5, 125.0, 123.5, 108.2, 107.9, 102.1, 43.4, 40.6; (ESI HRMS) m/z calcd. for $C_{15}H_{12}N_2O_3Na$ 291.0746 $(M+Na)^+$, found 291.0716.

(1-(*Tert*-butyl)-3-phenylaziridin-2-yl)(phenyl)methanone (72)

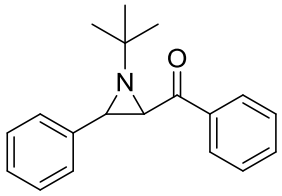

Trans-chalcone (521 mg, 2.5 mmol, 1 eq.) was added to a flame dried, nitrogen purged flask and dissolved in anhydrous diethyl ether (90 mL). I_2 (635 mg, 2.5 mmol, 1 eq.) was then added, followed by a solution of *tert*-butylamine (1.3 mL, 12.5 mmol, 5 eq.) in anhydrous diethyl ether (10 mL), resulting in an orange solution. The reaction was left to stir under nitrogen for 72 hours. The HI salt was filtered from the reaction and the filtrate was washed with H_2O (4x) and brine (1 x). The organic layer was dried over magnesium sulphate and reduced under pressure. The product was recrystallised from pentane to yield a yellow crystalline solid (212 mg, 30%). mp 105-110 °C. υ_{max} (film)/cm^{-1}: 2976 (m), 2541 (m), 1665 (s), 1634 (s), 1525 (s), 1450 (m), 1373 (s); ^{1}H NMR (300 MHz, $CDCl_3$): δH 7.91-7.88 (m, 2H, Ar), 7.29-7.47 (m, 1H, Ar), 7.41-7.36 (m, 4H, Ar), 7.21-7.10 (m, 3H, Az) 3.50-3.45 (m, 2H, 2CH), 1.18 (s, 9H, $3CH_3$); ^{13}C NMR (75 MHz, $CDCl_3$): δC 194.0,

137.4, 136.1, 132.7, 128.3, 128.1, 127.9, 127.6, 53.8, 44.2, 43.2, 26.4; (ESI HRMS) m/z calcd. for $C_{19}H_{22}NOH$ 280.1701 $(M+H)^+$, found 280.1702. Data in accordance with the literature.[117]

(1-Chloro-3-phenylaziridin-2-yl)(phenyl)methanone (131)

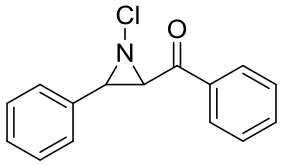

77 was dissolved in 4:1 dimethoxy ethane/H_2O mixture (20 mL) in a round bottom flask. NCS (65.8 mg, 0.50 mmol, 1.1 eq.) was then added and the reaction was left to stir under nitrogen for 60 hours. The solvent was reduced under pressure and purified by flash column chromatography on a GRACE Reveleris® X2 Flash Chromatography System, [Ethyl Acetate/Petroleum Ether 0-10% (3 CV), 20% (2 CV), 30% (2 CV), 40% (2 CV), 50% (2 CV), 50-100% (7 CV)]. The isolated product yielded a yellow oil (66.8 mg, 57%). υ_{max} (film)/cm^{-1}: 3060 (m), 2957 (m), 2806 (m), 1771 (s), 1683 (s); ^{1}H NMR (500 MHz, $CDCl_3$): Invertomers observed in a ratio of 2:1. Invertomer 1: δH 8.18-8.16 (m, 2H, Ar), 7.59-7.56 (m, 3H, Ar), 7.40-7.33 (m, 5H, Ar), 4.10 (d, J = 5.2 Hz, 1H, CH), 3.98 (d, J = 5.2 Hz, 1H, CH), Invertomer 2: δH 8.14-8.11 (m, 2H, Ar), 7.69-7.66 (m, 3H, Ar), 7.51-7.47 (m, 5H, Ar), 4.22 (d, J = 5.9 Hz, 1H, CH), 4.05 (d, J = 5.9 Hz, 1H, CH); ^{13}C NMR (75 MHz, $CDCl_3$): δC 192.8, 134.2, 130.3, 129.4, 128.9, 128.7, 128.5, 128.4, 126.6, 52.5, 52.1; (ESI HRMS) m/z calcd. for $C_{16}H_{15}NO_2H$ 260.0791 $(M+H)^+$, found 260.0818. Data in accordance with the literature.[118]

5.3. Spectroscopic Measurements

Specific experimental details are given with the associated text in the results chapters.

GC-MS Data

GC-MS data was collected on an Agilent 7890A Gas Chromatograph with a capillary column (30 m × 0.320 mm internal diameter) coated with HP-5 [(5% phenyl)-methylpolysiloxane] as the stationary phase providing a 0.25 μm film thickness. Helium was used as the mobile phase with a flow rate of 1.2 mL/min. The GC was coupled with an Agilent 5975C inert MSD with Triple Axis Detector.

Fluorescence Experiments

Fluorescence measurements were carried out on a Perkin Elmer LS50B Luminescence Spectrometer connected to a circulating water bath to regulate the temperature to 20 °C. Excitation and emission slit widths were set as stated in the experimental discussions. 3D excitation-emission profiles were obtained by varying the excitation wavelength every 2 nm from 200 nm to 348 nm. The emission was measured at each excitation wavelength. The baseline of MeCN was subtracted from each data set at the corresponding slit widths.

Magnetic Field Effect Studies were carried out using a custom fibre optic cable mounted to the fluorimeter with the excitation slit width set to 15 nm. The fibre optic cable was mounted in the optical table setup shown in Chapter 3.

UV-Visible Measurements

Absorbance data was collected on an Agilent Cary 60 UV-vis spectrometer using a 1 cm path length quartz cuvette.

Stopped-Flow Measurements

Stopped-flow UV and fluorescence kinetics were obtained on a Hi-Tech Scientific Stopped-Flow instrument with slit widths set to 5 nm. A linear polariser was used with this setup for polarisation experiments.

Circular Dichroism (CD) Measurements

CD spectra were recorded using a 1 cm path length quartz cuvette on an Applied Photophysics Chirascan spectrophotometer.

Optical Rotations

Optical rotations were measured using an Optical Activity Ltd. AA-10 automatic polarimeter. The cell volume was 1.5 mL with a path length of 1 dm. Measurements were recorded in $CHCl_3$ at room temperature, approximately 23 °C

6. References

1. J. B. Sweeney, *Chem. Soc. Rev.*, 2002, **31**, 247–258.

2. A. Armstrong and A. Ferguson, *Beilstein J. Org. Chem.*, 2012, **8**, 1747–1752.

3. G. E. Ham, *J. Org. Chem.*, 1964, **29**, 3052–3055.

4. Gilchrist, Thomas L., *Heterocyclic Chemistry*, Harlow : Longman, Essex, England, 3rd edn., 1997.

5. A. Padwa and A. Battisti, *J. Org. Chem.*, 1971, **36**, 230–231.

6. R. S. Atkinson and C. W. Rees, *J. Chem. Soc. C. Org.*, **1969**, 772–778.

7. T. Ando, S. Minakata, I. Ryu and M. Komatsu, *Tetrahedron Lett.*, 1998, **39**, 309–312.

8. J. U. Jeong, B. Tao, I. Sagasser, H. Henniges and K. B. Sharpless, *J. Am. Chem. Soc.*, 1998, **120**, 6844–6845.

9. K. Guthikonda and J. Du Bois, *J. Am. Chem. Soc.*, 2002, **124**, 13672–13673.

10. E. C. McLaughlin, A. Shrestha, M. H. Fletcher, N. S. Steinauer, M. K. Shinn and S. M. Shahid, *Tetrahedron Lett.*, 2013, **54**, 5461–5463.

11. W. Lwowski and T. W. Mattingly, *J. Am. Chem. Soc.*, 1965, **87**, 1947–1958.

12. L. B. Krasnova and A. K. Yudin, *Org. Lett.*, 2006, **8**, 2011–2014.

13. L. B. Krasnova, R. M. Hili, O. V. Chernoloz and A. K. Yudin, *Arkivoc*, 2004, **4**, 26–38.

14. T. Siu and A. K. Yudin, *J. Am. Chem. Soc.*, 2002, **124**, 530–531.

15. R. Vyas, B. M. Chanda and A. V. Bedekar, *Tetrahedron Lett.*, 1998, **39**, 4715–4716.

16. R. Vyas, B. M. Chanda, A. A. Belhekar, D. R. Patel, R. N. Ram and A. V. Bedekar, *J. Mol. Catal. Chem.*, 2000, **160**, 237–241.

17. A. M. M. Antunes, S. J. L. Marto, P. S. Branco, S. Prabhakar and A. M. Lobo, *Chem. Commun.*, 2001, **30**, 405–406.

18. D. Colantoni, S. Fioravanti, L. Pellacani and P. A. Tardella, *J. Org. Chem.*, 2005, **70**, 9648–9650.

19. A. K. Yudin, Ed., *Aziridines and epoxides in organic synthesis*, Wiley, Weinheim ; Chichester, 2006.

20. A. L. Williams and J. N. Johnston, *J. Am. Chem. Soc.*, 2004, **126**, 1612–1613.

21. F. A. Davis, P. Zhou and G. V. Reddy, *J. Org. Chem.*, 1994, **59**, 3243.

22. S. Gabriel, *Chem. Ber*, 1888, **21**, 1094.

23. H. Wenker, *J. Am. Chem. Soc.*, 1935, **57**, 2328–2328.

24. J. Li, J.-L. Liang, P. W. H. Chan and C.-M. Che, *Tetrahedron Lett.*, 2004, **45**, 2685-2688.

25. J. Li, P. W. H. Chan and C.-M. Che, *Org. Lett.*, 2005, **7**, 5801–5804.

26. A. Yoshimura, K. R. Middleton, C. Zhu, V. N. Nemykin and V. V. Zhdankin, *Angew. Chem. Int. Ed.*, 2012, **51**, 8059–8062.

27. R. Fan, H. Wang, Y. Ye and J. Gan, *Tetrahedron Lett.*, 2010, **51**, 453–456.

28. I. Washington, K. N. Houk and A. Armstrong, *J. Org. Chem.*, 2003, **68**, 6497–6501.

29. E. Schmitz, K. Jähnisck, *J. Geterozikl. Soedin.*, 1974, **12**, 1629.

30. K. Hori, H. Sugihara, Y. N. Ito, T. Katsuki, *Tetrahedron Lett.*, 1999, **40**, 5207.

31. R. Fan and Y. Ye, *Adv. Synth. Catal.*, 2008, **350**, 1526–1530.

32. P. W. Neber and A. V. Friedolsheim, *Justus Liebigs Ann. Chem.*, 1926, **449**, 109–134.

33. F. A. Davis, C.-H. Liang and H. Liu, *J. Org. Chem.*, 1997, **62**, 3796–3797.

34. M. J. Alves, G. Fortes, E. Guimarães and A. Lemos, *Synlett*, **2003**, 1403–1406.

35. Y. Matano, M. Yoshimune and H. Suzuki, *J. Org. Chem.*, 1995, **60**, 4663–4665.

36. L. Yadav and R. Kapoor, *Synlett*, **2009**, 3123–3126.

37. E. J. Corey and M. Chaykovsky, *J. Am. Chem. Soc.*, 1965, **87**, 1353–1364.

38. I. Ikeda, Y. Machii and M. Okahara, *Synthesis*, **1980**, 650–651.

39. J. Xu and P. Jiao, *J. Chem. Soc. [Perkin 1]*, **2002**, 1491–1493.

40. G. A. Olah, M. B. Sassaman, M. Zuanic, C. B. Rao, G. K. S. Prakash, R. Gilardi, J. Flippen-Anderson and C. George, *J. Org. Chem.*, 1992, **57**, 1585–1588.

41. A. Armstrong, D. Carbery, S. Lamont, A. Pape and R. Wincewicz, *Synlett*, **2006**, 2504–2506.

42. A. Armstrong, C. A. Baxter, S. G. Lamont, A. R. Pape and R. Wincewicz, *Org. Lett.*, 2007, **9**, 351–353.

43. L. Ma, D.-M. Du and J. Xu, *Chirality*, 2006, **18**, 575–580.

44. H. Ishihara, K. Hori, H. Sugihara, Y. N. Ito and T. Katsuki, *Helv. Chim. Acta*, 2002, **85**, 4272–4286.

45. A. Armstrong, R. D. C. Pullin, C. R. Jenner and J. N. Scutt, *J. Org. Chem.*, 2010, **75**, 3499–3502.

46. H. A. Samimi and A. R. Momeni, *J. Iran. Chem. Soc.*, 2015, **12**, 2221–2225.

47. Y.-M. Shen, M.-X. Zhao, J. Xu and Y. Shi, *Angew. Chem. Int. Ed.*, 2006, **45**, 8005–8008.

48. J. Wang, J. Lao, X. Li, R. Lu, H. Miao and M. Yan, *Synth. Commun.*, 2012, **42**, 1577–1584.

49. L. Kaplan, J. W. Pavlik and K. E. Wilzbach, *J. Am. Chem. Soc.*, 1972, **94**, 3283–3284.

50. A. Mishra, S. N. Rice and W. Lwowski, *J. Org. Chem.*, 1968, **33**, 481–486.

51. R. Ling, M. Yoshida and P. S. Mariano, *J. Org. Chem.*, 1996, **61**, 4439–4449.

52. H. Morita, A. Tatami, T. Maeda, B. Ju Kim, W. Kawashima, T. Yoshimura, H. Abe and T. Akasaka, *J. Org. Chem.*, 2008, **73**, 7159–7163.

53. N. Furukawa, S. Oae and T. Yoshimura, *Synthesis*, **1976**, 30–32.

54. J. Cossy and J. P. Pete, *Tetrahedron Lett.*, 1980, **21**, 2947–2948.

55. H. A. Samimi, H. Kiyani and Z. Shams, *J. Chem. Res.*, 2013, **37**, 282–284.

56. H. A. Samimi, B. Yamin and F. Saberi, *Synthesis*, 2014, **47**, 129–133.

57. H. A. Samimi, A. Mostafavi and M. R. Farsani, *J. Iran. Chem. Soc.*, 2015, **12**, 2031–

2035.

58. S.-L. Cui, J. Wang and Y.-G. Wang, *Org. Lett.*, 2007, **9**, 5023–5025.

59. H. A. Samimi and F. Dadvar, *Synthesis*, 2015, **47**, 1899–1904.

60. I. Coldham, A. J. Collis, R. J. Mould and R. E. Rathmell, *Tetrahedron Lett.*, 1995, **36**, 3557–3560.

61. J. M. Schomaker, A. R. Geiser, R. Huang and B. Borhan, *J. Am. Chem. Soc.*, 2007, **129**, 3794–3795.

62. D. Wenkert, S. B. Ferguson, B. Porter, A. Qvarnstrom and A. T. McPhail, *J. Org. Chem.*, 1985, **50**, 4114–4119.

63. L. M. Litvinenko and A. I. Kirichenko, *Dokl Chem*, **1967**, 763–766.

64. W. Steglich and G. Hoefle, *Angew. Chem. Int. Ed. Engl.*, 1969, **8**, 981.

65. G. P. Moss, *Pure Appl. Chem.*, 1996, **68**, 2193–2222.

66. R. P. Wurz, *Chem. Rev.*, 2007, **107**, 5570–5595.

67. K. Kondo, T. Kurosaki and Y. Murakami, *Synlett*, **1998**, 725–726.

68. A. G. Al-Sehemi, R. S. Atkinson, J. Fawcett and D. R. Russell, *Tetrahedron Lett.*, 2000, **41**, 2239–2242.

69. S. Arai, S. Bellemin-Laponnaz and G. C. Fu, *Angew. Chem.*, 2001, **113**, 240–242.

70. F. O. Arp and G. C. Fu, *J. Am. Chem. Soc.*, 2006, **128**, 14264–14265.

71. S. Arseniyadis, A. Valleix, A. Wagner and C. Mioskowski, *Angew. Chem. Int. Ed.*, 2004, **43**, 3314–3317.

72. V. B. Birman, H. Jiang, X. Li, L. Guo and E. W. Uffman, *J. Am. Chem. Soc.*, 2006, **128**, 6536–6537.

73. C. K. De, E. G. Klauber and D. Seidel, *J. Am. Chem. Soc.*, 2009, **131**, 17060–17061.

74. M. Crittall, H. S. Rzepa and D. R. Carbery, *Org. Lett.*, 2011, **13**, 1250–1253.

75. M. R. Crittall, N. W. Fairhurst and D. R. Carbery, *Chem. Commun.*, 2012, **48**, 11181–11183.

76. A. Padwa and L. Hamilton, *J. Am. Chem. Soc.*, 1967, **89**, 102–112.

77. A. Padwa and W. Eisenhardt, *J. Am. Chem. Soc.*, 1971, **93**, 1400–1408.

78. V. Bhat and M. V. George, *Tetrahedron Lett.*, 1977, **18**, 4133–4136.

79. A. G. Anastassiou and R. B. Hammer, *J. Am. Chem. Soc.*, 1972, **94**, 303–305.

80. A. M. Trozzolo, T. M. Leslie, A. S. Sarpotdar, R. D. Small, G. J. Ferraudi, T. D. Minh and R. L. Hartless, *Pure Appl. Chem.*, 1979, **51**.

81. K. Bhattacharyya, D. Ramaiah, P. K. Das, and M. V. George, *J. Phys. Chem.*, 1986, **90**, 3221–3229.

82. D. Ramaiah, D. R. Cyr, R. Barik, K. R. Gopidas, P. K. Das and M. V. George, *J. Phys. Chem.*, 1992, **96**, 1271–1278.

83. D. Ramaiah, M. Muneer, K. R. Gopidas, P. K. Das, N. P. Rath and M. V. George, *J. Org. Chem.*, 1996, **61**, 4240–4246.

84. R. Huisgen, H. Hermann and H. Maeder, *J. Am. Chem. Soc.*, 1971, **93**, 1779–1780.

85. E. Vedejs and M. Jure, *Angew. Chem. Int. Ed.*, 2005, **44**, 3974–4001.

86. U. F. Franck, *Angew. Chem. Int. Ed. Engl.*, 1978, **17**, 1–15.

87. A. J. Bissette and S. P. Fletcher, *Angew. Chem. Int. Ed.*, 2013, **52**, 12800–12826.

88. I. R. Epstein and K. Showalter, *J. Phys. Chem.*, 1996, **100**, 13132–13147.

89. M. Orbán, K. Kurin-Csörgei and I. R. Epstein, *Acc. Chem. Res.*, 2015, **48**, 593–601.

90. R. N. Jones, *J. Am. Chem. Soc.*, 1961, **83**, 3544–3545.

91. J. P. Knowles, L. D. Elliott and K. I. Booker-Milburn, *Beilstein J. Org. Chem.*, 2012, **8**, 2025–2052.

92. J. R. Lakowicz, *Principles of fluorescence spectroscopy*, Springer, New York, 3rd ed., 2006.

93. C. T. Rodgers and P. J. Hore, *Proc. Natl. Acad. Sci.*, 2009, **106**, 353–360.

94. I. R. Gould, N. J. Turro and M. B. Zimmt, in *Advances in Physical Organic Chemistry*, Elsevier, 1984, vol. 20, pp. 1–53.

95. J. R. Woodward, *Prog. React. Kinet. Mech.*, 2002, **27**, 165–207.

96. J. R. Woodward, T. J. Foster, A. R. Jones, A. T. Salaoru and N. S. Scrutton, *Biochem. Soc. Trans.*, 2009, **37**, 358–362.

97. U. E. Steiner and T. Ulrich, *Chem. Rev.*, 1989, **89**, 51–147.

98. B. Wardle, *Principles and applications of photochemistry*, Wiley, Chichester, U.K, 2009.

99. A. Albini and M. Fagnoni, Eds., *Handbook of synthetic photochemistry*, Wiley-VCH, Weinheim, 2010.

100. Philips Lighting. *TUV PL-L 36W/4P*, Guildford Surrey, UK, 2015.

101. Polysciences, Inc., *Methyl Methacrylate Casting & Embedding Kit-Technical Data Sheet 517*, Warrington, Pennsylvania, USA, 2013.

102. E. Frick, H. A. Ernst, D. Voll, T. J. A. Wolf, A.-N. Unterreiner and C. Barner Kowollik, *Polym. Chem.*, 2014, **5**, 5053–5068.

103. N. Yamagiwa, H. Qin, S. Matsunaga and M. Shibasaki, *J. Am. Chem. Soc.*, 2005, **127**, 13419–13427.

104. G. L. J. A. Rikken and E. Raupach, *Nature*, 1997, **390**, 493–494.

105. G. L. J. A. Rikken and E. Raupach, *Nature*, 2000, **405**, 932–935.

106. B. Chae, S. W. Lee, S. B. Kim, B. Lee and M. Ree, *Langmuir*, 2003, **19**, 6039–6049.

107. N. Kawatsuki, A. Yamashita, M. Kondo, H. Ono and A. Emoto, *J. Photopolym. Sci. Technol.*, 2010, **23**, 343–348.

108. R. D. Richardson, M. G. J. Baud, C. E. Weston, H. S. Rzepa, M. K. Kuimova and M. J. Fuchter, *Chem Sci*, 2015, **6**, 3853–3862.

109. Y. Zhang and G. B. Schuster, *J. Org. Chem.*, 1995, **60**, 7192–7197.

110. D. S. Kliger and J. W. Lewis, *Polarized Light in Optics and Spectroscopy*, Elsevier, 2012.

111. N. Rastogi, J. Abaul, K. S. Goh, A. Devallois, E. Philogène and P. Bourgeois, *FEMS Immunol. Med. Microbiol.*, 1998, **20**, 267–273.

112. A. C. Giddens, H. I. M. Boshoff, S. G. Franzblau, C. E. Barry III and B. R. Copp, *Tetrahedron Lett.*, 2005, **46**, 7355–7357.

113. H. A. Samimi, M. Mamaghani and K. Tabatabaeian, *J. Heterocycl. Chem.*, 2008, **45**, 1765–1770.

114. Q. Jiang, J. Jia, B. Xu, A. Zhao and C.-C. Guo, *J. Org. Chem.*, 2015, **80**, 3586–3596.

115. D. Ogawa, K. Hyodo, M. Suetsugu, J. Li, Y. Inoue, M. Fujisawa, M. Iwasaki, K. Takagi and Y. Nishihara, *Tetrahedron*, 2013, **69**, 2565–2571.

116. Z. Gonda and Z. Novák, *Chem. Eur. J.*, 2015, **21**, 16801–16806.

117. P. Tarburton, C. A. Kingsbury, A. E. Sopchik and N. H. Cromwell, *J. Org. Chem.*, 1978, **43**, 1350–1355.

118. P. Baret, M. Bourgeois, C. Gey and J. L. Pierre, *Tetrahedron*, 1979, **35**, 189–196.